UNIVERSITY OF CALIFORNIA

Santa Barbara

A Journey Through the Chemistry of Reactive Intermediates: From a Trimethylenemethane Diyl to Electrochemically-Generated Radical Ions

A Dissertation submitted in partial satisfaction of the

requirements for the degree Doctor of Philosophy

in Chemistry

by

Randi Kathleen Gbur

Committee in charge:

Professor R. Daniel Little, Committee Chair

Professor Alison Butler

Professor Craig J. Hawker

Professor Javier Read de Alaniz

September 2013

ProQuest LLC.
789 East Eisenhower Parkway
P.O. Box 1346
Ann Arbor, MI 48106 - 1346

The dissertation of Randi Kathleen Gbur is approved.

_____

Alison Butler

_____

Craig J. Hawker

_____

Javier Read de Alaniz

_____

R. Daniel Little, Committee Chair

July 2013

A Journey Through the Chemistry of Reactive Intermediates:
From a Trimethylenemethane Diyl to Electrochemically-Generated Radical Ions

By

Randi Kathleen Gbur

ACKNOWLEDGEMENTS

I would like to express my sincerest gratitude to my advisor and friend, Dr. R. Daniel Little, for providing me with the opportunity to work on a variety of projects in his research group, expand my breadth of knowledge in organic chemistry, and for his continual support and guidance both academically and in life. It has been an honor and my pleasure to work with a true gentleman and scholar.

I gratefully acknowledge my committee members, Dr. Craig Hawker and Dr. Javier Read de Alaniz for their insight and constructive criticism during my candidacy exam. I especially wish to thank Dr. Alison Butler for her warm encouragement throughout the course of my graduate studies.

I sincerely appreciate the guidance and friendships that I have gained from past and present Little group members. I am particularly indebted to Ms. Jinnie Myung, who taught me the fine art of careful manipulation and handling of small molecules. Furthermore, I am appreciative of Dr. G. Leslie Burnett IV for engaging in many intellectually stimulating scientific discussions, which have undoubtedly shaped my graduate career. Additionally, the opportunity provided by Dr. Cheng-chu Zeng to gain a better understanding and appreciation of the Chinese culture has left a lasting impression, and I am grateful for his hospitality for the duration of my stays in Beijing.

I am certain I would not be where I am without the unconditional love and support of my friends and family. I am incredibly grateful for my rock in shining armor, Stacey Gdula, and "The J. Wrights," Jaclynn and Jason, for comprising my

invaluable long distance support group, and to my "Santa Barbara Family"—especially Amy Chalker, Elizabeth Ilardi, Agustin Pierri, Bethany Wigington, Ash Wright, Sara Nownes, and Jo Little—for being my home away from home. My deepest appreciation is extended to my mother, Linda, and my sister, Jenn, for their love and support throughout my life. Finally, I am grateful to my father, Ed, the other gentleman and scholar in my life, for being an unwavering source of encouragement and advice.

CURRICULUM VITAE

Education:

University of California, Santa Barbara

Ph.D. Advisor: Prof. R. Daniel Little; July 2013.

University of Texas at Arlington

B. S. Biochemistry (*magna cum laude*), minor in Physics; May 2008

Awards:

NSF Partnership for International Research and Education: Electron Chemistry and Catalysis Intefaces (PIRE-ECCI) Fellow, **2011–2013**

Robert H. DeWolfe Graduate Teaching Fellowship, **2010–2012**

Bruce Rickborn-Ross Johnson Fellowship, **2008**

University of Texas at Arlington University Scholar Award, **2007**

NSF Research Experience for Undergraduates (REU) Fellow, **2007**

Experience:

Graduate Researcher, University of California Santa Barbara, 7/2008 – 7/2013

Visiting Researcher, Beijing University of Technology, 4/2012 – 6/2012

Undergraduate Research Intern, The Ohio State University, 6/2007 – 8/2007

Undergraduate Researcher, University of Texas at Arlington, 5/2006 – 3/2008

Publications:

1) Gbur, R. K.; Little, R. D. "Electrosynthesis of Bioactive Materials," in *Organic Electrochemistry*, 5th ed., B. Speiser and O. Hammerich, Eds. Chapt. 26, **2013**, *in press*.

2) Zhang, N.-t.; Zeng, C.-c.; Lam, C. M., Gbur, R. K.; Little, R. D. "Triarylimidazole Redox Catalysts: Electrochemical Analysis and Empirical Correlations," [Howard Zimmerman Memorial Issue] *J. Org. Chem.* **2013**, *78*, 2104–2110.

3) Gbur, R. K.; Little, R. D. "Unveiling the Role of Molecule Assisted Homolysis: A Mechanistic Probe into the Chemistry of a Bicyclic Peroxide," [Featured Article] *J. Org. Chem.* **2012**, *77*, 2134–2141.

Presentations:

Dept. of Chemistry Symposium in Honor of Professor R. Daniel Little,
Santa Barbara, CA, **2012**

National Science Foundation PIRE-ECCI Annual Meeting
Shanghai, China, **2012**

63rd Annual Meeting of the International Society of Electrochemistry
Prague, Czech Republic, **2012**

College of Life Science & Bioengineering Departmental Seminar
Beijing, China, **2012**

Chemical Sciences Interdepartmental Graduate Student Seminar Series

Santa Barbara, CA, **2012**

239th National Meeting of the American Chemical Society

San Francisco, CA, **2010**

The Ohio State University Chemistry REU Symposium

Columbus, OH, **2007**

Meeting in Miniature, Southwest Division of the American Chemical Society

Ft. Worth, TX, **2007**

ABSTRACT

A Journey Through the Chemistry of Reactive Intermediates:
From a Trimethylenemethane Diyl to Electrochemically-Generated Radical Ions

by

Randi Kathleen Gbur

Reactive intermediates, such as those derived from trimethylenemethane (TMM) diyls or electrochemically-generated radical ions, provide a versatile platform for exploring a wide variety of unique and interesting chemistries. A particular emphasis is placed on gaining a fundamental understanding of these intermediates through (a) mechanistic investigations or (b) method development, both of which are discussed herein.

Unlike the reaction of aryl-substituted diazenes, pyrolysis of alkyl-substituted diazenes in the presence of molecular oxygen generates an unexpectedly complex product mixture. Using deuterium labeling studies, in conjunction with quantum calculations, a reasonable mechanistic hypothesis for the decomposition of the resultant [3.3.0] peroxide, and subsequent formation of the keto-alcohol and Z-configured α,β-unsaturated keto-aldehyde, is proposed. Surprisingly, molecule-assisted homolysis plays a key role in this transformation, the details of which are discussed.

While fulvenes have a rich history taking advantage of their aromatic and olefinic characteristics, very little is known about the electrochemical properties of these compounds. One interesting aspect of their electrochemical behavior—the elecroreductive cyclization of a fulvene tethered to an α,β-unsaturated ester—is examined. In particular, the details concerning directed product formation via temperature control and concentration effects toward dimerization, or toward cyclization through a variation of the length of the tether joining the fulvene core to the second electrophore are discussed.

Indirect electron transfer using electrochemical mediators allows many reactions to be run under milder redox conditions, e.g. requiring less total energy consumption. Unfortunately, in the majority of cases the mediators can't be recovered; therefore a recoverable mediator source would be both economically and ecologically attractive. Taking advantage of a generally underappreciated tool in organic electrochemistry, *viz.*, the electrode surface, progress towards the modification of electrode surfaces with mediator-functionalized terthiophene polymers is presented. The aim of the investigation is to provide a method to recover and reuse electrochemical mediators, and thus a sustainable alternative to traditional mediated electrochemistry. One application of interest that will be explored is the anodic oxidative degradation of lignin model compounds.

ABBREVIATIONS

Abbreviation or symbol	Term
AcOH	acetic acid
AFM	atomic force microscopy
aq.	aqueous
ATC	atom transfer cyclization
BDD	boron doped diamond
br	broad
Bu	butyl
°C	degrees Celsius
C	coulomb
cat.	catalytic
COSY	correlation spectroscopy
CpH	cyclopentadiene
CV	cyclic voltammetry
δ	chemical shift(s)
d	doublet
DBU	1,8-diazabicyclo[5.4.0]undec-7-ene
DCC	*N,N′*-dicyclohexylcarbodiimide
DEAD	diethyl azodicarboxylate
DMAP	4-(dimethylamino)pyridine
DMF	*N,N*-dimethylformamide

DMSO	dimethyl sulfoxide
DPPA	diphenylphosphoryl azide
E	entgegen
E_p	peak potential
EI	electron ionization
equiv	equivalent
ESI	electrospray ionization
ESR	electron spin resonance
Et	ethyl
Et_2O	diethyl ether
EtOAc	ethyl acetate
EtOH	ethanol
FI	field ionization
FMO	frontier molecular orbital
FTO	fluorine-doped indium tin oxide
g	gram(s)
GC	glassy carbon
h	hour(s)
HOMO	highest occupied molecular orbital
HPLC	high-performance liquid chromatography
HRMS	high resolution mass spectroscopy
Hz	hertz

i	iso
i_p	peak current
IR	infrared spectroscopy
IRC	intrinsic reaction coordinate
J	coupling constant
KHMDS	potassium hexamethyldisilazide
LAH	lithium aluminum hydride
LDA	lithium diisopropylamide
LHMDS	lithium hexamethyldisilazide
LUMO	lowest unoccupied molecular orbital
m	multiplet
M	molar
mA	milliampere
MAH	molecule-assisted homolysis
MAO	methylaluminoxane
Me	methyl
MeCN	acetonitrile
MeOH	methanol
mg	milligram(s)
MHz	megahertz
min	minute(s)
mL	milliliter(s)

mmol	millimole
MO	molecular orbital
Ms	methanesulfonyl
ν	scan rate
n-BuLi	*n*-butyllithium
NAD^+/NADH	nicotinamide adenine dinucleotide
NBS	N-bromosuccinimide
NMR	nuclear magnetic resonance
NOESY	Nuclear Overhauser effect spectroscopy
Nu	nucleophile
Ph	phenyl
PIDA	(diacetoxyiodo)benzene
PIFA	bis(trifluoroacetoxy)iodobenzene
ppm	parts per million
pTTh	poly(terthiophene)
q	quartet
quint	quintet
R_f	retention factor
RDS	rate determining step
rt	room temperature
RVC	reticulated vitreous carbon
s	singlet

SCE	saturated calomel electrode
SEM	scanning eletron microscopy
SOMO	singularly occupied molecular orbital
t	triplet
T	temperature
t-Bu	tert-butyl
THF	tetrahydrofuran
TLC	thin layer chromatography
TMM	trimethylenemethane
TMS	trimethylsilyl
Ts	4-toluenesulfonyl
TTh	terthiophene
UV	ultraviolet
V	volt
Z	zusammen
2D	two dimensional

TABLE OF CONTENTS

FIGURES

SCHEMES

TABLES

Chapter 1

A Mechanistic Investigation of a Bicyclic Peroxide and the Unanticipated Role of Molecule-Assisted Homolysis

1.1 Introduction

1.1.1 Organic Peroxides

Organic peroxides are an important structural motif, and although peroxides are traditionally thought of as being unstable or even hazardous substances, this need not be the case. They are commonly used in the initiation of industrial polymerization processes,[1] as active ingredients in personal care products, such as acne medication,[2] and in the synthesis of biologically relevant natural products.[3] For instance, oxygen labeling experiments have shown that endoperoxides are important intermediates in the biosynthesis of several of the prostaglandins.[4] Alkyl peroxyl radicals generated from the homolytic cleavage of a peroxide bond, in particular, have long been under scrutiny. While many of these reactive oxygen species are considered toxic,[5] evidence suggests that others are biologically relevant, most notably the antimalarial, **1**–**3**, and antitumor agents, **6**–**7**, or the prostaglandins PGG_2, **4**, and PGH_2, **5** (Figure 1). For example, it has been shown that cleavage of the peroxide bond plays a key role in the expression of artemisinin's antimalarial activity.[6] Herein we describe the chemistry of a remarkably stable bicyclic peroxide generated from a trimethylenemethane diyl, and delve into the factors that eventually lead to cleavage of the peroxide bond.

Figure 1. Biologically active natural products containing a peroxide bond.

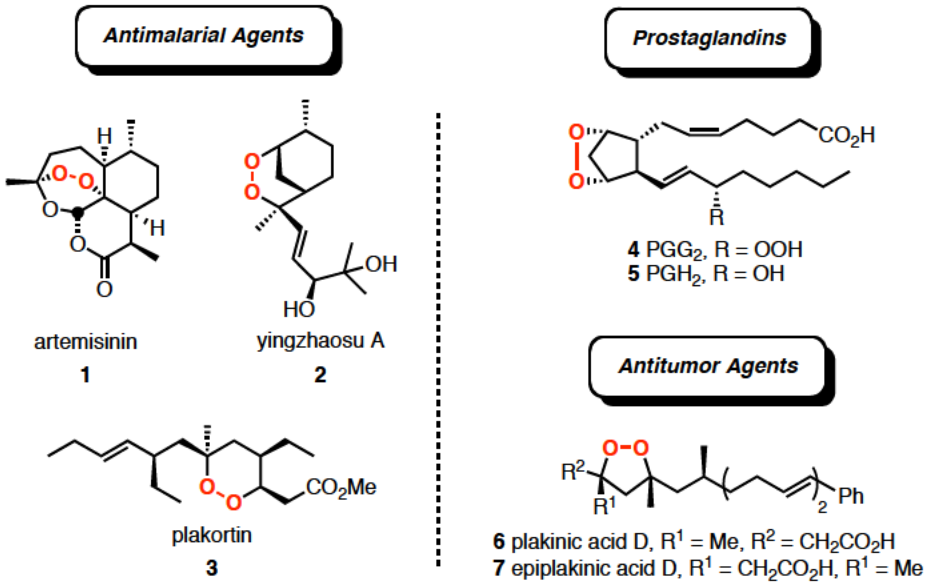

1.1.2 Trimethylenemethane

Trimethylenemethane (TMM), a simple diradical **8**, has been a focus of researchers for many years due to its unique reactivity. Simple Hückel MO calculations indicate that there are two degenerate nonbonding orbitals.[7] Application of Hund's rule predicts that the triplet should to be the ground state (Figure 2).[8] In practice, the existence of singlet and triplet spin states for the diradical (diyl) provide very different reactivities.

Figure 2. Molecular orbitals for trimethylenemethane (TMM).

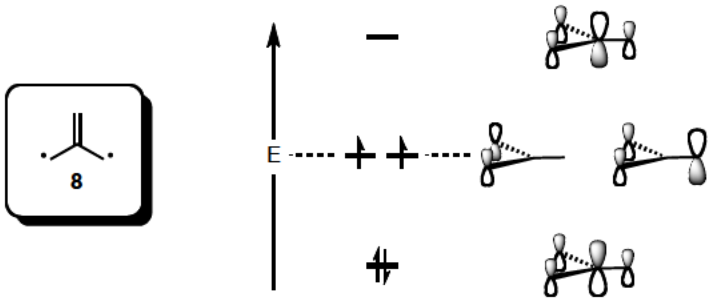

The parent diyl was first generated and studied by Dowd in 1966 using ESR spectroscopy.[9] Upon irradiation of 4-methylenepyrazoline, **9**, with light at –196 °C, a spectrum consistent with a triplet species, **11**, was observed (Scheme 1). The signal remained constant up to a month, as long as the low temperature was maintained. As soon as the temperature was raised above –150 °C, the triplet signal diminished within minutes. Subsequent experimental and theoretical efforts proved that the triplet was indeed the ground state.[10]

Scheme 1. Photochemical generation of the triplet TMM diyl.

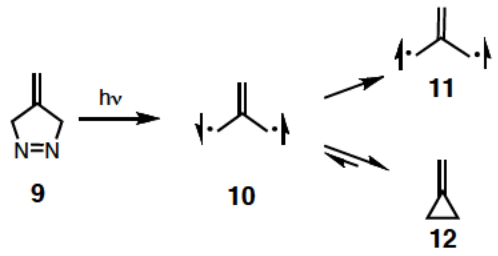

1.2 Diyl Trapping Reactions

Initial efforts were aimed at using the parent TMM diyl in cycloaddition reactions with alkenes. However, the initially formed singlet diyl, **10**, rapidly closes

to form methylenecyclopropane, **12**, requiring an activiation energy of 42 kcal/mol to revert to the ring-opened form.[10] This problem was circumvented by generating analogs of the parent diyl. Thus in 1971, Berson and coworkers formed 2-isopropylidene-1,3-diyl, **14**, by heating diazene **13** (R = R′ = CH_3).[11] This diyl was shown to dimerize through a triplet-triplet interaction and could be intercepted by a variety of diylophiles to form mixtures of bridged and fused cycloadducts (Scheme 2).[12] These findings provided abundant opportunities for additional exploration.

Scheme 2. Reactivities of TMM diyl derivatives in the intermolecular diyl trapping reaction.

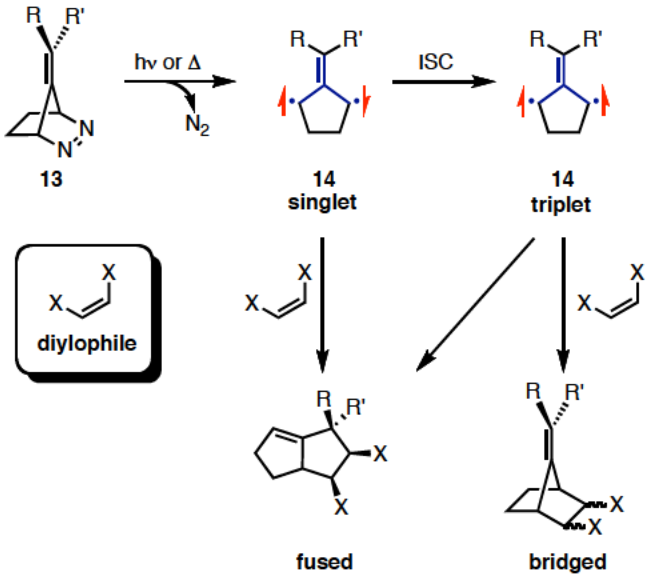

1.2.1 Singlet vs. Triplet Reactivity

TMM diyl derivatives can be generated either thermally or photochemically from bicyclic azo compounds, e.g. **13**, through the loss of nitrogen to produce the singlet TMM diyl, **14**. The temperatures at which the diyls can be generated range from

–20 °C for R = R′ = OMe, to refluxing acetonitrile.[13] Photochemical generation of the diyl occurs through an n–π* excitation of the azo linkage at wavelengths between 315 nm and 340 nm.[14] The singlet that is produced can undergo rapid interconversion with the methylenecyclopropane analog or intersystem cross to generate the triplet species, **14**. The rate at which the singlet diyl can be intercepted relative to the rate of intersystem crossing determines the ratio of products formed from the two spin states. Trapping of the singlet diyl is believed to proceed concertedly and stereospecifically and is regiospecific for the formation of fused products.[15] Cycloaddition with the triplet species, however, is regio-random and proceeds with loss of stereocontrol due to the stepwise, diradical nature of the transformation.

The differences in lifetime of the singlet and triplet TMM diyl can be understood by the differences in orbital geometry of the two species. The lowest singlet state exists in a bisected geometry while the triplet maintains a planar, delocalized π-framework (Figure 3).[16] Goodman and coworkers used time-resolved photoacoustic calorimetry (PAC) to determine experimentally that the enthalpic barrier between the singlet and triplet diyl was 12.7 kcal/mol,[17] resulting in a significant difference in their lifetimes, *viz*., 0.28 ns for the singlet and ~900 ns for the triplet diyl.[18]

Figure 3. Bisected singlet vs. planar triplet orbital geometries.

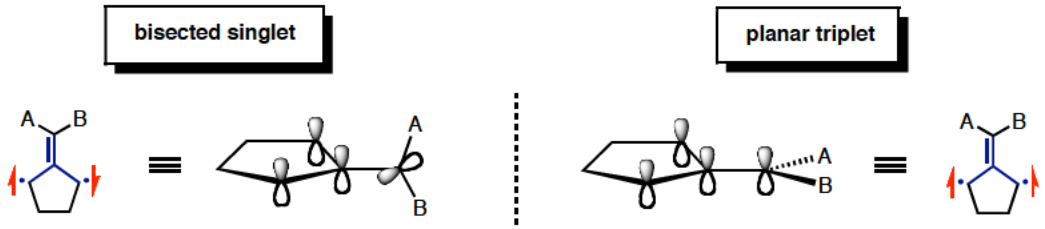

Based on the FMO diagram shown in Figure 4, the origin of the singlet selectivity can be ascertained. The degeneracy of the parent TMM diyl nonbonding orbitals is removed by the addition of the ethano bridge seen in the diyl analogs (Figure 4).[19] As a result of the Jahn-Teller distortion, the antisymmetric MO becomes higher in energy than the symmetric MO due to the destabilizing through-space interactions of the diyl π-system with the σ-orbitals of the ethano bridge. In contrast, through space interaction stabilizes the symmetric MO.[12,20]

Figure 4. Energy profile of non-degenerate singlet TMM molecular orbitals.

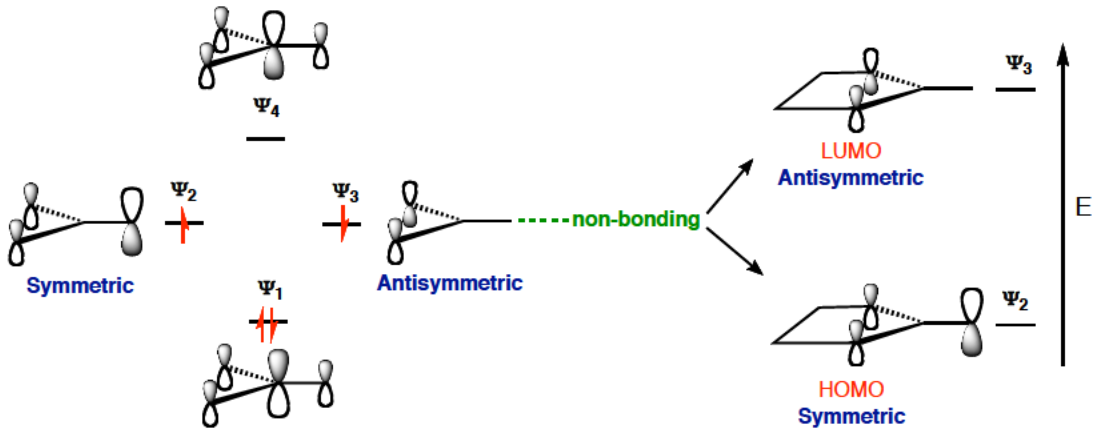

Because the diyl behaves as an electron rich species, the symmetric MO, acting as the HOMO, will interact with the LUMO of the diylophile (Scheme 3).[21]

Unfavorable anti-bonding interactions of the C_1 and C_3 p-orbitals with the LUMO of the diylophile occur during formation of the bridged cycloadduct. On the other hand, favorable bonding interactions occur during the formation of the fused cycloadduct.

Scheme 3. Rationale for observed regioselectivity of the singlet TMM diyl.

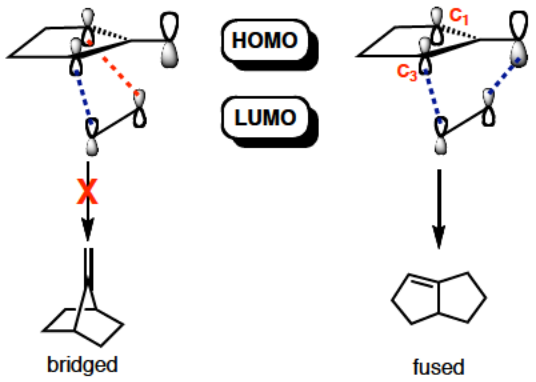

1.2.2 Diylophile Reactivity

The nature of the substituents appended to the diylophile can be used to control product formation. For example, an electron deficient diylophile will be reactive enough such that the rate of cycloaddition with the singlet exceeds the rate of intersystem crossing and more singlet-derived products will be formed. A bulky-substituent on the alkene or a more electron rich alkene will result in slow cycloaddition, allowing sufficient time for intersystem crossing and the formation of more triplet-derived cycloadducts.[22]

1.2.3 Application of the Diyl Trapping Reaction

TMM diyl derivatives provide a versatile platform for accessing a variety of interesting and complex structures through different modes of reactivity, including inter- and intramolecular cycloaddition reactions, atom transfer cyclization, and fragmentation cyclization cascades (Figure 5).

Figure 5. Versatile applications of TMM diyl derivatives.

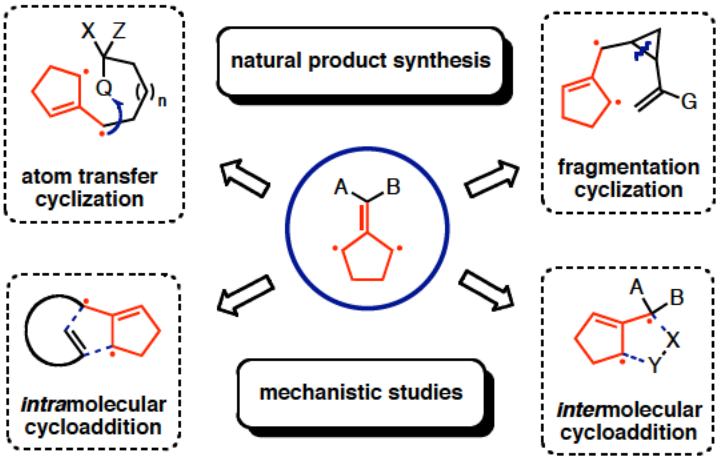

*Inter*molecular diyl trapping is an efficient process, but lacks the elements of stereo- and regiochemical control that are inherent to the intramolecular chemistry. Thus, when using an *intra*molecular variant many of these issues can be resolved by varying the tether length and substitution on the diylophile.[23] For example, Little and coworkers demonstrated that linearly fused cycloaddition products dominate when the tether length, *n*, is one or four methylene units, whereas a mixture of bridged and linear products are observed when *n* = 2 or 3 (Scheme 4).[24]

Scheme 4. Intramolecular cyclization reaction.

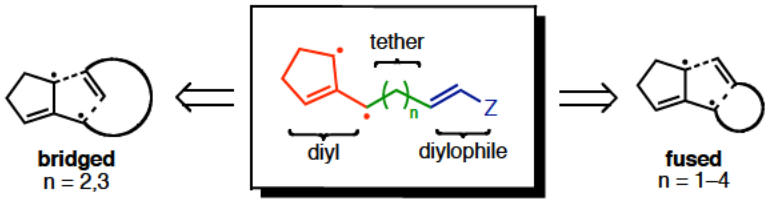

Initially, fused cycloadducts were desired for the use in natural product synthesis. Intramolecular diyl trapping was employed to form the linearly fused tricyclopentanoid core, which could be elaborated into natural products such as hypnophilin, **15,**[25] hirsutene, **16**,[26] Δ(9,12)-capnellene, **17**,[27] and coriolin, **18**[28] (Figure 6). It was also discovered that reversal of regiochemical control to afford bridged cycloadducts occurred when a bulky alkyl substitution was present on the internal carbon of the pendant olefin. This discovery proved useful for the synthesis towards natural products containing a bridged ring system such as taxol, **19**,[29] and aphidicolin, **20**.[30]

Figure 6. Natural products synthesized using a diyl trapping reaction.

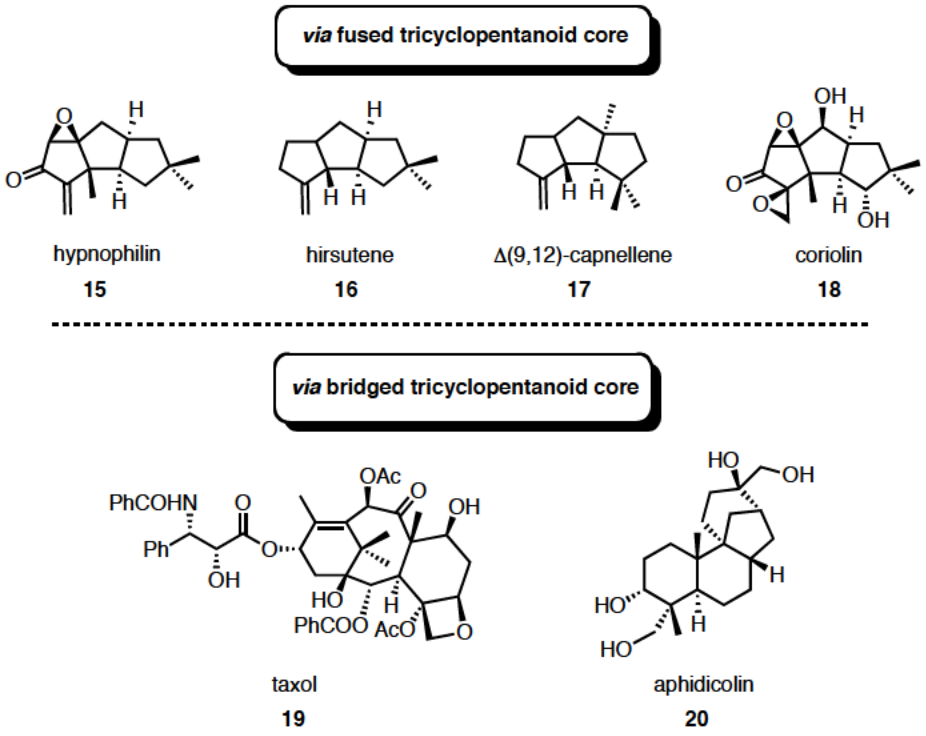

1.2.4 Atom Transfer Cyclization

Along with cycloaddition, TMM diyls can participate in atom transfer cyclization (ATC), despite the fact that the delocalized diyl is considered soft and unreactive when compared to its monoradical counterpart. Initial efforts by Adam and Finzel showed that TMM diyl **21** could in fact abstract a hydrogen atom from 1,4-cyclohexadiene (Scheme 5).[31]

Scheme 5. H-Abstraction by TMM Diyl.

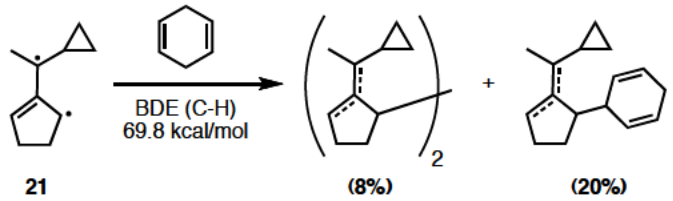

Little and coworkers later optimized the conditions for the ATC (Scheme 6).[24] Among other things, they suggested that the optimal transfer angle, i.e. θ in **22**, of the hydrogen atom is ~180°, thus the carbon tether must be sufficiently long, i.e. *d* in **22**, to accommodate this factor. Also, while not required, the "translocated" radical should be captodatively stabilized, i.e. appended to one electron donating group and one electron withdrawing group, X and Z in order to compensate for the loss in delocalization after atom transfer. For the latter case, ATC was the dominant pathway observed for diyl trapping.

Scheme 6. Optimal conditions for atom transfer cyclization.

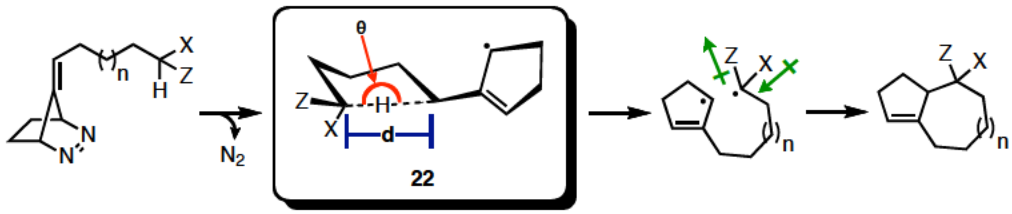

The importance of tether length in conjunction with captodative stabilization for ATC was demonstrated in the case of the simple diyl precursor, **25** (Table 1). When n = 2, cycloaddition and atom transfer cyclization did not occur; only dimerization products were isolated. Interestingly, an exception existed in the presence of a

Lewis acid, i.e. $ZnCl_2$. In this case, diazene **23** was converted to the [4.3.0] diene alcohol **24** in modest yields (Scheme 10). Because the reaction did not occur otherwise, it was theorized that complexation of the Lewis acid to the carbonyl oxygen polarized the carbonyl π-bond, thereby lowering the HOMO–LUMO gap and allowing attack by a dipolar diyl (i.e. a diyl exhibiting more dipolar character than diradical character).[32]

Scheme 7. Preferential cycloaddition in the presence of a Lewis Acid.

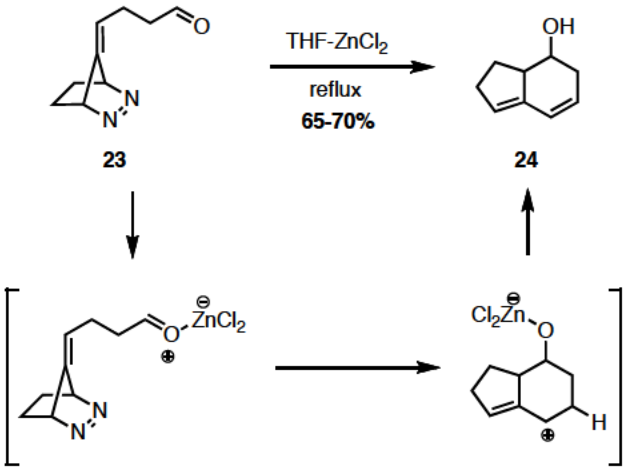

When the tether length was increased to three methylene units, cycloaddition was the preferred reaction pathway. Neither the use of $ZnCl_2$ or addition of an electron donating group (*p*-methoxybenzyl ether) alpha to the diylophile was sufficient to allow atom transfer cyclization to occur. The reaction pathway changed when an additional methylene unit existed between the diyl and the diylophile, i.e. when n = 4 in structure **25**. In this case, ATC dominated over cycloaddition, and became the

exclusive reaction pathway when captodative stabilization at the atom transfer site was present (Table 1).

Table 1. Effect of tether length on diyl trapping selectivity (cycloaddition vs. ATC).

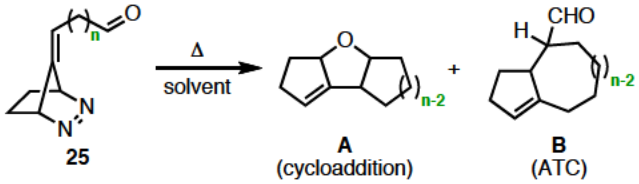

n	solvent	yield (%)	A : B
3	toluene	65	1 : 0
	$THF–ZnCl_2$	70	1 : 0
4	benzene	72	1 : 9
	$THF–ZnCl_2$	74	1 : 0

1.2.5 The Oxygen Trapping Reaction

On several occasions, molecular oxygen has been used to selectively probe the triplet chemistry of TMM diyls. It was used, for example, in determining the spin state responsible for formation of the linear and bridged cycloaddition products in the intramolecular diyl trapping reaction.[33] Initially, Berson and coworkers used this to study the singlet-derived products. It was proposed that if the triplet diyl could be trapped by molecular oxygen, singlet-derived products would be produced from cycloaddition with the diylophile.

Little and coworkers then used oxygen quenching studies in their quest to form predominantly bridged cycloaddition products starting from diazene **26**, shown in Table 2.[22] In the presence of molecular oxygen, no bridged adducts were formed and the yield of the fused adducts was significantly reduced, presumably as a result

of the reaction between oxygen and the triplet (Table 2). This confirmed that the triplet TMM diyl afforded both bridged and fused products, whereas the singlet TMM diyl afforded the fused cycloadduct.

Table 2. Selective triplet diyl quenching with molecular oxygen.

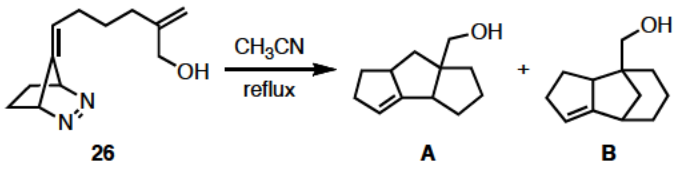

26 **A** **B**

	linear (**A**) : bridged (**B**) (% yield)
oxygen	44 : 46
no oxygen	17 : 0

The results of the oxygen diyl trapping studies were quite intriguing. Initial studies by Little and coworkers used dimethyl fumarate as the diylophile to compete with the oxygen in the trapping reaction.[34] No olefin cycloadducts were observed for the mono-*aryl* substituted diazenes **27** and **28**. A keto-alcohol (e.g., **29**) was the exclusive product, obtained in a 70-75% isolated yield (Scheme 8). Given its structural similarity to prostaglandins such as **30**, it was envisioned that by starting with a suitably alkyl-substituted diazene one might be able to use the oxygen trapping reaction to access prostanoids.

Scheme 8. The reaction of aryl-substituted diyls with oxygen.

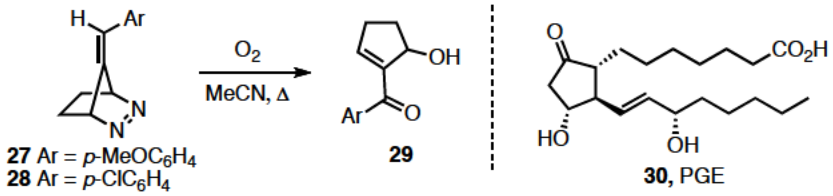

27 Ar = *p*-$MeOC_6H_4$
28 Ar = *p*-ClC_6H_4

29

30, PGE

Toward that end, they then elected to investigate the mono-*alkyl* substituted diazene.[35] As the subsequent discussion shows, its chemistry proved more complex than anticipated. For example, when the isopropyl-substituted azo compound, **31**, was subjected to pyrolysis in the presence of oxygen, three products were observed, viz., the keto alcohol **32**, a [3.3.0] endoperoxide, **33**, and an α,β-unsaturated keto-aldehyde, **34** (Scheme 12b). The cause of this unexpected outcome was never fully investigated until now.

Scheme 9. Pyrolysis of alkyl-substituted azo compounds in the presence of oxygen.

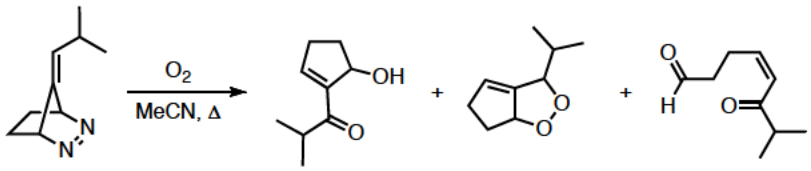

31 **32** **33** **34**

1.3 A Mechanistic Investigation

The following discussion is that of a mechanistic investigation into the behavior of mono-alkyl substituted systems in the presence of oxygen, highlighting in particular the unforeseen role of molecule-assisted homolysis (MAH) in the conversion of peroxide **39** into keto-alcohol **38** and keto-aldehyde **40**.

1.3.1 Synthesis of Diazene 9

To mitigate volatility problems that were encountered using the low molecular weight isopropyl-substituted diazene, and in preparation for a detailed mechanistic analysis, the *n*-heptyl-substituted diazene, **37**, was synthesized and its chemistry subsequently explored (note Scheme 11).

Synthesis of the alkyl substituted diazene **37** commenced in a slightly different fashion than previously reported by Dang (Scheme 10).[35] Following the Stone-Little procedure, heptyl fulvene, **35**, was prepared from octanal using cyclopentadiene and pyrrolidine followed by an acetic acid quench.[36] The fulvene was then converted to the [2.2.1] biscarbamate, **36**, through a sequential Diels-Alder reaction with DEAD and diimide reduction of the resulting $\Delta^{(4,5)}$ π-bond using dipotassium azodicarboxylate and glacial acetic acid in 85-95% yield over two steps. Saponification of the biscarbamate with KOH in refluxing ethanol, followed by oxidative decarboxylation using aqueous $K_3Fe(CN)_6$ provided diazene **37** in 55-64% yield.[37]

Scheme 10. Synthetic route used to assemble diazenes.

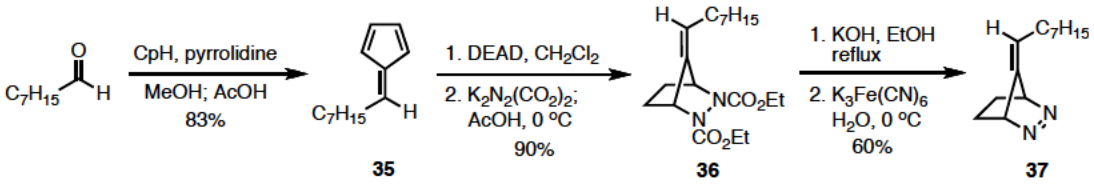

1.3.2 Initial Oxygen Trapping Results

Thermolysis was accomplished by heating **37** in a solution of acetonitrile in the presence of a continuous stream of oxygen (Scheme 11). Initially, the reaction was allowed to progress at reflux until the starting material was completely consumed. Three major products, viz., the expected keto-alcohol, **38**, as well as a [3.3.0] peroxide, **39**, and a *Z*-substituted α,β-unsaturated keto-aldehyde, **40**, were isolated and characterized. A peak showing correlation between the resonances at ~5.3 ppm, corresponding to the bridgehead proton, and ~4.9 ppm, corresponding to the methine proton, in a 2D NOESY NMR spectrum confirmed the relative *cis* stereochemistry of the [3.3.0] peroxide. While the crude reaction mixture contained a variety of additional products,[38] these three accounted for 76% of the isolated mass. Characterization of many of the side products proved futile because of the minute quantities in which they were isolated. However, mixtures of several regioisomeric products resulting from an apparent cycloaddition reaction with the carbonyl unit of an aldehyde, as well as dimeric products, were observed. Slow addition of the diazene to the pre-heated, pre-saturated solution of acetonitrile was attempted in order to minimize dimer formation, but no significant difference in the product ratios could be detected.

Scheme 11. The major products formed in the presence of oxygen.

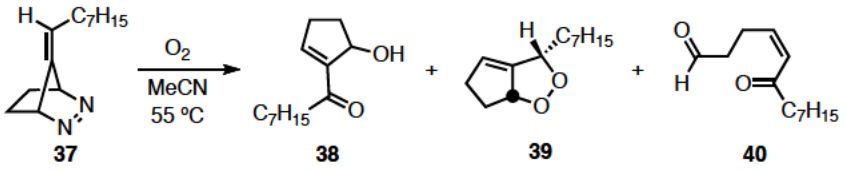

Assuming that the first intermediate formed is the fused peroxide rather than the bridged isomer, the qualitative observation of over 20 products in the crude reaction mixture is consistent with the work of Adam and coworkers.[39] In their case, the gas phase pyrolysis of the monocyclic 4-ethylidene-3,3,5,5-tetramethyl-1,2-dioxolane, **41**, generated numerous decomposition products when heated to 315 °C, the major product being the α,β-unsaturated ketone, **42** (Scheme 12). For the present mechanistic investigation, the reactions were run to low conversion and at a reduced temperature (55 °C) in an effort to minimize the formation of secondary products. As a result, recovered starting material accounted for an additional 14% of the isolated mass, and the main three products, **38-40**, formed the focus of our subsequent investigations. As the ensuing discussion will show, the relative amounts of each varied as a function of (a) time, (b) concentration of the starting diazene, and (c) the amount of keto-alcohol **38** present at any one time.

Scheme 12. Gas phase pyrolysis of dioxolane **41**.

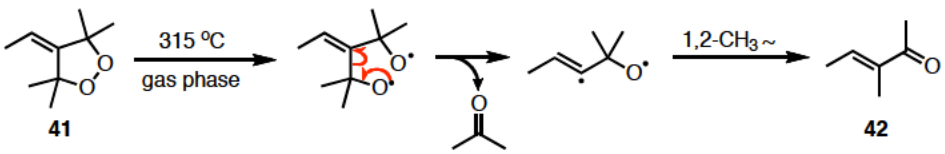

To assist in the elucidation of a reasonable mechanistic hypothesis, the order in which the products formed was determined. The peroxide, **11**, was the first to form, followed by the keto-alcohol, **10**, and finally the keto-aldehyde, **12**. From this information, we suspected that the peroxide might serve as the precursor of the other two products. This conclusion is consistent with observations made by Wilson and Geiser, who isolated and characterized a [3.3.0] endoperoxide as the sole product from thermolysis of a bis-substituted diazene in the presence of molecular oxygen. No bridged products were observed and the chemistry of the fused peroxide was not investigated further.[40]

1.3.3 Deuterium Labeling and Initial Thermolysis Results

To assist in determining the origin of these substances, the deuterium labeled diazene, **37-d_1**, was synthesized in the manner portrayed in Scheme 13. Thus, octanal, **43**, was converted to the dithiane, **44**, with 1,3-propanedithiol, using $ZnCl_2$ as a Lewis acid. Deuterium exchange to form **45** was accomplished by deprotonation with *n*-BuLi and a subsequent quench with D_2O, resulting in >90% deuterium incorporation as determined by ^1H NMR. The residual undeuterated material was carried throughout the ensuing experiments.

Scheme 13. Insertion of the deuterium label.

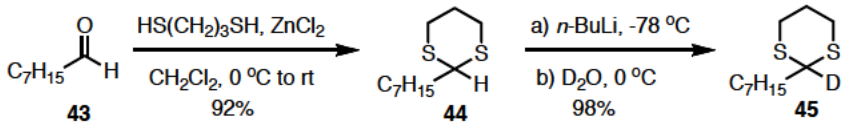

Interestingly, a modified procedure was required for the dithiane deprotection step. When directly following the procedure outlined by Stork and coworkers,[41] a single equivalent of PIFA was unsuccessful in removing the dithiane protecting group. Partial conversion of the starting material was observed after the addition of 2 equivalents, and the reaction proceeded smoothly in 96% yield with the addition of 5 equivalents of PIFA. Intrigued by this result, a further survey of the literature yielded precedence for this phenomenon from the work of Fleming and coworkers.[42] It is known that once a portion of the starting material is deprotected, several equivalents of PIFA are consumed by oxidizing the sulfur of the newly formed dithiolane, **46**, before the reaction can go to completion (Scheme 14).

Scheme 14. Deprotection of the aldehyde with PIFA and synthesis of the diazene.

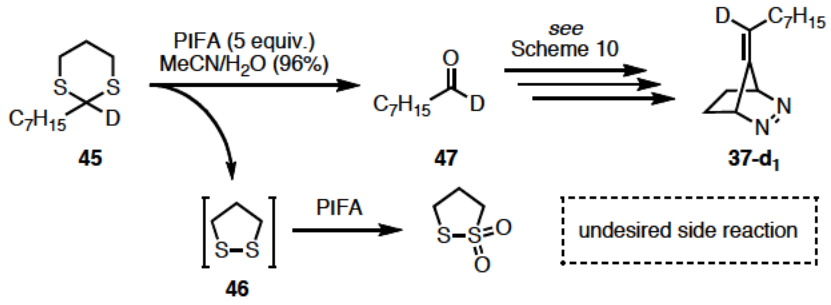

Once an efficient deprotection protocol of **45** using PIFA to yield octanal-d_1, **47**, had been developed, its subsequent conversion to the deuterated diazene, **37-d_1**, followed the synthetic approach illustrated in Scheme 10.

Thermolysis of the deuterated diazene, **37-d_1**, was conducted under the same conditions as its protio-counterpart, **37**. The location of the deuterium label in each of the three products was determined spectroscopically (Figure 7). A lack of signal change in the ^{1}H NMR for **38-d_1** corresponded to a proton exchange for the deuterium atom on the hydroxyl group.

Figure 7. Location of the deuterium label in the products formed from the reaction of the deuterated diazene, **37-d_1**, with oxygen.

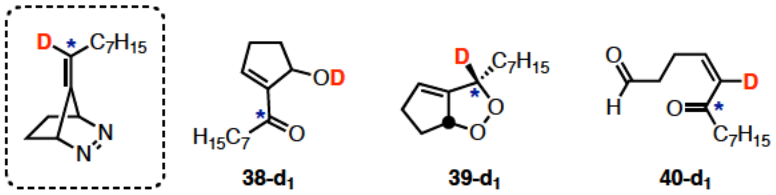

Examination of the structures for keto-alcohol **38-d_1** and enone **40-d_1** clearly reveals that the label has moved, as indicated by the originally labeled carbon marked with an asterisk; but how, and when? From these results, one can envision that the presence of dioxolane **39-d_1** is simply a result of the triplet diyl being trapped by the molecular oxygen (Scheme 15).

Scheme 15. Formation of the [3.3.0] endoperoxide.

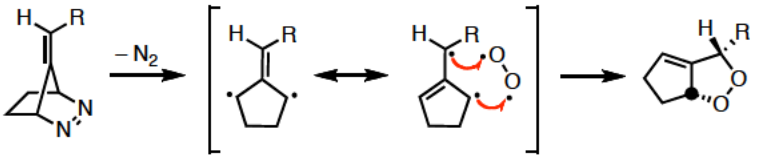

1.3.4 Unanticipated Concentration Effects

One of the more intriguing aspects of our initial findings was the dramatically different time needed for the conversion of the deuterated substrate, **37-d$_1$**, to the products relative to its protio-analog, **37**. This was obvious even when assessed qualitatively by TLC. In the protio case, for example, all three products were observed in approximately 2.5 hours, with peroxide **39** appearing after 1 hour and **38** and **40** appearing after 1.5 and 2 hours, respectively. In contrast, the deuterated substrate, **37-d$_1$**, required 2 hours before the peroxide, **39-d$_1$**, was visible by TLC, and even after an additional 2 hours of heating, no keto-alcohol or keto-aldehyde was observed.

To investigate further this unanticipated outcome, separate experiments were performed starting with the protio and deuterated diazenes **37** and **37-d$_1$**, respectively. The amount of peroxide (**39** and **39-d$_1$**) formed was measured as a function of time using ^{1}H NMR. Two diazene concentrations were examined, *viz*., 0.025 M and 0.05 M, the latter representing a 10-fold increase relative to the concentration normally used. Table 3 compares the results for the two systems at a starting diazene concentration of 0.05 M (note the black and red curves in Figure 8).

Notably after 2.5 h, there is nearly 20% more peroxide present when starting from the deuterated substrate, **37-d$_1$**, compared with its protio-counterpart, **37**. Why is this so? One option, discussed below, is that the deuterated peroxide, **39-d$_1$**, accumulates because its rate of conversion to the other two products is considerably slower than that of its protio-analog.

Table 3. Percentage of peroxide formed from pyrolysis of protio- and deuterated diazene **37** and **37-d$_1$** as a function of time and concentration of the diazene.

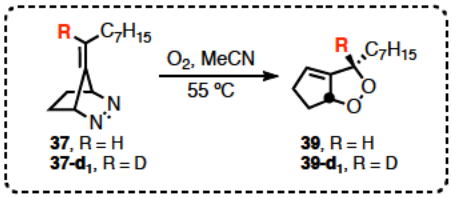

	from 0.025 M diazene:		from 0.05 M diazene:	
time (h)	**39** (%)	**39-d$_1$** (%)	**39** (%)	**39-d$_1$** (%)
0.5	10.	11	9.4	10.
1.0	20	21	18	27
1.5	31	32	27	37
2.0	38	42	33	48
2.5	44	50	37	56

Figure 8. Profile for **Table 3**.

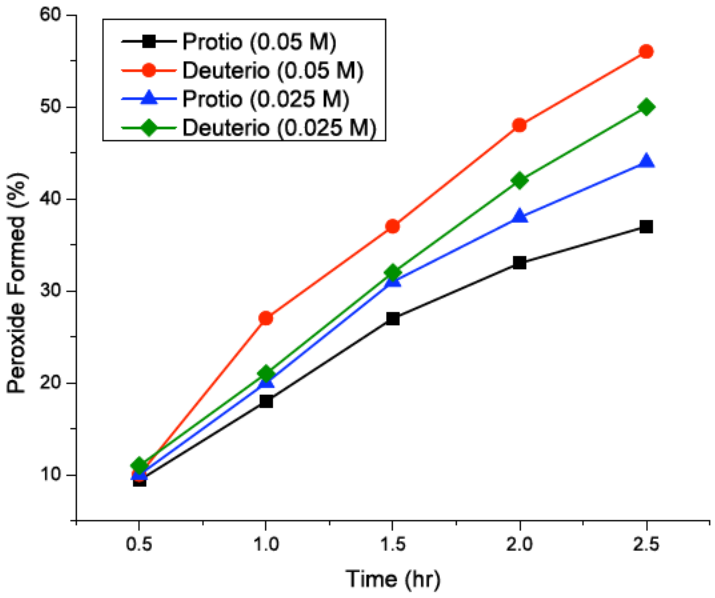

Since we suspected that **39-d$_1$** was the precursor of the other two products, we reheated it to the same temperature in an oxygen-rich solution similar to that used during its genesis, anticipating its facile conversion to **38-d$_1$** and **40-d$_1$**. Such was not the case. Only after prolonged heating (8 hours) at elevated temperatures (85 ºC) did we observe any sign of a reaction. This impasse led us to wonder whether there was something "special" about the reaction medium that existed as the products were being formed during the reaction with oxygen.

1.3.5 Molecule-Assisted Homolysis

In 1973, Nugteren and Hazelhof reported that the prostaglandin endoperoxide 9α,11α-epidioxy-15(*S*)-hydroxy-13-*trans*-prostenoic acid illustrated in Figure 9 decomposed with a half-life of only 30 minutes in an aqueous medium, while in non-

polar organic solvents the half-life increased to over 2 hours (Figure 9).[43] Their observation is not unprecedented.[44] It is known, for example, that peroxides are particularly sensitive to bond homolysis in the presence of hydrogen-bond donors and subsequent transformations are often accelerated.[45] We suspected that a similar molecule-assisted homolysis (MAH) pathway might be playing a role in the chemistry of peroxides **39** and **39-d$_1$**. Could it be, for example, that the conversion of the protio-peroxide **39** to the keto-alcohol **38** is facilitated as the concentration of the latter increases?

Figure 9. Stability of prostaglandin R_1 in organic vs. aqueous media.

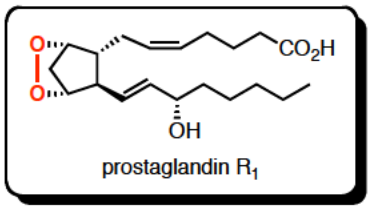

Half Life (20 °C)

H_2O (pH = 4-8): 0.5 h
organic solvents: 2.7 h

To explore this hypothesis, we first verified that the [3.3.0] peroxide was the sole precursor to keto-alcohol **38** and keto-aldehyde **40**. The bridged endoperoxide was initially entertained and then excluded as their precursor. When the isopropyl-substituted [2.2.1] system was independently synthesized and subjected to the reaction conditions, neither the keto-alcohol or the enone formed.[35] To our delight, the [3.3.0] endoperoxide provided both the keto-alcohol and the keto-alcohol upon heating in acetonitrile, both in the presence and absence of a stream of molecular oxygen. Furthermore, it can be envisioned that the keto-alcohol, **38**, is formed via an initial cleavage of the peroxide bond. Rotation about the exocyclic C–C bond in

structure **48** positions the terminal H atom for abstraction by the oxygen radical, forcing the formation of the alkyl substituted ketone, **38** (Scheme 16).

Scheme 16. Formation of the keto-alcohol from the [3.3.0] endoperoxide.

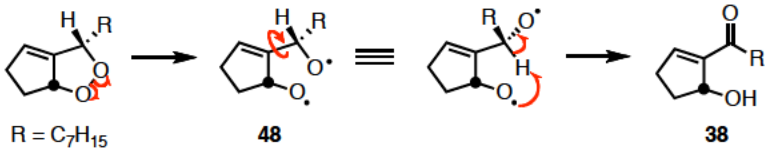

With that accomplished, we then used ^{1}H NMR to examine the chemistry of the peroxides as a function of time. To determine whether the presence of keto-alcohol **38** assisted the subsequent transformation of the peroxide, we compared the amount of keto-alcohol **38** and **38-d$_1$** produced when the peroxide was heated, both in its presence and absence.

Table 4. Percentage of keto-alcohol generated from pyrolysis of a 0.05 M solution of peroxide in the absence and presence of added **38**.

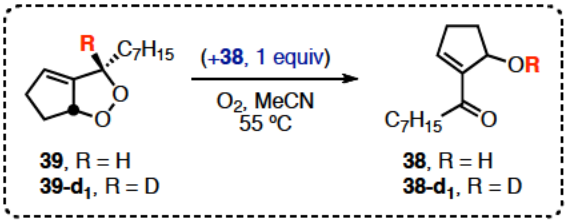

38 (%)			**38-d$_1$** (%)	
from: 39	**39 + 38**	time (h)	**from: 39-d$_1$**	**39-d$_1$ + 38**
3.5	6.4	0.5	2.4	5.2
4.1	16	1.0	3.1	6.8
6.6	44	1.5	4.1	9.0
8.3	50.	2.0	5.0	9.7
11	65	2.5	5.2	12

Figure 10. Profile for **Table 4**.

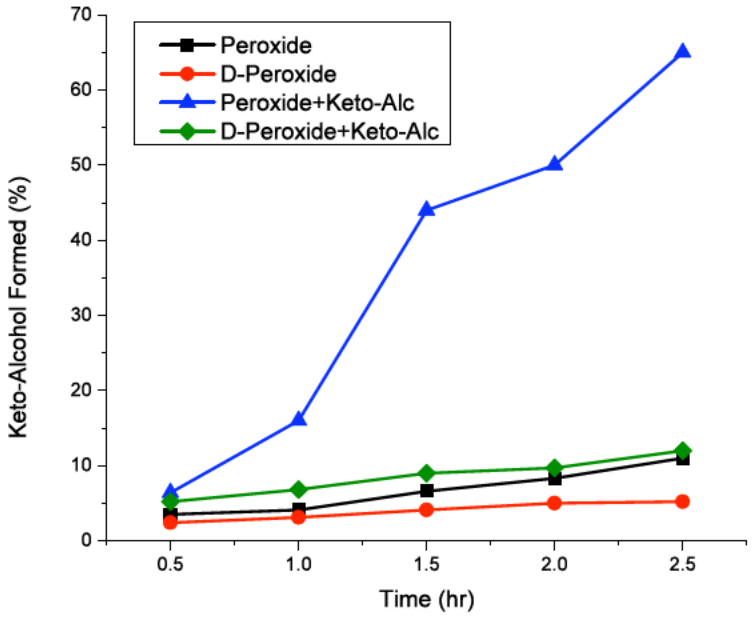

As indicated by the data listed in columns one and two of Table 4 (note particularly, the values at 2.5 hours) and illustrated in the graph, the addition of an equivalent of keto-alcohol *afforded a dramatic increase* in the amount of keto-alcohol generated from the protio-peroxide, **39**. This is consistent with the notion that the keto-alcohol assists in, and increases the rate of, conversion of peroxide **39** into keto-alcohol **38**, perhaps through hydrogen-bonding to the peroxide unit in the manner portrayed by **49**.[46] Comparison of the entries in columns two and five of Table 4 reveals that although the addition of keto-alcohol to the deuterated peroxide, **39-d$_1$**, leads to some **38-d$_1$** formation, the amount is significantly less than that of the protio-counterpart. While the added keto-alcohol presumably facilitates cleavage of the peroxide bond, the rate of C–D cleavage in the atom transfer step portrayed by the

conversion of **50** to **51** is presumably too slow to allow the amount of keto-alcohol to grow significantly during the timeframe of the investigation (Figure 11).

Figure 11. Conversion of the [3.3.0] endoperoxide to the keto-alcohol.

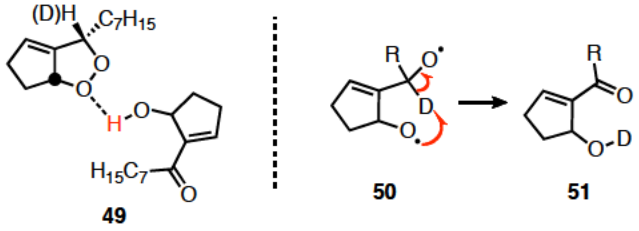

We then verified that this phenomenon was not limited to the case of the keto-alcohol. The amount of keto-aldehyde produced, as observed by ^{1}H NMR, also increased when the additional keto-alcohol was present. Furthermore, when protio-peroxide **39** was allowed to stand at room temperature in CD_3OH, it was converted to a 1 : 0.93 ratio of **39** to **38** in 12 hours.

1.3.6 Formation of the Keto-Aldehyde

One of the more challenging aspects of the present investigation was to determine a reasonable mechanism for the conversion of the peroxide, **39**, into the keto-aldehyde, **40**, in a manner that accounts for the *Z*-configuration. Of the options illustrated in Scheme 17, we find that neither pathway *a* involving oxetane **53**, nor pathway *b* involving allene oxide[47] **54** suffice since each leads to an *E*- rather than *Z*-configuration. Considering pathway *a* illustrated in Scheme 17, upon homolytic cleavage of the peroxide bond, closure of O• onto C_β generates oxetane **53**. For simplicity, the endo-configuration of R is illustrated, **53N**, although it is believed that

there is not preferential formation of either the exo- or endo-configuration upon oxetane ring formation. A 1,2-H• shift to generate the tertiary radical, followed by collapse of the resulting oxetane ring, produces the keto-aldehyde with the incorrect *E*-configuration. Alternatively, if closure of the oxygen-centered radical occurs at C_α of the olefin (pathway *b*), the resultant epoxide can be transformed into allene oxide **54**. Rearrangement of the allene oxide as described by Erden and coworkers,[47] ultimately generates the *E*-enone. A similar problem exists for pathways *c* and *d*, each involving a vinyl radical (*e.g.*, **55** or **56**) since rapid equilibration would ensure formation of the more stable *E*-configuration. Quantum calculations (UB3LYP/6-31G(d)) were in agreement with the notion that each of these pathways would lead to the *E*-stereochemical outcome.

Scheme 17. Mechanistic options that fail to deliver the *Z*-configuration found in the product enone.

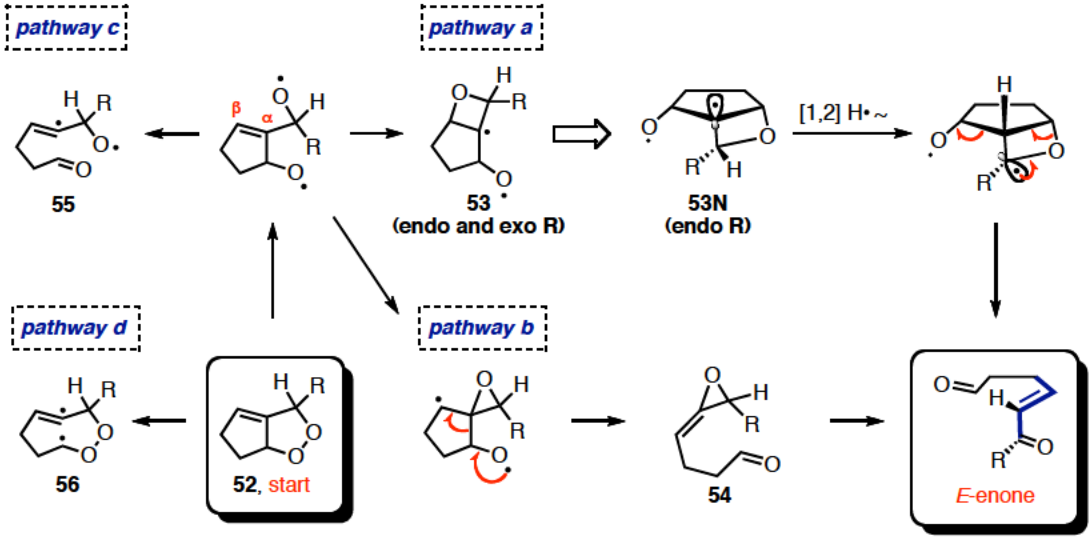

Taking into consideration that vinyl radicals are configurationally labile species, we examined the conditions under which it might be possible to "trap" the *Z*-configuration before equilibration to the more stable *E*-geometry could occur. Therefore, we propose that the enone is generated via a *concerted six-electron process* involving cleavage of the peroxide bond in concert with opening of the bridging C–C bond, and H-atom transfer in the manner portrayed in Scheme 6. Quantum calculations at the UB3LYP/6-31+G(d) level provide evidence in accord with our predictions. The calculations point to an exothermic transformation with a transition state 36.6 kcal/mol above the equilibrium geometry of the starting peroxide, **52** (Scheme 18). In the transition structure the peroxide bond has lengthened to 2.379 Å while the length of the bridging C–C bond has increased to 1.999 Å. The H-atom transfer to form the α,β-unsaturated ketone is just beginning

as is evidenced by the finding that the length of the C–H bond undergoing cleavage is 1.154 Å while that to which the migration terminates is 1.731 Å. Most interesting, however, is the angle about the emergent sp^2 center. As the a-b-c angle of the sp^2 center at *b* changes from 139° in the starting material to the *Z*-configuration found in the product, it must pass through a linear geometry. The calculated value of 152° in the transition structure indicates significant progress toward that end.

Scheme 18. Concerted six-electron pathway leading to the *Z*-enone.

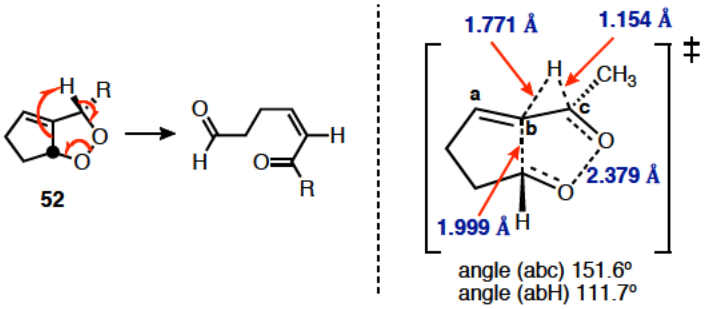

Once we identified a transition structure, an intrinsic reaction coordinate (IRC) calculation was performed in order to supply additional credibility to our proposal.[48] An IRC calculation provides a calculated structure that would produce a given transition state structure, as well as a projected product structure that would result from the same transition state structure. It is apparent from Figure 12 that the predicted starting and product structures are consistent with the experimental structures. In particular, note that the predicted peroxide bond length, *viz.,* 1.494 Å, directly correlates to that calculated for the starting structure (1.497 Å) during the transition state calculations.

Figure 12. Predicted starting material and product structures from IRC calculation.

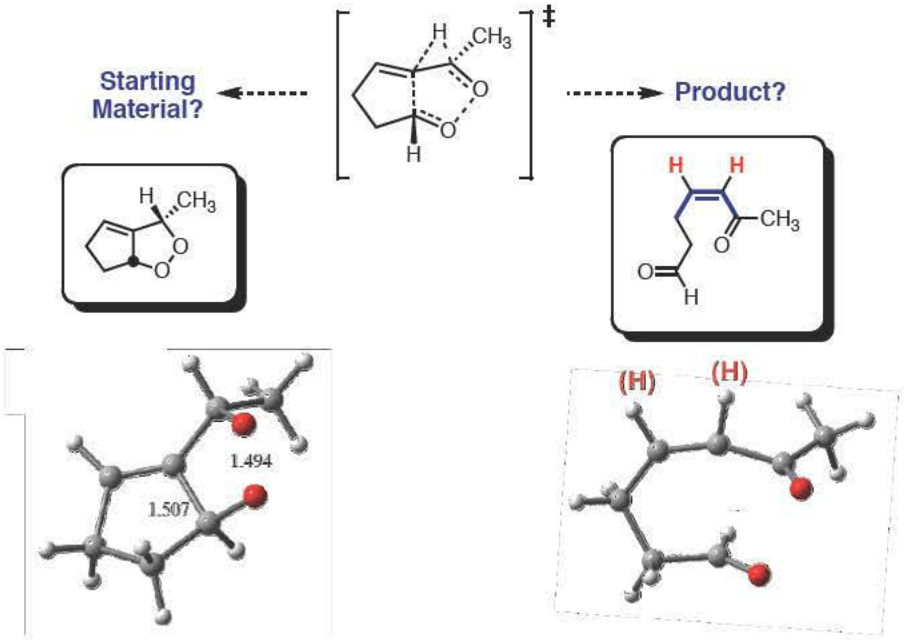

1.4 Conclusion

The importance of the peroxide functionality is apparent by its widespread presence, from biological to industrial applications. As such, the role that seemingly innocuous reaction components have on the decomposition of an otherwise notably stable peroxide bond is significant. When aryl-substituted trimethylenemethane diradical precursors are heated in the presence of molecular oxygen, keto-alcohols like **29** are produced cleanly. The chemical landscape changes dramatically when alkyl-substituted substrates are used. In these instances, a thermally stable [3.3.0] bicyclic peroxide is isolable in addition to the expected keto-alcohol and, interestingly, a *Z*-configured α,β-unsaturated keto-aldehyde. Deuterium labeling

studies were used to facilitate the elucidation of a mechanism for the transformation of the peroxide to the other two products. In the course of these studies, an unanticipated concentration effect was observed: it is only when heated in the presence of an additive, in this case keto-alcohol **38**, that the deuterated peroxide, **39-d$_1$**, is converted to the other two products. Such is not the case for the protio-counterpart, **39**, in which decomposition is unassisted in the absence of, and accelerated in the presence of, **38**. Further inquiry uncovered molecule-assisted homolysis of the peroxide bond via hydrogen-bonding with the keto-alcohol and the existence of a kinetic isotope effect.

Chapter 2

Blushing Fulvenes With a Splash of Radical for Flavor: Insight Into Electrohydrocyclization

2.1 Introduction

2.1.1 The Chemistry of Fulvenes

Thiele synthesized and described the first pentafulvenes in 1900.[49] He examined the condensation of cyclopentadiene with various ketones and aldehydes in the presence of an alkoxide base, e.g. **57-59**. (Scheme 19). Since the pioneering work, several variations have been developed to synthesize substituted fulvenes.[50]

Scheme 19. Original fulvenes synthesized and studied by Thiele.

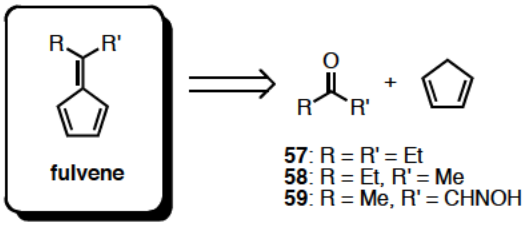

In 1976, Büchi and coworkers employed Freiesleben's procedure, using Et_2NH as a base, to form 6-(4-oxopentyl) fulvene, **60**.[51] This was a useful procedure for the assembly of monosubstituted fulvenes but was not efficient for the formation of fulvenes starting from sterically hindered aldehydes. For example, α-substituted aldehydes, such as isobutyraldehyde, gave diminished yields as compared to those with an unsubstituted α-C (Scheme 20).

Scheme 20. α-Substitution effect on the efficiency of fulvene formation.

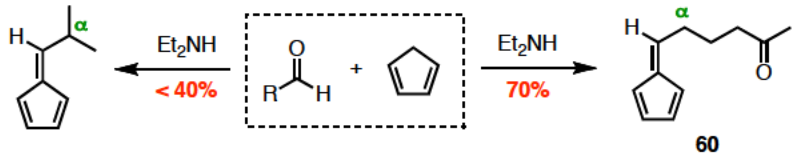

60

A modified procedure using pyrrolidine as a base and nucleophile was subsequently described by Stone and Little.[52] They observed the formation of a transient iminium ion that was intercepted by the cyclopentadienyl anion. In the presence of α,β-unsaturated esters, they found it was necessary to use Et_2NH, a less nucleophilic base, in order to avoid conjugate addition (Table 5). Alternatively, Erden and coworkers determined that the use of alkoxide or hydroxide bases best facilitated the formation of the 6,6-disubstituted fulvenes, e.g. entries 4–6, because they do not readily form the iminium intermediate.[53]

Table 5. Base-dependent formation of fulvenes.

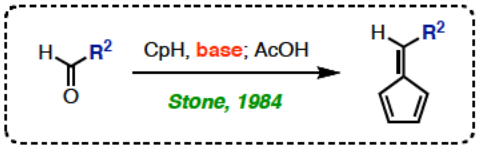

entry	R^2	base	% yield
1	Ph	pyrrolidine	70
		Et_2NH	45
2	*i*-Pr	pyrrolidine	98
		Et_2NH	45
3	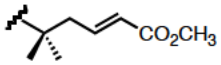	pyrrolidine	–
		Et_2NH	91

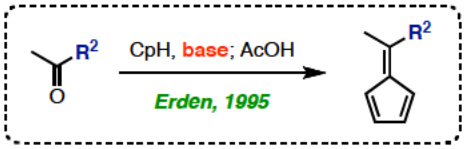

entry	R^2	base	% yield
4		NaOMe	94
5	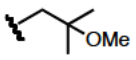	NaOMe	94
		NaOH	43
6	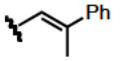	NaOH	67

Fulvene chemistry is interesting for a variety of reasons, not the least of which is associated with its unique reactivity patterns that are characteristic of both aromatic compounds and olefins. In the 1960's, William Little took advantage of the aromatic character of the cyclopentadienyl anion generated *in situ* from fulvenes as a way to make ferrocene complexes, e.g. **61** and **62** (Figure 13).[54] Similar studies designed to access metallocenes from fulvene-type structures have proven to be fruitful. For example, fulvene-derived *ansa*-metallocene catalysts, *viz.*, **63**, when used in conjunction with methylaluminoxane (MAO), provide a dramatic improvement in polymerization efficiency over traditional Ziegler-Natta catalysts.[55] More recently, titanocene complexes derived from fulvenes, such as **64**, have been studied and show promising activity as anti-cancer agents.[56]

Figure 13. Fulvene-derived metallocene complexes.

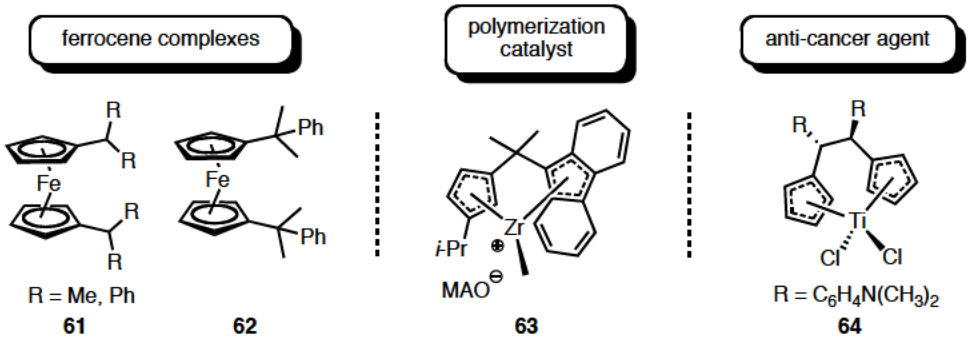

The olefinic nature of fulvenes has also been exploited considerably, in particular as a tool in cycloaddition chemistry.[57] Beginning in the early 1970's, Houk and coworkers carried out extensive studies on the use of fulvenes in [6+4] cycloaddition reactions,[58] thus providing the first examples of fulvenes acting as 6π electron

addends in conjunction with electron-rich 4π addends (Scheme 21). The [6+4] reaction proved useful for a variety of applications, including the synthesis of azulene derivatives such as **65**. Later, Wu demonstrated that the exocyclic olefin of fulvene **66** acts as the dienophile in a [4+2] cycloaddition reaction with a tethered electron rich diene to generate tricyclic structures, *viz.,* **67** (Scheme 22).[59] More recently, Hong and coworkers explored the use of fulvenes in mild [6+2] cycloadditions to generate heterocycles, **68**,[60] and as the dienophile component, *viz.,* **69** and **70**, of Diels-Alder reactions to access densely packed cores of several natural products.[61]

Scheme 21. Pioneering use of fulvenes in cycloaddition chemistry.

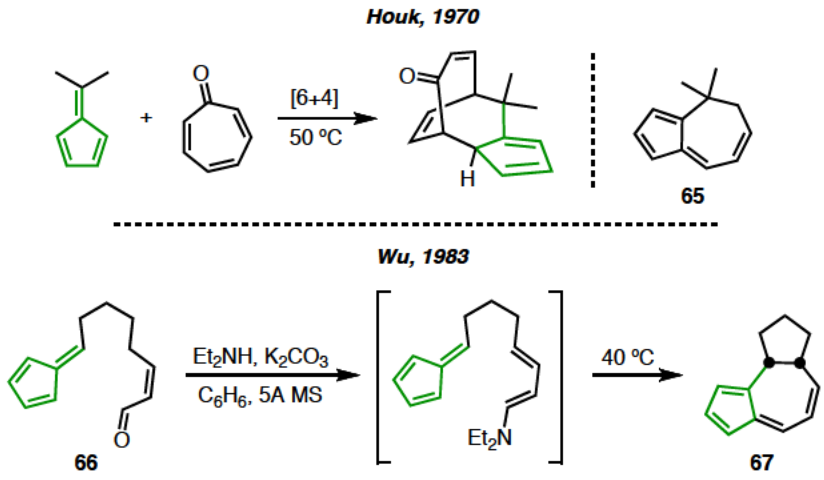

Scheme 22. Recent examples of fulvenes in cycloaddition chemistry.

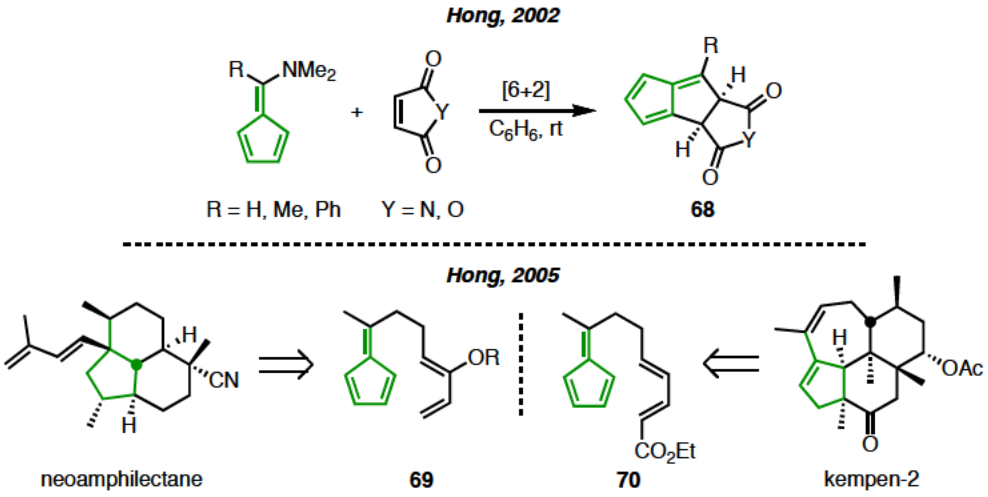

In 1976, Büchi demonstrated the carbonyl-like reactivity of fulvenes when he utilized a fulvene as part of a key intramolecular cyclization reaction in the synthesis of spirovetivane natural products (Scheme 23).[51] Addition of Gilman's reagent to fulvene **60** generated a lithium cyclopentadienide, which subsequently closed onto the pendant carbonyl, selectively forming the spirocyclic backbone of β-vetivone, **71**.

Scheme 23. Reductive cyclization of a fulvene towards the core of β-vetivone.

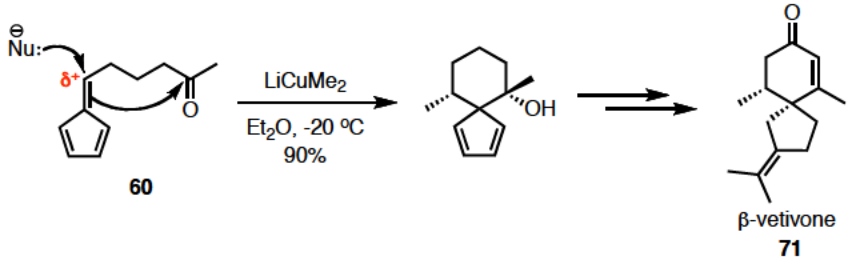

2.1.2 Redox Umpolung

While fulvenes have a rich history,[62] very little is known about the electrochemistry of these compounds.[63] Intrigued by Büchi's application of fulvenes, we were interested in determining whether we could employ electrochemistry to the same end via umpolung, or polarity reversal.[64] In this manner, the introduction of an electron to a fulvene core should convert the exocyclic carbon from having a partial positive character to one possessing nucleophilic character. This technique is not limited to reductions, as a single-electron oxidation of a nucleophilic center will generate a new electrophilic site (Scheme 24).

Scheme 24. Umpolung from single electron transfers.

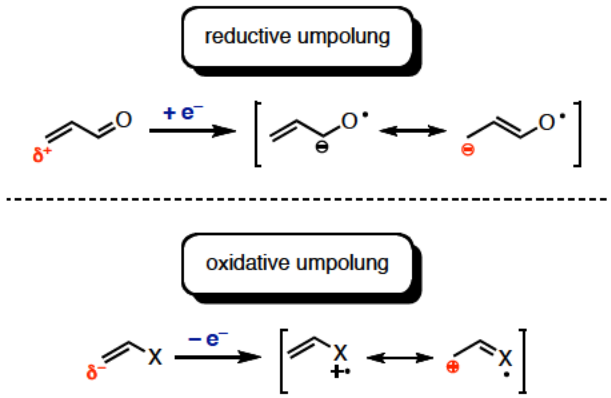

Baizer successfully demonstrated umpolung in the intermolecular electrohydrodimerization reaction used for the Monsanto synthesis of adiponitrile, **72**.[65] This key intermediate in the formation of Nylon 6-6 was generated

electrochemically from the reduction of acrylonitrile and its subsequent dimerization, consuming a total of two electrons and two protons (Scheme 25).

Scheme 25. Synthesis of adiponitrile using electrohydrodimerization.

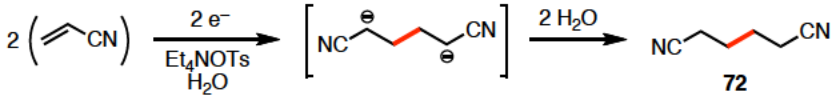

72

Alternatively, *intra*molecular electroreductive cyclization invoves σ-bond formation between two tethered electrophilic carbons, *viz.*, between the β-carbon of an electron deficient alkene and a remotely tethered carbonyl carbon. For example, electroreductive cyclization has been applied to the synthesis of natural products such as quadrone,[66] **73**, and the core framework of the phorbol esters,[67] i.e. **74** (Scheme 26).

Scheme 26. Natural product targets for electroreductive cyclization.

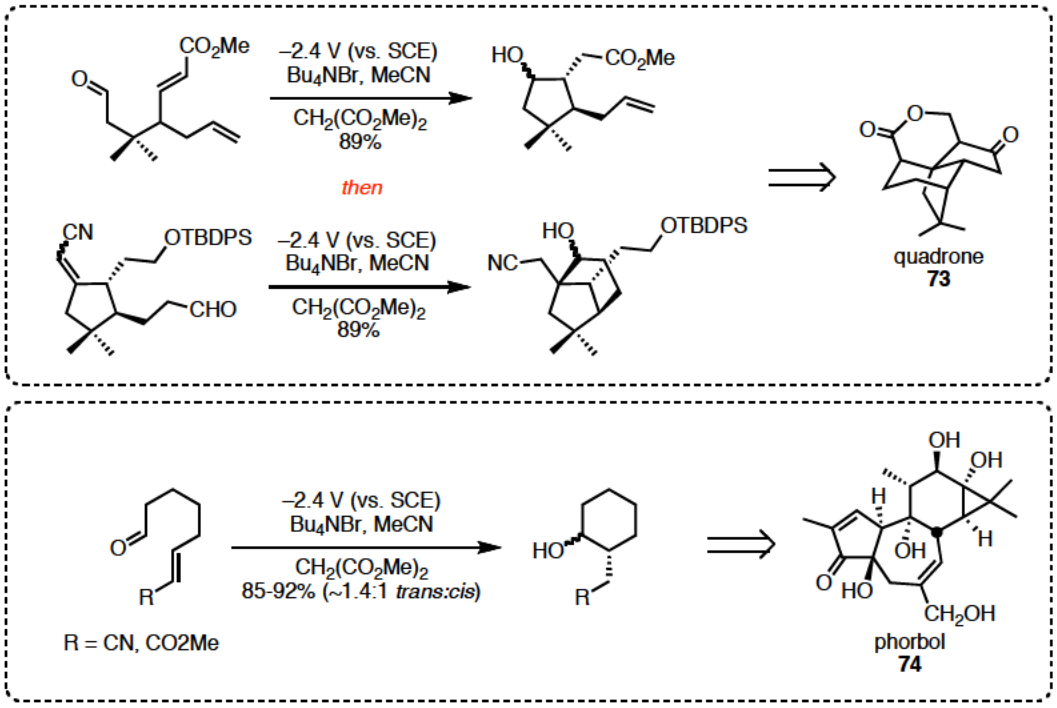

Using linear sweep voltammetry and chemical arguments, Fry, Leonetti, and Little systematically outlined a general mechanism by which electroreductive cyclization reactions can occur.[68] They concluded that five independent steps are involved: heterogeneous electron transfer (e), protonation (p), cyclization (c), homogeneous electron transfer (d), and a second protonation step (p). The rate determining step and the order in which these steps occur are dependent upon the substrates involved. For the electroreductive cyclization reaction of **75**, the sequence proceeded via an e-P-d-c-p pathway, i.e. electron transfer at the electrode "e", a rate determining protonation "P", the addition of a second electron via a homogeneous electron transfer "d", and the addition of the second proton "p" (Scheme 27).

Scheme 27. Mechanism for electroreductive cyclization.

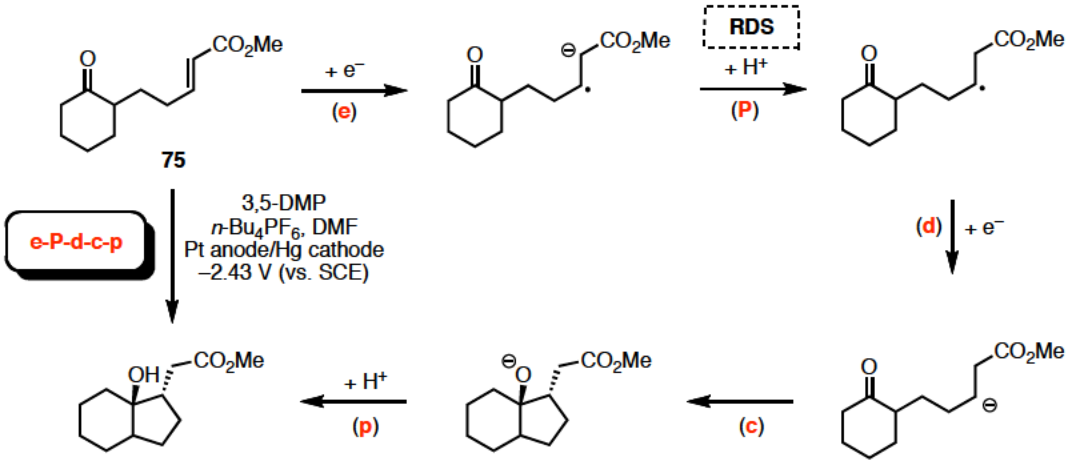

Although single electron donors such as SmI_2,[69] V(II) species,[70] and Zn[71] can induce umpolung and subsequent diastereoselective intramolecular cyclization, the electrochemical method offers the advantage of chemoselectivity between electrophores simply by adusting the applied potential to match that of the chosen electrophore and often requires less rigorous reaction conditions.

2.2 Insight into the Electroreductive Cyclization of Fulvenes

The use of redox umpolung of fulvenes to accomplish intramolecular cyclization has the potential to afford useful and interesting chemistry, especially if selectivity between two electrophores can be acheived. Owing to the facile nature of their synthesis, we elected to investigate a system in which a monosubstituted fulvene, acting as the carbonyl surrogate *cf.* **76**, is tethered to an α,β-unsaturated ester (Figure 14).

Figure 14. Fulvene systems of interest and related subunit reduction potentials.

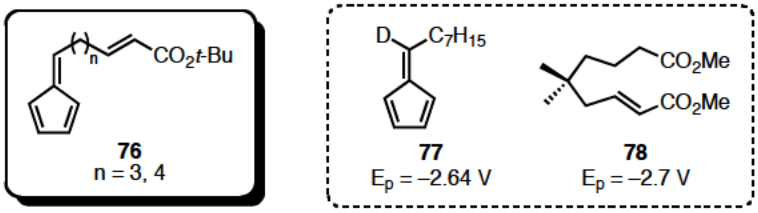

2.2.1 Theoretical Considerations

As previously alluded, one of our initial interests resided in determining if one of the two electrophores present in fulvene **76** could be selectively reduced. And if so, would the resulting radical anion be localized on the fulvene substructure (**79-a**)$^{\bullet-}$, or the unsaturated ester (**79-b**)$^{\bullet-}$ illustrated in Figure 15a? Comparing reduction potentials of an alkyl-substituted fulvene, **77**, to an α,β-unsaturated ester, **78**, *viz.,* –2.64 V and –2.7 V (vs. Ag/0.1 M $AgNO_3$) respectively, the answer is not so clear. While our view is that the fulvene should reduce first, quantum calculations using the UB3LYP method and a 6-31+G(d) basis set were carried out to add credibility to this opinion. The results indicated that spin and charge are unambiguously localized on the fulvene subunit (Figure 15b-d);[72] therefore, it is reasonable to assume that chemistry will originate there and subsequent discussions are based on this assumption.

Figure 15. Calculated (b) spin (c) SOMO and (d) electron density map for the radical anion of fulvene **79** in (a)

(a)

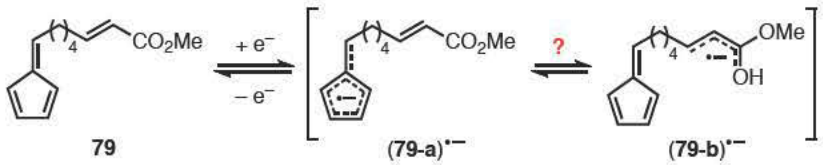

(b)

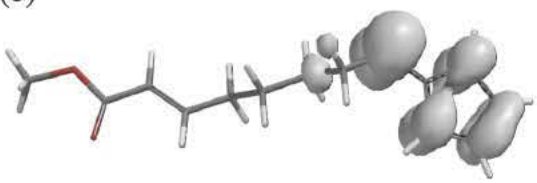

(c)

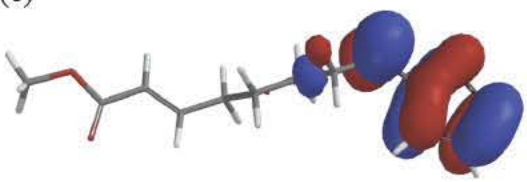

(d)

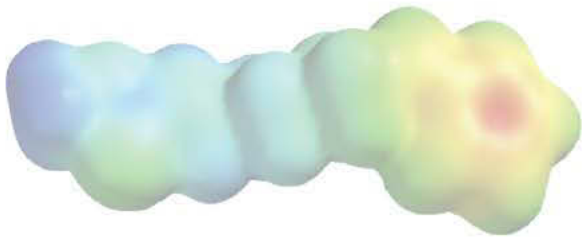

We hypothesized that, after the first electron transfer, two viable routes exist through which the initially formed radical anion could react (Scheme 28). For example, in the presence of a proton donor (path **a**), we envisioned that the initially formed radical anion, **80,** could be protonated to form the cyclopentadienyl radical, **81,** and then a second electron transfer would provide the anion, **82**. We speculated that cyclization onto the pendant unsaturated ester would be the predominant route should this sequence occur. Alternatively, in the absence of a proton donor (path **b**),

we suspected that radical anion dimerization to form the dimeric dianion, **83**, would primarily occur.[73]

Scheme 28. Viable reaction pathways for the reduced substrate.

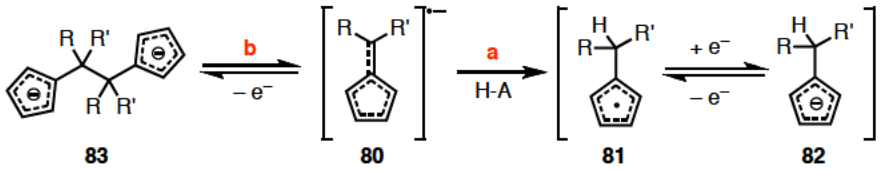

2.2.2 Synthesis of the Substrate

We began our investigation with the synthesis of substrates that possessed either a 3- or 4-C tether separating the fulvene core from an unsaturated *t*-butyl ester (Scheme 29). Oxidative cleavage of diol **84** with PIFA, followed by a Wittig reaction with the pre-formed ylide, **87**, yielded the fulvene precursor, **85**, in 83% yield over two steps.[74] Following the Stone-Little procedure, the fulvene, **86**, was generated using Et_2NH as the nucleophile and base in 88% yield.[52]

Scheme 29. Synthesis of the fulvene substrates.

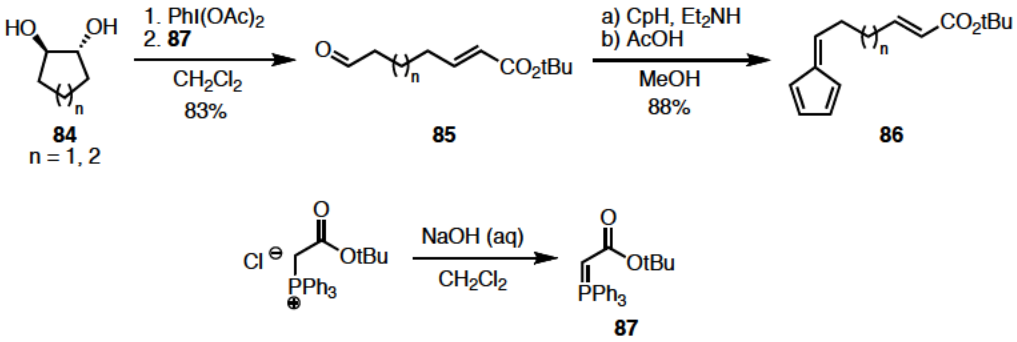

2.3 Voltammetric Studies

Initial cyclic voltammetric studies examined the substrate with a 4-C tether separating the electrophores. All CV experiments were performed using glassy carbon working and platinum counter electrodes, a Ag/0.1 M $AgNO_3$ reference electrode, and *n*-Bu_4NBF_4 (0.1 M in MeCN) as the supporting electrolyte at a scan rate of 100 mV/s.

2.3.1 In the absence of a Proton Donor

The voltammogram for the reduction of fulvene **F** in the absence of a proton donor is illustrated in Figure 16. Two irreversible peaks are observed, one at –2.65 V and a smaller peak at ca., –0.65 V. Consistent with the reduction peak observed for an alkyl substituted fulvene, **77**, at –2.64 V under the same conditions, the more negative of the two is attributed to the formation of the fulvene radical anion, $\mathbf{F}^{\bullet-}$.

Figure 16. CV of 4-C tether substrate in the absence of a proton donor.

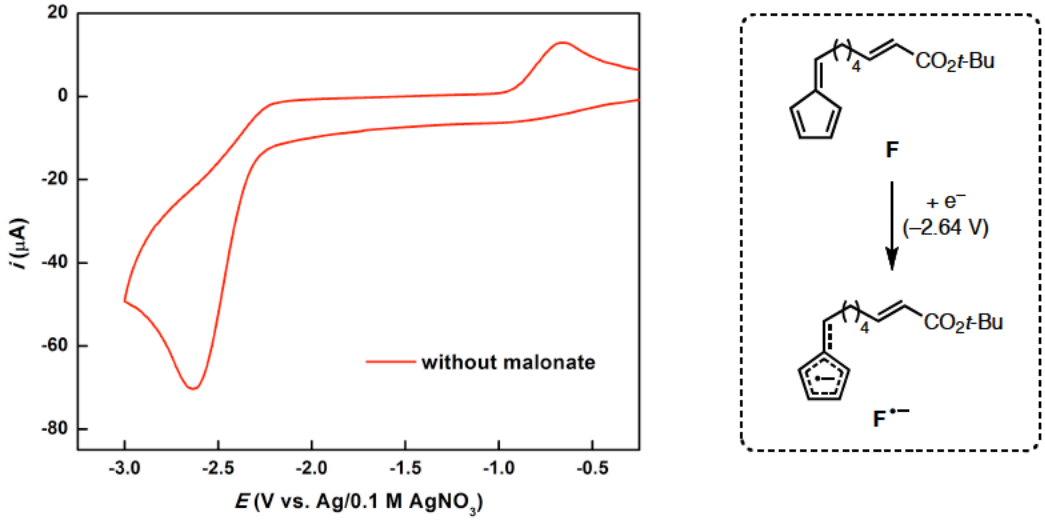

Without the intervention of a proton donor, what becomes of the initially formed radical anion? To answer this, one must consider the environment at the electrode surface, in particular the existence of an ~1 mm "double layer." In 1924 Stern introduced the idea of an electrochemical double layer by combining the earlier theories of Helmholtz[75] and Gouy,[76] describing a compact layer, d_1, directly adjacent to the electrode surface and a diffuse layer, d_2, between the compact layer and the bulk solution (Figure 17).[77] Within the compact layer, a highly ordered arrangement of counter ions balances the excess charge present on the electrode. The radius of the solvated counter ion, denoted as the Outer Helmholtz Plane (OHP), determines the thickness of d_1. As the distance from the electrode increases, the electric field decreases, therefore allowing a more diffuse ordering of ion pairs until at a certain distance, complete interspersion, i.e. the bulk solution, is reached. The chemistry that can occur in the double layer depends on the rate of diffusion of the substrate into the bulk solution. Interestingly, this suggests that temperature might be used to achieve differential product formation. If, for example, the temperature is increased, will the radical ions formed at the electrode gain enough thermal energy to diffuse more efficiently/rapidly to the bulk solution? If so, then differing chemistries might be anticipated.

Figure 17. Schematic of the "double layer" at a cathode.

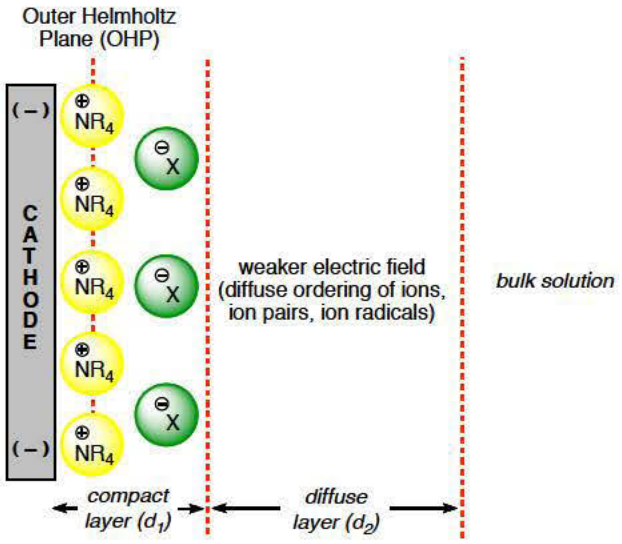

Could this phenomenon be, at least in part, responsible for the appearance of the peak at –0.65 V (note Figure 16)? Suppose that upon reduction of fulvene, **F**, slow diffusion of $\mathbf{F}^{\bullet-}$ to the bulk solution allows elevated concentrations to exist within the double layer. If so, then it is not unreasonable to intimate that dimerization of two fulvene radical anions $\mathbf{F}^{\bullet-}$ could afford a dimeric dianion, designated as $(\mathbf{F–F})^{2-}$ (Scheme 30). In the absence of an alternative reaction pathway, we suggest that the dimeric dianion builds up in solution, allowing sufficient time for oxidation of one of the cyclopentadienyl anions during the reverse scan. Thus, oxidation to form a dimeric radical anion, $\mathbf{(F–F)}^{\bullet-}$, may be responsible for appearance of the peak at –0.65 V. Bordwell and coworkers demonstrated that oxidation of cyclopentadienyl anion occurs at –0.62 V when recorded in DMSO (vs. Ag/0.1 M $AgNO_3$), lending credibility to our theory on the origin of this peak.[78]

Scheme 30. Fate of the reduced fulvene in the absence of a proton donor.

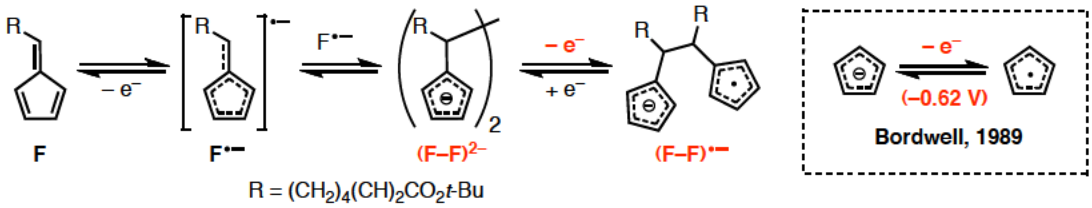

2.3.2 Addition of a Proton Donor

Two significant changes are observed when diethyl malonate is added to serve as a proton donor (H–A), namely, the small peak disappears and the larger peak is shifted anodically by > 100 mV (Figure 18). The proton donor presumably intercepts the fulvene radical anion $\mathbf{F}^{\bullet-}$ to shift the equilibrium between the radical anion and dianion, $\mathbf{(F–F)}^{2-}$, toward the protonated cyclopentadienyl framework $\mathbf{(F–H)}^{\bullet}$. If the protonation event is significantly fast such that the dimer dianion does not form, then the oxidation peak should disappear, as observed. This suggestion is also consistent with the > 100 mV anodic shift, reflecting the existence of one or more post equilibrium steps that drains radical anion, $\mathbf{F}^{\bullet-}$, from the redox couple leading to a Nernstian shift in the observed peak potential (Scheme 31).

Figure 18. Voltammogram of **F** before and after the addition of a proton donor.

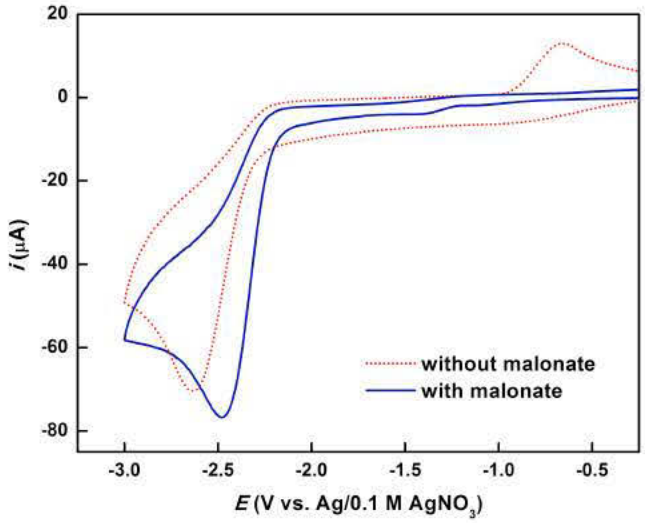

Scheme 31. Origin of the anodic potential shift in the presence of a proton donor.

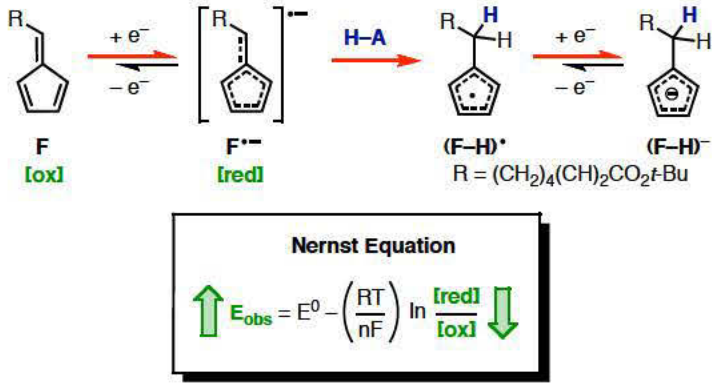

This is not without precedent. Little and Baizer demonstrated that the ester-aldehyde, **89**, was easier to reduce than either of the model structures, **90** and **91**, each of which possesses one of the two electrophores found in **89**. This implies a fast follow-up reation of the radical anion formed via the reduction of **89**, i.e. cyclization (Figure 19).[79]

Figure 19. Nernstian shift in reduction potential observed for substrate **89**.

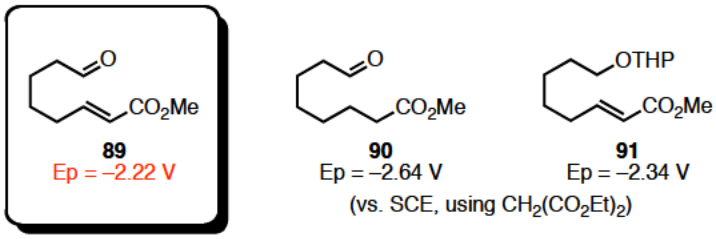

More relevant to our interest in the effect of tether-length was a case provided by Moeller and coworkers in which the oxidation potential of the substrate directly correlated with the ring size formed in the product (Figure 20).[80] This is not surprising if one applies the steady state approximation to the Nernst equation, as illustrated in equations (1) – (4). Given that the observed oxidation potential, E_{obs}, is proportional to the rate of cyclization, k_c, as the rate increases with decreasing ring size, following the trend $k_7 < k_6 \sim k_5$, the observed potential will undergo a positive shift.

Figure 20. Dependence of E_{obs} on the rates of cyclization.

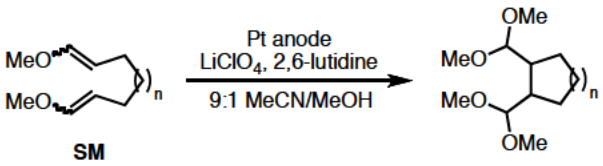

n	ring size	$E_{obs/2}$ (V)
1	5	+1.20
2	6	+1.30
3	7	+1.40

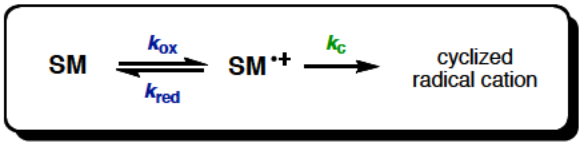

applying the steady-state approximation:

$$\frac{d[SM^{\bullet+}]}{dt} = 0 = k_{ox}[SM] - k_{red}[SM^{\bullet+}] - k_c[SM^{\bullet+}] \qquad (1)$$

if:

$$E_{obs} = E^0 - \left(\frac{RT}{nF}\right) \ln \frac{[SM]}{[SM^{\bullet+}]} \quad \textit{and} \quad [SM^{\bullet+}] = \frac{k_{ox}[SM]}{(k_{red}+k_c)} \qquad (2) \text{ and } (3)$$

then:

$$E_{obs} = E^0 + \left(\frac{RT}{nF}\right) \ln \frac{(k_{red}+k_c)}{k_{ox}} \qquad (4)$$

Two reasonable post-equilibrium reaction pathways are considered for the fulvene chemistry in the presence of a proton donor. The first possibility, portrayed in Scheme 32, involves a 6-exo-trig cyclization of the initially formed radical anion ($\mathbf{F}^{\bullet-}$) onto the unsaturated ester, followed by protonation of the resulting enolate. The subsequent addition of a second electron and a second proton would lead to what we term a "co-joined" structure, **92**. Analogous to the formalism presented earlier, the latter sequence can be described as one that follows an e-c-p-d-p mechanism.[68] The cyclization event could also occur after an initial protonation step, or by an e-p-c-d-p mechanism.

Scheme 32. One possible follow-up reaction leading to a co-joined structure.

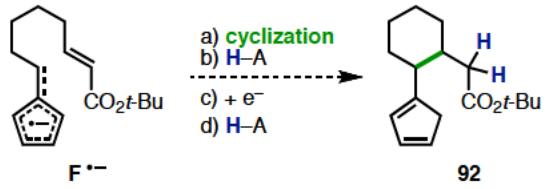

Alternatively, one can imagine that protonation of the radical anion on the exocyclic carbon of the fulvene framework to deliver structure **(F–H)**$^{\bullet}$ can be followed by a second electron transfer to generate **(F–H)**$^{-}$. Several options are available to the protonated anion, **(F–H)**$^{-}$. As shown in Scheme 33, it could undergo oxidation to afford the corresponding cyclopentadienyl radical, **(F–H)**$^{\bullet}$, or the pendant unsaturated ester could be reduced to form the doubly reduced species, **93**. By far the more interesting fate would be intramolecular cyclization. For example, cyclization between carbons C_a and C_β and subsequent protonation would deliver the spirocyclic structure, **94**. Alternatively, cyclization between C_b and C_β followed by protonation would afford a fused adduct, **95**.

Scheme 33. Possible reaction pathways of $(\mathbf{F–H})^{-}$.

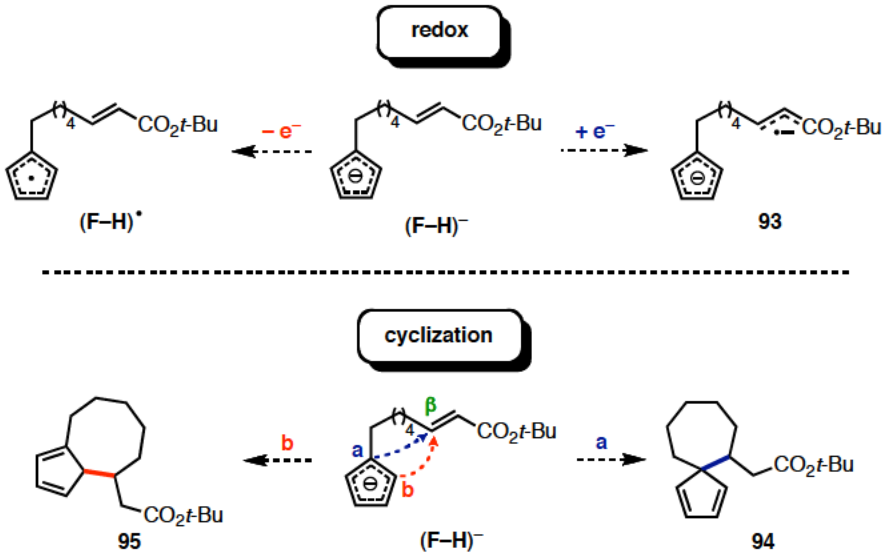

We believe that insight concerning the fate of $(\mathbf{F–H})^{-}$ is apparent from an examination of the voltammetric information portrayed in Figure 21a. Here, one finds the superposition of three voltammograms, recorded sequentially (1st scan shown in red, 3rd scan in blue, and 7th scan in green). Of particular interest is the appearance of two new peaks, one at ca. –2.8 V, the other at –1.5 V. Given that the previously published peak potential for reduction of the α,β-unsaturated ester **78** is ca. –2.7 V vs $Ag/AgNO_3$,[81] we speculate that the peak at –2.8 V may be due to reduction of the pendant unsaturated ester found in $(\mathbf{F–H})^{-}$, to produce the previously mentioned radical dianion, **93**.

Figure 21. (a) Voltammogram after 1, 3, and 7 scans and (b) the potential origin of the irreversible peak at ca. –2.8 V.

(a)

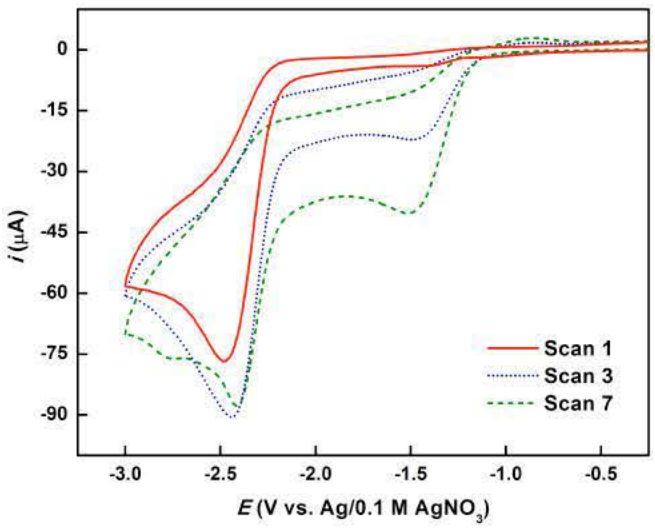

(b)

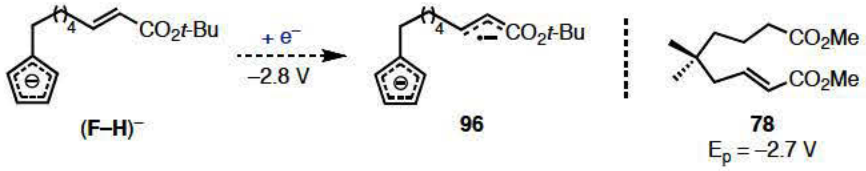

The more interesting peak is the one appearing at ca. –1.5 V. What species is responsible for its appearance? We suggest that it may correspond to reduction of the cyclopentadienyl radical $(\mathbf{F–H})^{\bullet}$ to establish an equilibrium between it and $(\mathbf{F–H})^{-}$, as illustrated in Scheme 34. This theory is consistent with the work of Sitzmann and coworkers, who reported that a sterically "protected" cyclopentadienyl radical reduces to the anion at –1.54 V (vs $Ag/AgNO_3$).[82]

Scheme 34. Potential origin of the reduction peak at ca. –1.54 V.

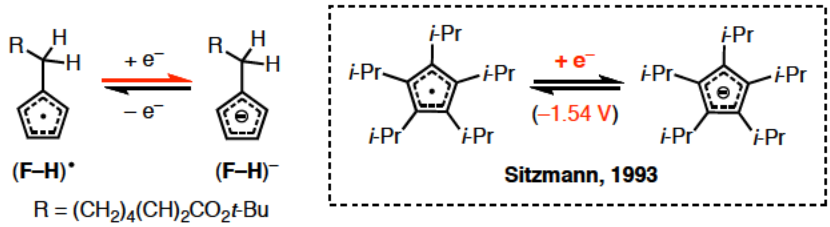

Why does the peak at ca. –1.5 V build over time? To address this query, suppose that there is a reason for the protonated fulvene-derived anion $(\mathbf{F–H})^-$ to accumulate. It would then shuttle forth-and-back in equilibrium with its radical precursor to create a temporary bottleneck until either of the species reacted and the equilibrium could be drained (note Scheme 34). This begs the question, *why* should $(\mathbf{F–H})^-$ accumulate? We believe the reason is simple since both of the cyclization pathways, one leading from structure $(\mathbf{F–H})^-$ to a seven-membered spirocyclic framework, **94**, the other to an eight membered ring in a fused frame, **95**, should be slow.

If this rationale is accurate, then one would anticipate that little-to-no accumulation would be observed if the length of the tether connecting the fulvene core to the pendant unsaturated ester was adjusted so that cyclization occurred more rapidly. Such proved to be the case when the number of intervening methylene units was reduced from four to three. In this case, spirocyclization would lead to a 6-membered ring, and should be significantly faster than alternative cyclization pathways. The resulting voltammogram is illustrated in Figure 22. Consistent with our hypothesis is the complete absence of a new species being formed during repetitive scans. Also of interest is the fact that the peak potential for the initial

wave is shifted by roughly another 100 mV to a still more positive value (note Figure 23), an outcome that is consistent with an increase in the rate of the cyclization step.

Figure 22. Absence of new species being formed during repetitive scans of the 3-C tether substrate.

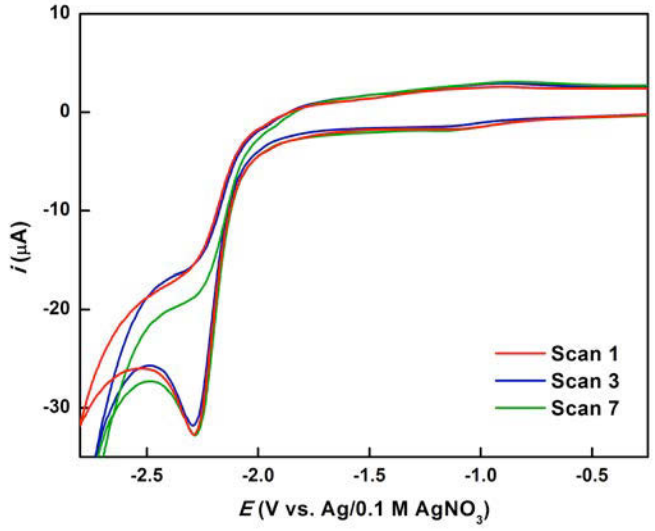

Figure 23. A Nernstian shift in the reduction potential observed for the 3-C tether substrate in the presence of a proton donor.

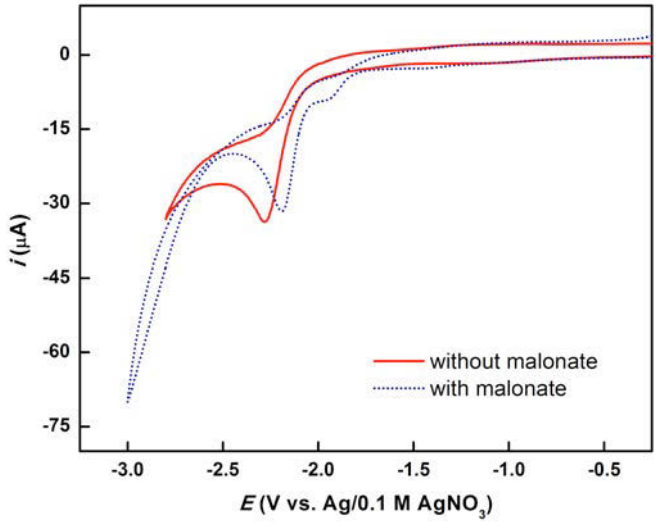

2.4 Bulk Electrolysis

Intrigued by the results of the voltammetric studies, we were keenly interested in determining the products that would be derived from the bulk electrolysis of both the 3- and 4-C tether substrates. We began by tailoring the experimental conditions to maximize the formation of cyclized products. Thus, preparative scale experiments were carried out with a dilute solution of fulvene (5 mM in MeCN) in a divided cell in the presence of two equivalents of a proton donor, in this case, 3,5-dimethylphenol. Graphite rods were used for the working and counter electrodes, and a Ag/0.1 M $AgNO_3$ for the reference electrode. Due to its hygroscopic nature, we elected to use Et_4NOTs (0.1 M) as the supporting electrolyte in place of the Bu_4NBF_4 because it could be easily removed during an aqueous work-up.

2.4.1 The "4-C Tether" Substrate

Controlled potential electrolysis of **F**, the substrate with a 4-C tether, was accomplished at the reduction potential of the fulvene obtained in the CV studies, *viz.,* –2.7 V (vs. Ag/0.1 M $AgNO_3$; note Figure 18). Following an aqueous work-up and isolation by prep-TLC, exhaustive purification by HPLC still afforded a complex mixture of products. Unfortunately, due to the extensive manipulation that was needed for the purification process, an accurate yield of each type of product has not been possible; however the mass recovery is good, viz., 87%. The HPLC trace for the electrolysis performed at room temperature provided two peaks in a 75 : 25 ratio (red line, Figure 29a). While spectroscopic characterization of the HPLC

fractions proved to be an arduous task due to the presence of double bond and stereoisomers, the nature of the products within each peak was examined using ^{1}H NMR. As described below, the first, and major, peak was attributed to cyclized products and the minor peak to a dimer/cyclized product mixture.

It was evident that more than one product was isolated in the fraction from the major peak in the HPLC trace (Figure 29a), therefore a 2D COSY spectrum was crucial for differentiating product structures. Three major signals exist in the vinyl region from 5.95 – 6.45 ppm, labeled as A–C in the ^{1}H NMR spectrum (Figure 24). If one considers the correlation signals between these protons in the COSY spectrum, it is evident that H_A couples to H_B, which in turn is coupled to H_C (Figure 25). While this could be consistent with the "fused" structure, such as **95** illustrated in Figure 25, two contradictions arise when one examines the signals corresponding to the doubly allylic protons at 2.9 ppm, labeled D/D'.[83] First, it can be seen from the COSY NMR spectrum that these diastereotopic protons couple exclusively with the signal attributed to H_C. If the product structure were consistent with **95**, the allylic proton, H_5, would show a correlation not only to the vinyl proton, H_C, but also to a neighboring alkyl proton, H_6. This is not the case. In addition, the second order splitting pattern for H_C should be less complex if it coupled solely with H_B and H_5 in the fused structure, **95**. Thus, it was postulated that the dominant cyclized product possessed the co-joined structure with the double bond configuration as indicated in structure **92**.

Figure 24. Paritial ^{1}H NMR spectrum of the co-joined product, **92**.

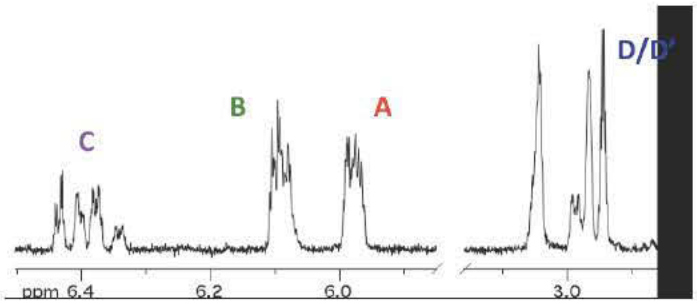

Figure 25. COSY spectrum (zoomed to the region of interest) for the product mixture isolated from the major peak in the HPLC trace.

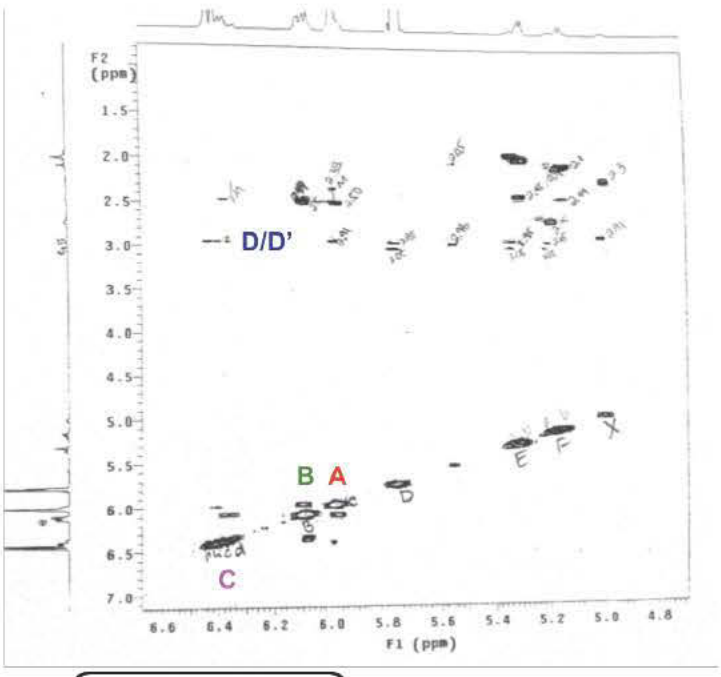

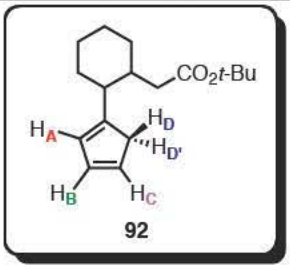

92

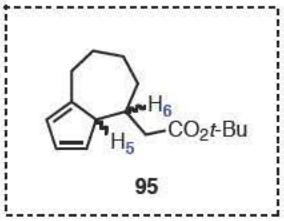

95

The transition states corresponding to the formation of each of the three products were determined, in a vacuum and as a single point calculation in acetonitrile, at the 6-31+G(d) level using the B3LYP method (Figure 26). The spirocyclic product had the highest activation barrier (35.1 kcal/mol in MeCN) relative to the fulvene structure **F-Me**. This is not completely unexpected as the transition structure revealed a loss in planarity of, and therefore an unfavorable loss of delocalization in, the cyclopentadienyl anion. While the fused product had a lower activation barrier (19.3 kcal/mol), the co-joined product provided the most favorable transition state, lying only 2.7 kcal/mol above the starting fulvene. Do the theoretical calculations agree with the experimental results? At least qualitatively, the answer is yes.

Figure 26. Calculated transition structure and corresponding energies for (a) spirocyclic, (b) fused, and (c) co-joined products starting from fulvene **F-Me**.

(a)

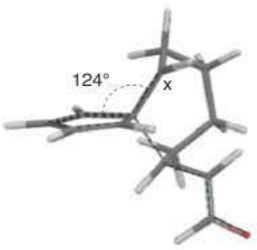

(b)

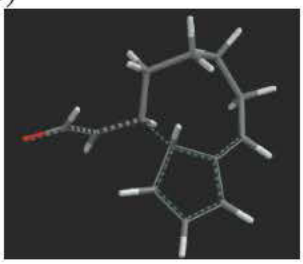

(c)

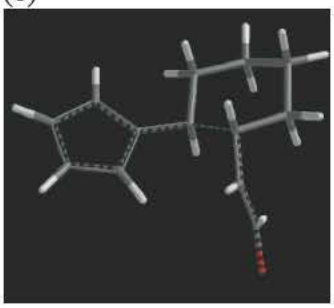

	$\Delta E^{\ddagger}$ (kcal/mol)	
	vacuum	MeCN
spirocyclic	37.5	35.1
fused	25.2	19.3
co-joined	3.4	2.7

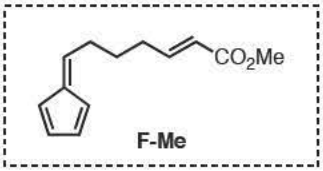

Dimers were easily identified by examining the aromatic region of the ^{1}H NMR spectrum. Interestingly, a single type of dimeric structure resulting from C–C bond formation at the C_6 position of the fulvene was observed, as evidenced by the presence of the α and β vinyl protons in the region of 5.65 and 6.8 ppm (Figure 27). Furthermore, the splitting patterns for the vinyl protons belonging to the fulvene subunit, labeled H_A and H_B in Scheme 6, were not conserved from the starting material ^{1}H NMR spectrum (i.e. they were absent in the spectrum of the dimer) and the exocyclic vinyl proton signal disappeared.

Figure 27. Vinyl region in the ^{1}H NMR for the dimerization product.

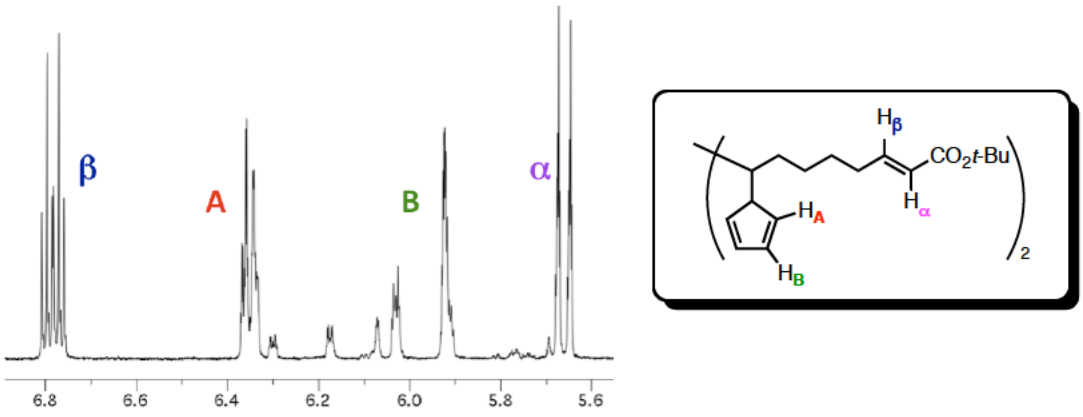

A 2D COSY NMR spectrum was helpful for elucidating the structure of the dimer. For example, the appearance of a new signal at 2.9 ppm, labeled D in Figure 28, shows a correlation signal for both H_A and H_B, and is attributed to the C_5 methine proton on the dimer. In addition, the peak at 2.2 ppm, showing a strong correlation to the H_β signal and a weak correlation to the H_α signal, is assigned to the allylic

protons, H_E. The combined results of the NMR experiments provide evidence in support of the conjecture made previously that the reduction, and subsequent reactions, occur preferentially at the fulvene subunit.

Figure 28. COSY spectrum (zoomed to the region of interest) for dimer/cyclized product mixture.

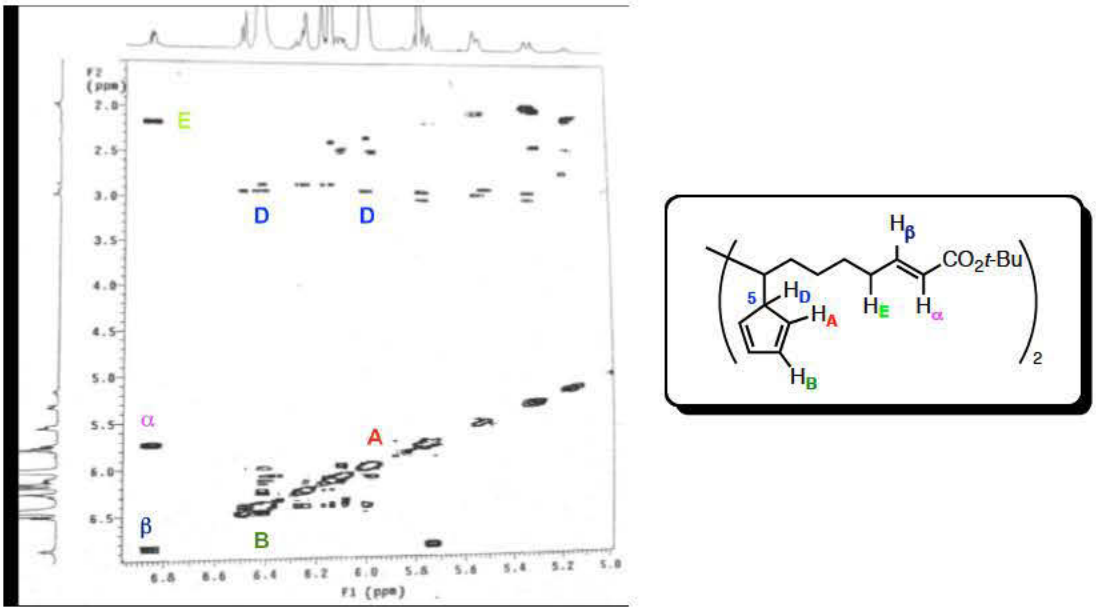

2.4.2 A Temperature Effect

We were curious to determine whether the product distribution could be directed to favor dimer formation. Recall the diffusion rate-dependence of chemistry that occurs within the "double layer" (vida supra). Could one take advantage of the kinetics surrounding the rate of diffusion from the double layer to the bulk solution by decreasing the reaction temperature, and thus "trapping" the initially formed

radical anion in the highly concentrated layer near the cathode? A subsequent reaction was performed at 0 ºC to test this hypothesis. The resultant HPLC trace was insightful from two perspectives. First, and much to our delight, an inverted ratio of cyclized products to dimer, *viz.,* 38 : 62, respectively, indicated that there was in fact a temperature-dependence on product distribution (Figure 29a). Second, a shoulder on the dimer peak became increasingly visible at the lower reaction temperature (blue line, Figure 29a).

Figure 29. (a) HPLC trace for product mixture from bulk electrolysis at 0 ºC (blue line) and 25 ºC (red line); (b) Racemic vs. *meso* dimeric isomers.

(a)

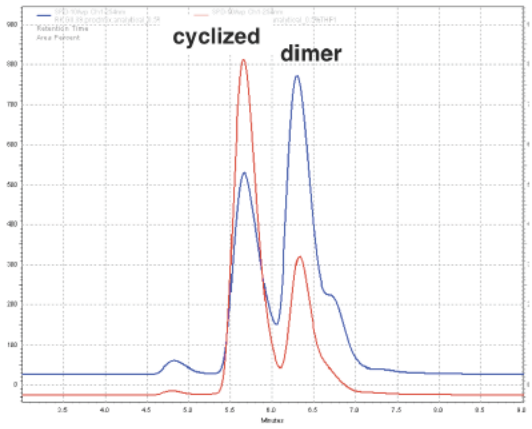

(b)

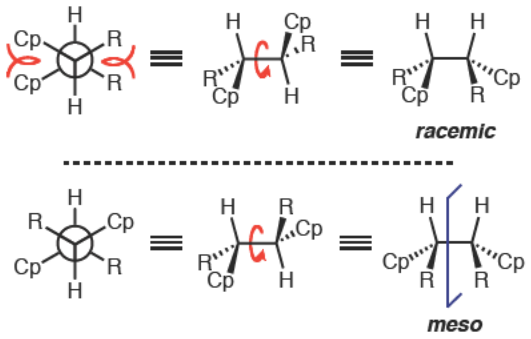

We suspected that its origin was the result of the formation of both *meso* and racemic dimeric structures, an event that only became prominent in the HPLC trace when a significant concentration of dimeric products existed. We rationalized that the *meso* dimer should be favored in order to minimize energy raising gauche interactions between the bulky cyclopentadienyl and acyclic units, and thus this form should

constitute the major peak (Figure 29b). If such a dramatic effect could be observed for a reduced reaction temperature, we wondered if this could also be applied to the reverse, that is, if the temperature was raised. Unfortunately, increasing the reaction temperature to 35 ºC did not have a proportionate effect on the product distribution, resulting in only a slight increase from a 75 : 25 to an 87 : 13 cyclized/dimer ratio.

2.4.3 The "3-C Tether" Substrate

What happens to the preparative chemistry when the tether length is decreased from four to three? A Nernstian shift in reduction potential was previously described during the CV studies of fulvene **76** (n = 3, note Figure 22), suggesting the existence of an efficient follow-up reaction, but is this reflected in the product distribution resulting from a bulk electrolysis? Preliminary results indicate that the chemistry is much cleaner for the substrate possessing a 3-C tether than for electrolysis of the 4-C tether substrate under identical conditions. At room temperature, for example, it appears by ^{1}H NMR that a single cyclized product consistent with the co-joined structure is formed with minimal dimeric side-products. Further spectroscopic characterization, *viz.,* 2D NMRs, as well as additional experiments regarding the temperature dependence, i.e. reactions carried out at 0 ºC and 35 ºC, are needed before direct correlations to the 4-C tether case can be made.

2.5 Conclusion

With the versatility of fulvenes being vast,[84] we endeavored to add to their repetoire by investigating one interesting aspect of their electrochemical behavior.

In particular, the elecroreductive cyclization of a fulvene tethered by either three or four methylene units to an α,β-unsaturated ester was explored. Ultimately, product formation could be directed via temperature control and concentration effects toward dimerization, or toward cyclization through a variation of the length of the tether joining the fulvene core to the second electrophore.

Chapter 3

Mediator Modified Electrodes for Use in Heterogeneous Catalysis

3.1 Introduction

3.1.1 Modified Electrodes

Electrochemistry has demonstrated its versatility across many disciplines, but the electrode surface is often underappreciated, particularly by practitioners of organic synthesis, as a powerful tool for tailoring electrochemical processes. In 1973, Lane and Hubbard were the first to report irreversible adsorption of organic molecules to a metal electrode surface.[85] Benefiting from the strong affinity of olefins for platinum, various olefin-containing quinones were chemisorbed to the electrode surface by soaking a platinum electrode in a solution containing the desired organic compound. Surface coverage experiments determined that the irreversible attachment resulted from π-bonds being replaced with Pt–C σ-bonds. Later, Murray and coworkers coined the term "chemically modified electrode" to describe a SnO_2 electrode surface functionalized with silanes tethered to a terminal amine, which effectively provided a platform for immobilizing Ru^{II} complexes to the surface.[86] In the ensuing decades, electrochemists have taken advantage of the ability to modify electrode surfaces with small molecules, polymers, and metals, turning "heterogeneous, unpredictive surfaces into chemically predictive ones."[86,87]

Since the pioneering work in the mid-1970's, numerous covalent attachment methods have been developed for immobilizing reagents onto electrode surfaces, including silanization of surface hydroxyls of metal oxides[88] and diazotization of carbon surfaces.[89] Alternatively, the most common non-covalent mode of

attachment is adsorption (Figure 30). For example, chemisorption, an adsorption technique that requires direct contact between an adsorbed molecule and the surface, deposits a monolayer of the substrate on the surface. Anson and coworkers provided one of the earliest examples, one where aromatic compounds were adsorbed to carbon electrodes via shared π-electron density.[90] Although many chemisorption methods do not offer fully irreversible attachment because of the occurrence of gradual leaching of the adsorbed molecule into the surrounding solution, recent advances in derivatizing gold surfaces with thiols seems to circumvent this issue.[91] In 1987, Facci described the Langmuir-Blodgett method to coat electrode surfaces in multilayer films. This adsorption technique takes advantage of the self-assembly properties of amphiphilic molecules, i.e. ones containing a redox active hydrophilic "head" group and a hydrophobic "tail," to generate highly ordered monolayers.[92] Polymer films, which were independently introduced by Miller[93] and Bard[94] in 1978, are arguably the most versatile multilayer adsorption method used. Redox active polymeric coatings can be generated from either a pre-formed polymer or by *in situ* polymerization of a monomer. Pre-formed polymers offer the advantage of being isolable materials, and therefore traditional purification and characterization techniques can be used before film deposition by spin casting, droplet evaporation or adsorption from solution.[88] However, it can be difficult to control the amount of polymer actually adsorbed on the electrode. *In situ* electrodeposition of the polymer film using cyclic voltammetry allows control over film thickness simply by varying the number of scans.

Figure 30. Methods of attachment for electrode modification.

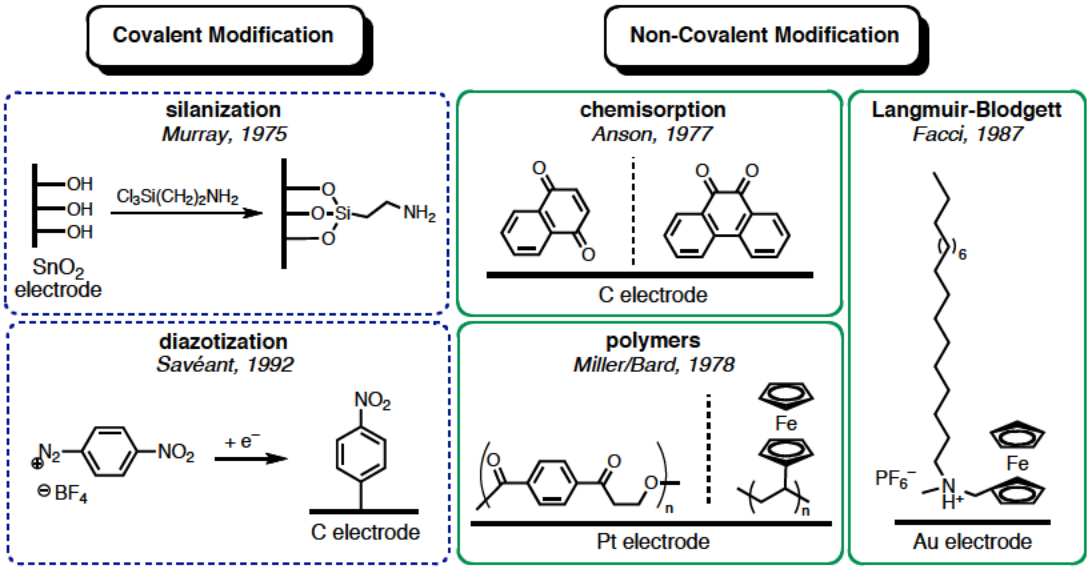

Polymer modified electrodes gained popularity relative to their monolayer counterparts because they were inherently easier to synthesize, exhibited increased stability during electrochemical cycling, demonstrated resistance to leaching into the surrounding solution, and offered greater diversity in the types of compounds that could be immobilized to the electrode surface.[95] The polymeric films used to modify electrodes can be grouped into three general categories. "Redox polymers" integrate redox-active molecules, such as ferrocene, into a non-redox active polymeric backbone, thus generating a localized charged site upon oxidation or reduction. "Ion exchange/coordination polymers" are also not redox active, but play host to redox active compounds through, for example, coordination of a metal to a polymer-bound ligand[96] or incorporation of an electroactive counterion as in the case of du Pont's Nafion® films.[97] The third category, "electroactive polymers," are inherently redox

active due to the presence of highly conjugated groups through which extensive charge delocalization can occur, resulting in conductive properties akin to metals. Commonly used electroactive polymers are polypyrrole, polyaniline, and polyacetylene. Thiophene-based polymers will form the focus of the discussions to follow.

3.1.2 Mediated Electrochemistry

The chemistry community is placing an overwhelming emphasis on developing methods that are considered environmentally sustainable. Indirect electrolysis using mediators offers the advantage of being able to use milder reaction conditions for electron transfer processes by requiring lower potentials and therefore a decrease in total energy consumption. In a typical electrochemical reaction, the substrate undergoes a direct oxidation or reduction at the electrode to generate the corresponding radical ion. Alternatively, indirect electrolysis of a substrate in the presence of a mediator involves two steps: heterogeneous electron transfer to oxidize/reduce the mediator and a subsequent homogeneous electron transfer from the mediator to the substrate, concurrently regenerating the neutral mediator (Figure 31). One consequence of the catalytic turnover of the mediator is an amplification of the current response, referred to as "catalytic current," due to the simultaneous presence of multiple ionic species near the electrode.

Figure 31. Mediated electron transfer.

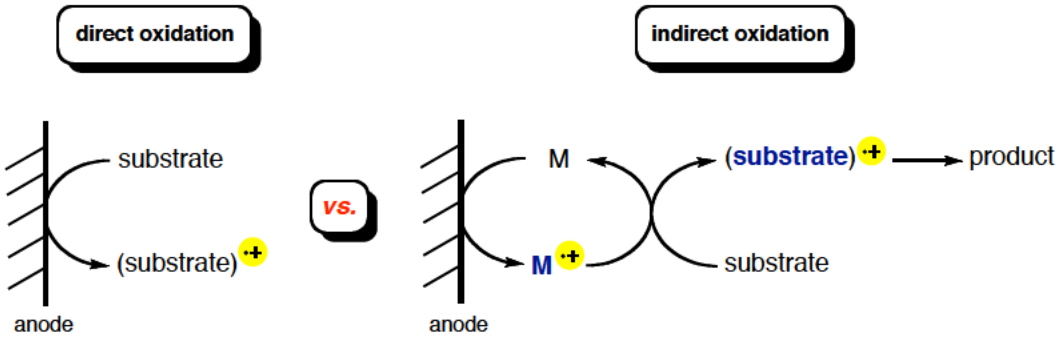

Electrocatalysis in this manner acts to accelerate the effective heterogeneous electron transfer rate of a substrate, which would otherwise be prohibitively slow at the same potential. What allows these processes to occur at the formal potential of the mediator? Consider equations 1 – 3 in Figure 32, which represent an indirect electron transfer process between a mediator (E_p^{ox} = +0.9 V) and a substrate that directly oxidizes at +1.4 V. In the case of a simple homogeneous electron transfer, follow-up reactions provide the kinetic drive for the electron transfer process. If the potential difference for the redox couple shown in equation 2 of Figure 32 is ca. < 500 mV,[111b] then the existence of a fast irreversible follow-up reaction (rate constant, *k*, in equation 3) can drain the unfavorable electron transfer equilibrium, redering the electron transfer feasible.

Figure 32. "Rule of thumb" for indirect electron transfer.

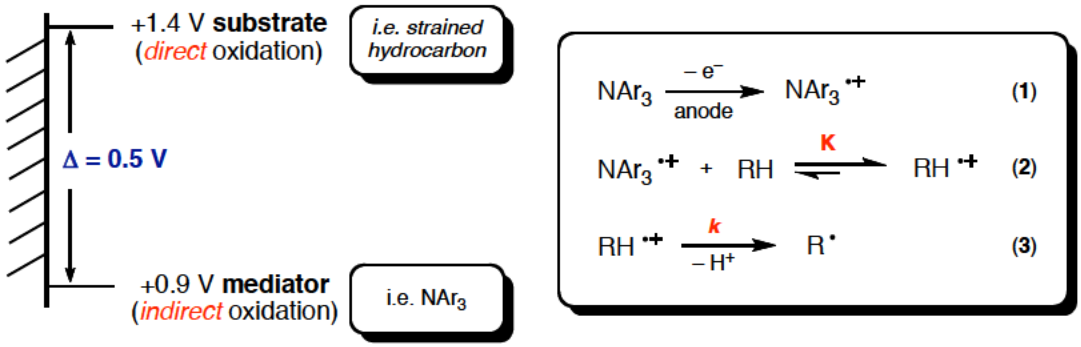

In addition to a thermodynamically favorable redox couple, the ideal mediator should satisfy other conditions.[98] For example, the charged mediator should be stable to both the solvent/electrolyte system and the substrates or additives in solution so as to avoid side reactions, which would rapidly decrease the catalytic efficiency. Furthermore, heterogenous electron transfer rates should be sufficiently fast and reversible, and all redox states of the mediator should be soluble in the solvent system being used. While inorganic mediators tend to be more stable to the reaction media than organic mediators, electron transfer processes are often slow. Organic mediators have the advantage of being easily manipulated synthetically to produce a diverse structure library, allowing versatility in accessible redox potentials.

Steckhan and coworkers described an early example of an indirect electrochemical reduction using an organic mediator; in this instance, viologens were used in conjunction with a redox enzyme to convert NAD^+ to NADH (Figure 33).[99] In this case, the reduced viologen, $V^{\bullet+}$, mediated an electron transfer to reduce the

enzyme, which then arbitrated a single electron transfer to the NAD^+ concurrently with a proton transfer to provide NADH.

Figure 33. Viologen-mediated reduction of NAD^+ to NADH.

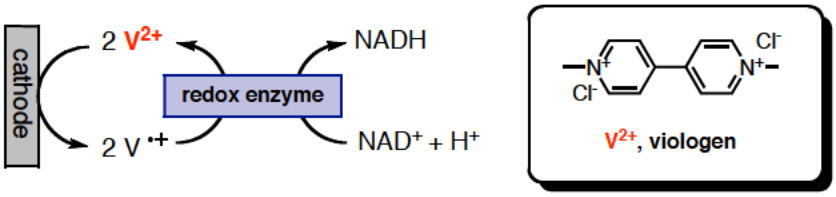

Other commonly used reduction mediators in electroorganic synthesis include polycyclic aromatic systems that reduce between ca. –1.67 V and –2.7 V (vs. SCE) (Figure 34).[98] On the other end of the spectrum, derivatives of the triarylamine framework provide reliable mediators, which prove stable over a wide range of conditions and redox potentials, viz., between +0.76 V and +1.96 V (vs. SCE) depending on the electronic substitution patterns.[120]

Figure 34. Commonly used organic redox mediators. Potentials listed refer to SCE as a reference.

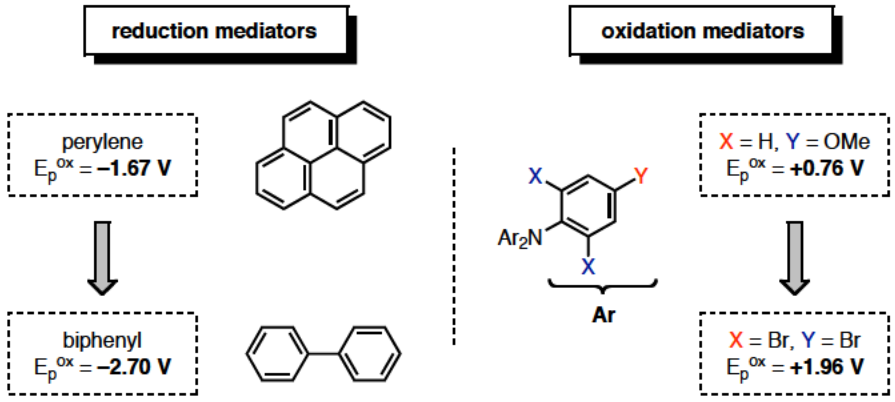

3.1.3 Mediator-Modified Electrodes

While electrochemical mediators allow many reactions to be run under milder redox conditions, in the majority of cases the mediators cannot be recovered. This frequently results in excessive waste and the need for additional workup procedures during their repeated synthesis and separation from the reaction mixture. One recent example from Little and coworkers demonstrated the use of tris(4-bromophenyl)amine to generate a key intermediate in the total synthesis of daucene, **98** (Scheme 35).[100] Unfortunately, 40 mol % of the mediator was required to obtain 70% of the desired product, **97**.

Scheme 35. Mediated electrochemistry in the synthesis of daucene.

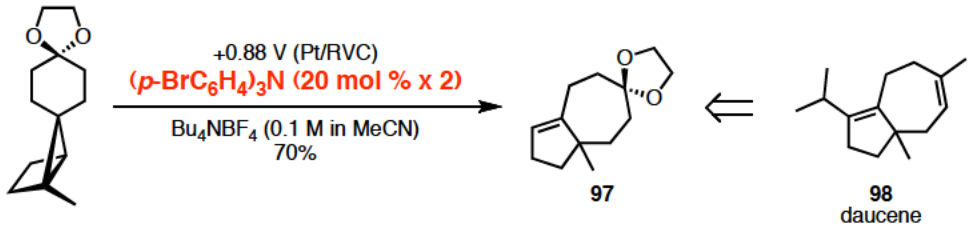

This leaves one to wonder how this process could be improved. One example, a recoverable mediator source, would be both economically and ecologically attractive. To this end, Fry and Mayers had modest success in their investigation of the behavior of triarylamines covalently bound to a carbon fiber electrode.[101] Unfortunately, the attached 4-amino-4',4"-dibromophenylamine underwent an undesirable dismutation. Recently, Stahl and Hamers demonstrated that a $Ru(typ)_2$ triazole tethered to the surface of a boron doped diamond (BDD) electrode was

stable for over 1 million cycles through the ruthenium redox potential range (Figure 35).[102]

Figure 35. Recent examples of mediator-modified electrodes.

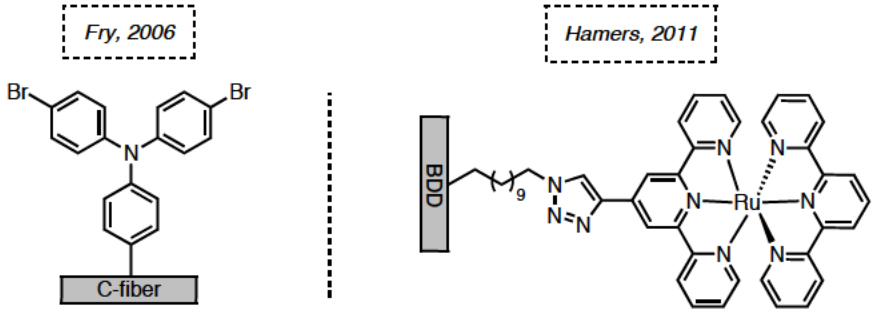

Progress towards the modification of electrode surfaces with mediator-functionalized polymers will be discussed (Figure 36). The aim of the investigation is to provide a method to recover and reuse mediators, and thus a sustainable alternative to traditional mediated electrochemistry. The focus will be upon easily synthesized mediators possessing a redox range such that catalysis of a variety of reactions is possible. Furthermore, differential functionalization of the monomer will maximize the efficiency for screening a variety of mediators for any given reaction. One application of interest that will be explored is the anodic oxidative degradation of lignin model compounds. Ultimately, we hope to increase the appeal of mediated electrochemistry to a broad, multi-disciplinary audience.

Figure 36. Approach to mediator-modified electrodes.

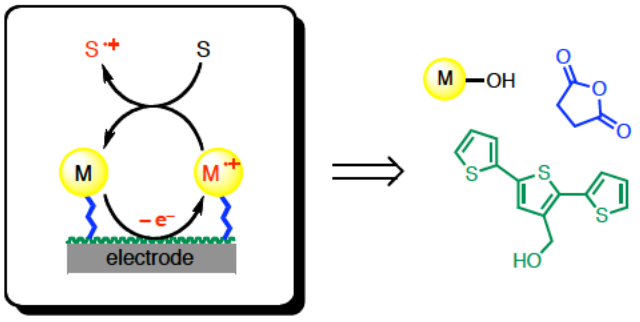

3.2 "Click" Chemistry Approach to Electrode Modification

3.2.1 Synthesis of the Terthiophene Monomer

Synthesis of the terthiophene monomer, **101**, that was polymerized on the electrode surface was completed in four steps (45% overall yield) from an inexpensive commercially available starting material (Scheme 36). Beginning with 3-thiophenecarboxaldehyde, **99**, bis-bromination was accomplished with a slightly modified procedure to that reported by Zhang and coworkers.[103] Using the reported 2.6 equivalents of Br_2 failed to yield the desired product, resulting in primarily mono-brominated substrate and some recovered starting material. After much trial and error, it was determined that *slow* addition of 7.5 equivalents of Br_2 generated the desired bis-brominated thiophene derivative **100**. A Suzuki cross-coupling reaction between **100** and boronic acid **102** efficiently produced 3-terthiophenecarboxaldehyde **101**.[104] Reduction to the alcohol using sodium borohydride[105] and subsequent azide substitution using diphenylphosphoryl azide and DBU[106] provided the desired terthiophene monomer.

Scheme 36. Synthesis of the terthiophene monomer, **101**.

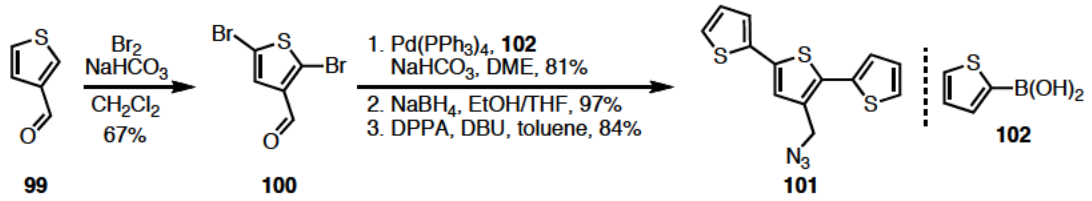

3.2.2 Modification and Characterization of the Electrode Surface

Once the terthiophene azide monomer was synthesized, the conditions necessary for electrochemical polymerization onto the anode were determined. An initial CV was obtained with a 3 mM solution of azide **101** in acetonitrile using a glassy carbon anode, platinum cathode and *n*-Bu_4NPF_6 (5 mM) as the supporting electrolyte. The monomer displayed an irreversible curve with an oxidation potential of +0.8 V (vs. Ag/0.1 M $AgNO_3$) (Figure 37a) and additional scans showed an increasingly broad and quasi-reversible curve (Figure 37b), which is agrees with the results reported by Wolf and coworkers for the oxidation of a similar terthiophene monomer.[107]

Figure 37. Cyclic voltammograms obtained for terthiophene monomer **101** after (a) 1 scan and (b) subsequent polymerization scans.

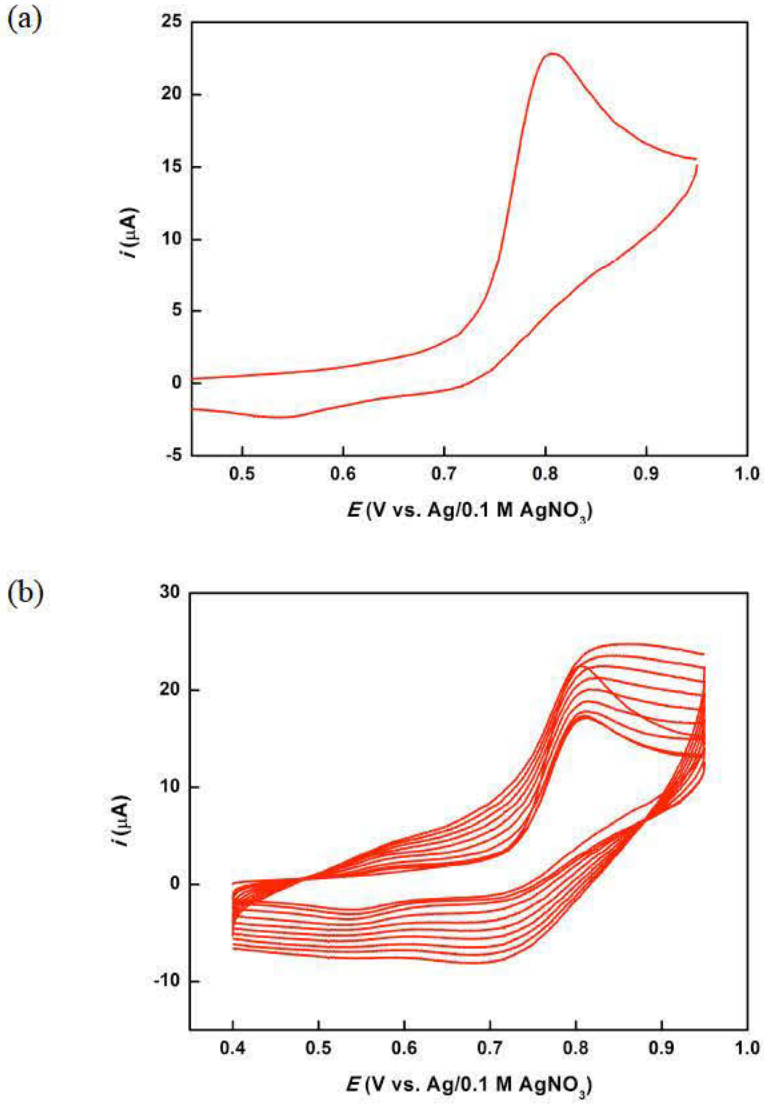

The broad shape of the oxidation wave observed in Figure 37b is associated with slow charge transport, a common characteristic of polymer-modified electrodes. For example, the diffusion coefficient for poly(2,2':5',2'-terthiophene) was determined to

be 6.5 x 10^{-11} m^2s^{-1},[108] *five orders of magnitude smaller* than a "tethered" ferrocene monolayer on a gold electrode,[109] which has a diffusion coefficient of 5.1 x 10^{-6} m^2s^{-1} in a similar solvent/electrolyte system. Simply explained, only a fraction of the electroactive sites, *viz.,* those near the electrode surface, can be oxidized in a thick multilayer film during a single votammetric scan. Thus a charge diffusion layer is created and, as accumulation of oxidized species occurs as the charge diffuses through the film and new oxidation sites become available, increases in current and peak tailing are observed. These effects become more pronounced as the film thickness grows with additional scans. The kinetic dependence on scan rate is consistent with the Randles-Sevcik equation, which will be discussed in more detail later. The appearance of the peak at approximately +0.7 V is attributed to the reduction of the bulk polymer (pTTh) to $pTTh^{-}$. Wakeham and coworkers report a similar observation in the electrochemical characterization of poly(2,2':5',2'-terthiophene).[108]

The presence of the polymeric film on the electrode was confirmed and its surface morphology examined using scanning electron microscopy (SEM) and atomic force microscopy (AFM).[110] Samples were prepared on a carbon paper and on a silicon wafer anode by sweeping for ten cycles between +0.45 and +0.95 V using the polymerization conditions described previously. It can be seen in the AFM (Figure 38a) and SEM (Figure 38b) images that a porous polymer film approximately 300 nm thick was deposited on the electrodes. The smooth surface of the silicon wafer was characterized by homogeneous film coverage, in contrast to the

carbon paper, which had regions of exposed electrode apparent in the SEM image. Wakeham observed similar porosity in the bulk poly(2,2':5',2'-terthiophene) deposited on indium tin oxide (ITO) on glass.[108] The ramifications of these inhomogeneities on the catalytic properties of this modified electrode are not clear. An IR spectrum of the modified carbon paper electrode produced a characteristic peak for azides at 2168 cm^{-1}, confirming that the azide functionality was able to withstand the polymerization conditions.

Figure 38. Polymeric film imaged by (a) AFM on a silicon wafer and (b) SEM on carbon paper

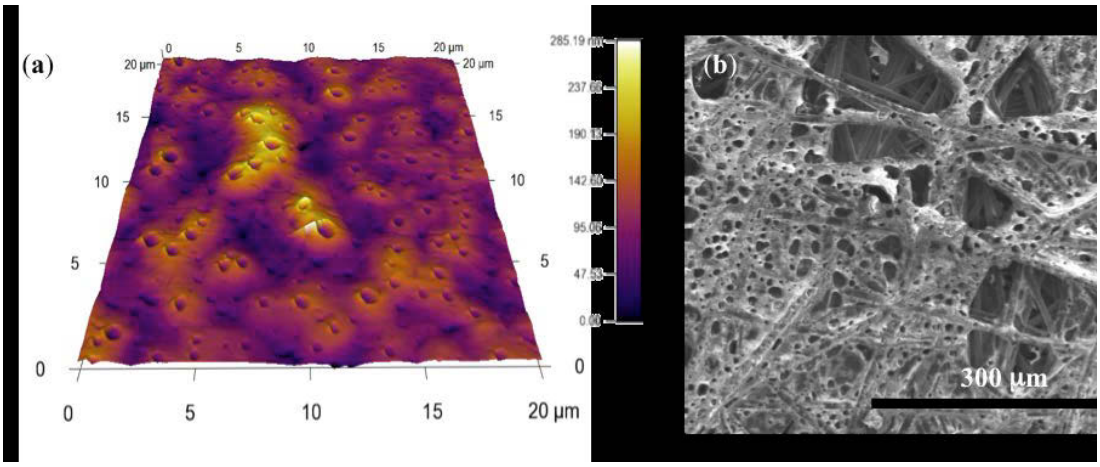

While the mediators were being synthesized, a test "click" reaction was performed using phenyl acetylene (Scheme 37). An azide-modified electrode was placed in a solution containing copper powder, $Cu(MeCN)_4PF_6$, and phenyl acetylene in acetonitrile for three days. Qualitatively, during that time, the orange polymeric sheen had faded to a matte hunter green, which suggested that a reaction had taken place. The "clicked" electrode was washed thoroughly with acetonitrile

and dried under vacuum. Although the phenyl-substituted triazole was not expected to act as a redox mediator — the electrode produced an irreversible CV curve — this example proved that the azide could be functionalized after polymerization.

Scheme 37. Test case for the heterogeneous "click" reaction conditions.

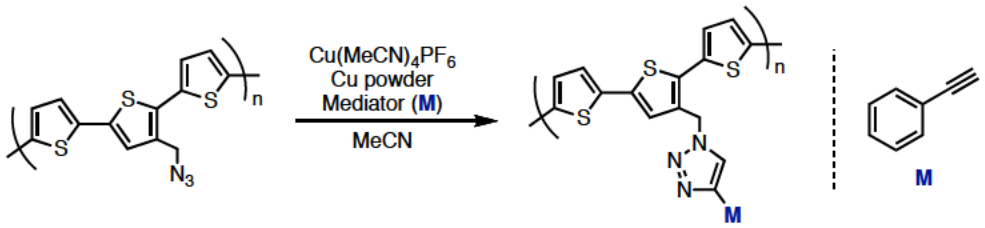

3.2.3 Triarylimidazole Mediators

With all indicators suggesting that modification of the electrode surface with a polymeric film was successful, the next task was to determine a suitable mediator to attach. Ideally, the redox mediator should be (a) easily synthesized or derivatized, (b) robust over a desired potential range and reaction conditions, and (c) amenable to a variety of reactions. Thus, our initial focus was on the use of oxidation mediators due to their widespread utility in organic electrochemistry.[98]

We recently reported a new class of over 30 redox catalysts based on the triarylimidazole framework, *viz.,* **103**.[111] Using the conditions set forth by Barekat,[112] we demonstrated that a variety of benzil derivatives undergo a condensation reaction with various aldehydes, methylamine and ammonium acetate in the presence of a catalytic amount of sodium dihydrogen phosphate when heated to 150 ºC for 5-7 hours, affording crystalline triarylimidazoles in yields generally

exceeding 85%. In addition to the wide range of accessible oxidation potentials, *viz.*, +0.71 V to 1.44 V (vs. Ag/0.1 M AgCl), their versatility was demonstrated by mediating the oxidation of electron rich benzylic alcohols and ethers to their corresponding carbonyl compounds (Scheme 38).

Scheme 38. Oxidation of aromatic compounds using triarylimidazole mediator.

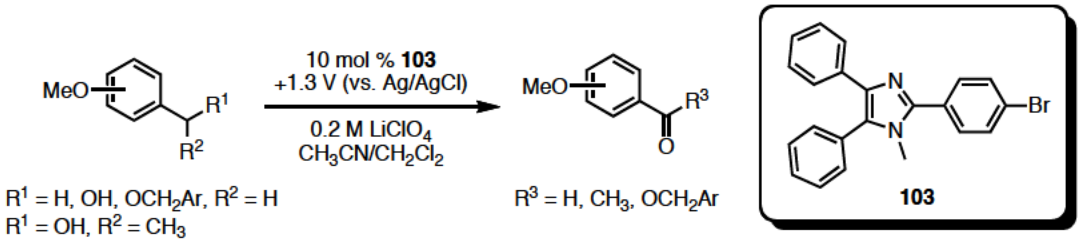

R^1 = H, OH, OCH_2Ar, R^2 = H
R^1 = OH, R^2 = CH_3

R^3 = H, CH_3, OCH_2Ar

Given the generality of the synthetic approach, we hoped to expand this methodology to derivatives that could be used for click chemistry. However, synthesis of the mediator with a pendant alkyne proved to more complicated than originally anticipated. It was envisioned that triarylimidazoles of the type **107** could be accessed using one of two synthetic sequences. Initially, we attempted installation of the ethynyl group first followed by condensation to form the triarylimidazole (Scheme 39). A Pd-catalyzed Sonogashira cross-coupling reaction was employed to attach TMS-protected acetylene **105** to 4-bromobenzaldehyde, **104**.[113] Removal of the TMS group with potassium carbonate in methanol produced 4-ethynylbenzaldehyde, **106**, in 92% yield over two steps.[114] Unfortunately, imidazole **107** could not be generated using the conditions described by Zeng and coworkers.[115]

Scheme 39. First approach to the synthesis of triarylimidazole **107**.

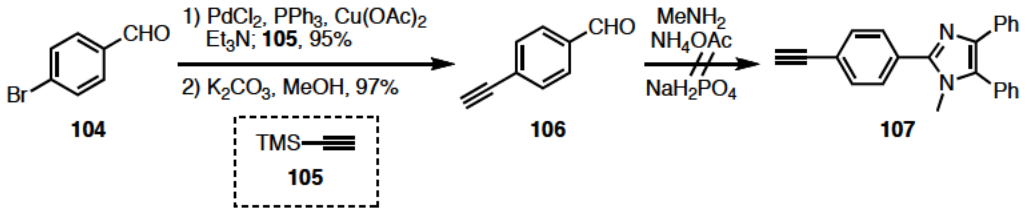

Examination of the literature revealed that terminal alkynes undergo coupling reactions, commonly termed A_3-coupling, with aldehydes and amines in the presence of base or transition metal catalysts at elevated temperatures (Scheme 40).[116]

Scheme 40. General metal-catalyzed A^3-coupling reaction.

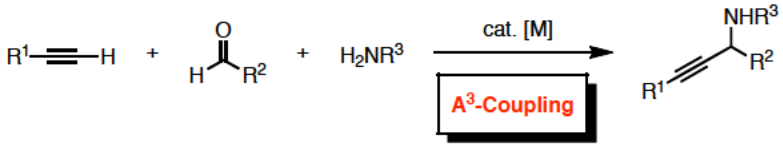

Fearing that our terminal alkyne could be susceptible to undesirable chemistry of this nature, or that it was unstable under the high temperature and pressure conditions required for the condensation reaction, we hoped to address the reactivity issue by masking the alkyne during the condensation reaction. We envisioned formation of the TMS-protected ethynylbenzaldehyde using a Sonogashira cross-coupling reaction, construction of the triarylimidazole using the condensation conditions described previously, and a final deprotection of the alkyne to generate the desired mediator, **9** (Scheme 41). After successfully coupling bromobenzaldehyde with TMS acetylene, the condensation reaction again produced only a myriad of decomposition products.

Scheme 41. Second approach to the synthesis of triarylimidazole **107**.

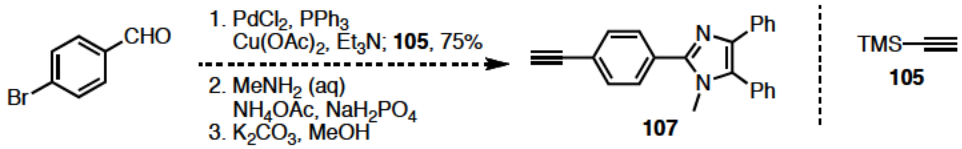

The glaring problem became *how* we could circumvent the stability and reactivity issues we had encountered thus far while still maintaining the highly versatile "click" chemistry method of attachment. The seemingly obvious solution involved changing the order of the synthesis such that the terminal alkyne was not present during the condensation step. Thus, the modified synthetic sequence generated imidazole **103** first using the condensation conditions reported previously (Scheme 42), followed by installation of the ethynyl group using a Sonogashira cross-coupling reaction with trimethylsilylacetylene.[114,117]

Scheme 42. Synthesis of the mediator precursor, triarylimidazole **103**.

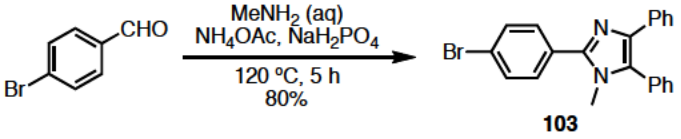

As illustrated in Table 6, a variety of palladium and copper sources were surveyed in conjunction with reaction temperatures ranging from room temperature to refluxing THF, as well as in the presence and absence of added ligand. Despite valiant efforts, the desired triarylimidazole, **108**, was never isolated and in most cases only starting material was recovered.

Table 6. Conditions for the Sonogashira cross-coupling reaction.

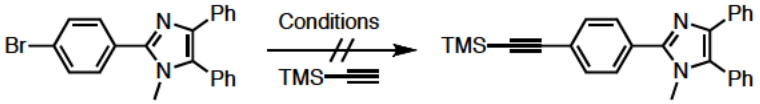

103 108

Pd Source	Cu Source	Ligand	Base	Solvent	T (° C)
$PdCl_2(PPh_3)_2$	CuI	PPh_3	Et_3N	N/A	80
$Pd(PPh_3)_4$	CuI	none	Et_3N	N/A	25
$PdCl_2$	$Cu(OAc)_2$	PPh_3	Et_3N	N/A	80
$Pd(PPh_3)_4$	CuI	none	Et_3N	N/A	50
$PdCl_2$	$Cu(OAc)_2$	PPh_3	Et_3N	THF	80
$Pd(PPh_3)_4$	CuI	none	Et_3N	THF	80

It was recently reported by Heravi and coworkers that the condensation reaction could be carried out between 25 and 60 ºC using $FeCl_3 \cdot 6H_2O$ as an additive.[118] We hoped that the milder reaction conditions would allow facile access to a variety of substitution patterns for the triarylimidazole framework containing an alkyne. Much to our dismay, the decreased reaction temperatures and increased reaction time (24 h) proved unsuccessful in yielding the desired triarylimidazole. We then wondered if we could simultaneously lower the temperature and pressure at which the condensation reaction took place. For example, if a higher-boiling amine was used in place of methylamine, could the need for a sealed tube be eliminated? Two subsequent reactions with cyclohexylamine and benzylamine were carried out at the boiling point of the respective amines using only a reflux condenser. Unfortunately, no desired product could be observed in either of these cases.

After exhaustive efforts to synthesize mediators with an aryl ethynyl moiety proved futile, an alternative mediator attachment site was considered. The most logical site for modification seemed to exist on the alkylated nitrogen of the imidazole ring. Acting as both a higher-boiling amine as well as providing an alternative attachment site, propargylamine appeared to be an ideal candidate. Thus, an ethanolic solution of benzil and benzaldehyde was heated to 35 °C in the presence of propargylamine, ammonium acetate, and the $FeCl_3 \cdot 6H_2O$ catalyst (Scheme 2). Limited success was achieved using this approach as substituted benzil derivatives, *viz.,* **110** and **111**, failed to react and the unsubstituted system, **109**, yielded less than 20% of the desired triarylimidazole.

Scheme 43. Synthesis of the mediator with an alternative attachment site.

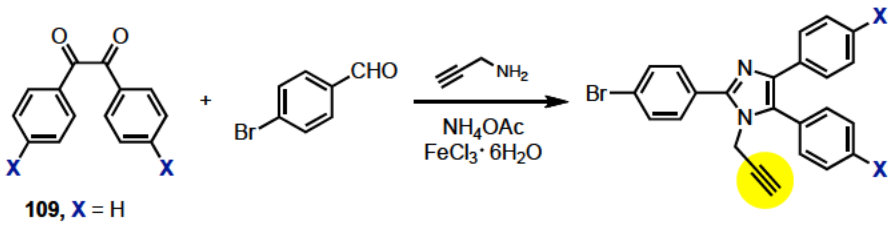

109, **X** = H
110, **X** = Br
111, **X** = OMe

3.2.4 Alternative Mediators

A crystal structure of the triarylimidazole mediator **Q** indicates that all three aryl groups reside out of plane (Figure 39a). Quantum calculations suggest that delocalization within the HOMO is limited as a result (Figure 39b). Therefore, in addition to benzil-derived triarylimidazoles, substrates with a "fused" core were investigated as possible mediators (e.g. structure **113** illustrated in Scheme 44). We

suspected, and calculations provided support for the conjecture, that by covalently linking the aryl groups appended to C4 and C5 of the imidazole core, greater delocalization would ensue, thereby allowing the electronic characteristics of the substituents to be more fully expressed, and leading to a larger range of accessible oxidation potentials (Figure 39c).

Figure 39. (a) Crystal structure of triarylimidazole mediator and calculated HOMO for an (b) unfused and (c) fused (d) triarylimidazole **Q**

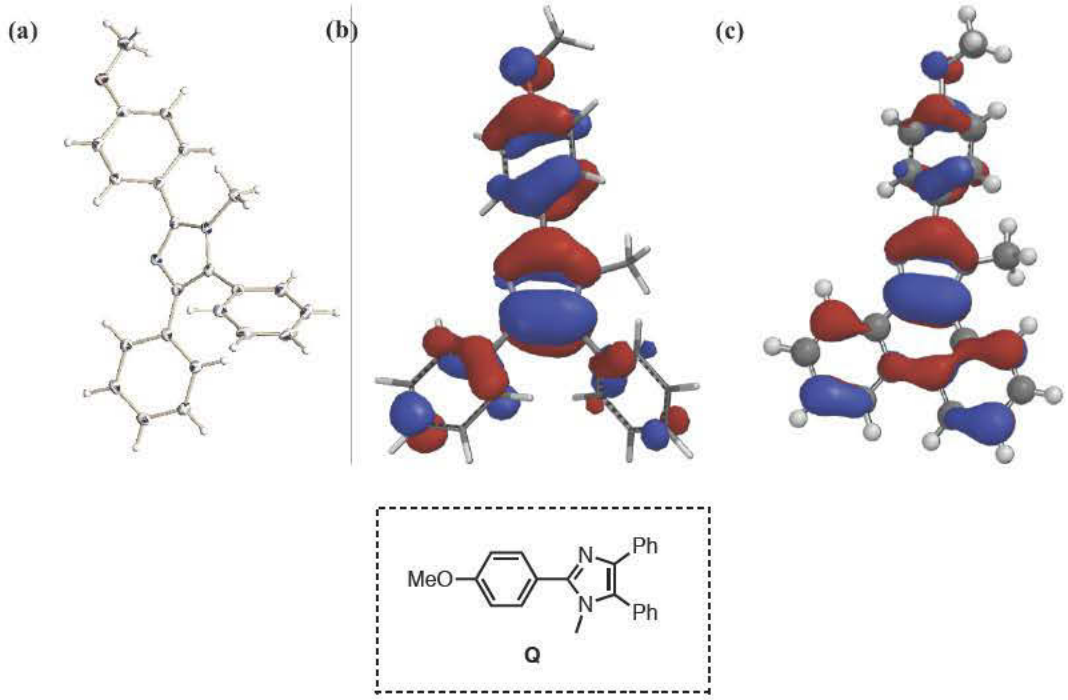

Unfortunately, only modest success was encountered in the synthesis of the "fused" triarylimidazoles. In this case, phenanthraquinone reacted with an electron deficient aldehyde, *viz.,* **114** and **113**, to produce the mono-substituted fused triarylimidazoles in < 20% yield. When the phenanthraquinone was substituted with

an electron-withdrawing group, *viz.*, **114**, at the *para* position, only recovered starting material was obtained (Scheme 44).

Scheme 44. Synthesis of selected "fused" triarylimidazoles.

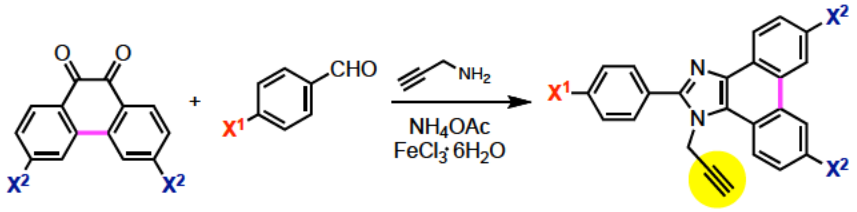

112, X^1 = Br, X^2 = H
113, X^1 = NO_2, X^2 = H
114, X^1 = X^2 = Br

Cyclic voltammograms of the ethynyl substituted triarylimidazoles, **109**, **112**, and **113**, revealed two important pieces of information. First, in accord with the predictions described above, fusion of the aromatic rings had a dramatic effect on the oxidation potential. For example, comparison of the oxidation potential for the fused analog, **112**, with that of its unfused analog, **109**, revealed a difference of nearly 300 mV (Figure 40). This suggests that delocalization of the cation radical is increased when the planarity of the core increased, and suggests that an even larger range of oxidation potentials could be accessed by expanding the substrate scope to this skeletal feature. Second, irreversible CV curves were obtained for all three mediators. This result was not unexpected. Irreversible electron transfer might reasonably occur as a result of polymerization or nucleophilic attack at the unprotected *para*-position when the mediator is free in solution, analogous to what is observed with unsubstituted triarylamines.[120a] However, even after clicking the mediator to the electrode, fully reversible CV curves were not obtained. Ultimately,

because the scope of the reaction was limited to phenanthraquinone and benzil (mediators **110**, **111**, and **114** were not successfully synthesized), we no longer pursued the ethynyl-substituted triarylimidazoles, and alternative mediator structures were explored.

Figure 40. Oxidation potentials for selected ethynyl-substituted triarylimidazoles.

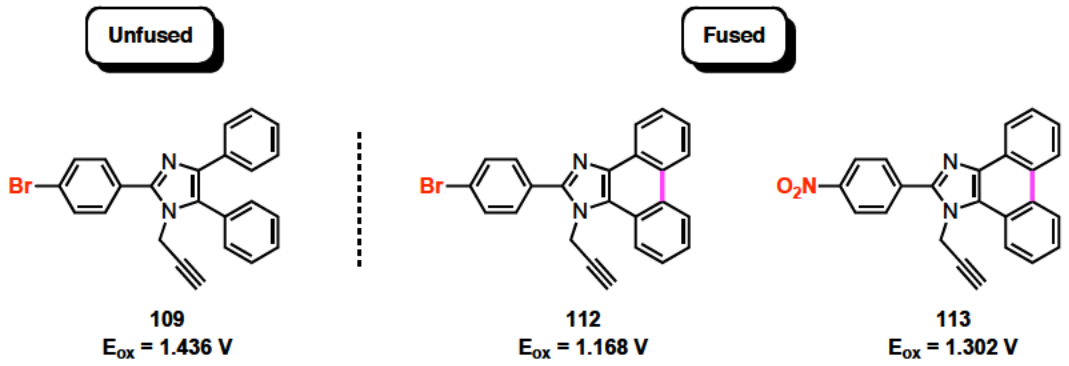

109
E_{ox} = 1.436 V

112
E_{ox} = 1.168 V

113
E_{ox} = 1.302 V

Recently, Brunner and coworkers reported oxidation potentials ranging from approximately +0.80 V to +1.3 V (vs. SCE) for a variety of carbazole derivatives.[119] Intrigued by the large range of accessible potentials, we hoped to capitalize on the ease of synthesis and diversity of carbazole structures. Although Brunner reported an irreversible curve for the unsubstituted carbazole, we were hopeful that immobilization of the substrate would eliminate any potential follow-up reactions (i.e. undesirable reactivity at the *para*-position)[120] that might be occurring. In addition to the unsubstituted derivative, **116**, the most simple *para*-substituted carbazole derivative, **117**, was also examined. The bis-brominated carbazole, **115**, was easily synthesized in good yields by adding NBS to carbazole in a SiO_2 slurry (Scheme 3).[121] Independent treatment of each carbazole and **117** with propargyl

bromide and aqueous sodium hydroxide, using Et_3BnNCl as a phase transfer catalyst, provided the alkylated substrates (Scheme 45).[122] With the alkyne readily available, the substrate was "clicked" to the terthiophene backbone both before (homogeneous coupling) and after (heterogeneous coupling) polymerization onto the electrode surface. Although both methods resulted in successful electrode functionalization, irreversible CV curves were obtained for both substrates and carbazole derivatives were abandoned as potential mediators.

Scheme 45. Synthesis of alkylated carbazole derivatives.

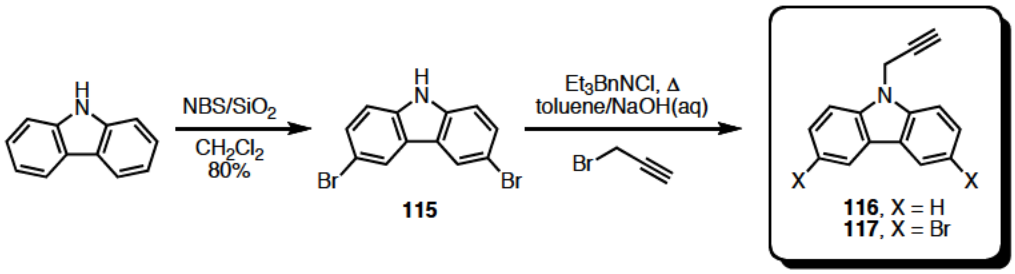

With an interest in expanding scope of the methodology to reductions, we elected to purse two well-studied metal-salen complexes.[123] Our investigation began with a facile condensation of 4-bromosaliciladehyde with ethylenediamine to cleanly generate the salen ligand, **118**, in 80% yield (Scheme 46).

Scheme 46. Synthesis of the salen ligand.

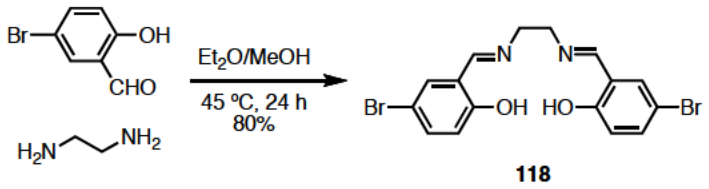

118

Regrettably, the synthesis of the derivatized Zn and Ni(salen) complexes, **119** and **120**, needed for the "click" reaction was not as straightforward as similar complexes described by Chang and coworkers.[124] Two possible orders for the synthetic routes to form the metal complex with a terminal alkyne were explored (Scheme 47). Initially, the bis-brominated complexes were generated in good yields by heating the salen ligand in the presence of the respective metal acetate ($M(OAc)_2$). Unfortunately, the subsequent coupling step proved unreliable; thus, the acetylation of the salen ligand was carried out first, followed by metal complexation. Solubility issues associated with the final metal complex prevented traditional characterization methods, i.e. NMR, from being used. More importantly, however, insolubility of the substrate in acetonitrile resulted in unsuccessful attachment of the mediator to the polymer modified electrode.

Scheme 47. Synthetic routes to M^{2+}(salen) click chemistry precursor.

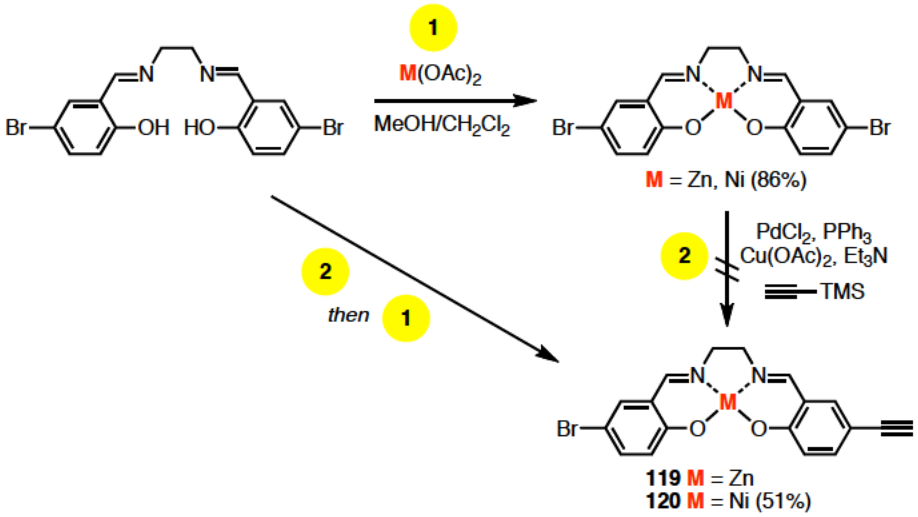

3.3 "Tethered" Approach to Electrode Modification

Although the triazole ring promised to provide durable connectivity, especially under the rigorous conditions necessary for our desired lignin degradation application, the appeal of the supposedly versatile "click" chemistry attachment method was lost when a large library of functional mediators could not be easily synthesized. In the interest of developing a methodology that would be valuable to a wide variety of applications, we wanted to consider alternative ways in which to incorporate the mediator. For example, could surface modification occur via polymerization of a fully functionalized monomer, as opposed to a post-modification heterogeneous attachment of the mediator? In light of this new perspective and with the terthiophene alcohol, **TTh**, readily available, could the hydroxyl group act as a handle in which to incorporate the mediator, i.e. by either S_N2 displacement or esterification, before carrying out the polymerization (Scheme 48)?

Scheme 48. Attachment methods for the tethered approach to mediator incorporation.

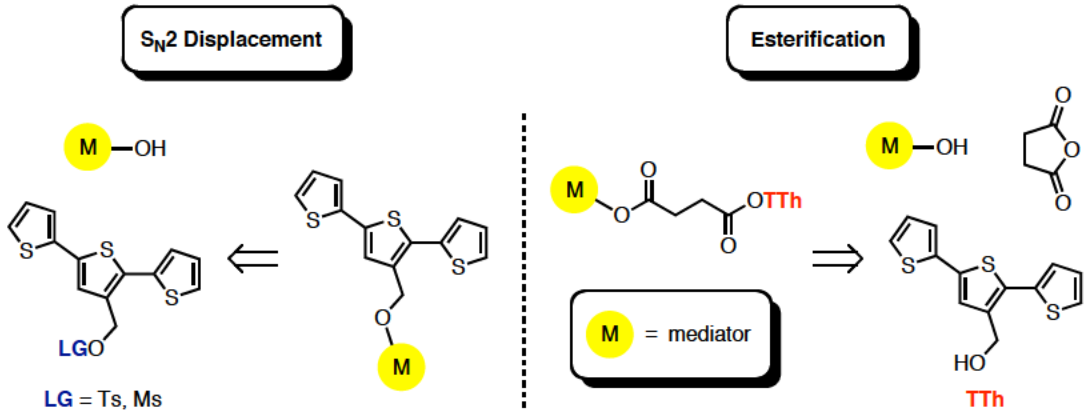

3.3.1 Attachment via S_N2

An S_N2 displacement of either the mesyl or tosyl protected terthiophene monomer by a hydroxyl-substituted mediator provided a straightforward starting point. Thus, the terthiophene alcohol was converted to the tosylate, **121**, using toluenesulfonyl chloride and sodium hydroxide,[125] or the mesylate, **122**, using methanesulfonyl chloride and triethylamine (Scheme 49).[126] The well-studied oxidation mediator, 4-hydroxy-TEMPO,[127,133] was used as a test case nucleophile. Unfortunately, the mesyl-protected terthiophene monomer proved unstable to purification and the tosyl-protected monomer exhibited solubility issues. Furthermore, the S_N2 reaction proceeded inefficiently, requiring up to 48 hours to achieve poor conversions when homogeneous displacement was attempted.

Scheme 49. Synthesis of TEMPO-functionalized terthiophene monomer.

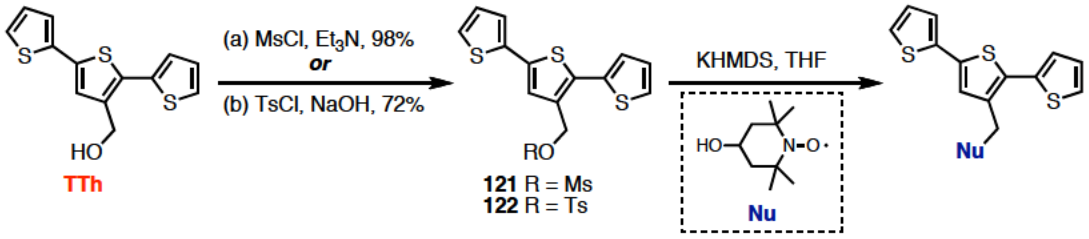

3.3.2 Attachment via Esterification

Unsatisfied with the outcome of the first method, we explored the use of two sequential esterification reactions to attach the mediator, **M** (Scheme 51). One appealing aspect of this method is the use of succinic anhydride as a linker between the mediator and monomer, allowing flexibility in the design of the modified surface. For example, if desired, a variable-length tether could be added between the mediator and the terthiophene backbone simply by changing the number of methylene units in the cyclic anhydride. Furthermore, hydroxy-substituted mediators should be synthetically easier to access than either alkynes or azides, and the terthiophene monomer precursor can be produced in one less step than its azide counterpart.

3.3.3 A New Mediator and a Test Reaction

We turned our attention to a member of the well-studied class of electrochemical oxidation mediators, the triarylamines, in order to test the new attachment method.[98,128] Synthesis of the triarylamine mediator, **124**, was accomplished in three steps (Scheme 50). From the commercially available triphenylamine, an

unoptimized Vilsmeier-Haack formylation reaction using $POCl_3$ in DMF afforded **123** in poor yields.[129] Fortunately, the triphenylamine starting material could be recovered and resubjected to the reaction conditions. Bis-bromination of crude **123** with NBS,[130] and subsequent reduction of the formyl group using $NaBH_4$ in a biphasic reaction mixture,[131] gave the desired mediator in 88% yield over two steps.

Scheme 50. Synthesis of the hydroxy-substituted triarylamine mediator.

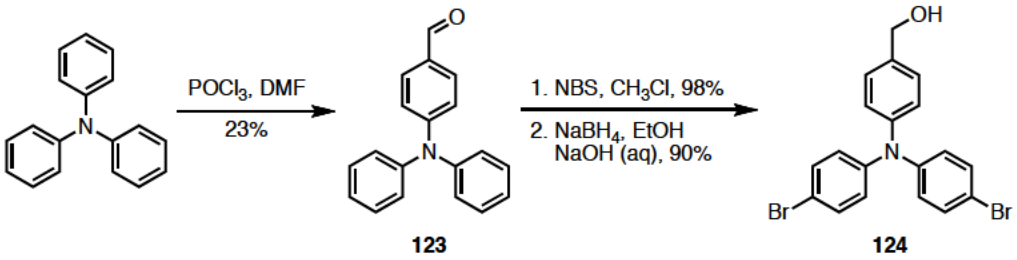

123 **124**

With the desired mediator in hand, alcohol **124** was coupled to succinic anhydride using DMAP to obtain the carboxylic acid analog, **125** (Scheme 51).[132] It was not necessary to purify this material before it was coupled to the terthiophene alcohol, **TTh**, using DMAP and DCC.[133] The final monomer, **126**, was purified using column chromatography and subsequently polymerized onto the carbon paper electrode surface following the same polymerization procedure described previously. After sweeping ten times between +0.40 and +0.95 V, the electrode was removed from the CV cell, rinsed, and dried under vacuum before further characterization was carried out.

Scheme 51. Attachment method employing a double esterification sequence.

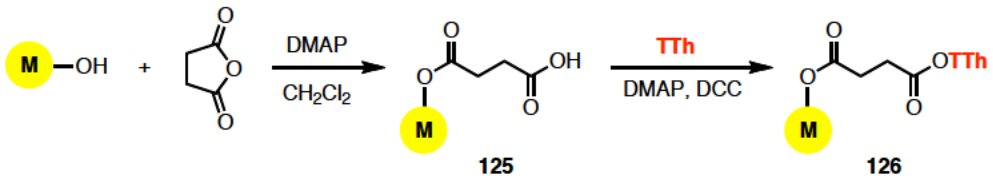

An initial CV obtained of the modified working electrode provided a reversible curve characteristic of triarylamines (Figure 41, red curve). Following precedence set forth by Zeng and coworkers, a simple oxidation of 4-methoxybenzyl alcohol, in the presence of excess 2,6-lutidine with a 0.1 M solution of Bu_4NPF_6 in acetonitrile, was used to probe the catalytic activity of the electrode (Scheme 52). Much to our delight, catalytic current was observed (Figure 41, blue curve).

Scheme 52. Oxidation reaction used to probe the catalytic activity of the modified electrode.

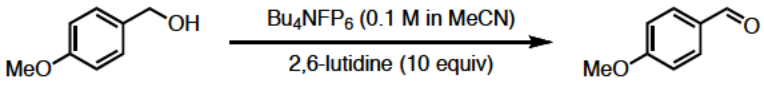

Figure 41. CV curve demonstrating catalytic current for the oxidation illustrated in **Scheme 52**.

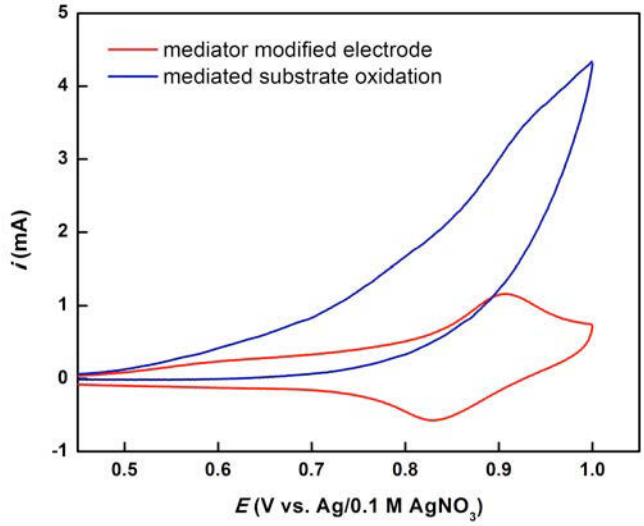

3.3.4 Lignin Model System

One goal is to use modified electrodes for electrochemical oxidative degradation of lignin. To this end, lignin model systems were synthesized following slightly modified procedures of Bolm and co-workers.[134] Initially, commercially available 2-methoxyphenol was alkylated using ethyl bromoacetate and potassium carbonate in acetone (Scheme 53). The resulting ester, **127**, was deprotonated using LHMDS at –78 ºC and then coupled to 3,4-dimethoxybenzaldehyde to generate the condensation product **129**. Unfortunately, this second step was low yielding with a nearly racemic mixture of diastereomers, which proved difficult to separate.

Scheme 53. Synthesis of lignin model compound precursor.

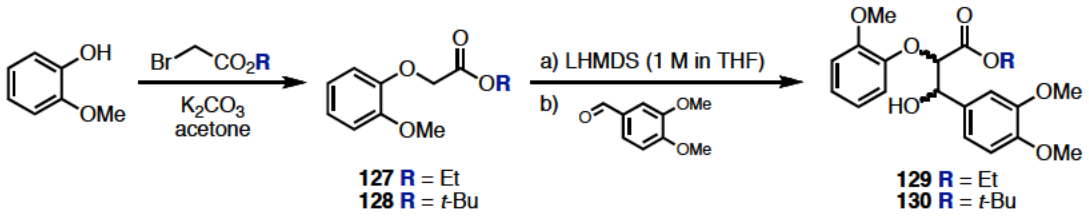

127 **R** = Et
128 **R** = *t*-Bu

129 **R** = Et
130 **R** = *t*-Bu

In an effort to maximize the yield of a single isolated diastereomer, *t*-butyl bromoacetate was substituted for the ethyl bromoacetate in the first alkylation step in order to increase the steric bulk near the forming stereocenter. Thus, the *t*-Bu ester, **128**, was subjected to the same Claisen-Schmidt reaction conditions described previously. Unfortunately, this again resulted in a low yield (< 30%) of the desired product mixture, **130**. This was attributed to the substitution of LHMDS for LDA as the base in the α-deprotonation step in the modified procedure. To account for the difference in base strength, subsequent deprotonations were carried out at 0 ºC with warming to room temperature after addition of the aldehyde, resulting in significantly increased yield of the desired product, **130**, e.g. from 30% to 74%. The major diastereomer, **131**, was easily separated using column chromatography and was subsequently reduced using LAH to yield the lignin dimer model compound, **132** (Scheme 54). In a preliminary study, catalytic current was observed in the CV for the oxidation of lignin model compound **132**.

Scheme 54. Synthesis of diastereomerically pure lignin model compound **132**.

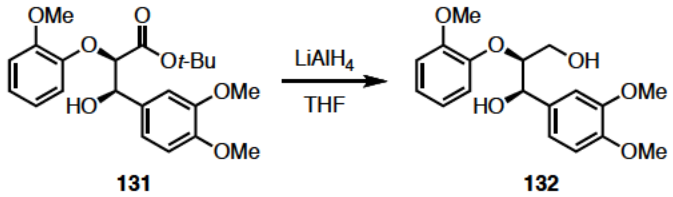

131 **132**

3.3.5 Additional Electrode Characterization

Although the surface morphology of the modified electrodes had been explored using AFM and SEM imaging (vide supra), the nature of the interaction between the electrode and the polymer film was also of interest. For example, is the polymer absorbed to the surface of the electrode and how robust is this interaction? Is there a relationship between the number of scans used during polymerization and the conductivity of the electrode, and is there a direct correlation to film thickness?

A scan rate study was used to gain a more thorough understanding of the modified electrode. For the present investigation, peak current was measured at variable scan rates (0.05 V/s to 0.55 V/s) for a carbon paper electrode modified in the usual way with the fully funcionalized polymeric complex. The data was then plotted to illustrate the peak current (i_p, mA) as a function of the square root of the scan rate ($v^{1/2}$) and fitted with a linear regression line (Figure 42).

Figure 42. Plot of the relationship between scan rate and peak current for the terthiophene-modified electrode.

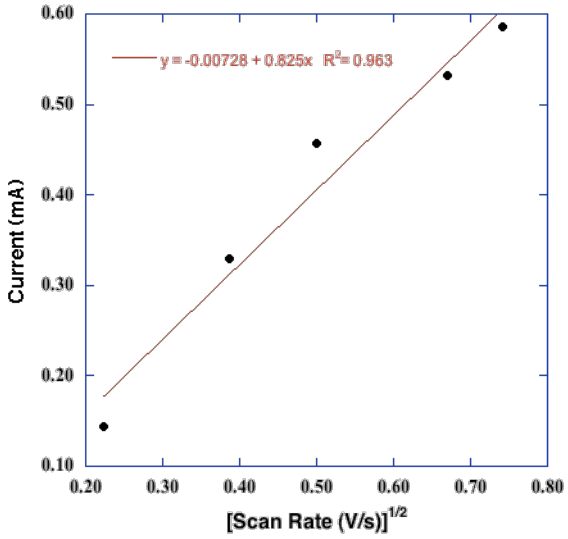

The Randles-Sevcik equation (Equation 1) predicts a positive, linear relationship between peak current, i_p, and the square root of the scan rate ($\nu^{1/2}$) for an electrochemically reversible, diffusion controlled process occurring at the electrode surface.[135] Current is a function of both charge and time; therefore, as the scan rate increases, the charge passed per unit time is greater resulting in an increase in the peak current. Obeying Randles-Sevcik-type kinetics, a reasonable coefficient of determination ($R^2 = 0.96$) was observed for this system, providing evidence that the polymer is adsorbed to the electrode surface and confirming that the electron transfer process is fully reversible, i.e. no degradation occurred upon repetitive cycling. These results, in conjunction with conserved reversibility of the triarylamine CV curve after 1000 consecutive scans ($\nu = 0.1$ V/s) over the potential range described previously, confirmed the durability of both the mediator and polymeric film.

Equation 1. Randles-Sevcik equation.

$$i_p = 0.4463\, nFAC \left(\frac{nF\nu D}{RT}\right)^{1/2}$$

i_p = peak current (A)
n = number of electrons transferred
A = electrode area (cm^2)
F = Faraday's constant (C/mol)
D = diffusion coefficient (cm^2/s)
C = concentration (mol/cm^3)
ν = scan rate (V/s)

Conducting-AFM (c-AFM) images were collected to determine the conductivity of the polymeric film as a function of CV scan cycles used during the electrochemical polymerization.[136] Because c-AFM is still in the relatively early stages of development, images could only be obtained for a 50 scan sample on carbon paper and on fluorine-doped indium tin oxide (FTO) on glass. Furthermore, the images indicated complete resistivity of the polythiophene film, which is inconsistent with other polythiophene-modified electrodes in the literature. Further investigation using this technique is necessary before a conclusion regarding the relationship between conductivity and number of scans can be made.[137]

3.4 Modified Electrodes for Bulk Electrolysis

Successful catalysis was observed on the CV scale, however, the important question remained: could this be expanded to practical quantities? Furthermore, what would be the best electrode material to maximize catalytic efficiency while still minimizing environmental impact? Wanting to avoid the use of precious metal electrodes, our investigations began with carbon electrodes. Several factors were taken into consideration when choosing the type of carbon electrode. "Hard" carbon electrodes (*viz.*, reticulated vitreous carbon, RVC, or glassy carbon, GC) are ideal

because polymer characterization can be carried out readily with using advanced imaging techniques (AFM, SEM, etc.), and it is possible for qualitative film deposition to be observed visually. "Soft" carbon electrodes (*viz.*, carbon felt, graphite rods) generally offer a larger surface area and are closer to the model system (carbon paper) used in the CV studies. Furthermore, the ability of the polymerized material to remain adsorbed to the smooth carbon surface of "hard" carbon electrodes could prove problematic, as was observed with the silicon wafers used during AFM/SEM sample preparation.

Therefore, the initial electrode modified for bulk electrolysis was an ~ 5 cm x 1.5 cm x .5 cm carbon felt strip "sewn" with copper wire to which the alligator clip could be attached. The polymerization was carried out by sweeping ten times between 0 and +0.95 V (vs. Ag/ 0.1 M $AgNO_3$), in a 0.1 M Bu_4NPF_6 solution in acetonitrile. Unfortunately, the larger quantity of substrate required for the modification of this electrode was not completely soluble in pure acetonitrile. A small amount of dichloromethane (< 500 ∝L) was added to ensure complete dissolution of the monomer into the electrolytic solution. When the carbon felt was immersed in the solution, a significant amount of solvent was absorbed, resulting in swelling of the electrode. This proved problematic for several reasons: unwanted absorption of the electrolyte solution could mean inefficient polymerization (i.e. does the monomer adsorb as readily as the supporting electrolyte, etc.) and inaccurate accountability for what is actually in/on the electrode during catalysis. When the electrode was pre-saturated in pure acetonitrile, no further swelling was

observed upon immersion in the electrolytic solution. This problem would most likely be circumvented with the use of a "hard" carbon electrode.

The modified electrode was used for the oxidation of *p*-methoxybenzyl alcohol, **133**, to the corresponding aldehyde, **134** (Scheme 55). However, when the potential was set to that of the triarylamine mediator, no reaction was observed when analyzed qualitatively by TLC.

Scheme 55. Bulk electrolysis of alcohol **133** using a modified electrode.

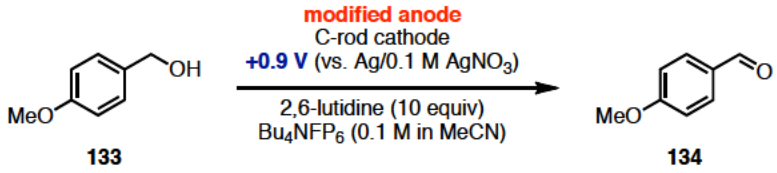

133 **134**

It was postulated that using CV for polymerization would not generate a sufficient amount of polymer-modified surface for the relatively large surface area of the felt electrode when compared to the carbon paper used in analytical studies. Thus, subsequent polymerizations were carried out in an H-cell under comparable conditions (0.1 M 0.1 M Bu_4NPF_6, 0.1 M monomer, graphite rod counter electrode) using controlled potential electrolysis (+0.95 V vs. $Ag/AgNO_3$) until the current fell below 5 mA or until 15 C of charge had passed, whichever occurred first. The felt electrode was removed, rinsed with copious amounts of pure acetonitrile and diethyl ether, and then dried under vacuum for at least one hour. In addition to the carbon felt electrode, two different mesh sizes of reticulated vitreous carbon (RVC) and a copper wire were also modified for comparison of "soft" vs. "hard" electrode materials.

All four modified electrode types were independently tested on the benzylic oxidation reaction depicted in Scheme 55. The carbon felt electrode showed almost complete conversion of the substrate to product by TLC. Although these results were very promising, a spot consistent with the starting monomer was also observed. This is indicative that even though the electrode was washed thoroughly after the polymerization step, some monomer remained absorbed in the electrode material. Even if excess monomer could be completely washed out of the electrode after polymerization, it would be difficult to ascertain if any reaction components remained absorbed in the felt after bulk electrolysis experiments. This would render the electrode unfit for reuse and therefore carbon felt was discounted as a viable electrode material. Partial conversion of the substrate (< 10%) was observed when using either of the modified RVC electrodes. For the RVC electrode with a smaller mesh size, attaching the copper wire proved precarious because the material was sufficiently brittle that any excessive force caused the electrode to chip away. Although the iridescent sheen characteristic of the polymeric film was observed on both types of RVC surfaces, after washing the electrodes with a stream of acetonitrile and ether, the sheen seemed to have disappeared. This was indicative of an insecure adsorption of the film to the electrode surface. It is possible that alternative washing methods, i.e. dipping in solvents, would temporarily solve these issues, however it would not attest to the robustness of the modification, a critical goal of this method. No reaction was observed when the modified copper wire was

used as the working electrode although charge was being consumed; presumably this was a result of the observed corrosion of the copper wire.

Several critical questions have yet to be answered: why does the polymeric complex adsorb irreversibly to the carbon paper electrode used in CV studies but this does not translate to bulk scale carbon electrode materials? Is it necessary to use a platinum electrode and does a lifecycle analysis allow for the turnover numbers of the catalyst to outweight the cost of using a precious metal electrode? And most importantly, is it necessary for a polymeric backbone to be employed or can these issues be circumvented with direct, covalent modification of an electrode surface?

3.5 Conclusion

With a continued drive to develop environmentally friendly chemical methods, this work described the modification of electrodes with electrochemical mediators for eventual use as heterogeneous catalysts in the oxidative degradation of lignin model compounds. Various attachment methods were explored, ranging from the use of "click" chemistry to S_N2 displacement reactions, and, most successfully, sequential esterifications. Furthermore, a variety of mediators were investigated, including the well-studied metal salens for reductions, and triarylamines and triarylimidazoles for oxidations. While this method shows promise for successful electrode modification, further investigations into the fundamental chemistry is required before widespread appeal to a broad audience can be achieved.

EXPERIMENTAL PROCEDURES AND SPECTRAL DATA

General Procedures. In reactions where water was not present as a solvent, reagent, or by-product, all glass vessels were flame-dried unless otherwise noted. A slight positive pressure of dry argon was maintained via rubber septum seal during the course of the reaction. Reagents were purchased from commercial vendors and used as received unless otherwise stated. Tetrahydrofuran (THF) was distilled from sodium and benzophenone. Methanol (MeOH) was distilled from $Mg(OMe)_2$. Ethanol (EtOH) was distilled from $Mg(OEt)_2$. Dichloromethane (CH_2Cl_2) and acetonitrile (MeCN) were distilled from CaH_2. Pyrrolidine and diethylamine were distilled from $Ba(OH)_2$ at atmospheric pressure. Reactions were monitored by analytical thin-layer chromatography on hard layer silica gel-60F-250. Visualization was effected by ultraviolet light (254 nm), followed by staining (*p*-anisaldehyde). Removal of solvents was typically accomplished using a rotary evaporator. Silica gel (60, particle size 0.043–0.063 mm) was used for flash column chromatography. NMR spectra were recorded on a 400, 500, or 600 MHz instrument and calibrated using residual undeuterated solvent as an internal reference. The following abbreviations (or combinations thereof) are used to explain the multiplicities: s = singlet, d = doublet, t = triplet, q = quartet, quint = quintet, m = multiplet.

General CV Procedures. The experiments were carried out in a conventional three electrode cell using a Potentiostat 600C (CH Instruments, Austin, Texas). A glassy carbon disc (diameter: 1 mm) served as working electrode and a platinum wire as the counter electrode unless otherwise noted. The glassy carbon disc was polished using polishing alumina (0.05 μm) before each experiment. The reference was a $Ag/AgNO_3$ electrode (silver wire in 0.1 M NBu_4BF_4/CH_3CN solution) and this compartment separated from the rest of the cell with a Vycor frit. Bu_4NBF_4 (0.1 M) was employed as supporting electrolyte in a dry acetonitrile solution. The electrolyte was degassed with argon for at least five minutes prior to performing the experiment.

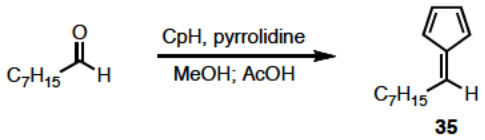

35

5-Octylidenecyclopenta-1,3-diene (6-heptylfulvene) (35). To a solution of octanal (100. mg, 0.780 mmol, 1.0 equiv) in dry methanol (0.780 mL, 1.0 M) was added freshly cracked cyclopentadiene (0.159 mL, 1.95 mmol, 2.5 equiv.). At room temperature, freshly distilled pyrrolidine (0.0960 mL, 1.17 mmol, 1.5 equiv) was added. The reaction was stirred at room temperature until determined to be complete by TLC (approximately 15 min). Glacial acetic acid (0.0730 mL, 1.25 mmol, 1.6 equiv) was added slowly to the reaction mixture. The crude reaction mixture was poured into water (2 mL) and extracted with ether (3 x 2 mL). The combined organic extracts were washed with $NaHCO_3$ (5 mL), water (5 mL) and brine (5 mL), dried over $MgSO_4$, and concentrated *in vacuo*. The fulvene was purified by flash

column chromatography, eluting with 100% pentane, to afford the product (125 mg, 0.709 mmol, 91%) as a bright yellow liquid. TLC: (100% pentane) R_f^{SM} = 0.05 (red), R_f^{PROD} = 0.6 (blue, UV). ^{1}H NMR (500 MHz; $CDCl_3$): δ 6.55 (dt, *J* = 3.6, 1.7 Hz, 1H), 6.52-6.51 (m, 1H), 6.46 (t, *J* = 5.6 Hz, 1H), 6.43 (t, *J* = 8.0 Hz, 1H), 6.21 (dt, *J* = 5.1, 1.7 Hz, 1H), 2.52 (t, *J* = 7.5 Hz, 2H), 1.55-1.52 (m, 2H), 1.35-1.28 (m, 8H), 0.89 (t, *J* = 6.5 Hz, 3H); ^{13}C NMR (125 MHz; $CDCl_3$): δ 146.1, 143.7, 133.1, 130.9, 125.8, 119.4, 32.0, 31.3, 29.7, 29.5, 29.3, 22.9, 14.3; IR (neat, cm^{-1}): 3102, 3071, 2955, 2924, 2781, 1651, 1458, 1377, 1339, 1134, 899, 818; HRMS (EI) calcd for $[C_{13}H_{20}]^+$ 176.1565, found 176.1564.

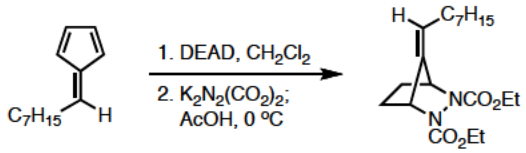

35 **36**

N,N′-Dicarboethoxy-2,3-diaza-7-(octylidene)-bicyclo[2.2.1]heptane (36). A solution of fulvene (80.0 mg, 0.454 mmol, 1.0 equiv) in dry dichloromethane (1.82 mL, 0.25 M) was prepared. Diethyl azodicarboxylate (0.0750 mL, 0.477 mmol, 1.05 equiv) was added at room temperature. The reaction was stored in the freezer at 0 °C. After 12 hours, dipotassium azodicarboxylate (881 mg, 4.54 mmol, 10 equiv) was added to the solution. For reactions of >1 g, a mechanical stirrer was installed. The reaction was cooled to 0 °C. Glacial acetic acid (0.400 mL, 6.81 mmol, 15 equiv) was added dropwise to the reaction mixture over 45 minutes. The reaction mixture was stirred for an additional four hours at 0 °C and then filtered through a sintered glass funnel, which was subsequently rinsed with ether (10 mL). The crude

reaction mixture was neutralized with $NaHCO_3$ (15 mL), dried over $MgSO_4$, and concentrated *in vacuo*. The crude biscarbamate was carried on to the next reaction as a foamy white solid (158 mg, 0.448 mmol, 98%). Due to "dynamic" processes involving the ethyl carbamate moiety, significantly broadened signals appeared in the NMR; thus, characteristic peaks were identified and no further characterization was carried out. TLC: *step 1*: (50% ether in pentane) R_f^{SM} = 0.99 (blue, UV), R_f^{DEAD} = 0.6 (yellow), R_f^{PROD} = 0.3 (purple); *step 2*: (50% ether in pentane) R_f^{PROD} = 0.3 (blue). ^{1}H NMR (600 MHz; $CDCl_3$): δ 6.56 (s, 2H), 5.30 (d, J = 0.4 Hz, 1H), 4.18 (q, J = 7.1 Hz, 6H), 2.03 (dt, J = 12.2, 6.4 Hz, 2H), 1.85 (t, J = 0.6 Hz, 2H), 1.25 (m, 18H), 0.85 (d, J = 7.1 Hz, 3H).

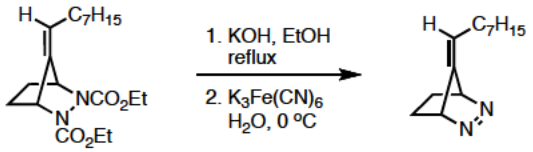

36 **37**

2,3-Diaza-7-(octylidene-1-d)-bicyclo[2.2.1]hept-2-ene (37). A solution of biscarbamate (158 mg, 0.448 mmol, 1.0 equiv) in dry ethanol (4.48 mL, 0.10 M) was prepared in a 3-neck round-bottomed flask and degassed by bubbling Ar through the solution while stirring for 30 minutes. Potassium hydroxide pellets (447 mg, 7.97 mmol, 17.8 equiv) were added at room temperature. A reflux condenser was attached and the reaction mixture was heated to reflux for 2.5 hours. The yellow-colored solution was then cooled to 0 °C. An addition funnel was attached and a solution of potassium ferricyanide powder (481 mg, 1.46 mmol, 3.25 equiv) in deionized water (3.84 mL, 0.38 M) was added dropwise over 30 minutes. The

reaction was stirred for an additional 2.5 hours at 0 °C. The mustard yellow, chalky mixture was then poured into water (20 mL) and ether (20 mL). If necessary, additional water was added to completely dissolve any remaining solids in order to avoid emulsion formation during extraction. The aqueous layer was extracted with ether (7 x 10 mL). The combined organic extracts were washed with brine (50 mL), dried over $MgSO_4$, and concentrated *in vacuo*. The diazene was purified by flash column chromatography, eluting with a 15–25% ether/pentane gradient as a light yellow oil (480. mg, 0.232 mmol, 52%). TLC: *step 1:* (50% ether in pentane) R_f^{SM} = 0.3 (blue), R_f^{PROD} = 0.0 (white/no stain); *step 2:* (25% ether in pentane) R_f^{PROD} = 0.5 (lime green, UV). ^{1}H NMR (500 MHz; $CDCl_3$): δ 5.41 (d, *J* = 2.2 Hz, 1H), 5.13 (dt, *J* = 4.6, 2.6 Hz, 2H), 2.04-1.92 (m, 2H), 1.71-1.60 (m, 2H), 1.36-1.21 (m, 10H), 1.15-1.10 (m, 2H), 0.90 (t, *J* = 7.0 Hz, 3H); ^{13}C NMR (150 MHz; $CDCl_3$): δ 144.8, 117.9, 77.1, 72.9, 32.0, 29.6, 29.3, 29.2, 29.2, 22.9, 21.8, 21.3, 14.3; IR (neat, cm^{-1}): 3019, 2926, 2855, 1479, 1456, 1377, 1285, 1273, 1113; HRMS (ESI) calcd for $[(C_{13}H_{22}N_2) + Na]^+$ 229.1681, found 229.1678.

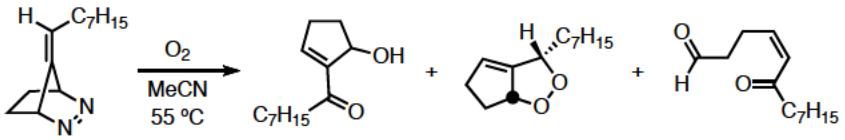

37 **38** **39** **40**

Pyrolysis of diazene 37 in the presence of molecular oxygen: formation of 38, 39, and 40. A round-bottomed flask containing an internal tube with a sintered glass tip of medium porosity (Figure 1SI) and condenser were dried in a vacuum oven overnight and subsequently cooled under argon. A solution of diazene (175 mg,

0.848 mmol, 1.0 equiv) in dry acetonitrile (17.0 mL, 0.05 M) was added to the reaction vessel and oxygen was bubbled through the solution for 10 minutes. The solution was heated to 55 °C, with continuous oxygen flow, until the presence of compounds **10**, **11**, and **12** were visualized by TLC. After cooling to room temperature, the crude acetonitrile solution was extracted with pentane (5 x 20 mL) to avoid heating and further reaction progress during evaporation of the solvent. The combined pentane extracts were concentrated *in vacuo*. The products (135 mg, 0.642 mmol, 76%) were separated and purified by, first, performing a prep-TLC with 5% ether in pentane to isolate the peroxide and then 10% ether in pentane to isolate the keto-alcohol and keto-aldehyde. Recovered starting material accounted for an additional 25.0 mg (14%) of the recovered mass and was isolated in the first prep-TLC. TLC: (25% ether in pentane) R_f^{SM} = 0.5 (lime green, UV), $R_f^{PEROXIDE}$ = 0.95 (brown, light UV), $R_f^{KETO\text{-}ALD}$ = 0.25 (blue, UV), $R_f^{KETO\text{-}ALC}$ = 0.2 (maroon, UV).

2-Heptyl-3,4-dioxabicyclo[3.3.0]oct-1(8)-ene (39). 32.0 mg, 0.152 mmol, 18% yield. ^{1}H NMR (600 MHz; $CDCl_3$): δ 5.58 (dq, *J* = 3.5, 1.8 Hz, 1H), 5.34-5.31 (m, 1H), 4.57-4.54 (m, 1H), 2.89 (dtdd, *J* = 16.0, 8.0, 3.8, 2.0 Hz, 1H), 2.76 (ddddd, *J* = 16.0, 8.0, 3.3, 2.2, 1.1 Hz, 1H), 2.21-2.17 (m, 1H), 1.81 (dtd, *J* = 12.6, 9.3, 7.3 Hz, 1H), 1.74-1.63 (m, 2H), 1.48-1.39 (m, 2H), 1.34-1.23 (m, 8H), 0.87 (t, *J* = 7.1 Hz, 3H); ^{13}C NMR (150 MHz; $CDCl_3$): δ 157.1, 121.7, 91.6, 78.5, 38.8, 34.6, 32.0, 30.6, 29.7, 29.4, 26.3, 22.9, 14.3; IR (neat, cm^{-1}): 3063, 2928, 2855, 1620, 1559, 1501, 1458, 1049; HRMS (ESI) calcd for $[C_{13}H_{22}O_2 + Na]^+$ 233.1517, found 233.1521.

1-(5-Hydroxycyclopent-1-enyl)octan-1-one (38). 91.0 mg, 0.434 mmol, 51% yield. ^{1}H NMR (600 MHz; $CDCl_3$): δ 6.83 (t, *J* = 2.5 Hz, 1H), 5.12 (t, *J* = 6.0 Hz, 1H), 3.10 (s, 1H), 2.71-2.63 (m, 3H), 2.46-2.40 (m, 1H), 2.34-2.29 (m, 1H), 1.84-1.79 (m, 1H), 1.61 (dd, *J* = 14.7, 7.4 Hz, 2H), 1.32-1.21 (m, 8H), 0.87 (t, *J* = 7.0 Hz, 3H); ^{13}C NMR (125 MHz; $CDCl_3$): δ 201.1, 145.7, 132.8, 75.9, 39.3, 31.9, 31.5, 31.3, 29.5, 29.3, 24.6, 22.8, 14.3; IR (neat, cm^{-1}): 3468, 3059, 2955, 2928, 2855, 1663, 1616, 1462, 1377, 1180, 1053, 984; HRMS (FI) calcd for $[C_{13}H_{22}O_2]^+$ 210.1620, found 210.1611.

(*Z*)-6-Oxotridec-4-enal (40). 12.0 mg, 0.0571 mmol, 7% yield. ^{1}H NMR (600 MHz; $CDCl_3$): δ 9.76 (t, *J* = 1.4 Hz, 1H), 6.17 (dt, *J* = 11.4, 1.4 Hz, 1H), 6.07 (dt, *J* = 11.4, 7.5 Hz, 1H), 2.89 (qd, *J* = 7.3, 1.3 Hz, 2H), 2.60 (td, *J* = 7.1, 1.3 Hz, 2H), 2.44 (t, *J* = 7.4 Hz, 2H), 1.57 (t, *J* = 7.2 Hz, 2H), 1.28-1.24 (m, 8H), 0.86 (t, *J* = 6.9 Hz, 3H); ^{13}C NMR (150 MHz; $CDCl_3$): δ 202.0, 201.7, 145.4, 127.9, 44.5, 43.4, 31.9, 29.4, 29.3, 24.2, 22.8, 22.5, 14.3; IR (neat, cm^{-1}): 3060, 2955, 2928, 2855, 2724, 1721, 1690, 1655, 1620, 1458, 1408, 1130, 1076; HRMS (ESI) calcd for $[(C_{13}H_{22}O_2) + Na]^+$ 233.1517, found 233.1515.

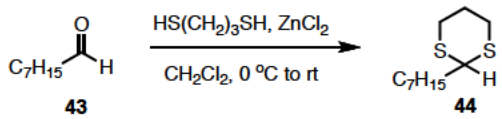

43 **44**

2-Heptyl-1,3-dithiane (44). A solution of octanal (12.2 mL, 78.0 mmol, 1.0 equiv) in dry dichloromethane (78.0 mL, 1.0 M) was prepared. Propane-1,3-dithiol (7.83 mL, 78.0 mmol, 1.0 equiv) was added and the resulting mixture was stirred at room

temperature for 1 hour. Zinc chloride (5.21 g, 38.2 mmol, 0.49 equiv) was added portion-wise at 0 °C, and the reaction mixture was allowed to warm to room temperature slowly. After stirring for an additional 15 hours, the colorless, cloudy solution was washed with water (3 x 20 mL), a 7% KOH solution (3 x 20 mL), and water (3 x 20 mL). The crude reaction mixture was dried over Na_2SO_4, filtered, and concentrated *in vacuo*. No purification of the crude product was necessary, yielding the dithiane as a pale yellow liquid (17.0 g, 77.8 mmol, 99%). TLC: (10% ether in pentane) R_f^{SM} = 0.4 (blue), R_f^{PROD} = 0.5 (yellow). ^{1}H NMR (500 MHz; $CDCl_3$): 4.04 (t, J = 6.9 Hz, 1H), 2.90-2.79 (m, 4H), 2.13-2.08 (m, 1H), 1.89-1.80 (m, 1H), 1.75-1.71 (m, 2H), 1.52-1.46 (m, 2H), 1.31-1.22 (m, 8H), 0.87 (t, J = 7.0 Hz, 3H); ^{13}C NMR (125 MHz; $CDCl_3$): δ 47.9, 35.7, 32.0, 30.8, 29.4, 29.3, 26.9, 26.3, 22.9, 14.3; IR (neat, cm^{-1}): 2951, 2928, 2854, 1462, 1420, 1377, 1273, 1180, 907; HRMS (FI) calcd for $[C_{11}H_{22}S_2]^+$ 218.1163, found 218.1139.

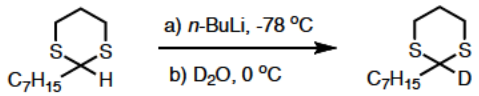

44 **45**

2-Heptyl-1,3-dithiane-2-d (45). A solution of dithiane (5.00 g, 22.9 mmol, 1.0 equiv) in dry THF (58.7 mL, 0.39 M) was prepared and cooled to –78 °C. A 2.05 M solution of *n*-BuLi in hexanes (11.7 mL, 24.0 mmol, 1.05 equiv) was added dropwise and the resulting mixture was allowed to warm to room temperature slowly. After stirring for 1.5 hours, the reaction mixture was cooled to 0 °C and deuterium oxide (3.92 mL, 196 mmol, 8.55 equiv) was added all at once. The crude

reaction was warmed to room temperature and extracted with ether (3 x 15 mL). The combined organic extracts were washed with water (3 x 25 mL), a 7% KOH solution (3 x 25 mL), and water (3 x 25 mL). The crude reaction mixture was dried over Na_2SO_4, filtered, and concentrated *in vacuo*. The deuterated dithiane from three 5.00 g reactions was combined and distilled (115-118 °C, 5 torr), yielding a clear, colorless liquid (13.4 g, 61.1 mmol, 89%). ^{1}H NMR (500 MHz; $CDCl_3$): δ 2.90-2.79 (m, 4H), 2.11 (dtt, J = 14.1, 4.7, 2.4 Hz, 1H), 1.90-1.81 (m, 1H), 1.81-1.71 (m, 2H), 1.49 (quintet, J = 7.5 Hz, 2H), 1.32-1.21 (m, 8H), 0.87 (t, J = 7.0 Hz, 3H); ^{13}C NMR (125 MHz; $CDCl_3$): δ 47.9, 35.6, 31.9, 30.7, 29.4, 29.2, 26.8, 26.3, 22.8, 14.3; IR (neat, cm^{-1}): 2953, 2924, 2854, 1456, 1422, 1275; HRMS (FI) calcd for $[C_{11}H_{21}DS_2]^+$ 219.1226, found 219.1220.

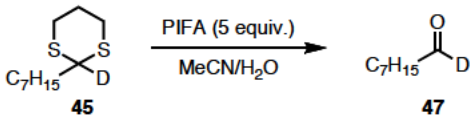

Octanal-1-d (47). To a solution of deuterated dithiane (100. mg, 0.456 mmol, 1.0 equiv) in a 9:1 mixture of acetonitrile and water (0.460 mL, 1.0 M) was added PIFA (391 mg, 0.912 mmol, 2.0 equiv). The reaction mixture was stirred at room temperature until found to be complete by TLC (approximately 35 min). The light yellow solution was neutralized with $NaHCO_3$ and extracted with ether (3 x 5 mL). The combined organic extracts were dried over $MgSO_4$, filtered, and concentrated *in vacuo*. The deuterated octanal was purified by flash column chromatography, eluting with 5%–10% gradient of ether in pentane as a light yellow oil (56.0 mg,

0.433 mmol, 95%). TLC: (10% ether in pentane) R_f^{SM} = 0.5 (yellow), R_f^{PROD} = 0.4 (blue). ^{1}H NMR (500 MHz; $CDCl_3$): δ 2.41 (t, *J* = 7.4 Hz, 2H), 1.62 (quintet, *J* = 7.2 Hz, 2H), 1.31-1.25 (m, 8H), 0.88 (t, *J* = 6.9 Hz, 3H); ^{13}C NMR (125 MHz; $CDCl_3$): δ 203.0, 44.10, 43.9, 31.8, 29.2, 22.8, 22.3, 14.3; IR (neat, cm^{-1}): 2955, 2924, 2854, 1716, 1464, 1456, 1378; HRMS (EI) calcd for $[C_8H_{15}DO]^+$ 129.1264, found 129.1268.

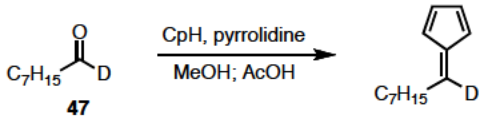

5-(Octylidene-1-d)cyclopenta-1,3-diene (6-Heptylfulvene-6-d). See experimental for compound **35** (60.0 mg, 0.338 mmol, 74%). ^{1}H NMR (500 MHz; $CDCl_3$): δ 6.55-6.51 (m, 2H), 6.47-6.41 (m, 1H), 6.21 (dt, *J* = 5.1, 1.7 Hz, 1H), 2.52 (t, *J* = 7.1 Hz, 2H), 1.53 (quintet, *J* = 7.4 Hz, 2H), 1.37-1.26 (m, 8H), 0.88 (t, *J* = 7.0 Hz, 3H); ^{13}C NMR (125 MHz; $CDCl_3$): δ 145.9, 143.6, 133.1, 130.8, 125.7, 119.3, 32.0, 31.2, 29.7, 29.6, 29.4, 22.9, 14.4; IR (neat, cm^{-1}): 3099, 3074, 2956, 2925, 2855, 1638, 1471, 1455, 1363, 1078, 886, 772, 766; HRMS (FI) calcd for $[C_{13}H_{19}D]^+$ 177.1628, found 177.1634.

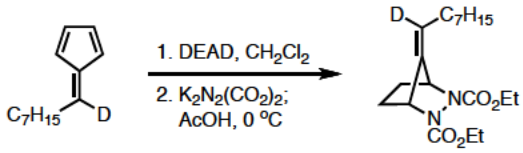

N,N′-Dicarboethoxy-2,3-diaza-7-(octylidene-1-d)-bicyclo[2.2.1]heptane. The procedure is the same as that for **36** with exception that the second step, starting with

the addition of dipotassium azodicarboxylate, is carried out after 1 hour instead of 12 hours. The crude biscarbamate was used in the next reaction as a foamy white solid (151 mg, 0.427 mmol, 130%). Due to "dynamic" processes of the ethyl carbamate subunit, significantly broadened signals appeared in the NMR; thus, characteristic peaks were identified and no further characterization was carried out. TLC: *step 1*: (50% ether in pentane) R_f^{SM} = 0.99 (blue, UV), R_f^{DEAD} = 0.6 (yellow), R_f^{PROD} = 0.3 (purple); *step 2*: (50% ether in pentane) R_f^{PROD} = 0.3 (blue). ^{1}H NMR (400 MHz; $CDCl_3$): δ 6.56 (s, 2H), 4.21 (q, *J* = 7.1 Hz, 4H), 2.05 (td, *J* = 7.1, 2.1 Hz, 2H), 1.89-1.80 (m, 2H), 1.28 (t, *J* = 7.1 Hz, 18H), 0.87 (t, *J* = 6.9 Hz, 3H); HRMS (ESI) calcd for $[(C_{19}H_{31}DN_2O_4) + Na]^+$ 376.2323, found 376.2314.

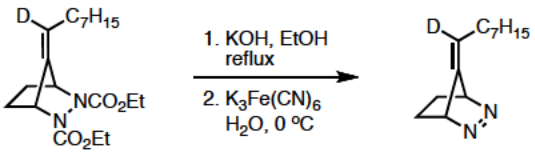

37-d$_1$

2,3-Diaza-7-(octylidene-1-d)-bicyclo[2.2.1]hept-2-ene (37-d$_1$). See experimental for compound **9** (30.0 mg, 0.145 mmol, 68%). ^{1}H NMR (500 MHz; $CDCl_3$): δ 5.39 (d, *J* = 2.6 Hz, 1H), 5.12-5.11 (m, 1H), 2.02-1.91 (m, 2H), 1.66-1.62 (m, 2H), 1.33-1.22 (m, 10H), 1.11 (dd, *J* = 9.4, 1.8 Hz, 2H), 0.89 (t, *J* = 14.0 Hz, 3H); ^{13}C NMR (125 MHz; $CDCl_3$): δ 144.6, 117.8, 72.9, 32.1, 30.0, 29.6, 29.3, 29.2, 29.16, 22.9, 21.8, 21.4, 14.4; IR (neat, cm^{-1}): 3018, 2950, 2925, 2854, 1455, 1278, 1114, 926; HRMS (ESI) calcd for $[C_{13}H_{21}DN_2 + Na]^+$ 230.1743, found 230.1740.

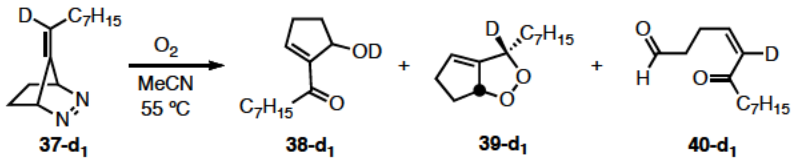

37-d$_1$ **38-d$_1$** **39-d$_1$** **40-d$_1$**

Pyrolysis of diazene 37-d$_1$ in the presence of molecular oxygen: formation of 38-d$_1$, 39-d$_1$, and 40-d$_1$. See experimental for compound **37** (63.0 mg, 0.300 mmol, 67%).

2-Heptyl-3,4-dioxabicyclo[3.3.0]oct-1(8)-ene-2-d (39-d$_1$). 33.0 mg, 0.157 mmol, 39%. ^{1}H NMR (600 MHz; $CDCl_3$): δ 5.59 (t, *J* = 1.7 Hz, 1H), 5.34-5.31 (m, 1H), 2.93-2.87 (m, 1H), 2.79-2.74 (m, 1H), 2.20 (dt, *J* = 12.7, 6.3 Hz, 1H), 1.85-1.80 (m, 1H), 1.69 (dqd, *J* = 18.3, 9.2, 5.5 Hz, 2H), 1.49-1.41 (m, 2H), 1.35-1.27 (m, 8H), 0.88 (t, *J* = 7.0 Hz, 3H); ^{13}C NMR (150 MHz; $CDCl_3$): δ 157.0, 121.8, 91.5, 78.5, 38.8, 34.5, 32.0, 30.6, 29.7, 29.4, 26.2, 22.9, 14.3; IR (neat, cm^{-1}): 3057, 2928, 2862, 1464, 1318, 1046, 817.67; HRMS (ESI) calcd for $[C_{13}H_{21}DO_2 + Na]^+$ 234.1580, found 234.1577.

1-(5-Hydroxycyclopent-1-enyl)octan-1-one (38-d$_1$). 16.0 mg, 0.0761 mmol, 19%. ^{1}H NMR (600 MHz; $CDCl_3$): δ 6.84 (t, *J* = 2.6 Hz, 1H), 5.14-5.12 (m, 1H), 3.09 (s, 1H), 2.67 (td, *J* = 7.5, 3.2 Hz, 3H), 2.48-2.42 (m, 1H), 2.33 (dddd, *J* = 13.7, 8.8, 7.9, 4.1 Hz, 1H), 1.86-1.80 (m, 1H), 1.65-1.60 (m, 2H), 1.31-1.25 (m, 8H), 0.88 (t, *J* = 7.0 Hz, 3H); ^{13}C NMR (151 MHz; $CDCl_3$): δ 201.1, 146.0, 145.8, 75.9, 39.3, 31.9, 31.5, 31.3, 29.5, 29.3, 24.6, 22.8, 14.3; IR (neat, cm^{-1}): 3441, 3028, 2955, 2928, 2051, 1667, 1651, 1616, 1512, 1458, 1373, 1049; HRMS (ESI) calcd for $[C_{13}H_{22}O_2 + Na]^+$ 233.1517, found 233.1519.

(*Z*)-6-Oxotridec-4-enal-5-d (40-d_1). 14.0 mg, 0.0665 mmol, 17%. ^{1}H NMR (600 MHz; $CDCl_3$): δ 9.78 (t, *J* = 1.4 Hz, 1H), 6.08 (dd, *J* = 9.5, 4.6 Hz, 1H), 2.92-2.88 (m, 2H), 2.62 (td, J = 7.08, 2.35 Hz, 2H), 2.45 (t, *J* = 7.4 Hz, 2H), 1.61-1.57 (m, 2H), 1.30-1.25 (m, 8H), 0.88 (t, *J* = 7.0 Hz, 3H); ^{13}C NMR (150 MHz; $CDCl_3$): δ 202.0, 201.7, 145.3, 127.9, 44.5, 43.4, 31.9, 29.4, 29.3, 24.1, 22.8, 22.4, 14.3; IR (neat, cm^{-1}): 3024, 2955, 2924, 2855, 2816, 2716, 1728, 1682, 1613, 1408, 1373, 1149, 1080; HRMS (ESI) calcd for $[C_{13}H_{21}DO_2 + Na]^+$ 234.1580, found 234.1580.

General procedure for ^{1}H NMR analysis of peroxide or diazene decomposition: A J young NMR tube was dried in a vacuum oven overnight and subsequently cooled under argon. A solution of the substrate in dry acetonitrile-d_3 was added to the NMR tube and oxygen was bubbled through the solution for 20 minutes. The NMR tube was sealed and an initial ^{1}H NMR spectrum was obtained as a baseline measurement. The solution was heated to 55 °C in an oil bath and subsequent ^{1}H NMR spectra were recorded at 30-minute intervals with an ice bath "quench" before each analysis.

Quantum calculations. Calculations carried out at UCSB used Spartan 08 for Macintosh software. Geometries were optimized using the B3LYP/6-31+G(d) method. The transition structure was characterized by a frequency calculation for which there was one and only one imaginary frequency. That the transition structure was an accurate representation for the conversion of the peroxide to the unsaturated keto-aldehyde was verified using an intrinsic reaction coordinate (IRC) calculation that was carried out by Professor D. J. Tantillo at UC Davis.

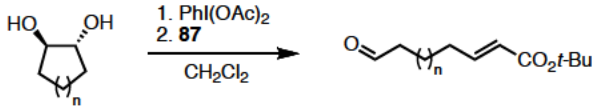

84
n = 1, 2

85

(*E*)-*tert*-butyl 7-oxohept-2-enoate (85, n = 1).[138] *See reference* (0.140 g, 0.706 mmol, 72%). ^{1}H NMR (500 MHz; CDCl3): δ 9.75 (s, 1H), 6.79 (dt, *J* = 15.6, 7.0 Hz, 1H), 5.74 (dt, *J* = 15.6, 1.5 Hz, 1H), 2.46 (td, *J* = 7.3, 1.3 Hz, 2H), 2.20 (qd, *J* = 7.3, 1.2 Hz, 2H), 1.78 (quintet, *J* = 7.4 Hz, 2H). ^{13}C NMR (151 MHz; $CDCl_3$): δ 201.9, 166.0, 146.4, 124.2, 80.5, 43.2, 31.3, 20.6; HRMS (ESI) calcd for $[C_{11}H_{18}O_3 + Na]^+$ 221.1154, found 221.1158.

(*E*)-*tert*-butyl 8-oxooct-2-enoate (85, n = 2).[138] *See reference* (0.154 g, 0.723 mmol, 84%). ^{1}H NMR (600 MHz; $CDCl_3$): δ 9.75 (t, *J* = 1.6 Hz, 1H), 6.81 (dt, *J* = 15.6, 7.0 Hz, 1H), 5.73 (dt, *J* = 15.6, 1.5 Hz, 1H), 2.44 (td, *J* = 7.3, 1.5 Hz, 2H), 2.21-2.17 (m, 4H), 1.67-1.62 (m, 2H). ^{13}C NMR (126 MHz; CDCl3): δ 202.2, 166.0, 147.1, 123.6, 80.2, 43.8, 31.9, 28.4, 27.7, 21.8.

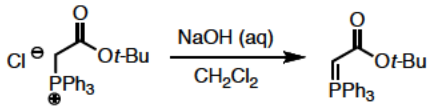

87

***tert*-Butyl 2-(triphenylphosphoranylidene)acetate (87).**[139] A 250 mL separatory funnel was charged with *t*-butyl 2-(triphenylphosphonium)acetate chloride (5.37 g, 13.0 mmol), dry $CHCl_3$ (39.0 mL), and aqueous 2 N NaOH solution (39.0 mL) and the mixture was shaken gently for 5 min. The organic phase was separated, dried over MgSO4, and concentrated in vacuo. The viscous residue was dissolved in 5 mL

of CH2Cl2, and the resulting solution was added 100% hexane (150 mL) upon vigorously stirring. The resulting white suspension was condensed in vacuo to give product III-17 (4.812 g, 98.4%) as a white powder which was used for the next step without further purification. The ^{1}H NMR was consistent with the published spectrum. ^{1}H NMR ($CDCl_3$, 400 MHz) δ 7.70-7.62 (m, 6 H), 7.55-7.51 (m, 3 H), 7.49-7.41 (m, 6 H), 2.69 (br s, 1 H), 1.22 (br s, 9 H).

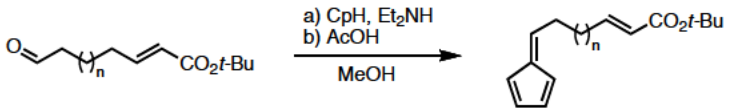

85 **86**

Fulvenes (86). See experimental for compound **35**. The procedure is the same as that for **35** with the exception that freshly distilled Et_2NH (3.0 equiv) was used in place of the pyrrolidine.

(*E*)-*tert*-butyl 7-(cyclopenta-2,4-dienylidene)hept-2-enoate (n = 1). (0.144 g, 0.586 mmol, 83%). ^{1}H NMR (500 MHz; $CDCl_3$): δ 6.84 (dt, *J* = 15.6, 7.0 Hz, 1H), 6.54 (td, *J* = 3.4, 1.7 Hz, 1H), 6.48-6.45 (m, 1H), 6.36 (t, *J* = 7.9 Hz, 1H), 6.19 (dt, *J* = 5.1, 1.7 Hz, 1H), 5.75 (dt, *J* = 15.6, 1.5 Hz, 1H), 2.55 (t, *J* = 11.3 Hz, 2H), 2.25-2.20 (m, 2H), 1.69 (quintet, *J* = 7.5 Hz, 2H). ^{13}C NMR (126 MHz; $CDCl_3$): δ 166.2, 147.1, 146.7, 141.9, 133.5, 131.2, 125.8, 123.9, 119.3, 80.3, 31.7, 30.6, 28.4, 28.0; IR (neat, cm^{-1}): 3075, 2976, 2933, 2862, 1713, 1650, 1474, 1456, 1367, 1156, 981, 767; HRMS (ESI) calcd for $[C_{16}H_{22}O_2 + Na]^+$ 269.1517, found 269.1505.

(*E*)-*tert*-butyl 8-(cyclopenta-2,4-dienylidene)oct-2-enoate (n = 2). (0.216 g, 0.830 mmol, 98%). ^{1}H NMR (500 MHz; $CDCl_3$): δ 6.84 (dt, *J* = 15.6, 7.0 Hz, 1H), 6.55

(dq, J = 5.3, 1.7 Hz, 1H), 6.50-6.46 (m, 2H), 6.39 (t, J = 7.9 Hz, 1H), 6.20 (dt, J = 5.2, 1.7 Hz, 1H), 5.74 (dt, J = 15.6, 1.5 Hz, 1H), 2.54 (q, J = 7.4 Hz, 2H), 2.20 (qd, J = 7.1, 1.4 Hz, 2H), 1.59-1.50 (m, 4H). ^{13}C NMR (126 MHz; $CDCl_3$): δ 166.2, 147.6, 146.4, 142.6, 133.4, 131.1, 125.8, 123.5, 119.3, 80.3, 32.1, 31.1, 29.2, 28.5, 28.1; IR (neat, cm^{-1}): 3074, 2956, 2930, 1715, 1650, 1471, 1455, 1363, 1078; HRMS (FI) calcd for $[C_{17}H_{24}O_2]^+$ 260.1776, found 260.1781.

General procedure for bulk electrolysis of fulvenes 84 (n = 3, 4). An H-cell (Figure 2SI) with a stir bar in each of the two chambers, connected by a fine porosity glass frit, was dried in a vacuum oven for 4 hours and then cooled under argon. During that time, a 0.1 M solution of the supporting electrolyte, Et_4NOTs, in dry acetonitrile (0.01 M relative to the fulvene) was degassed by bubbling with argon for 25-30 minutes. The anode and cathode chambers were equipped with freshly cleaned carbon rods and an equal volume of the supporting electrolyte solution was added to each chamber. To the cathode chamber was added the fulvene (1 equiv) and proton donor, dimethyl phenol (2 equiv), and the reference electrode (Ag/0.1 M $AgNO_3$) was positioned as close to the cathode as possible. The fixed potential (–2.7 V) was applied until the theoretical number of coulombs were consumed, or until complete conversion of the fulvene was observed by TLC. The cathode solution was removed and extracted with pentane (3 x twice the volume of MeCN). If product was still present in the acetonitrile layer, as determined by TLC, additional extractions were performed. The combined pentane extracts were washed once with 3 N NaOH to remove dimethyl phenol, once with brine, and then dried over $MgSO_4$.

The dried pentane extracts were concentrated *in vacuo* with careful attention paid to the vacuum pressure so that the volatile products were not also removed. The crude reaction mixture was purified by prep-TLC, isolating the top product mixture spot after two sequential elutions in 5% ether in pentane. The product mixture was then separated by HPLC in a 0.5% THF in hexanes solvent system. TLC: (10% ether in pentane) $R_f^{SM} = 0.5$ (UV, blue), $R_f^{PROD} = 0.8$ (UV, magenta/blue), $R_f^{DMP} = 0.25$ (hot pink).

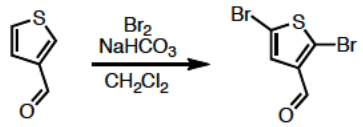

99 **100**

2,5-dibromothiophene-3-carbaldehyde (100).[140] To a solution of thiophene-3-carbaldehyde (1.00 g, 8.91 mmol, 1.0 equiv) in dichloromethane (22.3 mL, 0.40 M) in a 3-neck round-bottom flask was added $NaHCO_3$ (5.61 g, 66.8 mmol, 7.5 equiv). The argon inlet from the Schlenk line to the reaction flask was replaced with an argon-filled balloon and the round-bottom flask was covered in aluminum foil. A solution of Br_2 (3.45 mL, 66.8 mmol, 7.5 equiv) in dichloromethane (66.9 mL, 1.0 M) was added to an addition funnel covered in aluminum foil and then subsequently attached to the 3-neck flask. The Br_2 solution was added *slowly* at a rate of ca. 1 drop every 30-60 seconds. The reaction mixture was stirred at room temperature until found to be complete by TLC (approximately 5 days). The solids were removed by filtering the crude reaction over a pad of Celite. The filtrate was collected and washed with water (200 mL), quenched carefully with aqueous $Na_2S_2O_3$ (2 x 200

mL), and an additional wash with water (200 mL). The organic layer was dried over $MgSO_4$, filtered, and concentrated *in vacuo*. The crude material was carried on without further purification. (1.62 g, 5.97 mmol, 67%). ^{1}H NMR (500 MHz; $CDCl_3$): δ 9.79 (s, 1H), 7.34-7.34 (m, 1H).

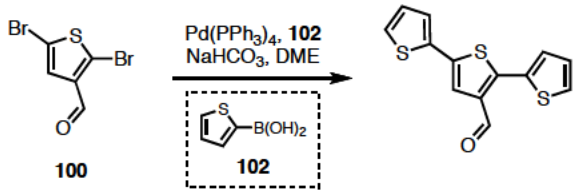

3′-formyl-2,2′:5′,2″-terthiophene.[141] *See reference* (34.0 mg, 0.123 mmol, 81%) ^{1}H NMR (500 MHz; $CDCl_3$): δ 10.09 (s, 1H), 7.57 (s, 1H), 7.49 (dd, *J* = 5.2, 1.2 Hz, 1H), 7.31 (dd, *J* = 3.6, 1.2 Hz, 1H), 7.29 (dd, *J* = 5.1, 1.1 Hz, 1H), 7.23 (dd, *J* = 3.6, 1.2 Hz, 1H), 7.16 (dd, *J* = 5.2, 3.6 Hz, 1H), 7.05 (dd, *J* = 5.1, 3.6 Hz, 1H).

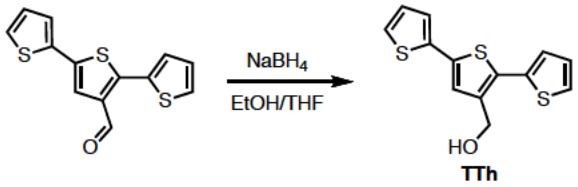

3′-(Hydroxymethyl)-2,2′:5′,2″-terthiophene (TTh).[142] *See reference* (33.0 mg, 0.119 mmol, 97%). ^{1}H NMR (500 MHz; $CDCl_3$): δ 7.35-7.34 (m, 1H), 7.25-7.23 (m, 2H), 7.21 (dt, *J* = 3.6, 0.6 Hz, 1H), 7.19-7.18 (m, 1H), 7.10-7.09 (m, 1H), 7.04-7.02 (m, 1H), 4.76 (d, *J* = 5.8 Hz, 2H), 1.68 (t, *J* = 5.8 Hz, 1H); ^{13}C NMR (126 MHz; $CDCl_3$): δ 138.4, 137.0, 136.2, 134.9, 132.3, 128.11, 128.07, 126.8, 126.3, 126.0, 124.9, 124.1, 59.3

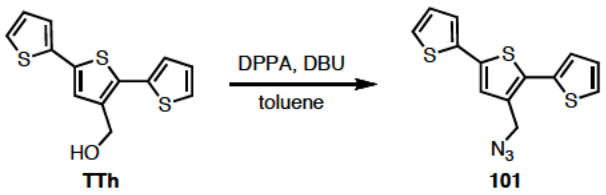

TTh 101

3′-azido-2,2′:5′,2″-terthiophene (101). To a solution of 3′-(Hydroxymethyl)-2,2′:5′,2″-terthiophene (33.0 mg, .119 mmol, 1.0 equiv) in toluene (0.349 mL, 0.34 M) was added diphenylphosphoryl azide (DPPA) (31.0 μL, 0.142 mmol, 1.2 equiv). The reaction mixture was cooled to 0 ºC and DBU (21.0 μL, 0.142 mmol, 1.2 equiv) was added dropwise. The reaction was then warmed to room temperature and stirred overnight before washing with water (2 x 1 mL) and 5% aq. HCl (1 mL). The organic layer was dried over $MgSO_4$, filtered, and concentrated *in vacuo*. The deuterated octanal was purified by prep-TLC, eluting with 15% dichloromethane in pentane as a light yellow amorphous solid (30.0 mg, 0.100 mmol, 84%). ^{1}H NMR (600 MHz; $CDCl_3$): δ 7.38 (dd, J = 5.2, 1.1 Hz, 1H), 7.25 (d, J = 1.1 Hz, 1H), 7.19 (ddd, J = 6.7, 3.6, 1.1 Hz, 2H), 7.16 (s, 1H), 7.11 (dd, J = 5.1, 3.6 Hz, 1H), 7.04 (dd, J = 5.1, 3.6 Hz, 1H), 4.43 (s, 3H). ^{13}C NMR NMR (151 MHz; $CDCl_3$): δ 136.85, 136.70, 134.3, 133.6, 132.8, 128.24, 128.22, 127.3, 126.9, 125.9, 125.3, 124.5, 48.5; IR (neat, cm^{-1}): 3106, 3171, 2924, 2851, 2168, 2095, 1490, 1269, 1184, 964, 833; HRMS (EI) calcd for $[C_{13}H_9N_3S_3]^+$ 302.9959, found 302.9960.

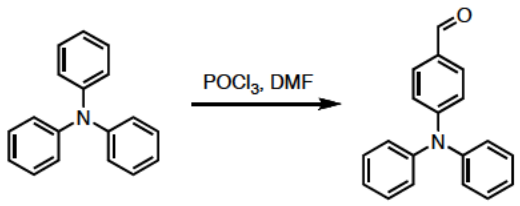

123

4-(diphenylamino)benzaldehyde (123).[143] *See reference* (1.30 g, 4.76 mmol, 39%). ^{1}H NMR (500 MHz; $CDCl_3$): δ 9.82 (s, 1H), 7.70 (d, J = 8.7 Hz, 2H), 7.44-7.43 (m, 4H), 6.93-6.91 (m, 4H).

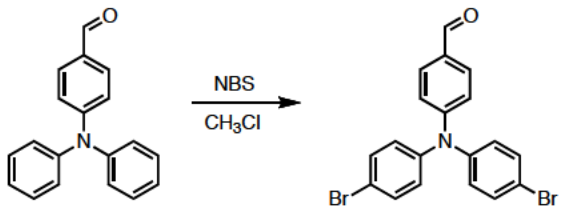

123

4-(bis(4-bromophenyl)amino)benzaldehyde.[144] A solution of **123** (1.21 g, 4.46 mmol, 1.0 equiv) in chloroform (60.0 mL, 0.08 M) was degassed by bubbling Ar through the solution while stirring for 30 minutes. The reaction was cooled to 0 ºC and NBS (1.75 g, 9.81 mmol, 2.2 equiv) was added over four portions in 20 min. intervals. After stirring for an additional hour at 0 ºC, the reaction was heated at reflux for 15 hours. The crude reaction mixture was cooled to room temperature and washed with water (100 mL) and back-extracted with CH_2Cl_2 (50 mL). The combined organic extracts were washed with saturated sodium thiosulfate (100 mL), brine (100 mL), dried over $MgSO_4$, filtered, and concentrated *in vacuo*. The tar-like crude solid was used without further purification. (1.93 g, 4.46 mmol, 100%). ^{1}H

NMR (500 MHz; $CDCl_3$): δ 9.82 (s, 1H), 7.70 (d, J = 8.7 Hz, 2H), 7.44-7.43 (m, 4H), 6.93-6.91 (m, 4H).

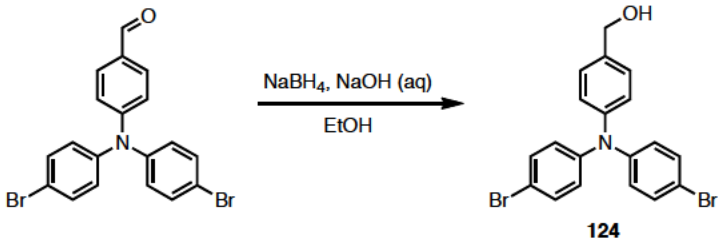

124

(4-(bis(4-bromophenyl)amino)phenyl)methanol (124).[144] *See reference* (1.74 g, 4.01 mmol, 90%). ^{1}H NMR (600 MHz; $CDCl_3$): δ 7.34-7.33 (m, 4H), 7.28 (s, 2H), 7.05 (d, J = 8.5 Hz, 2H), 6.93 (d, J = 8.9 Hz, 4H), 4.65 (s, 2H).

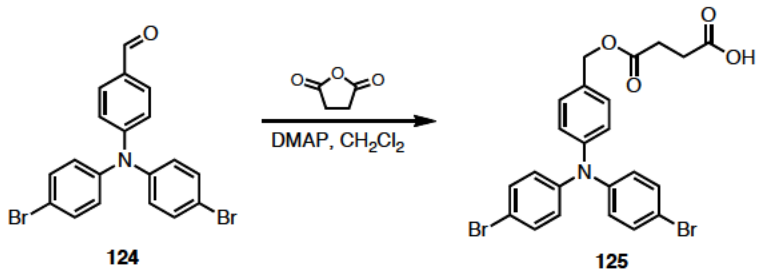

124 **125**

4-(4-(bis(4-bromophenyl)amino)benzyloxy)-4-oxobutanoic acid (125). A solution of **124** (110. mg, 0.254 mmol, 1.0 equiv) in dichloromethane (0.49 mL, 0.50 M) was cooled to 0 °C. A solution of DMAP (93.0 mg, 0.762 mmol, 3.0 equiv) in dichloromethane (0.64 mL, 1.2 M) was added to the amine solution at 0 °C, followed by the addition of a solution of succinic anhydride (76.0 mg, 0.762 mmol, 3.0 equiv) in dichloromethane (3.8 mL, 0.2 M). The reaction mixture was warmed to room temperature and stirred overnight. The crude reaction mixture was quenched with 2 M HCl (~3 mL) and aqueous layer was extracted with CH_2Cl_2 (3 x 5 mL). The

combined organic extracts were dried over $NaSO_4$, filtered, and concentrated *in vacuo*. The amorphous yellow crude solid contained < 10% contaminants (as determined by ^{1}H NMR) and was therefore used without further purification – the extra mass was attributed to trapped solvent/moisture because the fluffy solid turned tar-like upon standing until re-concentrated *in vacuo*. (163 mg, 0.305 mmol, 120%). ^{1}H NMR (500 MHz; $CDCl_3$): (1.30 g, 4.76 mmol, 39%). δ 7.35 (q, J = 4.9 Hz, 4H), 7.23 (d, J = 8.6 Hz, 2H), 7.02 (d, J = 8.6 Hz, 2H), 6.93 (d, J = 4.6 Hz, 4H), 5.09 (s, 2H), 2.71-2.69 (m, 4H).

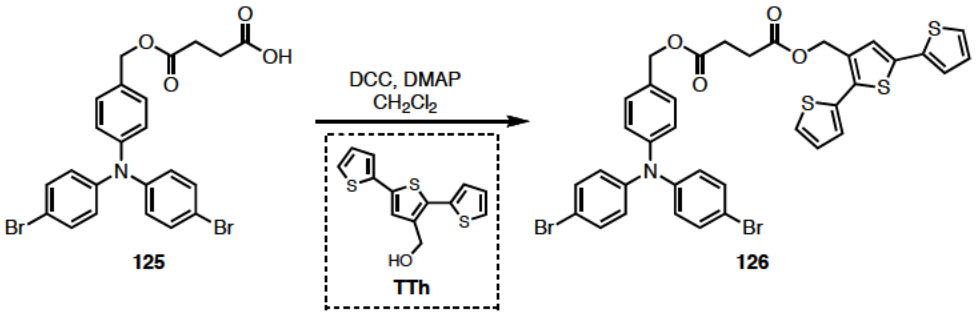

3′-(4-(4-(bis(4-bromophenyl)amino)benzyloxy)-4-oxobutanoxy)-2,2′:5′,2″-terthiophene (126). To a solution of **125** (47.0 mg, 0.0878 mmol, 1.0 equiv) and **TTh** (24.0 mg, 0.0878 mmol, 1 equiv) in ethyl acetate (0.176 mL, 0.5 M) cooled to 0 ºC, was added DMAP (0.100 mg, 0.000878 mmol, 0.010 equiv). A solution of DCC (200. mg, 0.0966 mmol, 1.1 equiv) in ethyl acetate (0.11 mL, 0.85 M) was added to the reaction mixture at 0 ºC. The reaction warmed to room temperature and stirred for an additional 2.5 hours at room temperature. The crude reaction mixture was filtered over a pad of Celite to remove the solids and the filtrate was concentrated *in vacuo*. The crude material was purified using prep-TLC, eluting in a

1:1 mixture of ethyl acetate to hexanes, to yield a pale yellow solid (28.4 mg, 0.0360 mmol, 41%). ^{1}H NMR (500 MHz; $CDCl_3$): δ 7.35-7.32 (m, 4H), 7.23-7.16 (m, 5H), 7.08 (dd, *J* = 5.1, 3.6 Hz, 1H), 7.02-6.98 (m, 3H), 6.93-6.90 (m, 4H), 5.16 (s, 2H), 5.06 (s, 2H), 2.74-2.70 (m, 4H); ^{13}C NMR (151 MHz; $CDCl_3$): δ 172.26, 172.21, 147.2, 146.5, 136.75, 136.71, 136.3, 134.4, 132.9, 132.6, 130.9, 129.9, 128.1, 127.08, 127.05, 126.81, 126.76, 126.6, 125.9, 125.13, 125.09, 124.31, 124.27, 124.16, 116.0, 77.4, 77.2, 77.0, 66.4, 60.6, 29.4; IR (neat, cm^{-1}): 3105, 3068, 3033, 2930, 2853, 1732, 1611, 1578, 1510, 1485, 1311, 1271, 1151, 1071, 1006, 821, 697; HRMS (ESI) calcd for $[C_{36}H_{27}O_4NS_3Br_2 + Na]^+$ 813.9367, found 813.9350.

General procedure for electrochemical polymerization of terthiophene derivatives. In a dried CV cell, a light yellow solution of terthiophene monomer (5.0 mM) and Bu_4NPF_6 (0.1 M) in dry acetonitrile was degassed by bubbling with a constant stream of argon for 10 minutes. The CV set-up was then assembled with a glassy carbon counter electrode, the Ag/0.1 M AgNO3 reference electrode, and carbon paper working electrode. Sweeping ten cycles between +0.4 and +0.95 V at a scan rate of 100 mV/s changed the solution to a bright yellow-green (Figure 3SI) and deposited a visible layer of polymer on the working electrode. The working electrode was removed, rinsed with copious amounts of acetonitrile, to remove residual monomer, and subsequently dried *in vacuo* before further use.

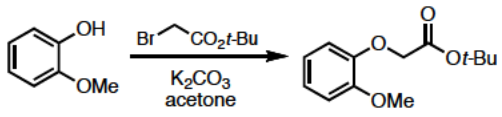

128

***tert*-butyl 2-(2-methoxyphenoxy)acetate (128).**[145] *See reference* (11.7 g, 55.7 mmol 62%). ^{1}H NMR (400 MHz; $CDCl_3$): δ 6.96 (td, J = 7.6, 1.3 Hz, 1H), 6.88 (ddd, J = 15.9, 7.8, 1.7 Hz, 2H), 6.80 (dd, J = 7.9, 1.6 Hz, 1H), 4.58 (s, 2H), 3.88 (s, 3H), 1.47 (s, 9H).

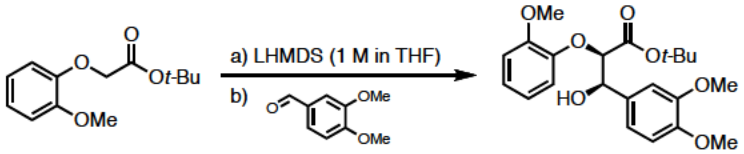

128 **131**

(2*R*,3*R*)-*tert*-butyl 3-(3,4-dimethoxyphenyl)-3-hydroxy-2-(2-methoxyphenoxy) propanoate (131).[145] The procedure follows that as reported in the reference with the exception that LHMDS (1.0 M in THF, 23.1 mL, 23.1 mmol, 1.1 equiv) was used as the base and addition occurred at 0 ºC with rooming to warm temperature after 10 minutes (5.60 g, 13.8 mmol, 60%). ^{1}H NMR (400 MHz; $CDCl_3$): δ 7.11 (d, J = 1.8 Hz, 1H), 7.01-6.97 (m, 2H), 6.93-6.81 (m, 4H), 5.11 (d, J = 4.7 Hz, 1H), 4.66 (d, J = 4.8 Hz, 1H), 3.87 (s, 3H), 3.85 (s, 3H), 3.84 (s, 3H), 1.30 (s, 9H).

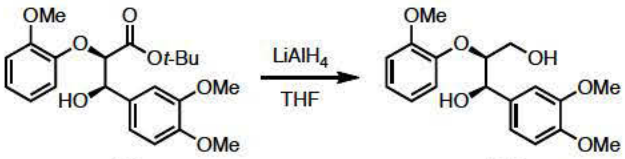

131 132

(1R,2S)-1-(3,4-dimethoxyphenyl)-2-(2-methoxyphenoxy)propane-1,3-diol (132).[145] *See reference* (1.29 g, 3.86 mmol, 78%). ^{1}H NMR (600 MHz; $CDCl_3$): δ 7.08-7.05 (m, 1H), 6.98-6.88 (m, 5H), 6.83 (d, J = 8.3 Hz, 1H), 4.98 (t, J = 4.0 Hz, 1H), 4.16 (ddd, J = 6.0, 4.7, 3.5 Hz, 1H), 3.91 (dd, J = 12.1, 5.7 Hz, 1H), 3.88 (s, 3H), 3.87 (s, 3H), 3.86 (s, 3H), 3.65 (ddd, J = 12.1, 7.8, 3.4 Hz, 1H), 3.43 (d, J = 3.2 Hz, 1H), 2.69 (dd, J = 7.6, 5.5 Hz, 1H).

Figure 1SI. Apparatus used for oxygen trapping reaction.

Figure 2SI. H-cell apparatus used for bulk electrolysis.

(a) "fulvene yellow" cathodic solution (b) "blushing" fulvene cathodic solution

Figure 3SI. Solution color change during electrochemical polymerization.

(a) pre-polymerization solution (b) post-polymerization solution

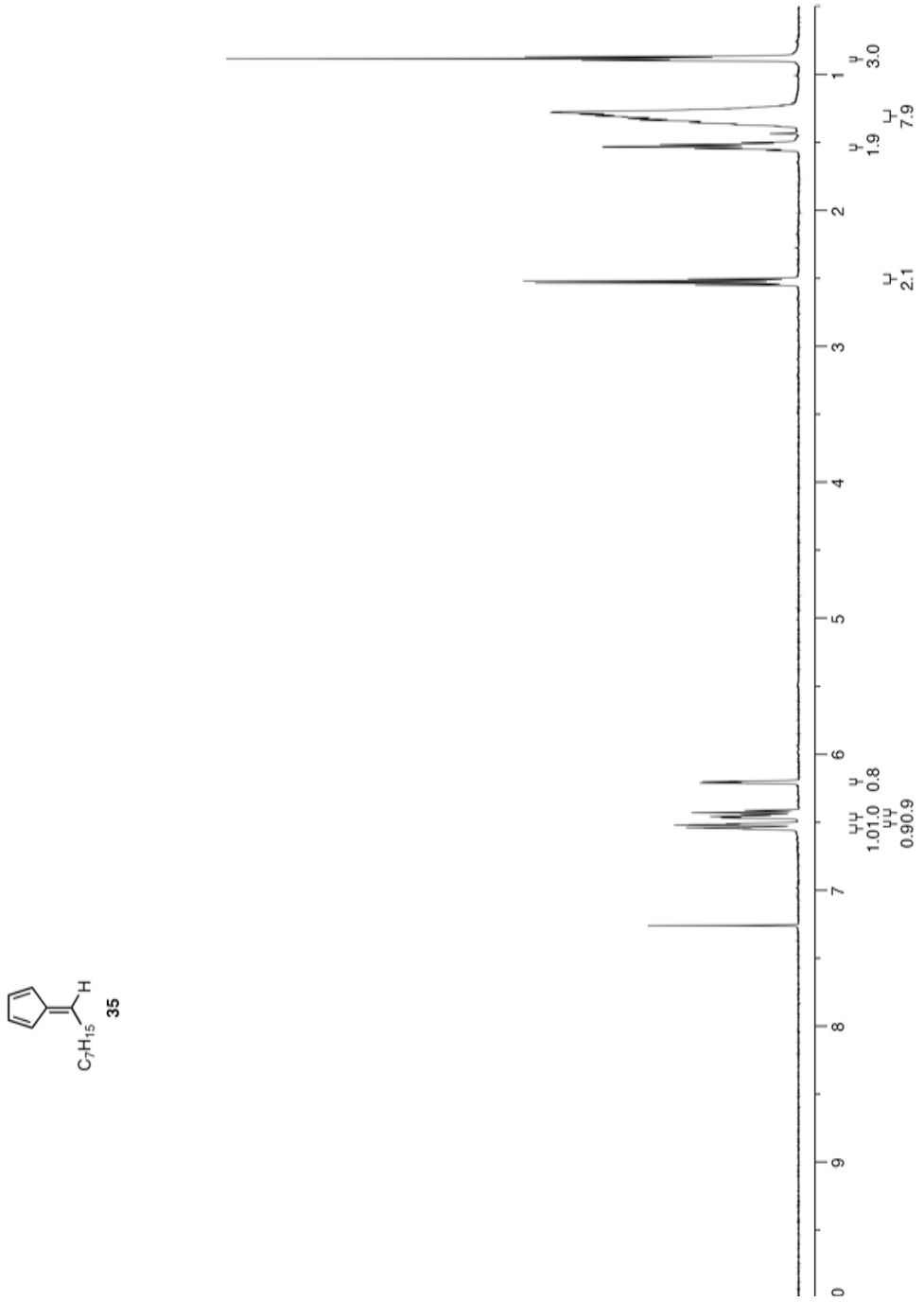
C7H15
H
35
0
1
2
3
4
5
6
7
8
9
3.0
1.9
7.9
2.1
1.01.0
0.8
0.90.9

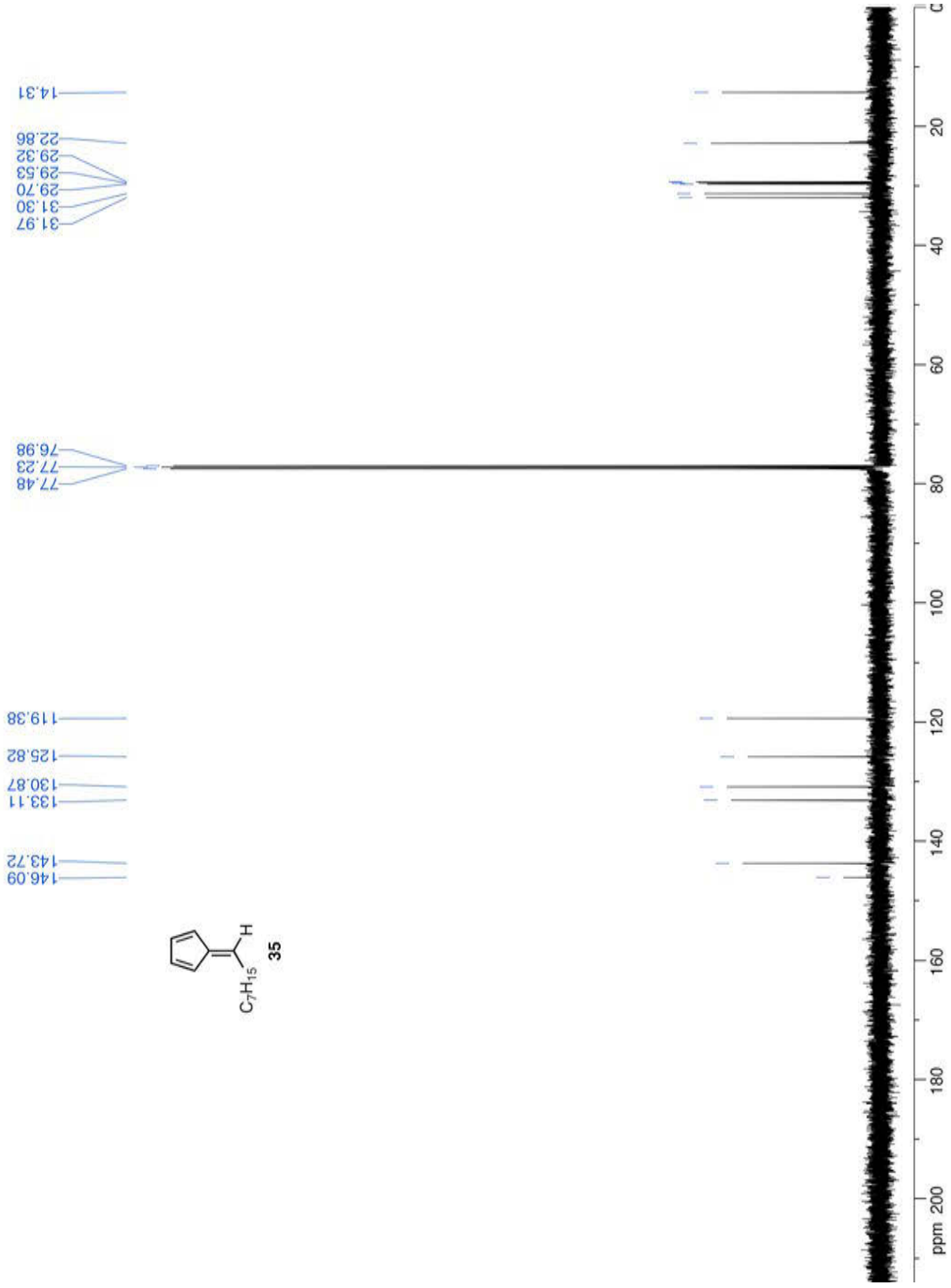
14.31
22.86
29.32
29.53
29.70
31.30
31.97
76.98
77.23
77.48
119.38
125.82
130.87
133.11
143.72
146.09
H
C7H15
35
ppm 200
180
160
140
120
100
80
60
40
20

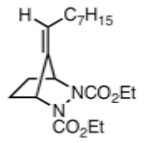

36

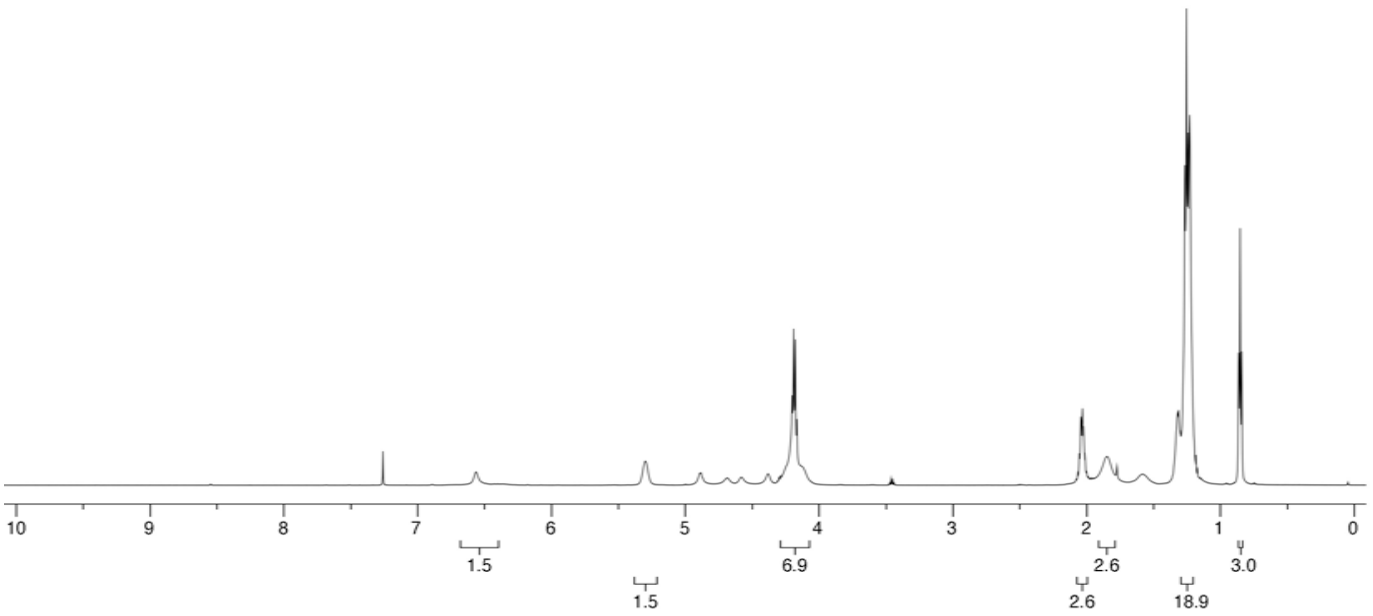

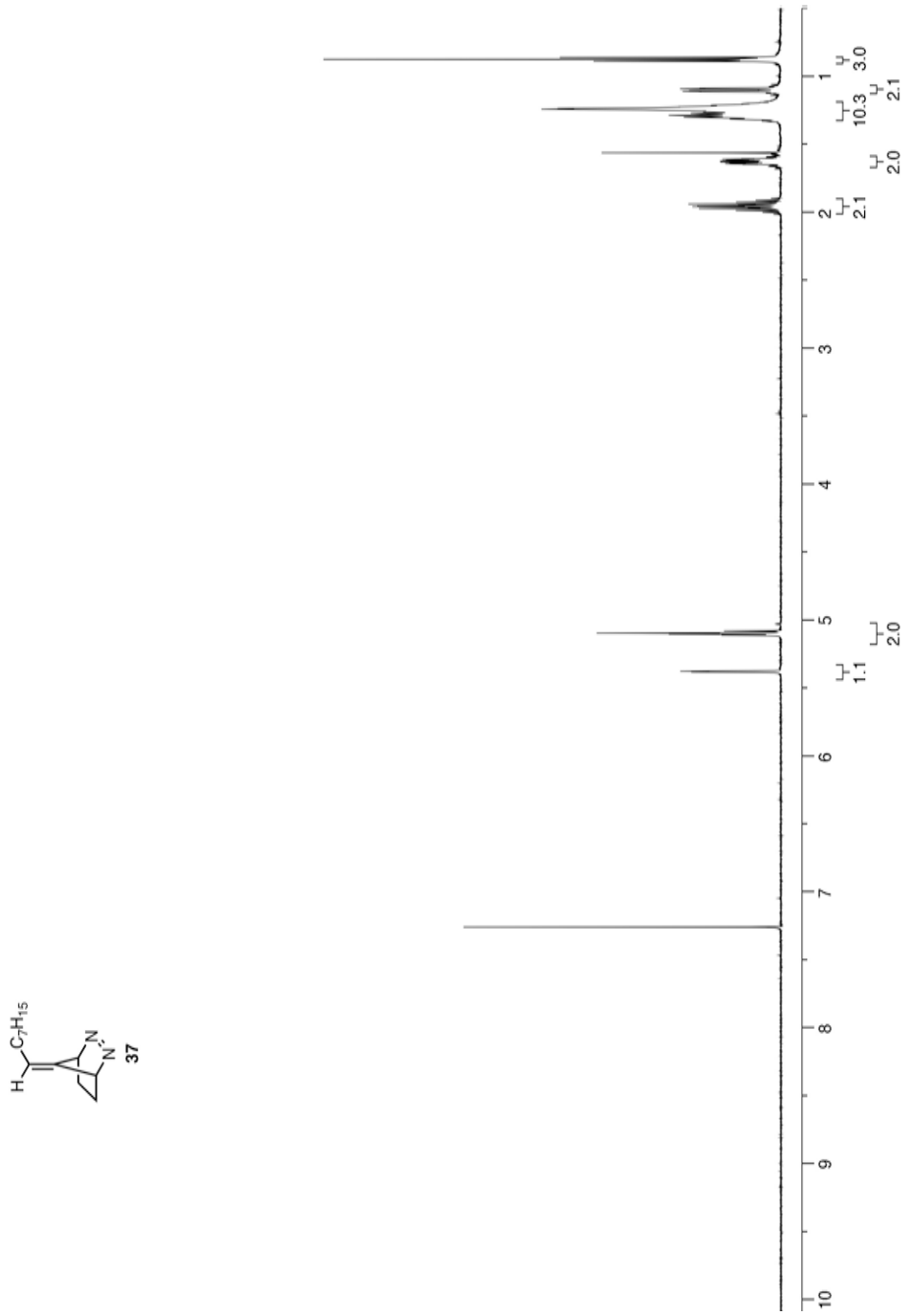
H
C7H15
N
N
37
10
9
8
7
6
5
4
3
2
1
1.1
2.0
2.1
2.0
10.3
2.1
3.0

14.30
22.84
26.29
26.84
29.25
29.41
30.73
31.95
35.69
47.91
77.02
77.23
77.44
S
S
H
C7H15
44
0
20
40
60
80
100
120
140
160
180
200

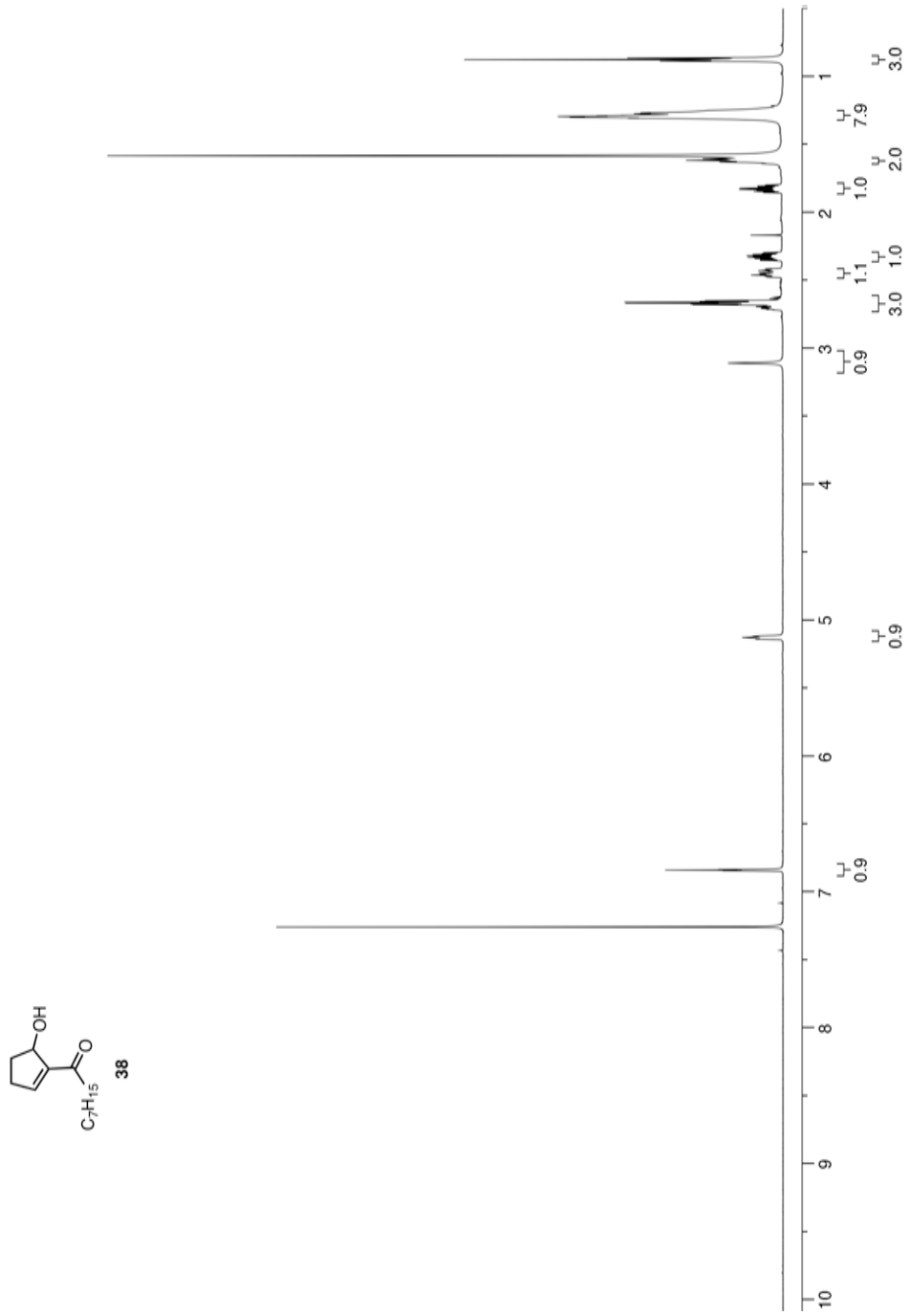
OH
O
C7H15
38

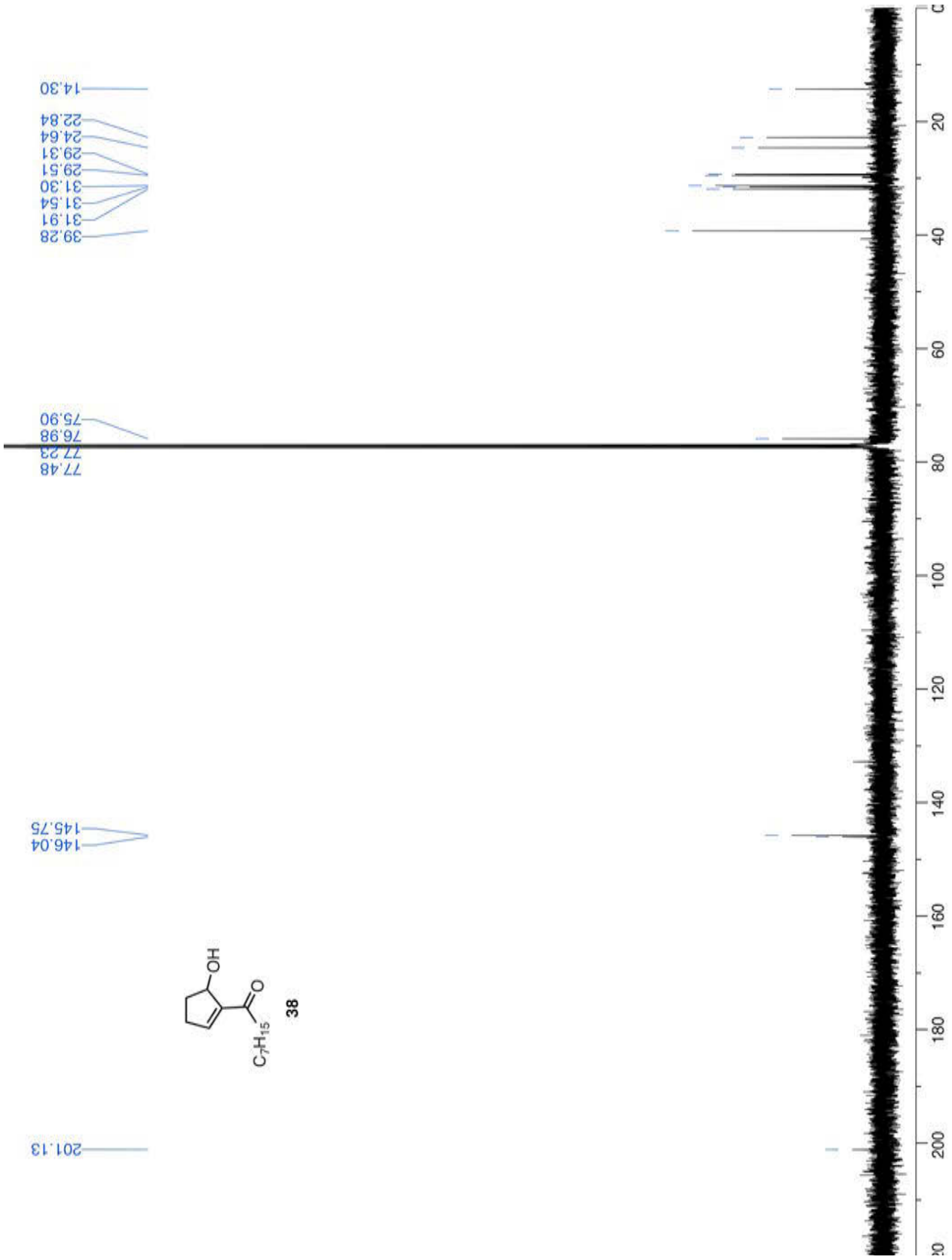
14.30
22.84
24.64
29.31
29.51
31.30
31.54
31.91
39.28
75.90
76.98
77.23
77.48
145.75
146.04
201.13
OH
O
C7H15
38

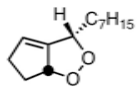

39

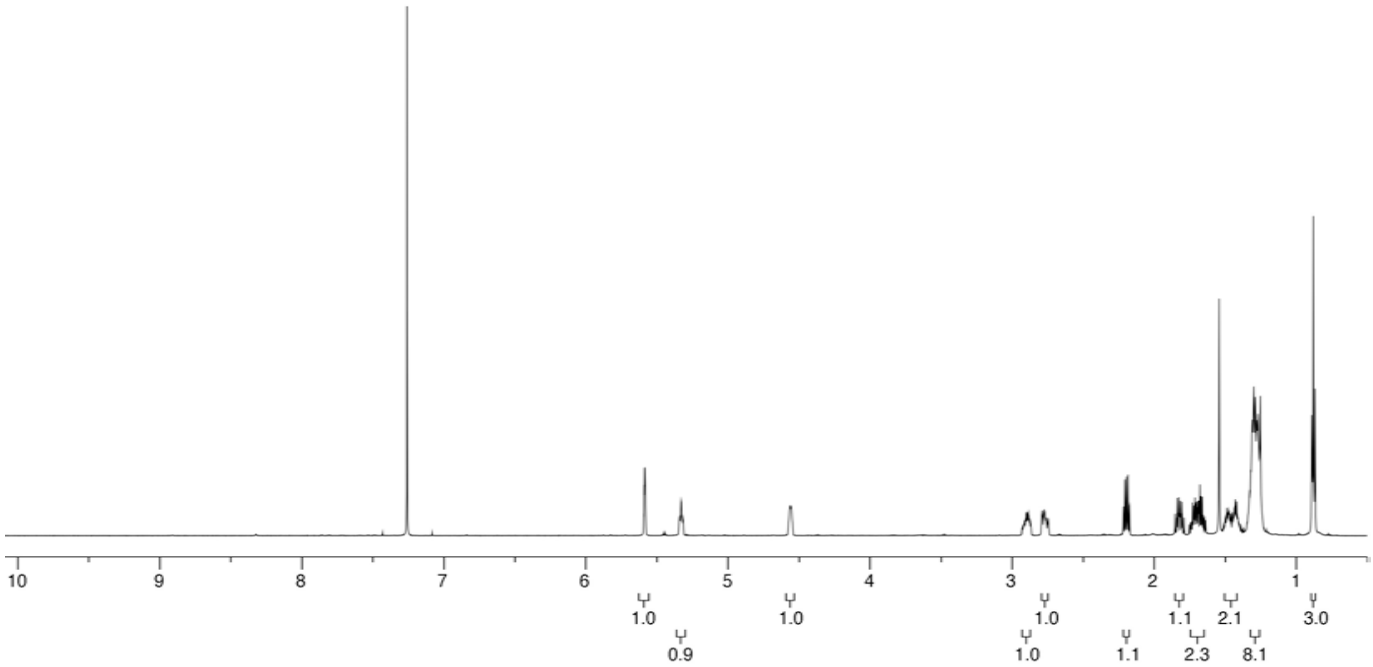

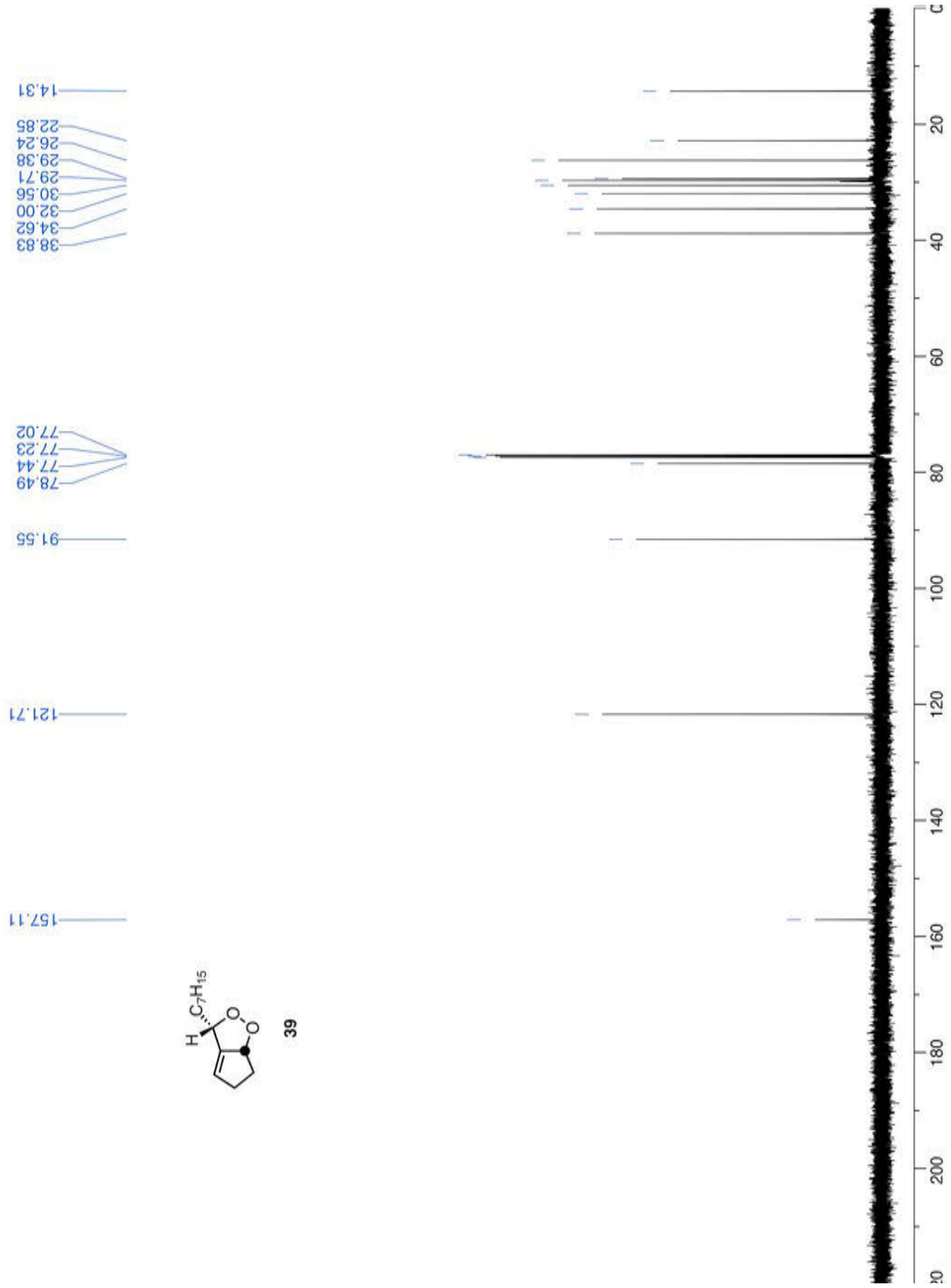
14.31
22.85
26.24
29.38
29.71
30.56
32.00
34.62
38.83
77.02
77.23
77.44
78.49
91.55
121.71
157.11
39

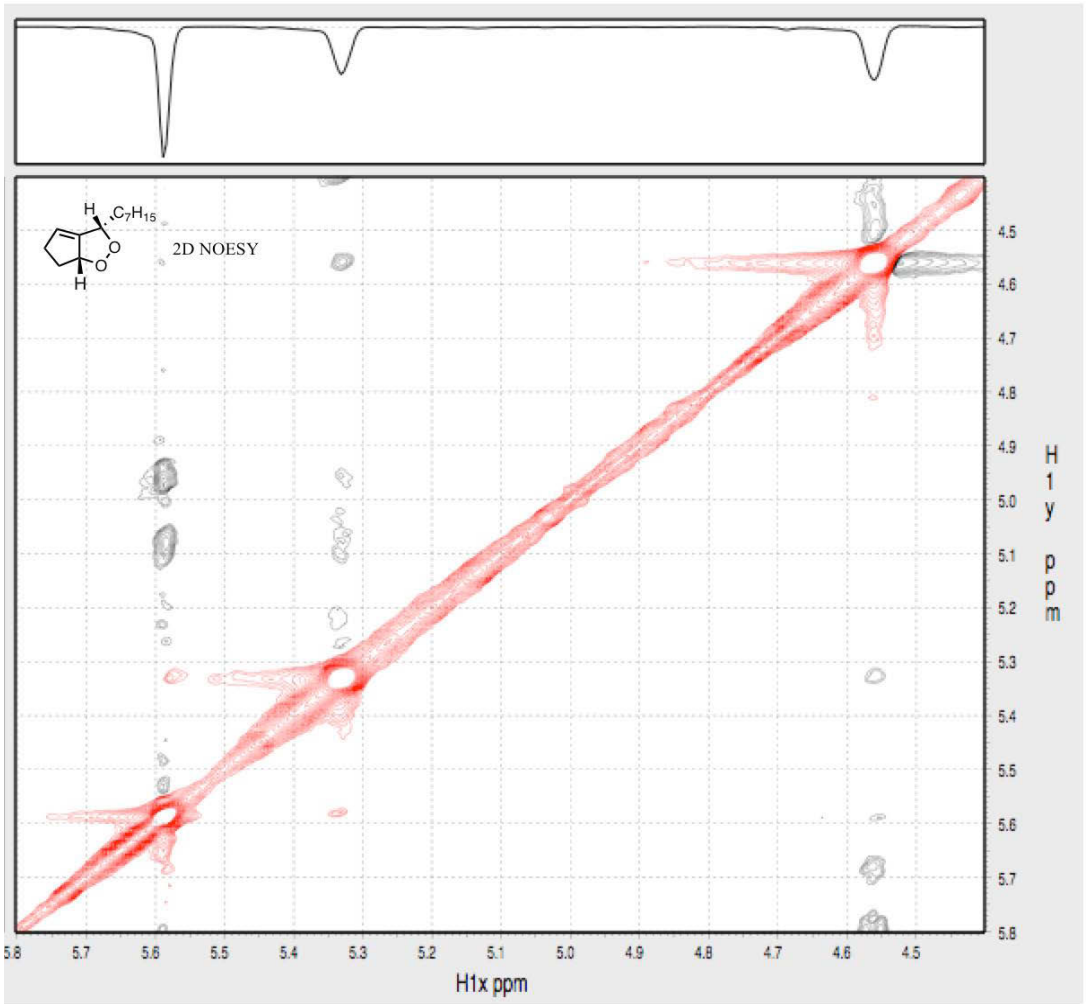
2D NOESY
H1x ppm
H1y ppm

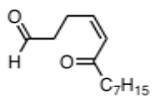

40

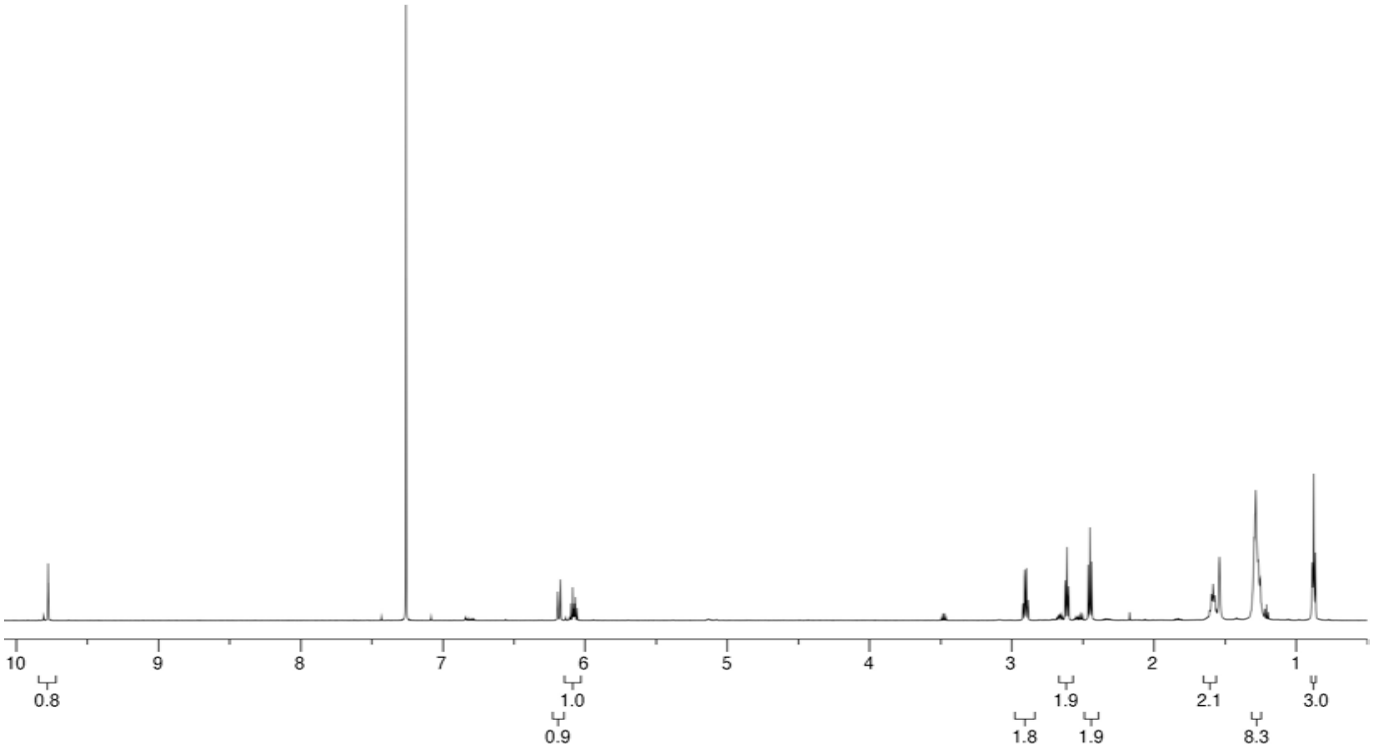

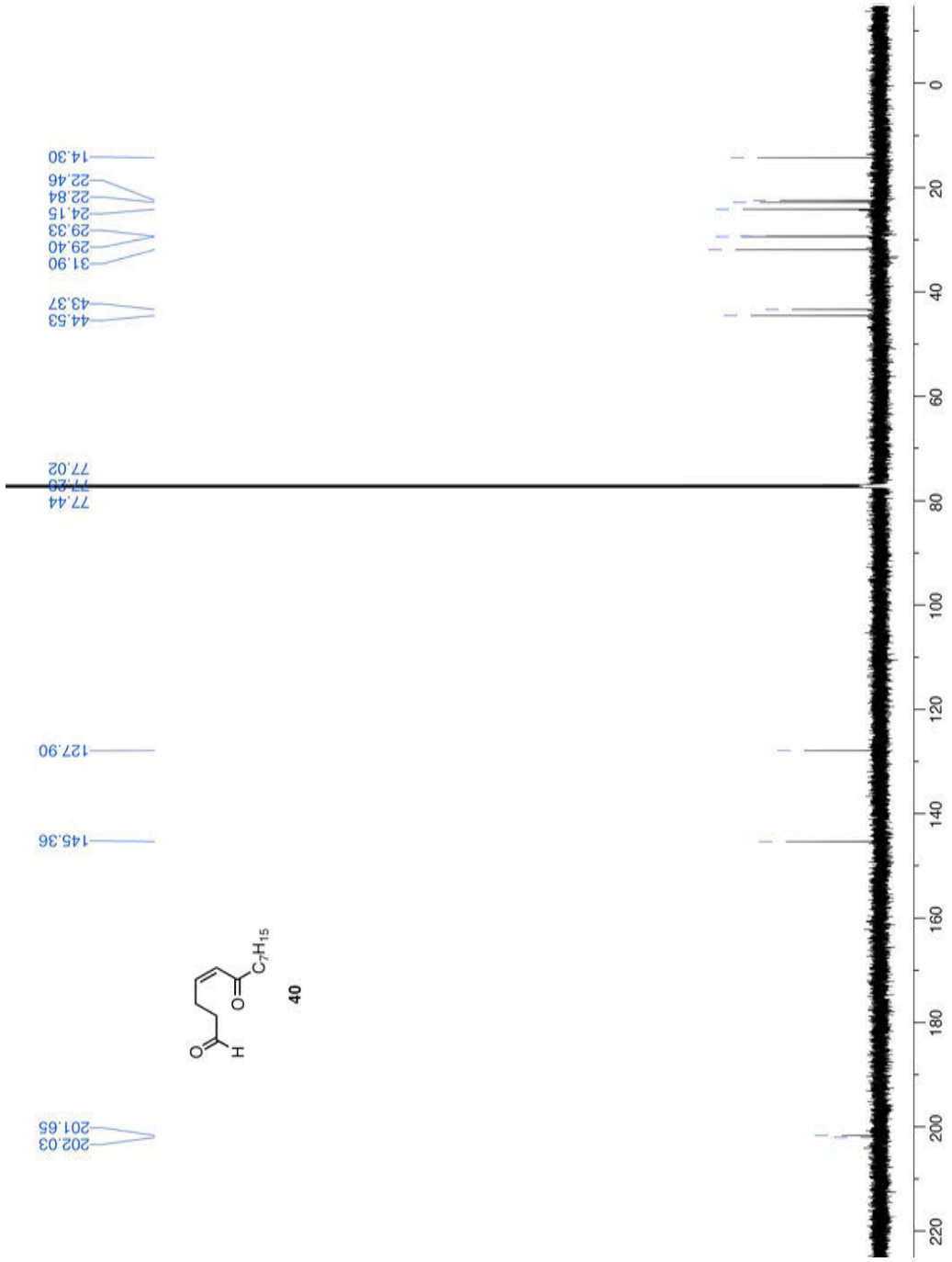
14.30
22.46
22.84
24.15
29.33
29.40
31.90
43.37
44.53
77.44
77.65
77.02
127.90
145.36
202.03
201.65
0
20
40
60
80
100
120
140
160
180
200
220
O
H
O
C7H15
40

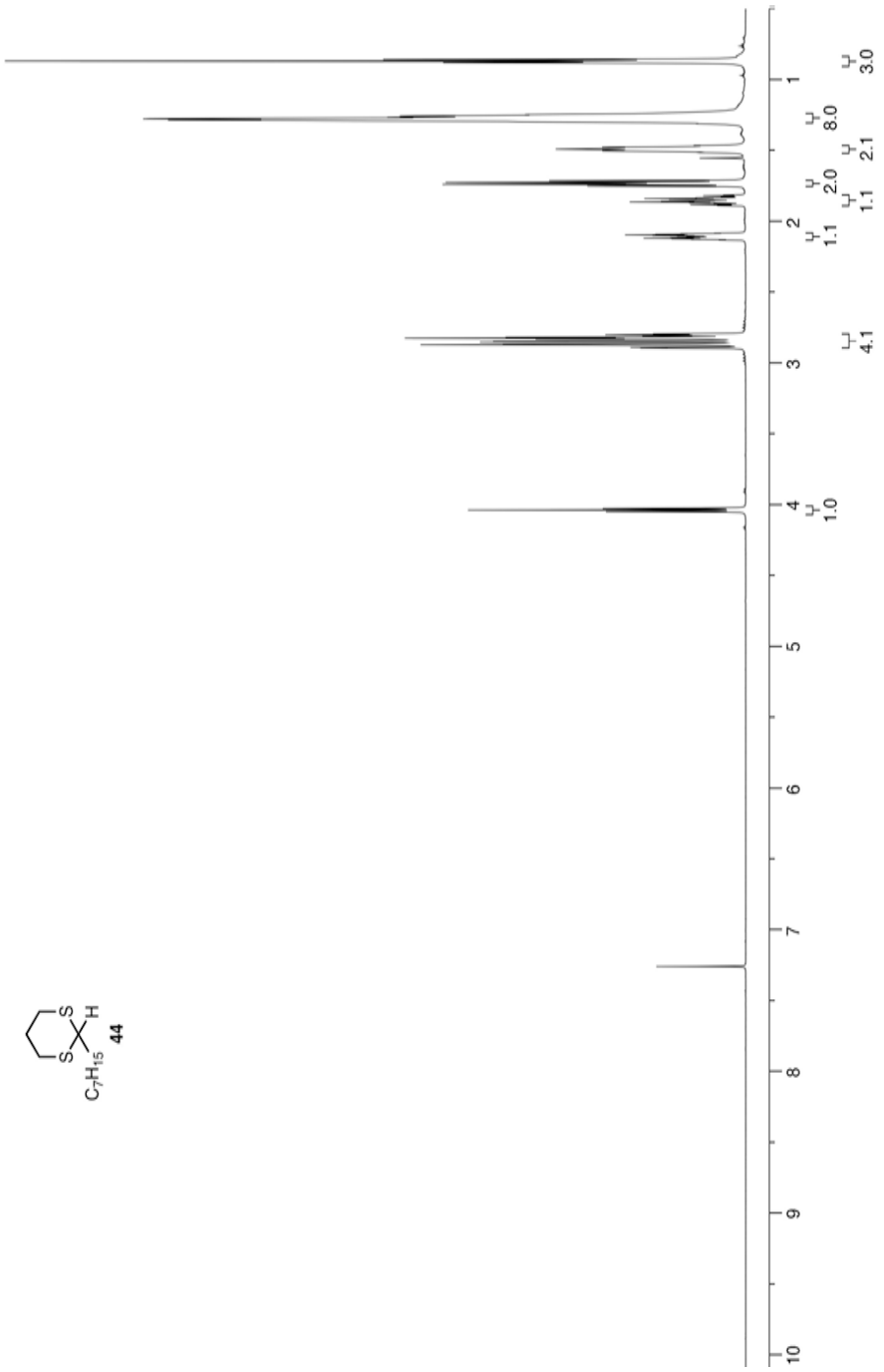
S
S
H
C7H15
44
10
9
8
7
6
5
4
1.0
3
4.1
2
1.1
2.0
1.1
2.1
8.0
1
3.0

14.30
22.84
26.29
26.84
29.25
29.41
30.73
31.95
35.69
47.91
77.02
77.23
77.44
S
S
H
C7H15
44
20
40
60
80
100
120
140
160
180
200

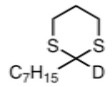

45

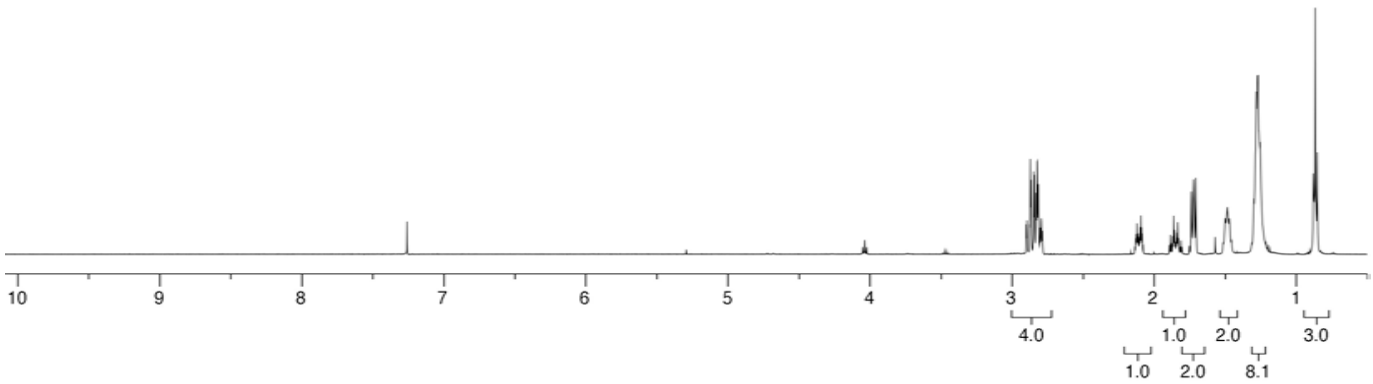

14.30
22.84
26.27
26.78
29.24
29.39
30.67
31.94
35.55
47.89
S
S
D
C_7H_{15}
45
ppm 200
180
160
140
120
100
80
60
40
20

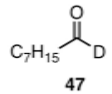

47

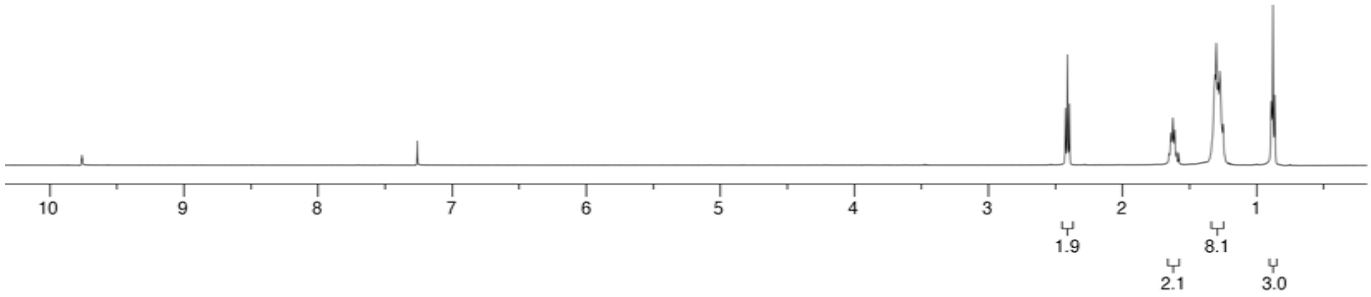

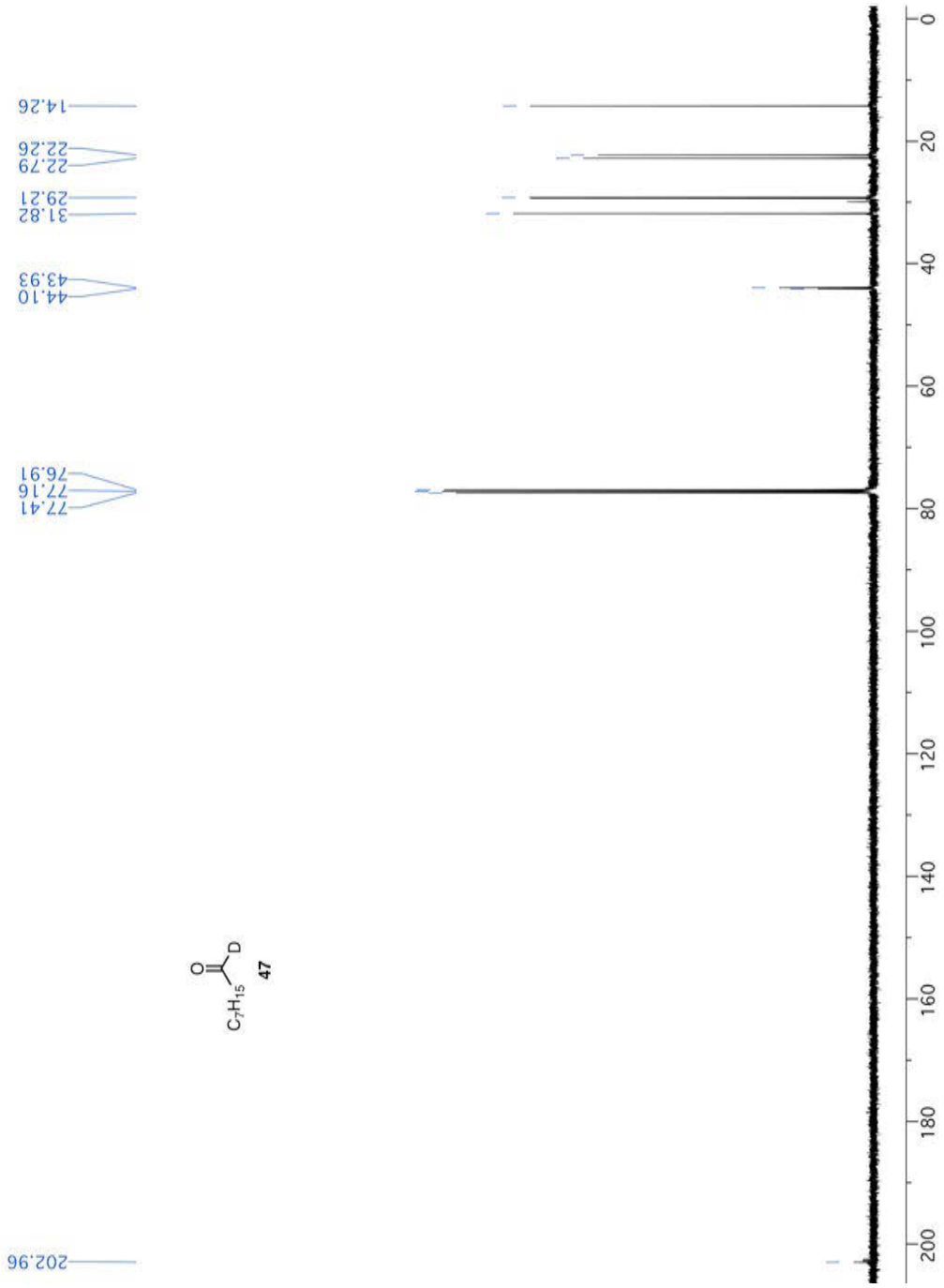
14.26
22.79
22.26
29.21
31.82
43.93
44.10
76.91
77.16
77.41
202.96
O
D
C7H15
47
0
20
40
60
80
100
120
140
160
180
200

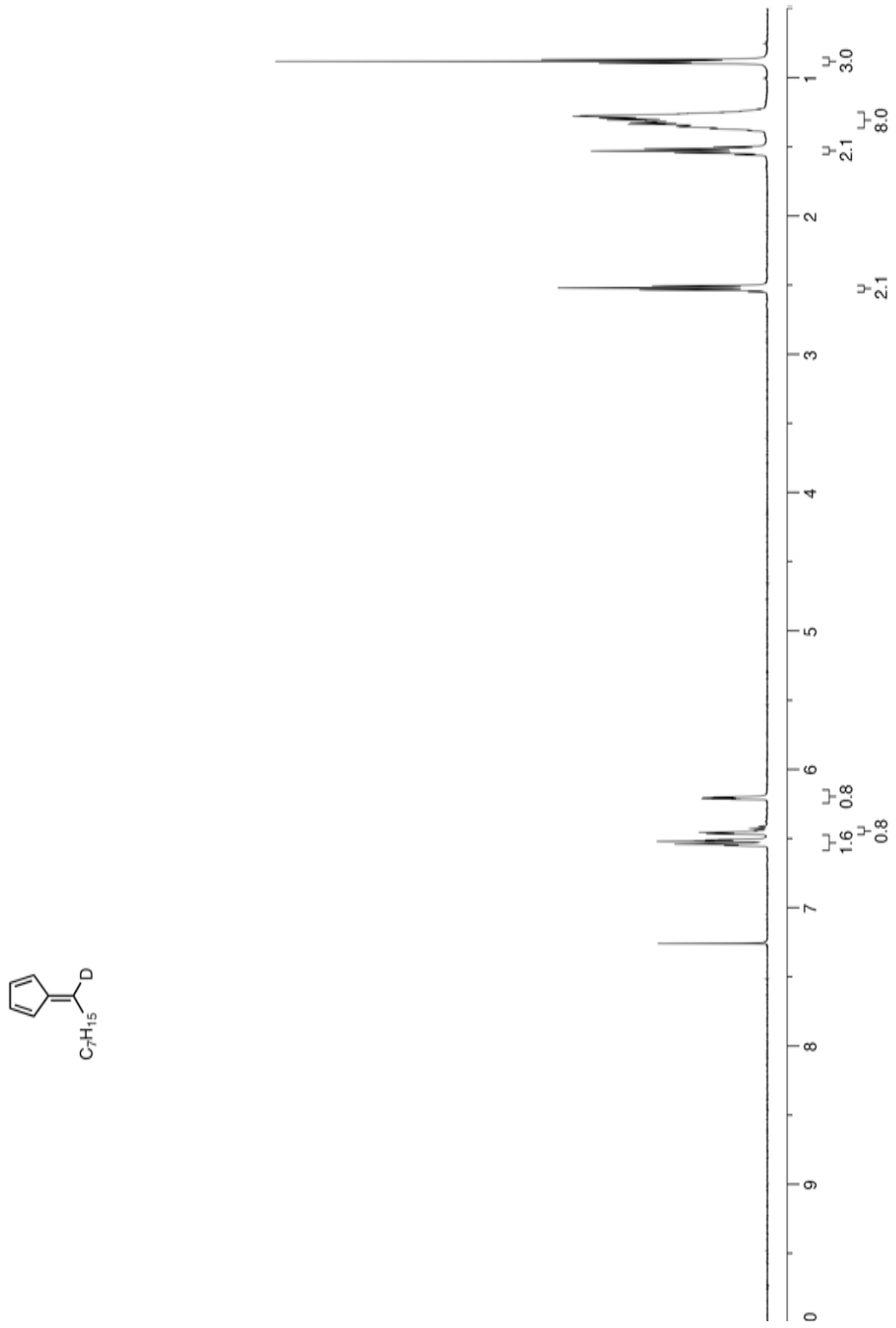
C7H15
D
0
1
2
3
4
5
6
7
8
9
3.0
8.0
2.1
2.1
1.6
0.8
0.8

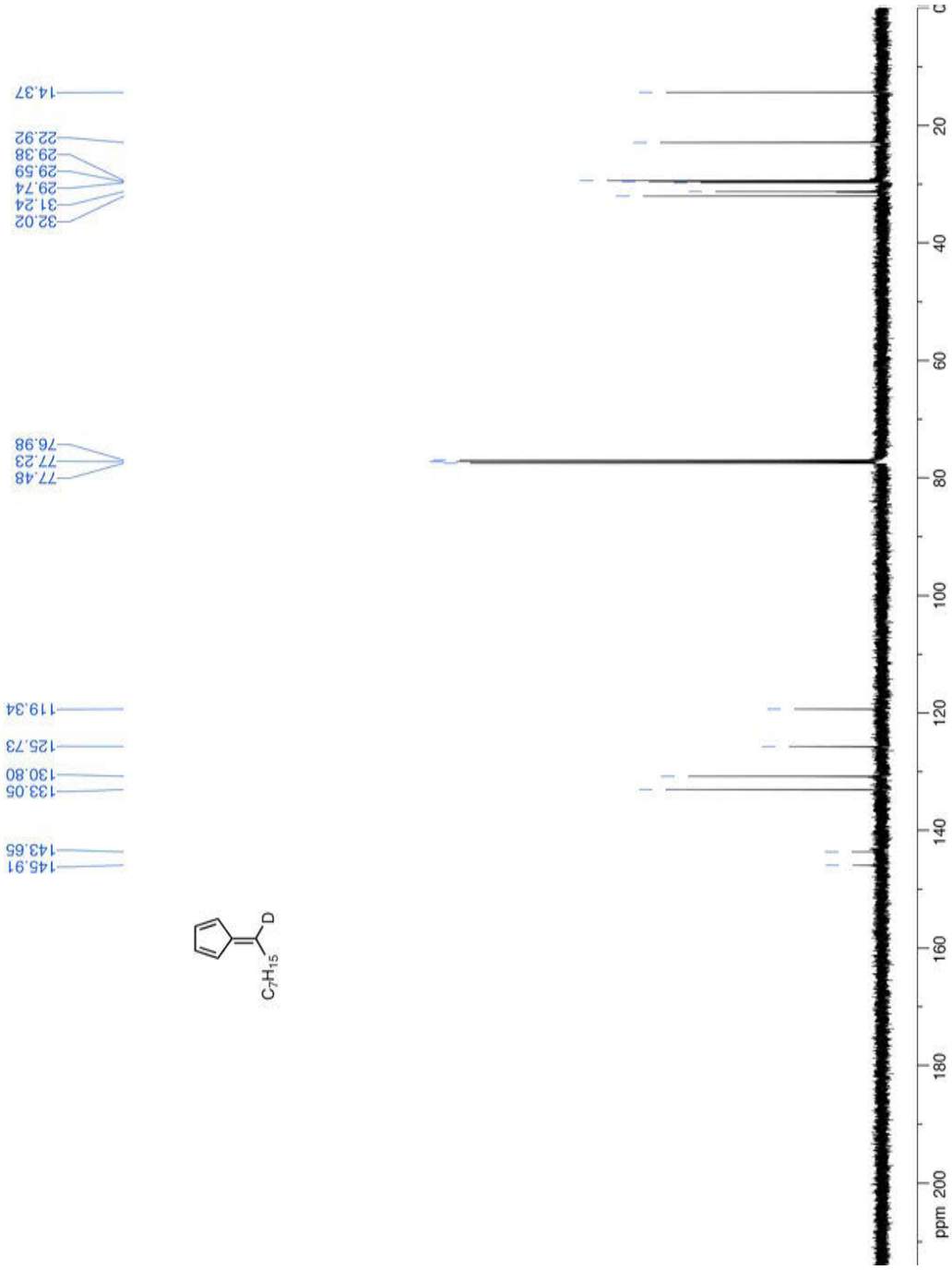
14.37
22.92
29.38
29.59
29.74
31.24
32.02
76.98
77.23
77.48
119.34
125.73
130.80
133.05
143.65
145.91
D
C7H15
ppm 200
180
160
140
120
100
80
60
40
20

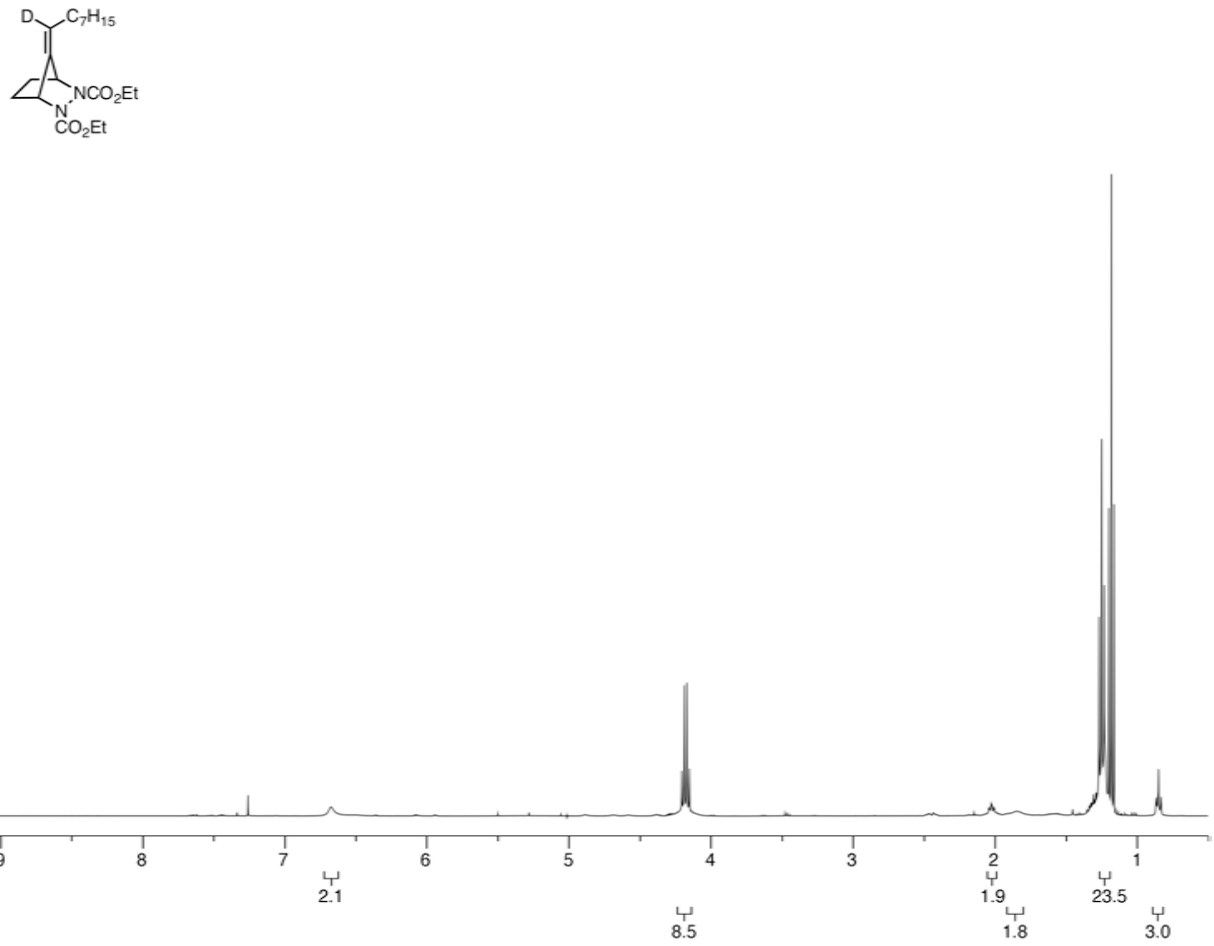
D
C7H15
NCO2Et
N
CO2Et
10
9
8
7
6
5
4
3
2
1
2.1
8.5
1.9
1.8
23.5
3.0

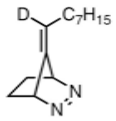

37-d_1

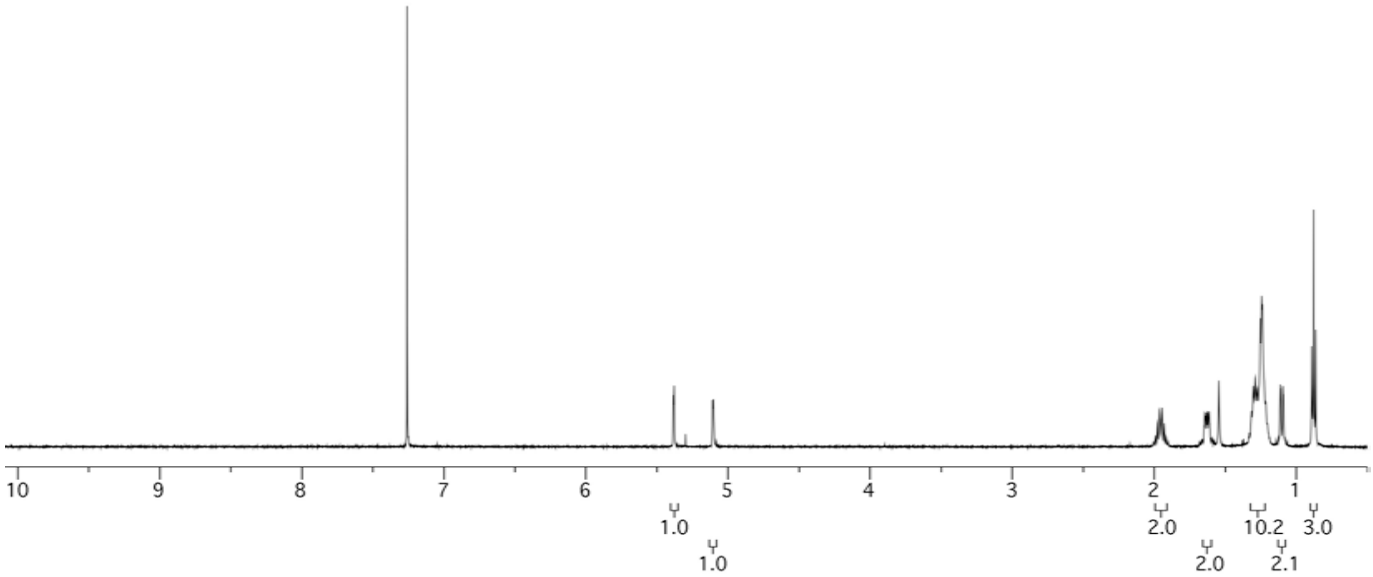

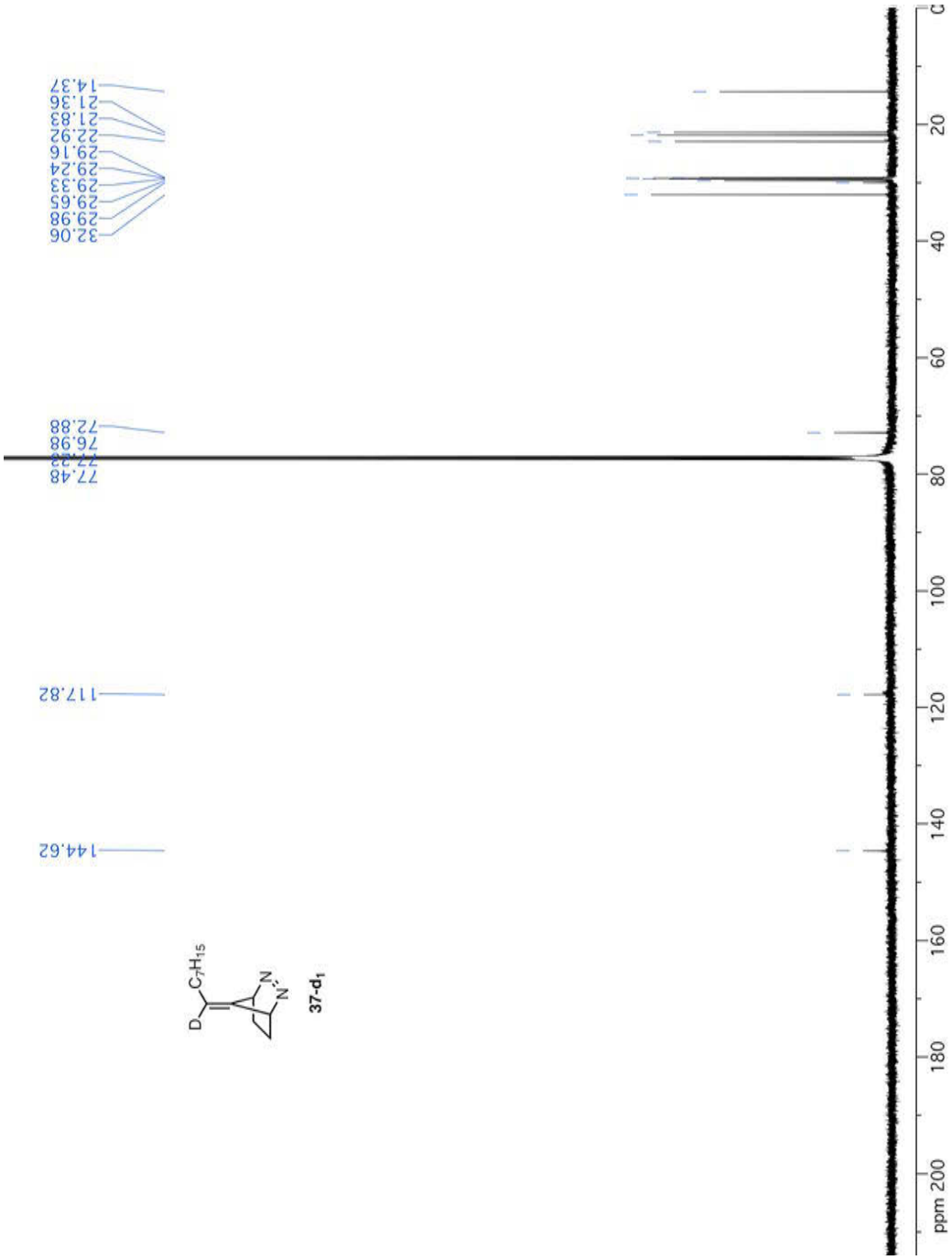
14.37
21.36
21.83
22.92
29.16
29.24
29.33
29.65
29.98
32.06
72.88
76.98
77.23
77.48
117.82
144.62
ppm 200
180
160
140
120
100
80
60
40
20
D
C7H15
N
N
37-d1

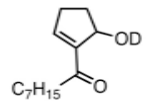

38-d_1

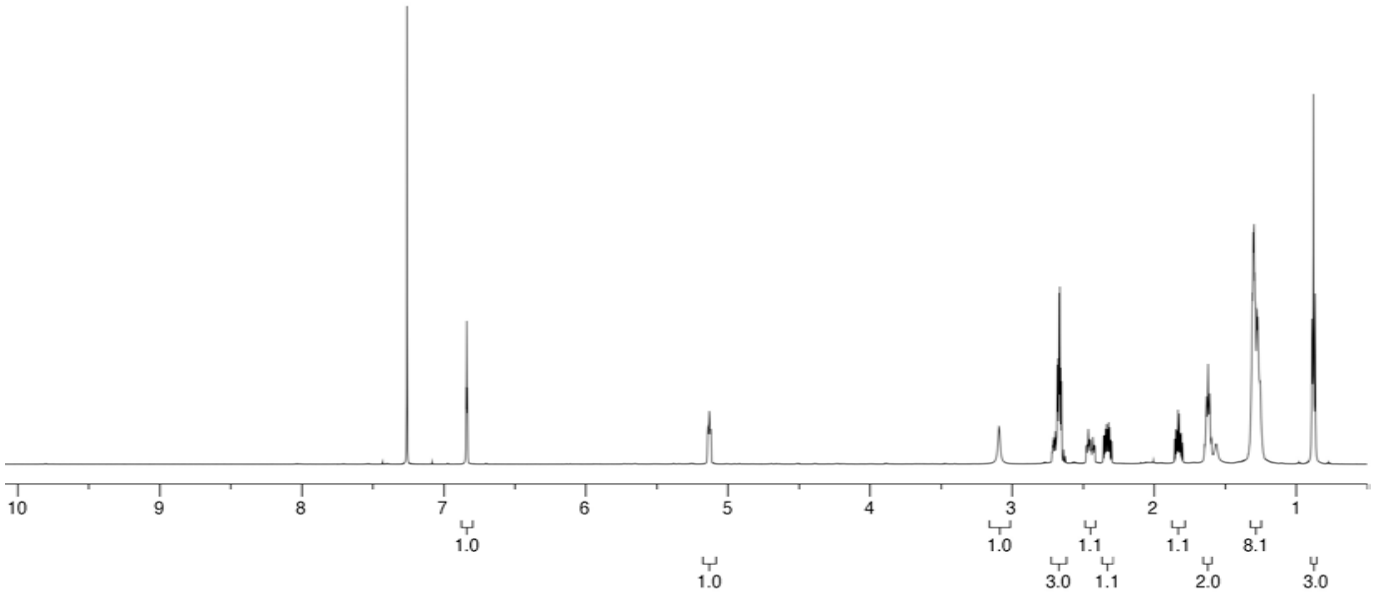

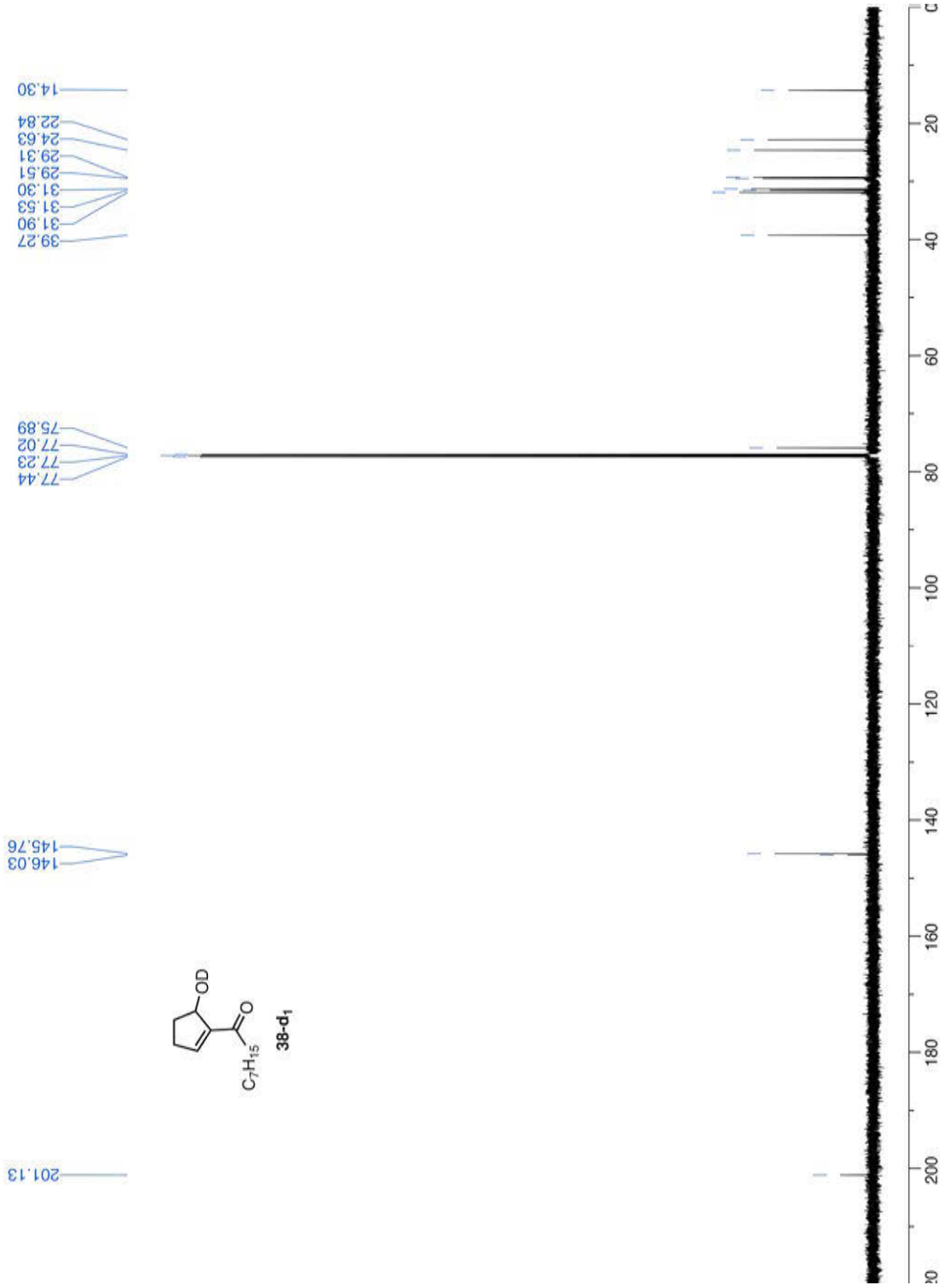
14.30
22.84
24.63
29.31
29.51
31.30
31.53
31.90
39.27
75.89
77.02
77.23
77.44
145.76
146.03
201.13
OD
O
C_7H_{15}
38-d_1
0
20
40
60
80
100
120
140
160
180
200

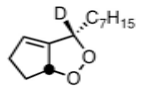

39-d_1

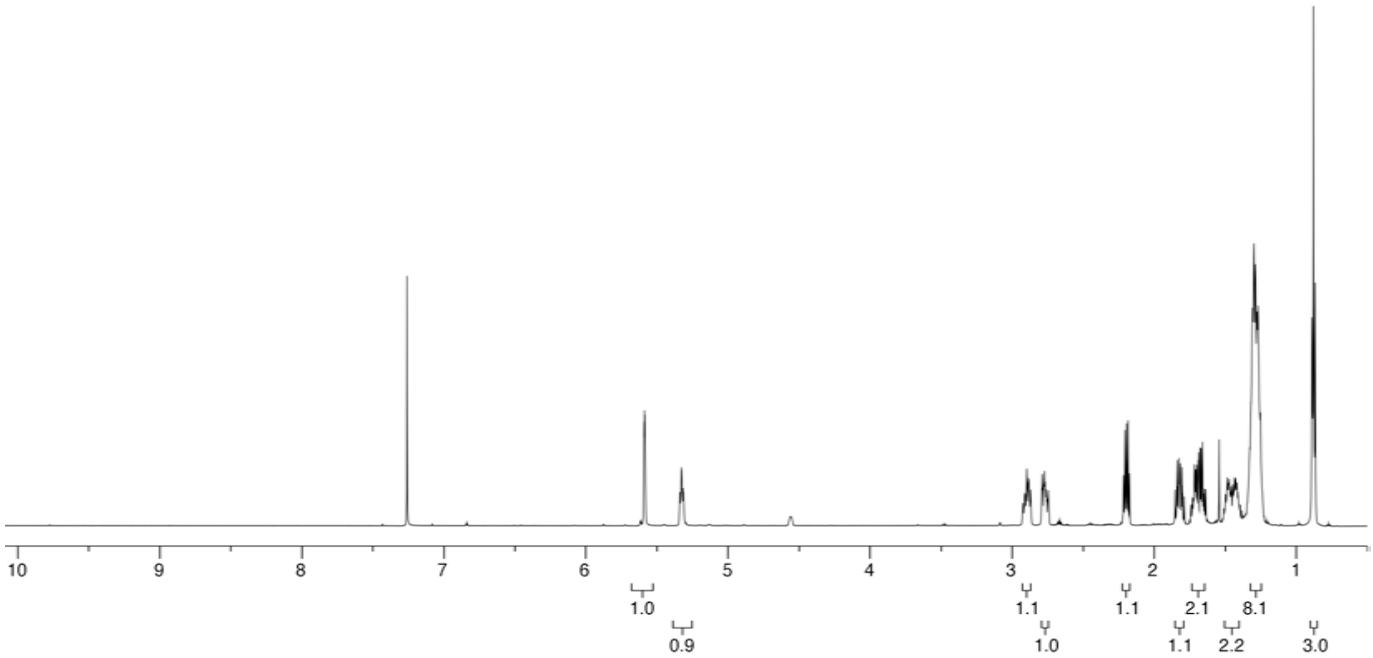

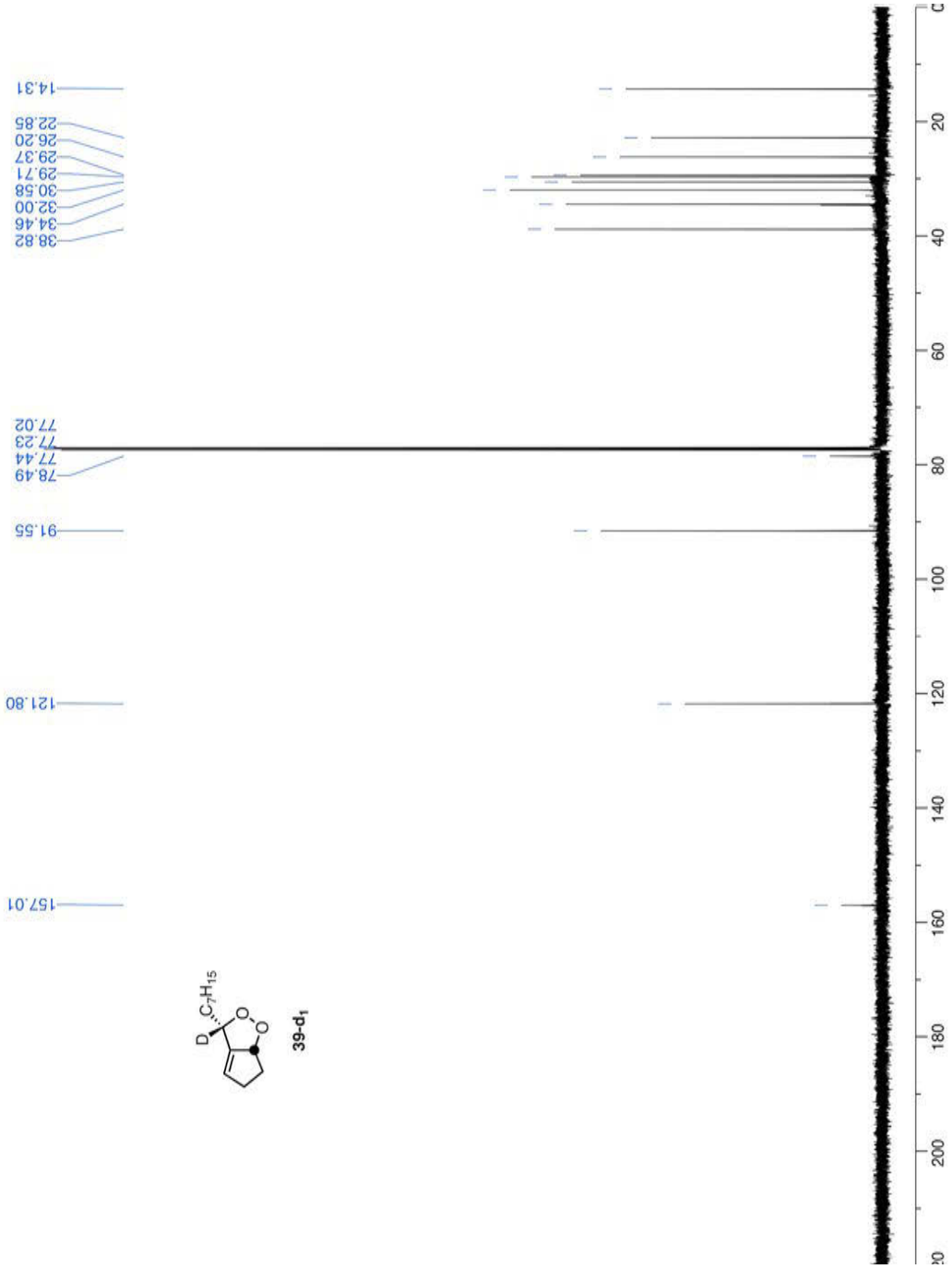
14.31
22.85
26.20
29.37
29.71
30.58
32.00
34.46
38.82
77.02
77.23
77.44
78.49
91.55
121.80
157.01
39-d1

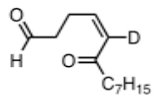

40-d_1

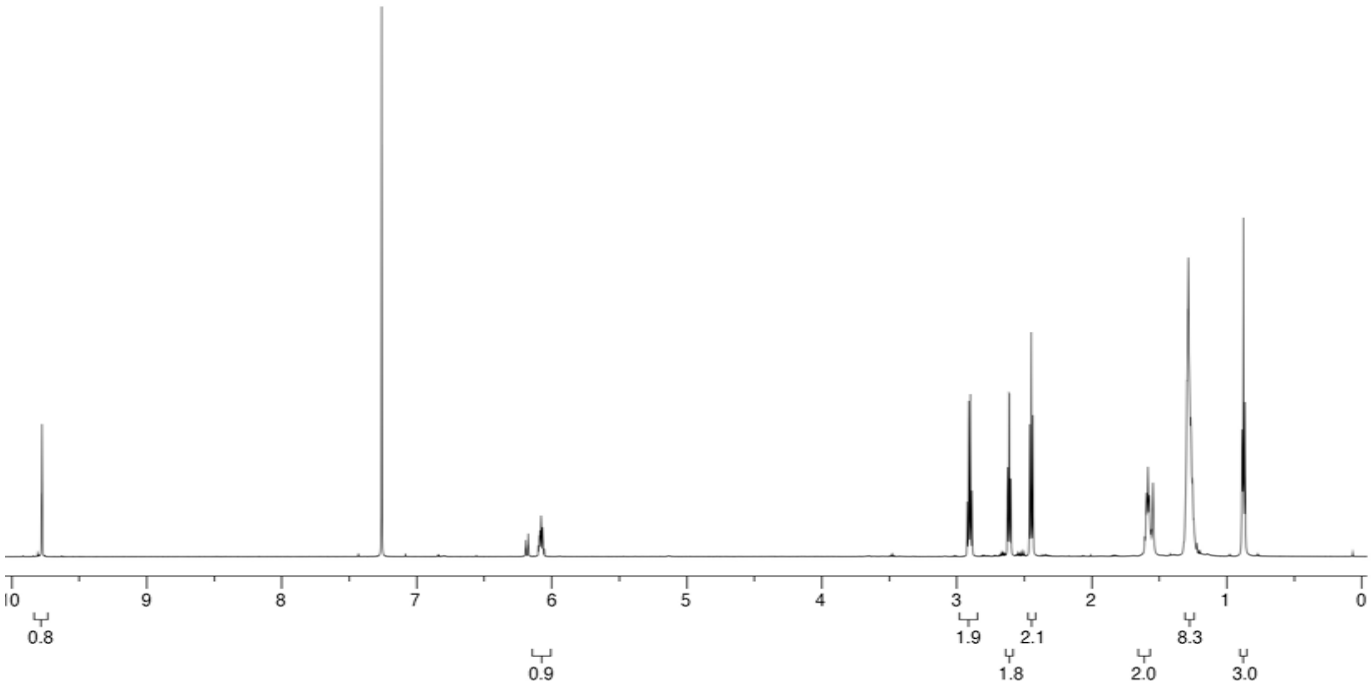

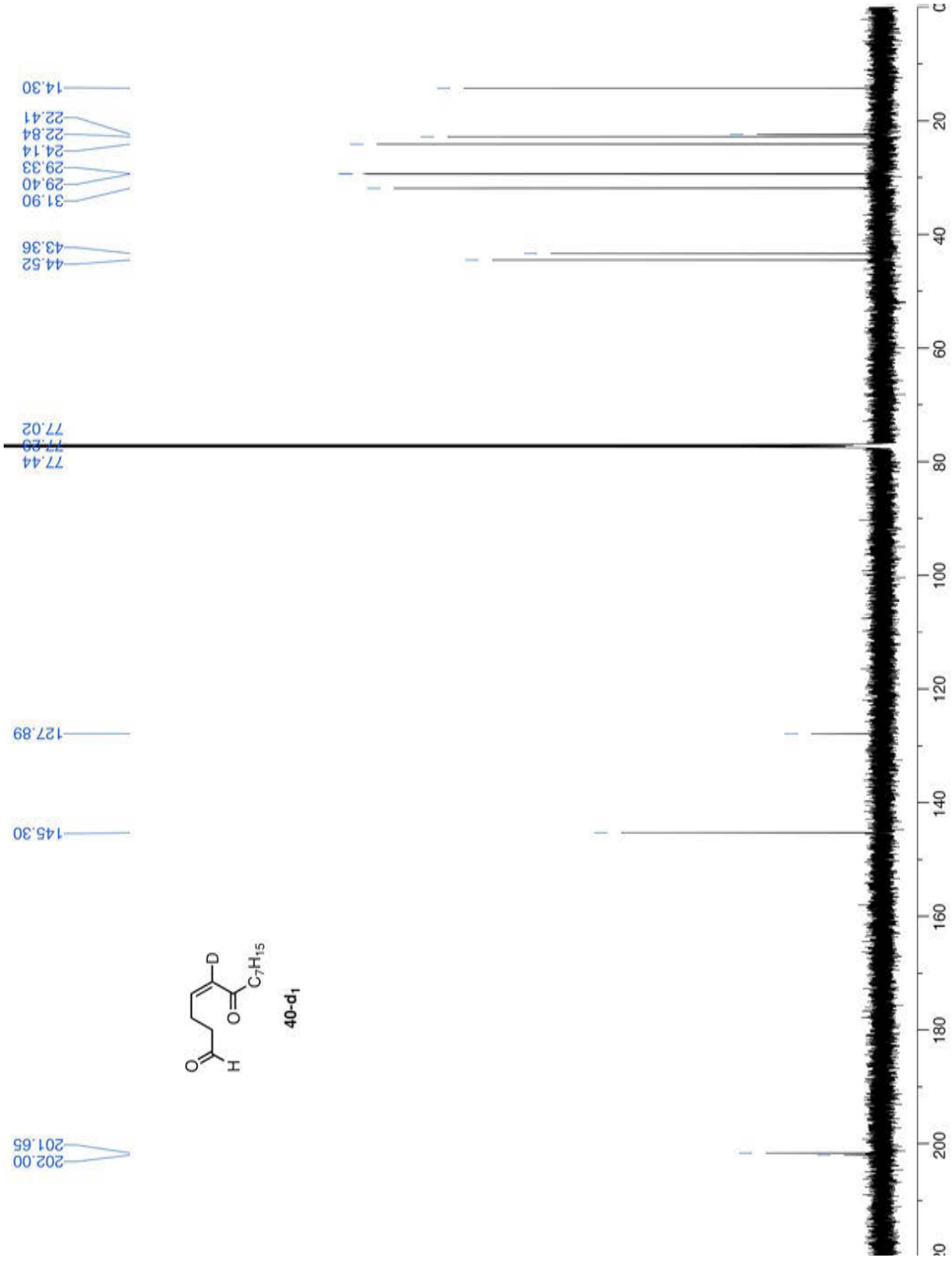
14.30
22.41
22.84
24.14
29.33
29.40
31.90
43.36
44.52
77.02
77.29
77.44
127.89
145.30
201.65
202.00
O
H
O
D
C7H15
40-d1

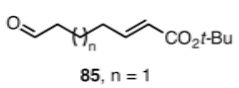

85, n = 1

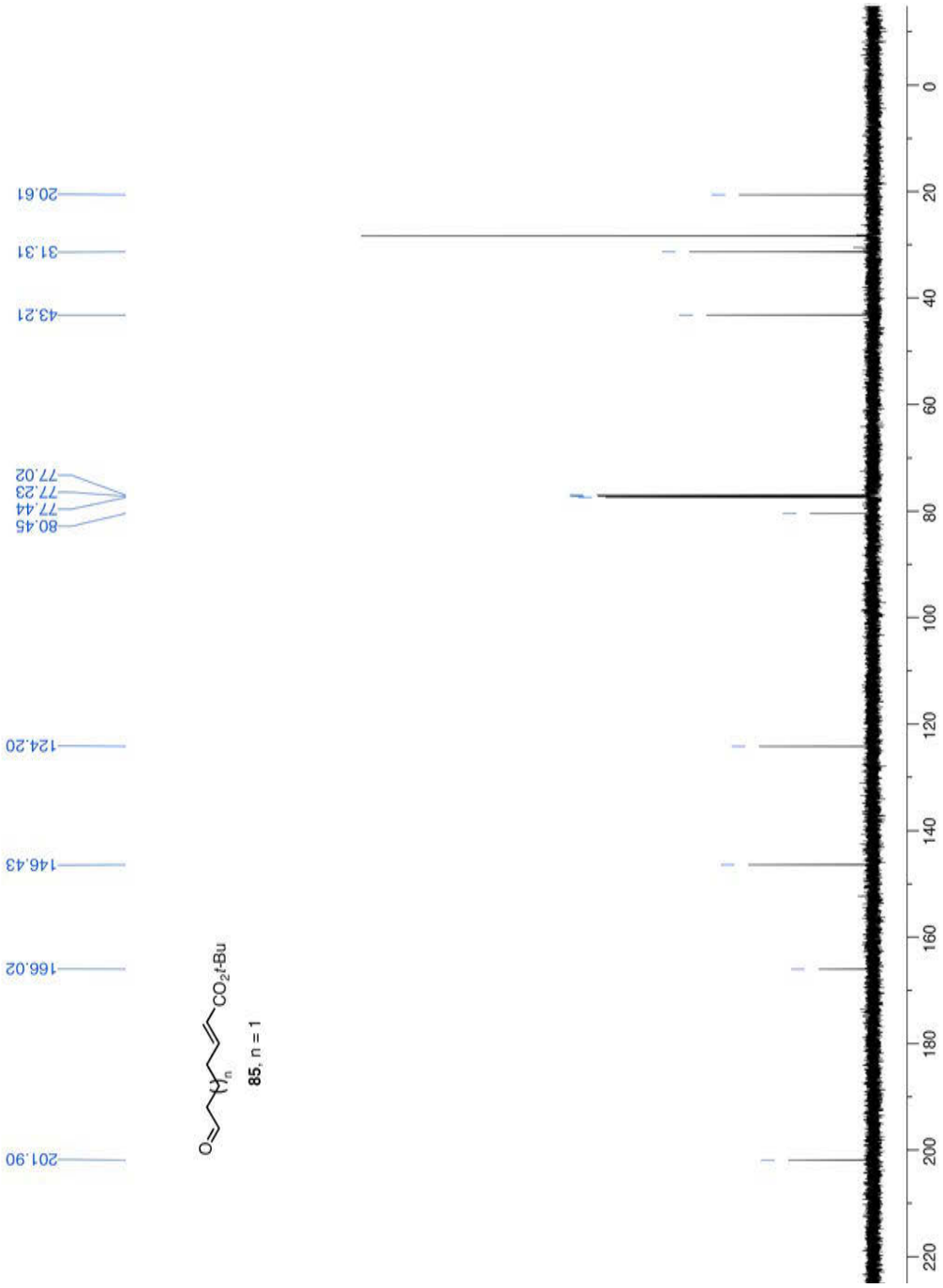
20.61
31.31
43.21
77.02
77.23
77.44
80.45
124.20
146.43
166.02
201.90
CO2t-Bu
85, n = 1
0
20
40
60
80
100
120
140
160
180
200
220

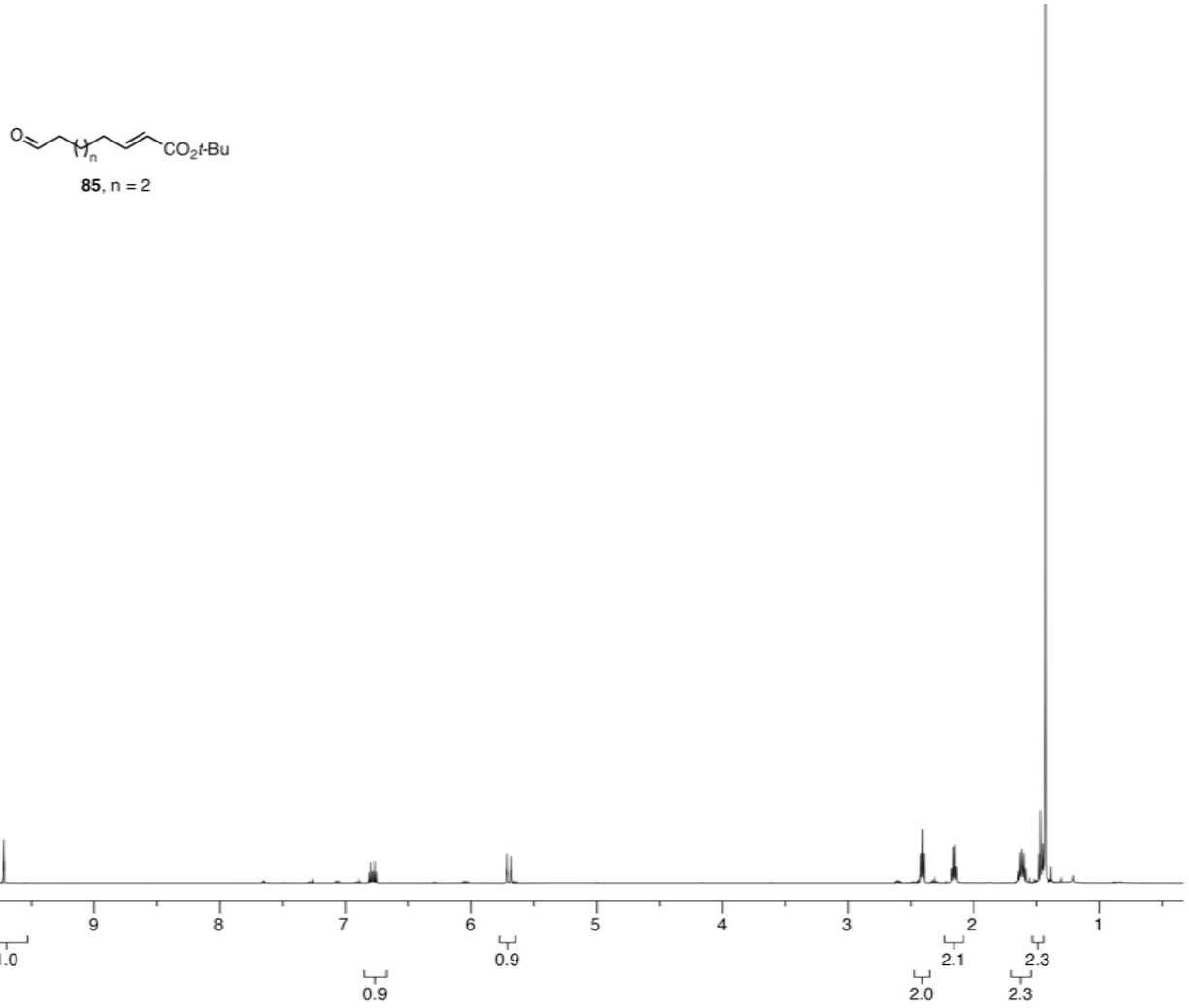
O
n
CO2t-Bu
85, n = 2
ppm 10
9
8
7
6
5
4
3
2
1
1.0
0.9
0.9
2.0
2.1
2.3
2.3

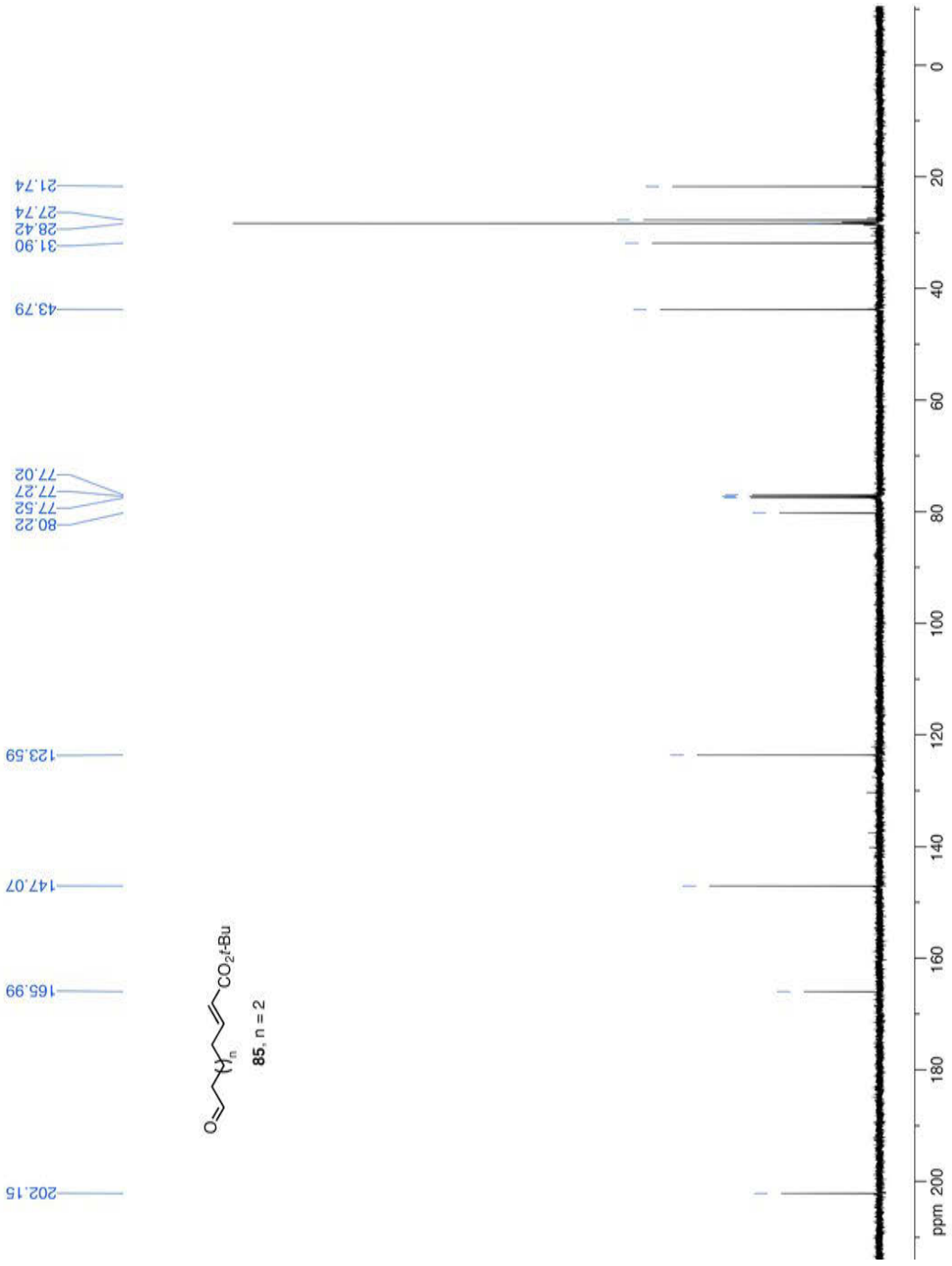
21.74
27.74
28.42
31.90
43.79
77.02
77.27
77.52
80.22
123.59
147.07
165.99
202.15
O
CO2t-Bu
n
85, n = 2
0
20
40
60
80
100
120
140
160
180
200
ppm

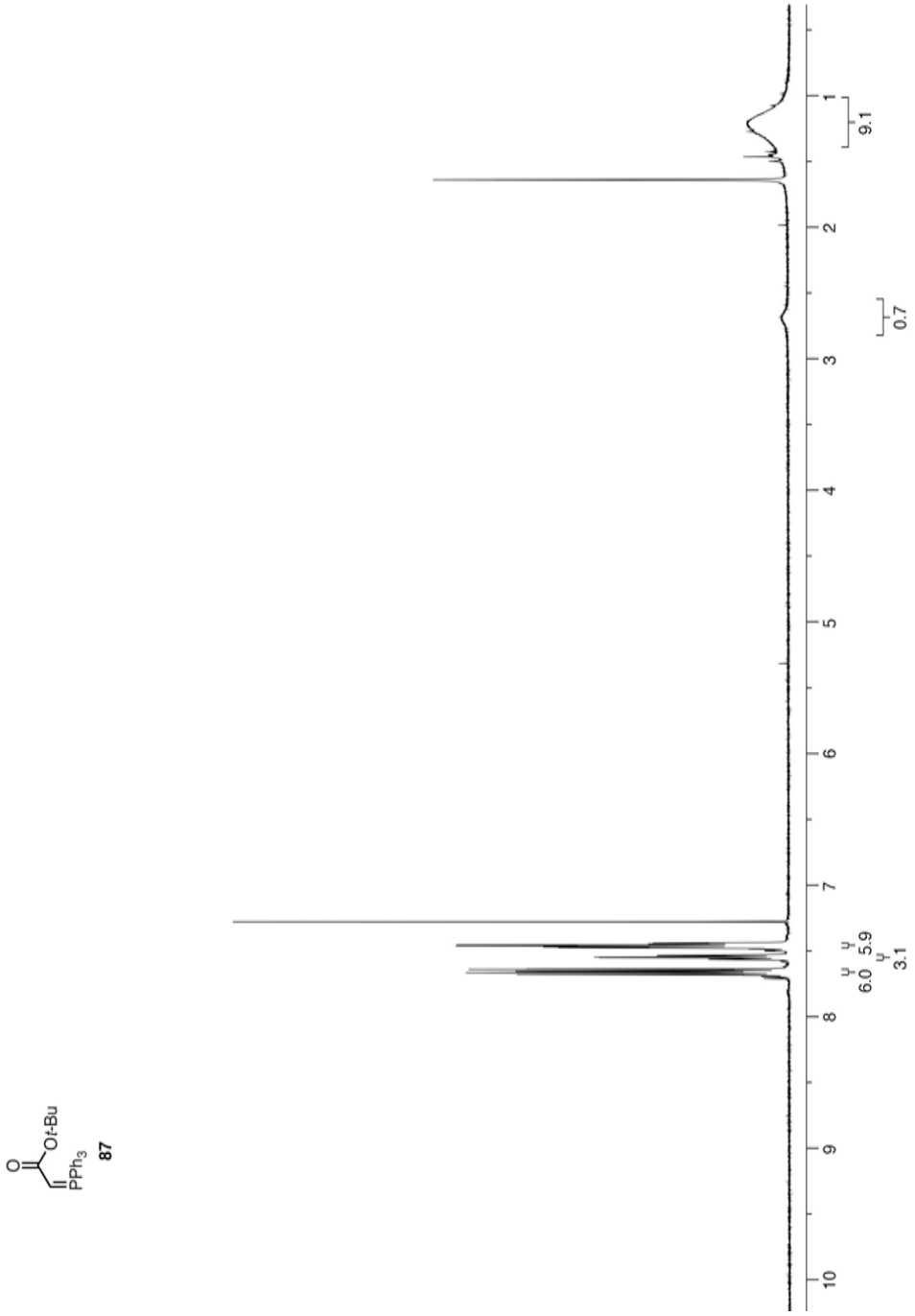
O
Ot-Bu
PPh3
87
9.1
0.7
6.0
5.9
3.1

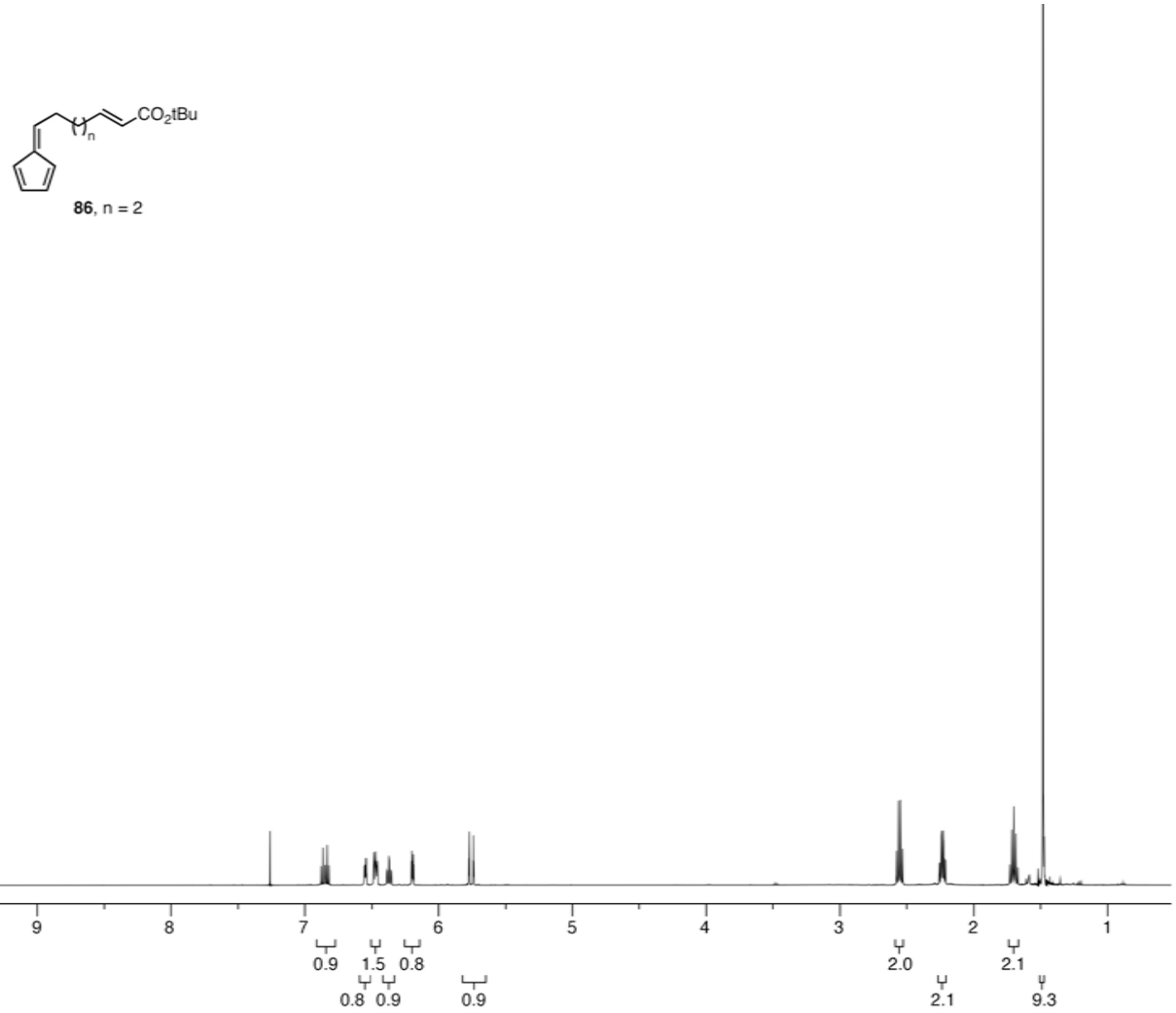
CO2tBu
n
86, n = 2
ppm 10
9
8
7
6
5
4
3
2
1
0.9
1.5
0.8
0.8
0.9
0.9
2.0
2.1
2.1
9.3

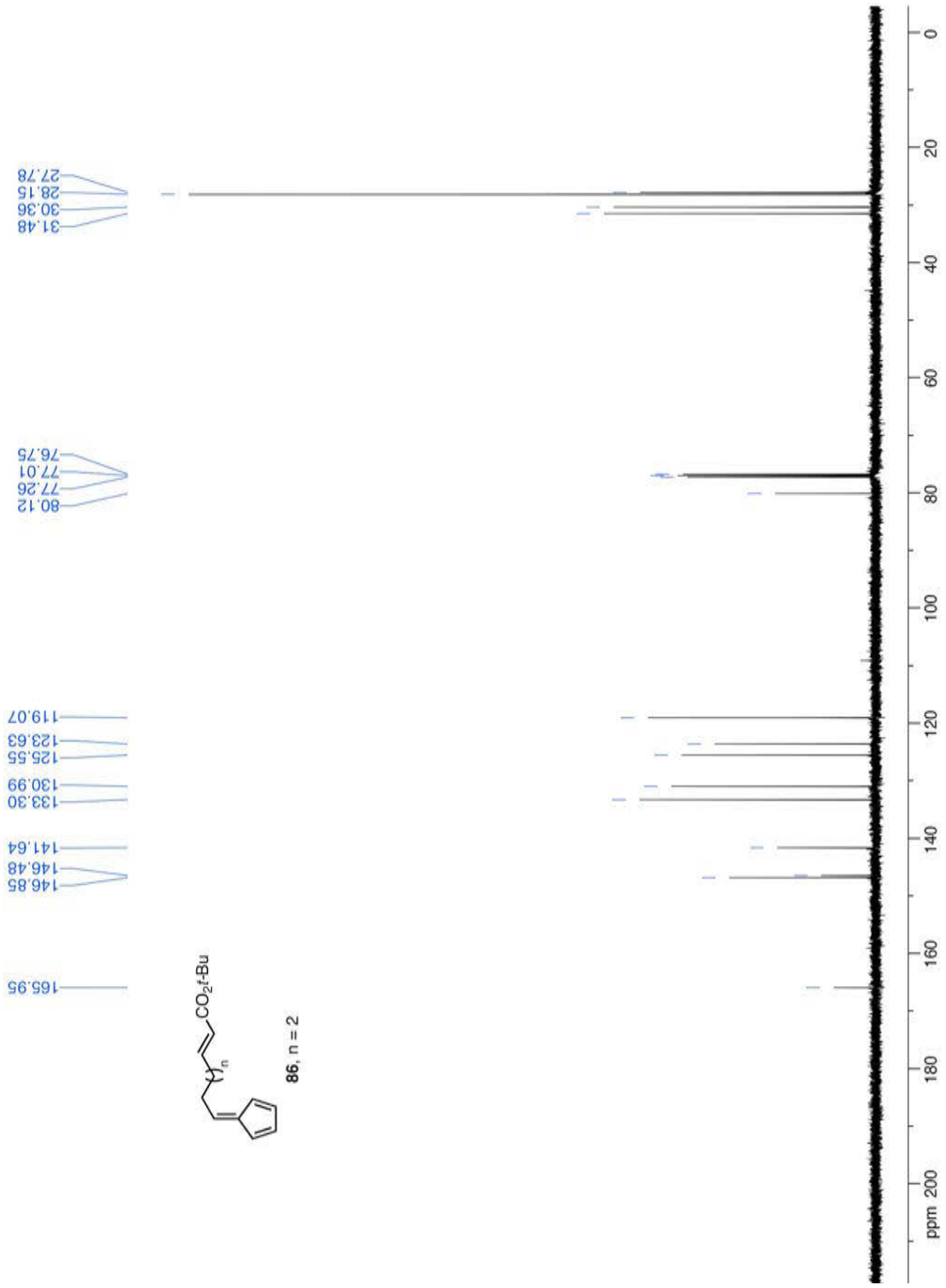
27.78
28.15
30.36
31.48
76.75
77.01
77.26
80.12
119.07
123.63
125.55
130.99
133.30
141.64
146.48
146.85
165.95
CO2t-Bu
n
86, n = 2
0
20
40
60
80
100
120
140
160
180
200
ppm

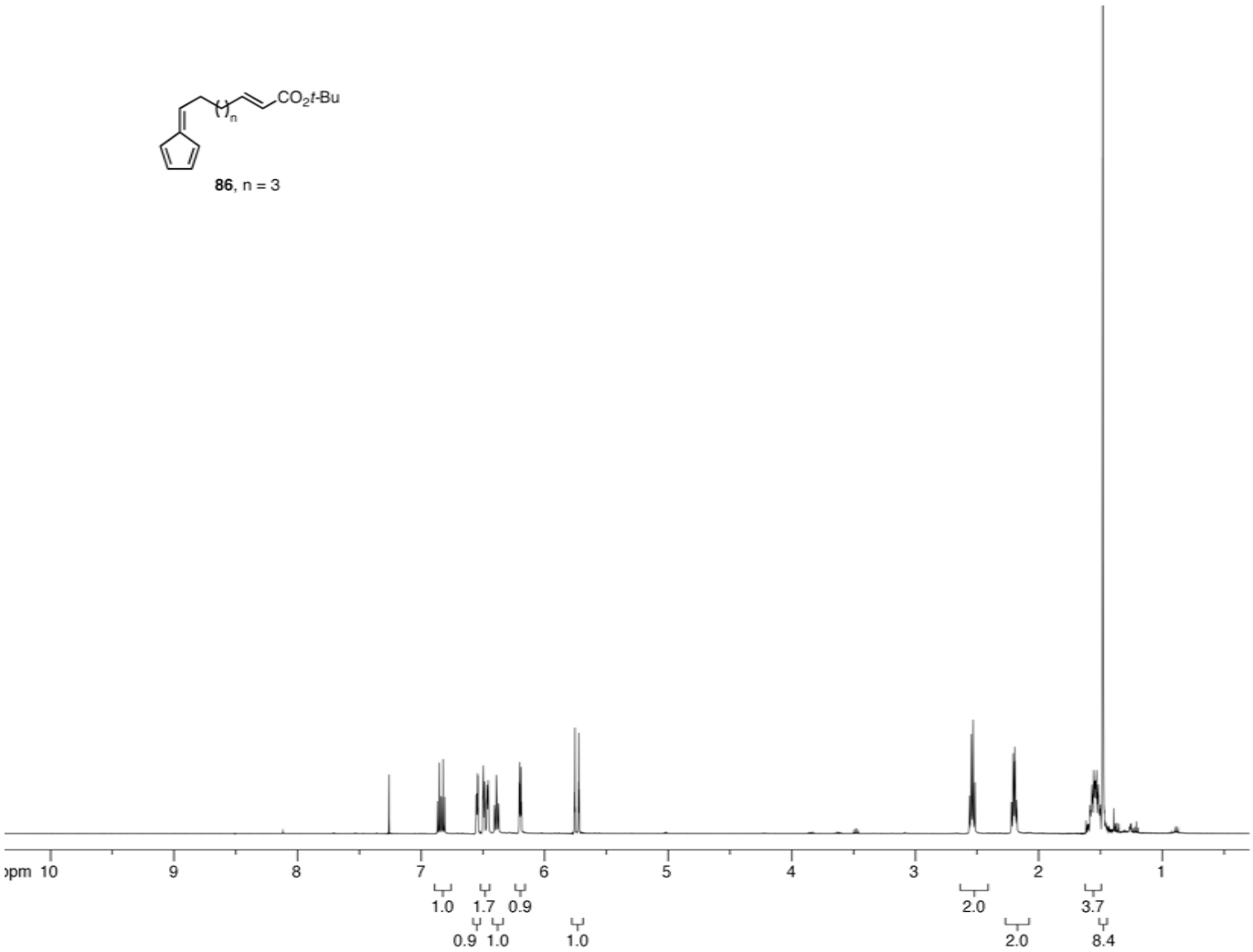
CO2t-Bu
n
86, n = 3
ppm 10
9
8
7
6
5
4
3
2
1
1.0
1.7
0.9
0.9
1.0
1.0
2.0
2.0
3.7
8.4

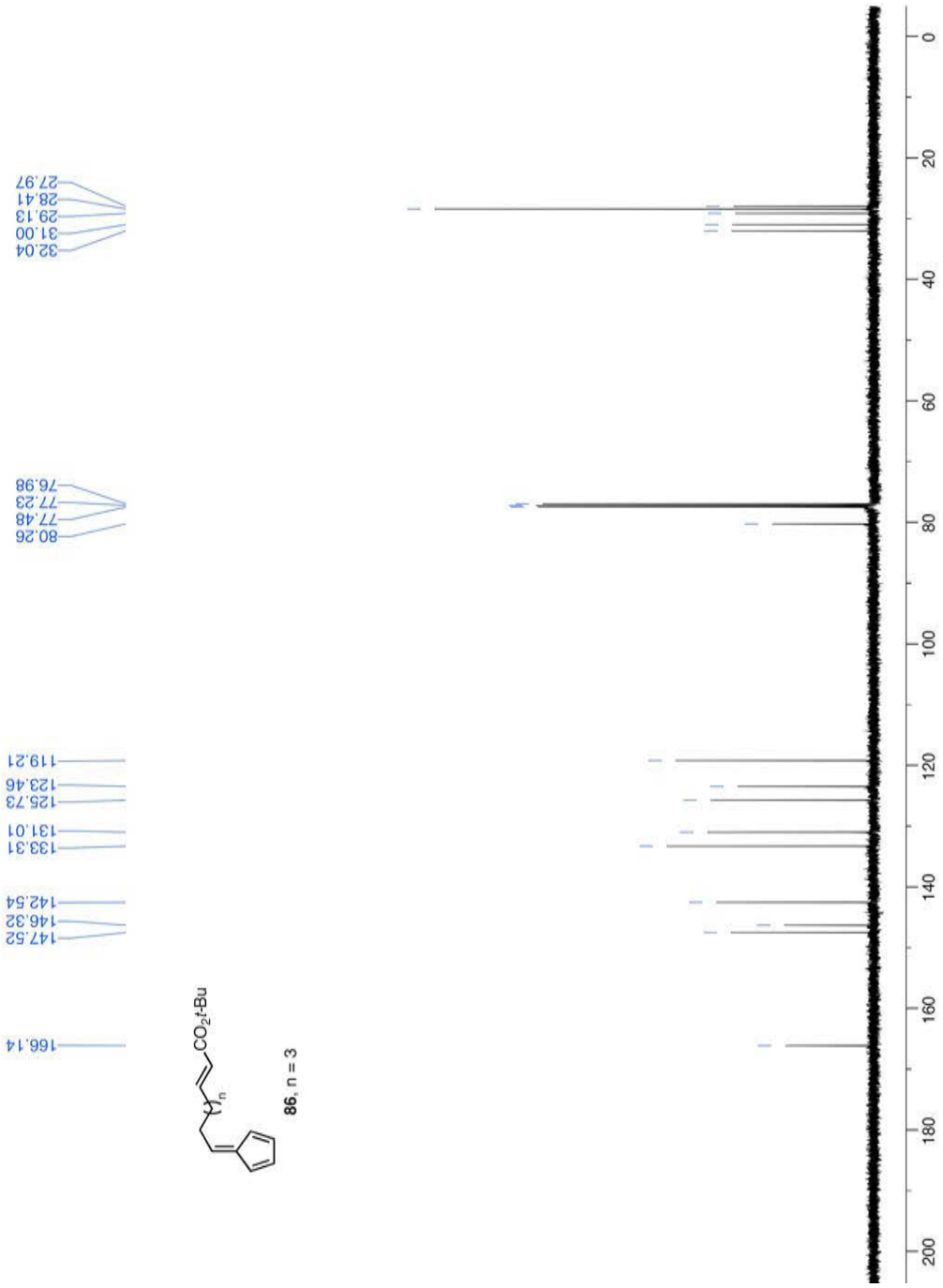
27.97
28.41
29.13
31.00
32.04
76.98
77.23
77.48
80.26
119.21
123.46
125.73
131.01
133.31
142.54
146.32
147.52
166.14
CO2t-Bu
n
86, n = 3
0
20
40
60
80
100
120
140
160
180
200

From bulk electrolysis of:

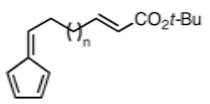

86, n = 2

From bulk electrolysis of:

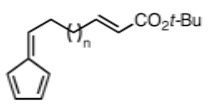

86, n = 3

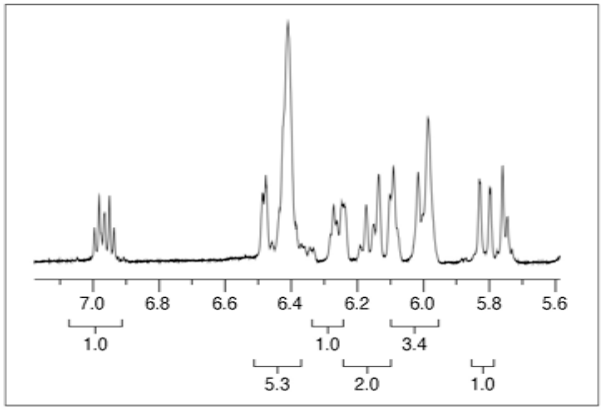

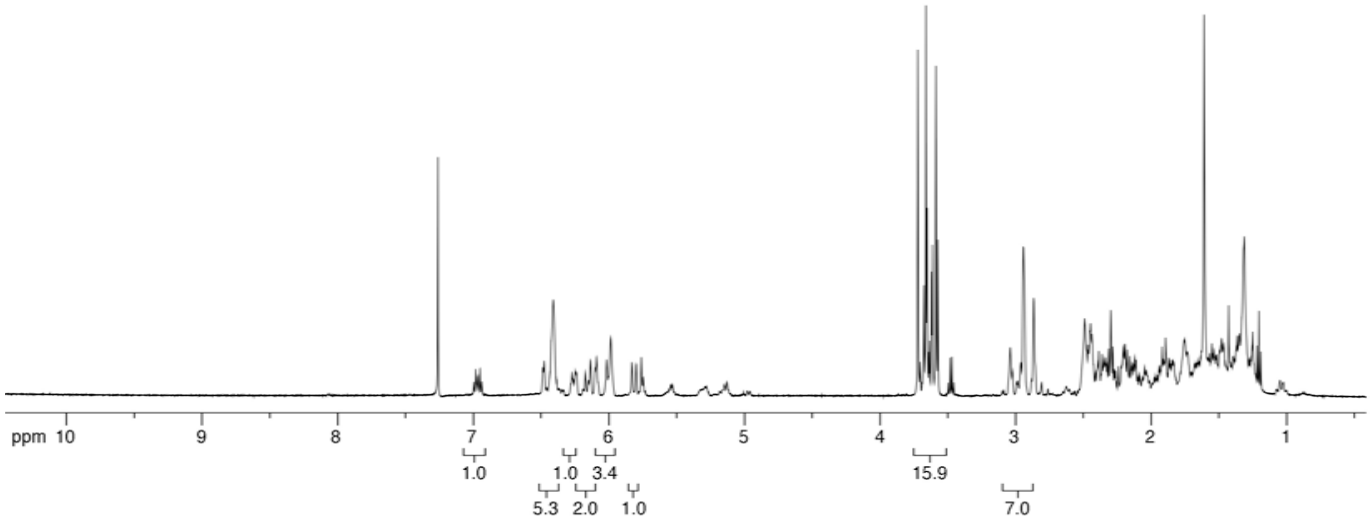

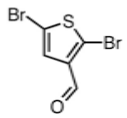

100

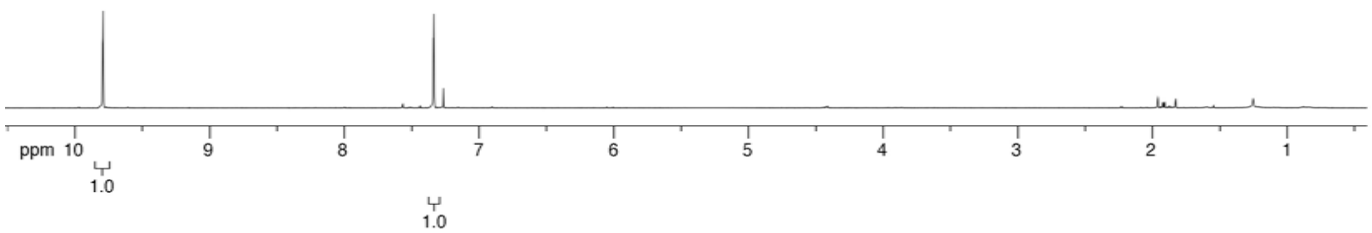

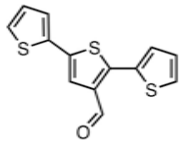
S
S
S
O

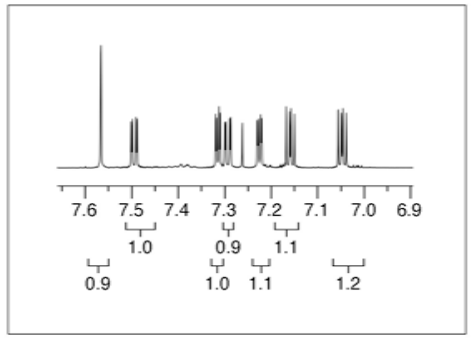
7.6 7.5 7.4 7.3 7.2 7.1 7.0 6.9
1.0
0.9
1.1
0.9
1.0 1.1
1.2

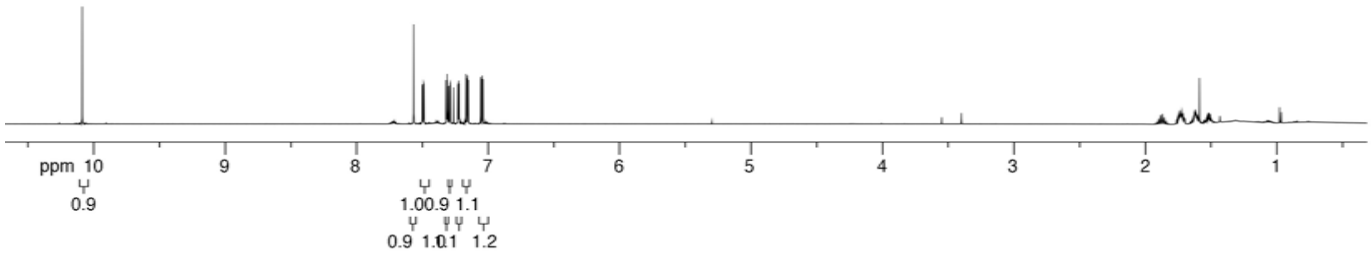
ppm 10
9
8
7
6
5
4
3
2
1
0.9
1.00.9 1.1
0.9 1.0 1.1 1.2

TTh
HO
S
S
S
7.3
7.2
7.1
7.0
1.0
0.9
1.1
2.3
0.9
1.0
2.3
1.2
1.0
1.1
1.0

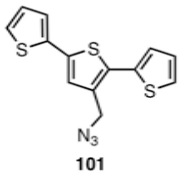
S
S
S
N3

101

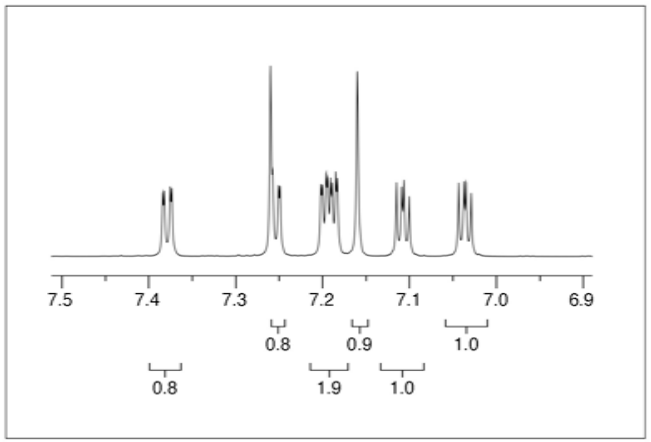
7.5
7.4
7.3
7.2
7.1
7.0
6.9
0.8
0.9
1.0
0.8
1.9
1.0

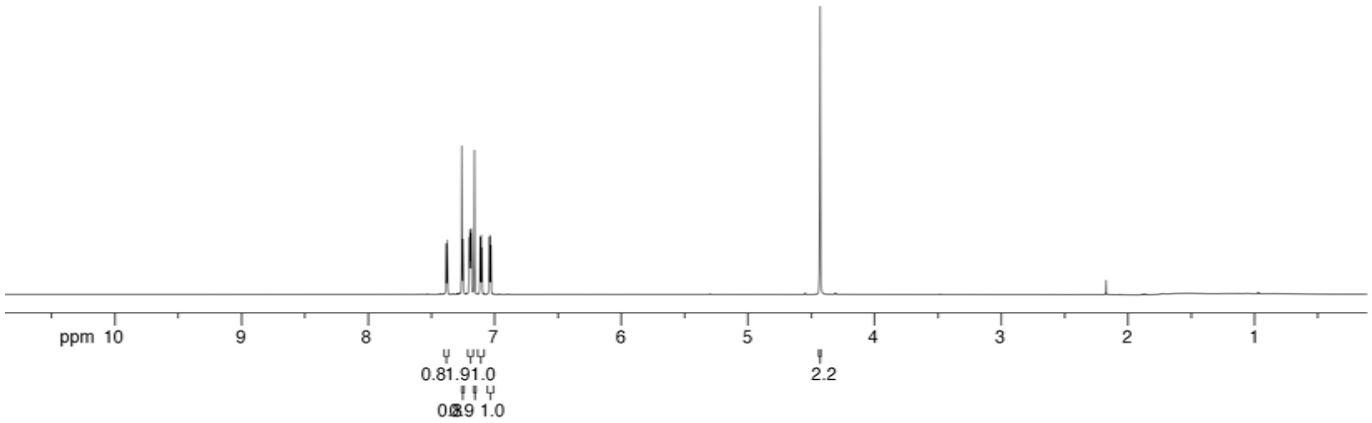
ppm 10
9
8
7
6
5
4
3
2
1
0.8
1.9
1.0
2.2
1.0

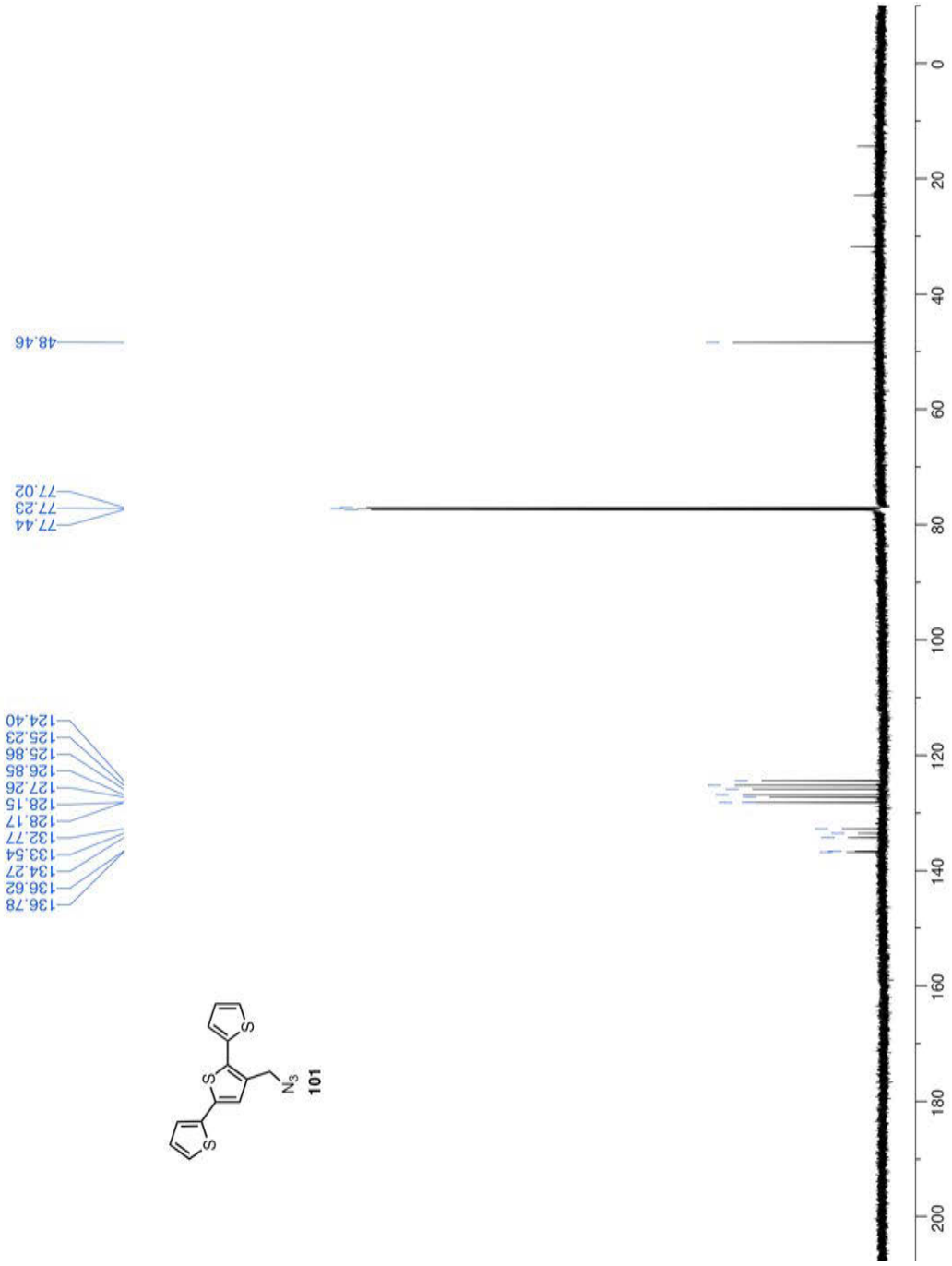
48.46
77.44
77.23
77.02
136.78
136.62
134.27
133.54
132.77
128.17
128.15
127.26
126.85
125.86
125.23
124.40
0
20
40
60
80
100
120
140
160
180
200
S
S
S
N3
101

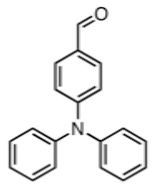

123

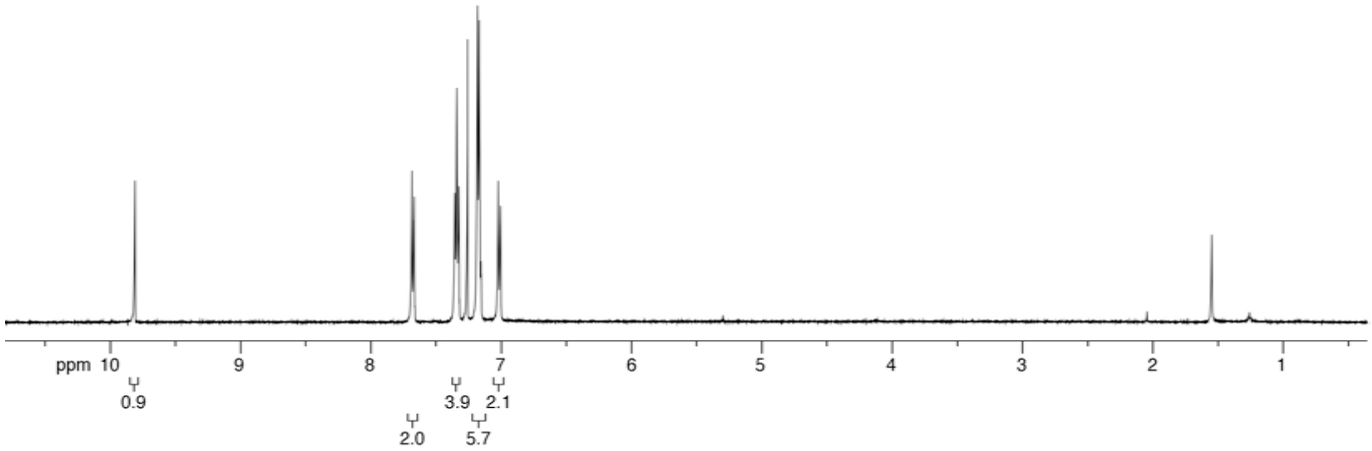

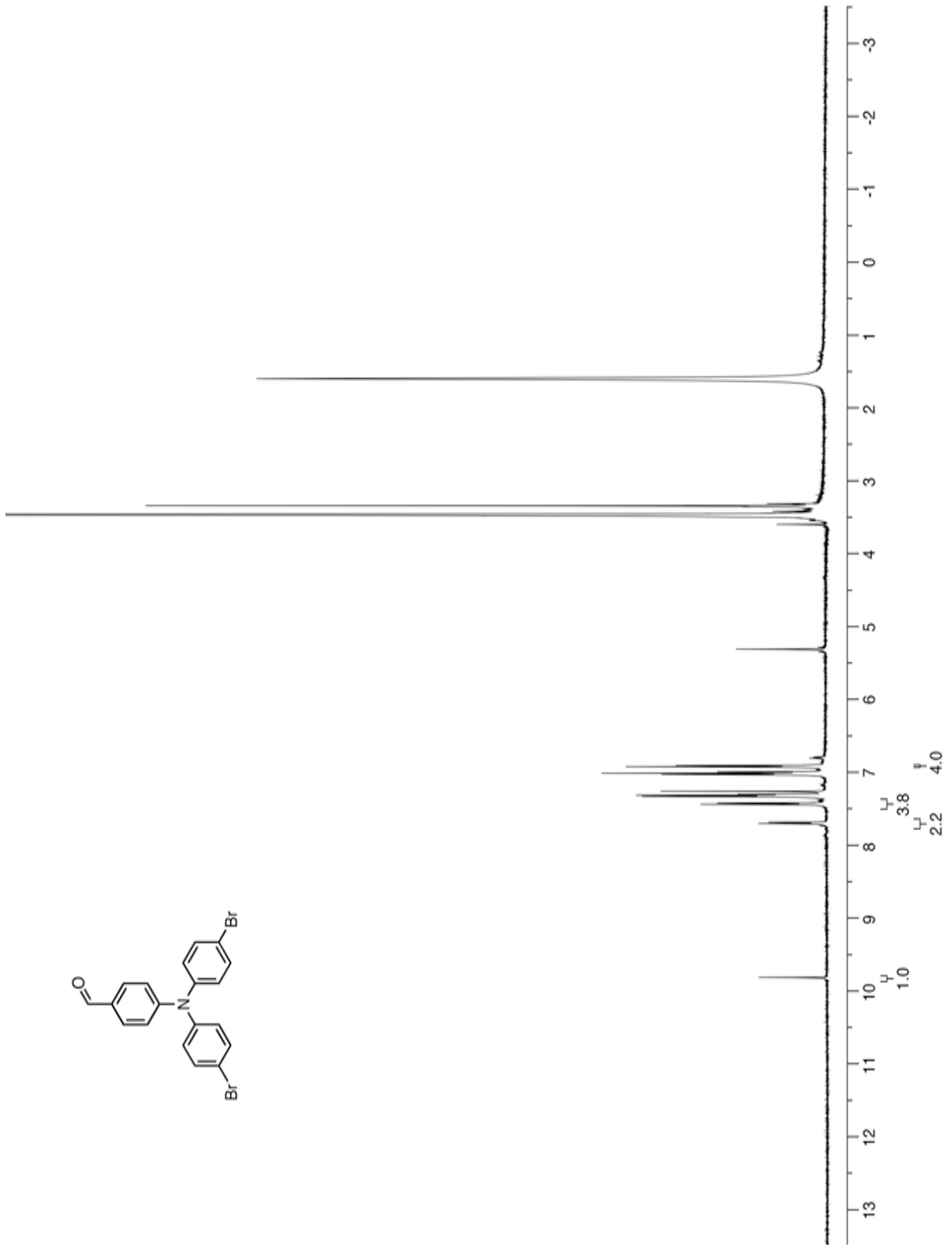
O
N
Br
Br
13
12
11
10
9
8
7
6
5
4
3
2
1
0
-1
-2
-3
1.0
2.2
3.8
4.0

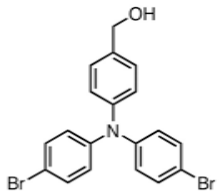

124

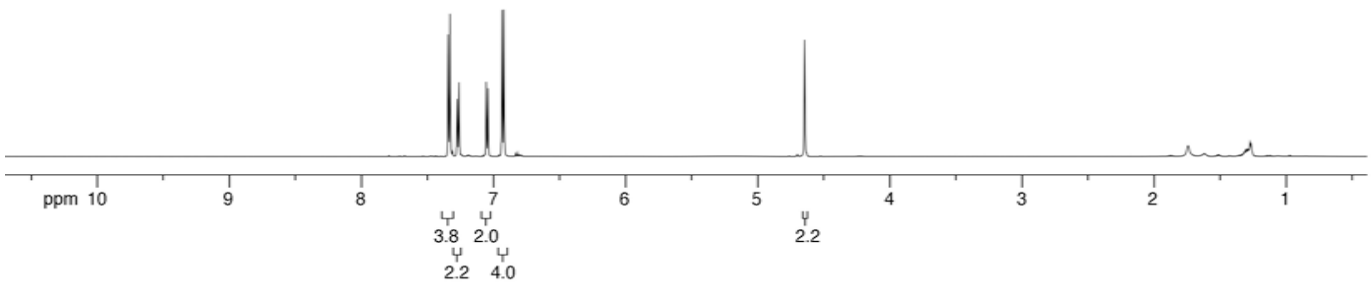

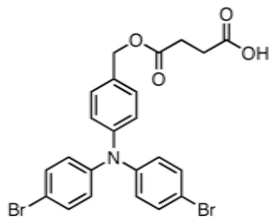

125

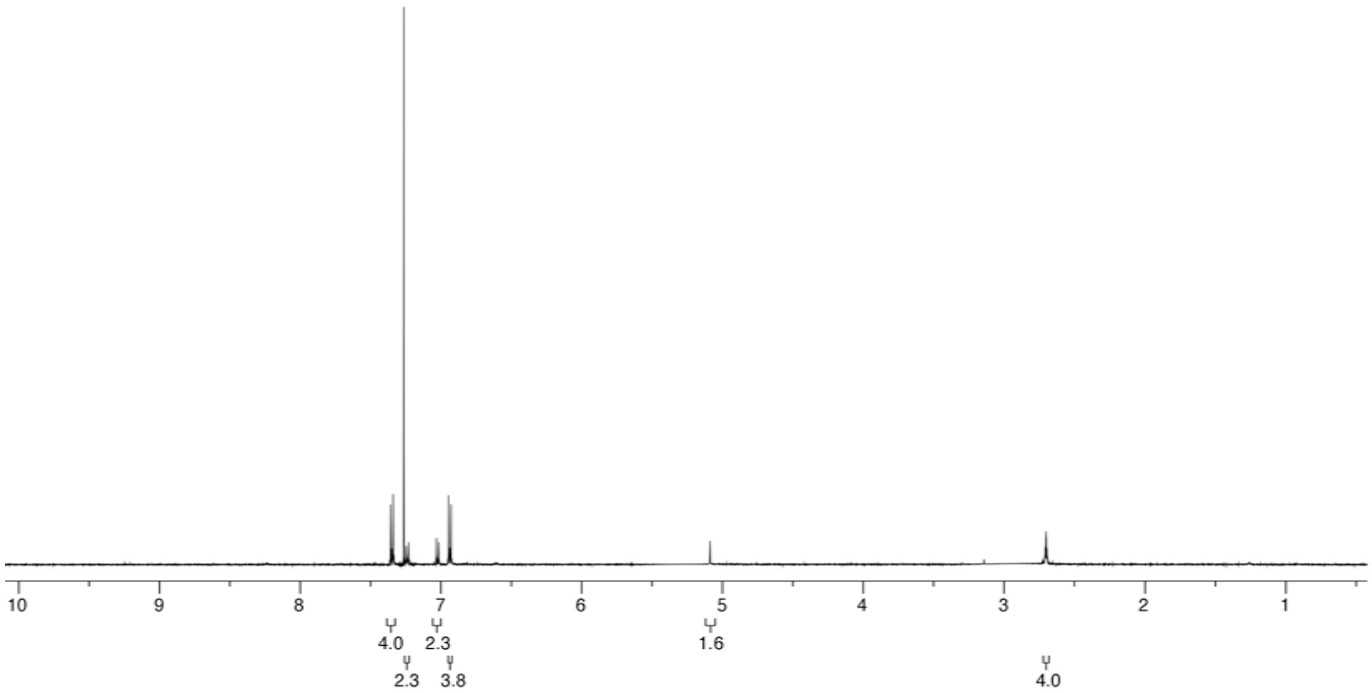

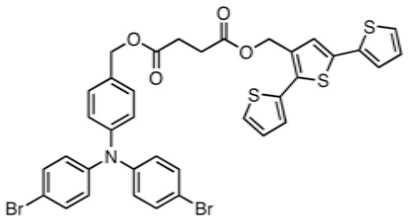

126

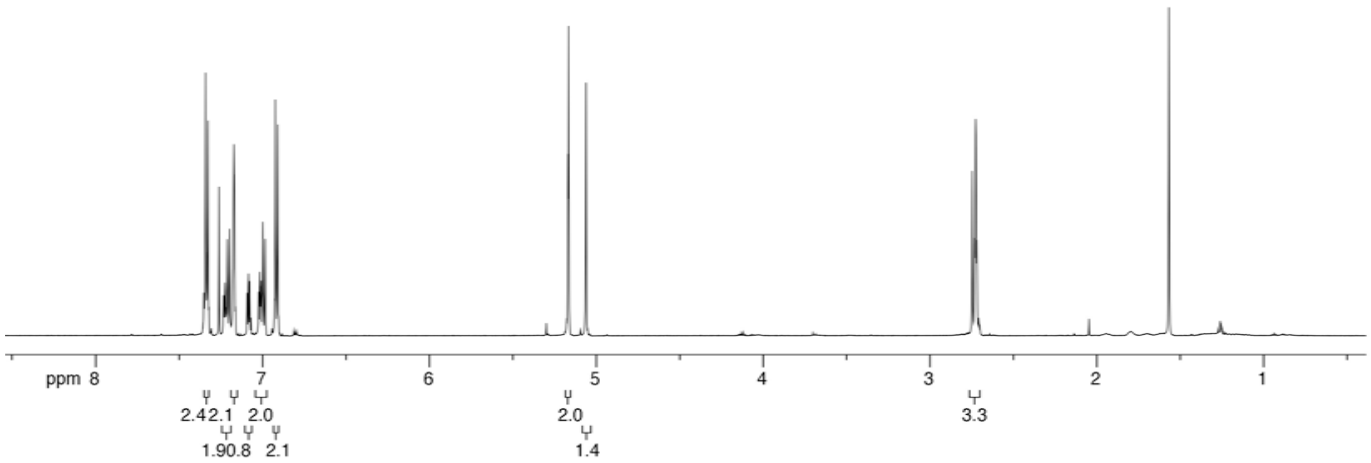

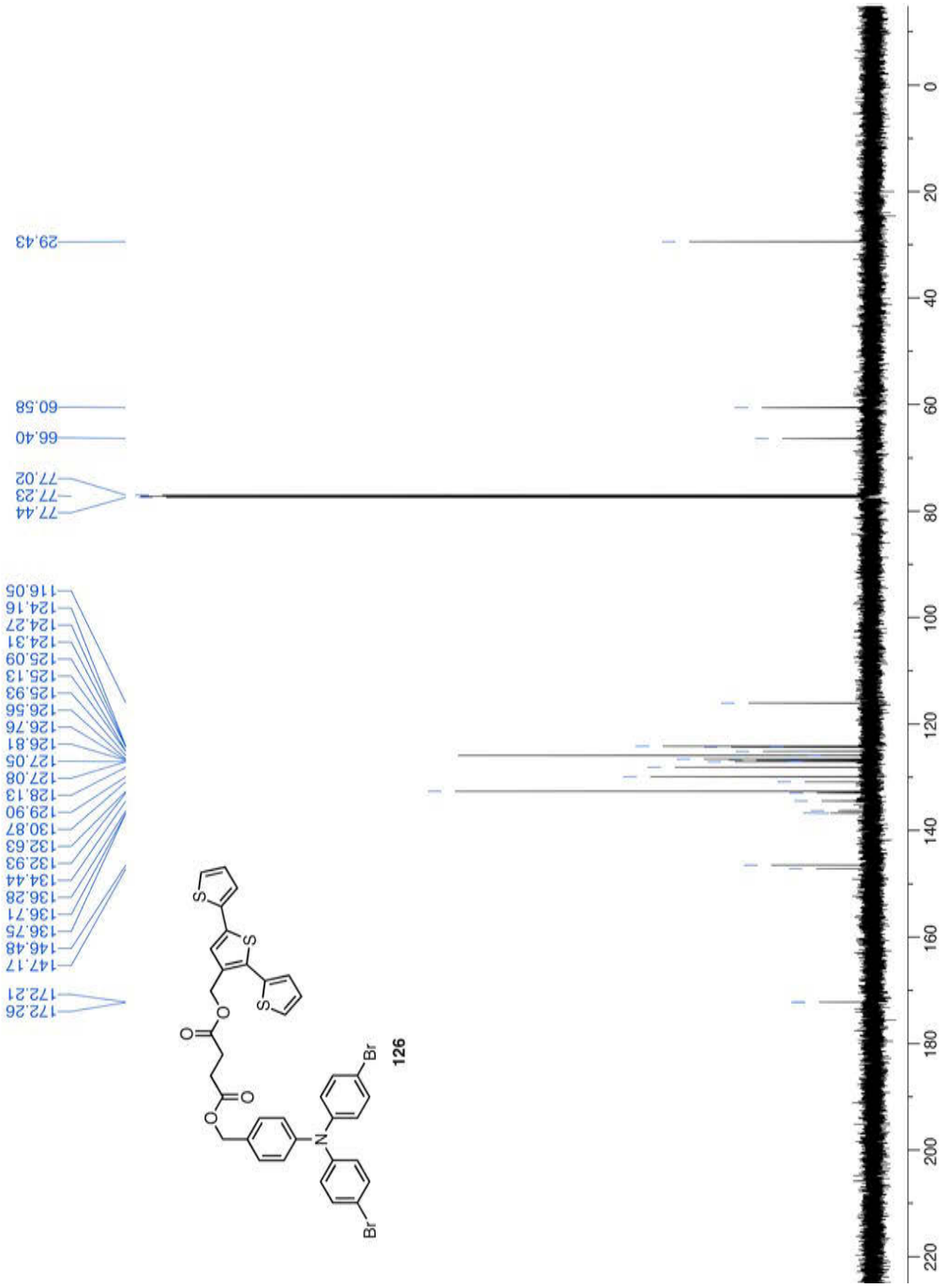
29.43
60.58
66.40
77.02
77.23
77.44
116.05
124.16
124.27
124.31
125.09
125.13
125.93
126.56
126.76
126.81
127.05
127.08
128.13
129.90
130.87
132.63
132.93
134.44
136.28
136.71
136.75
146.48
147.17
172.21
172.26
126

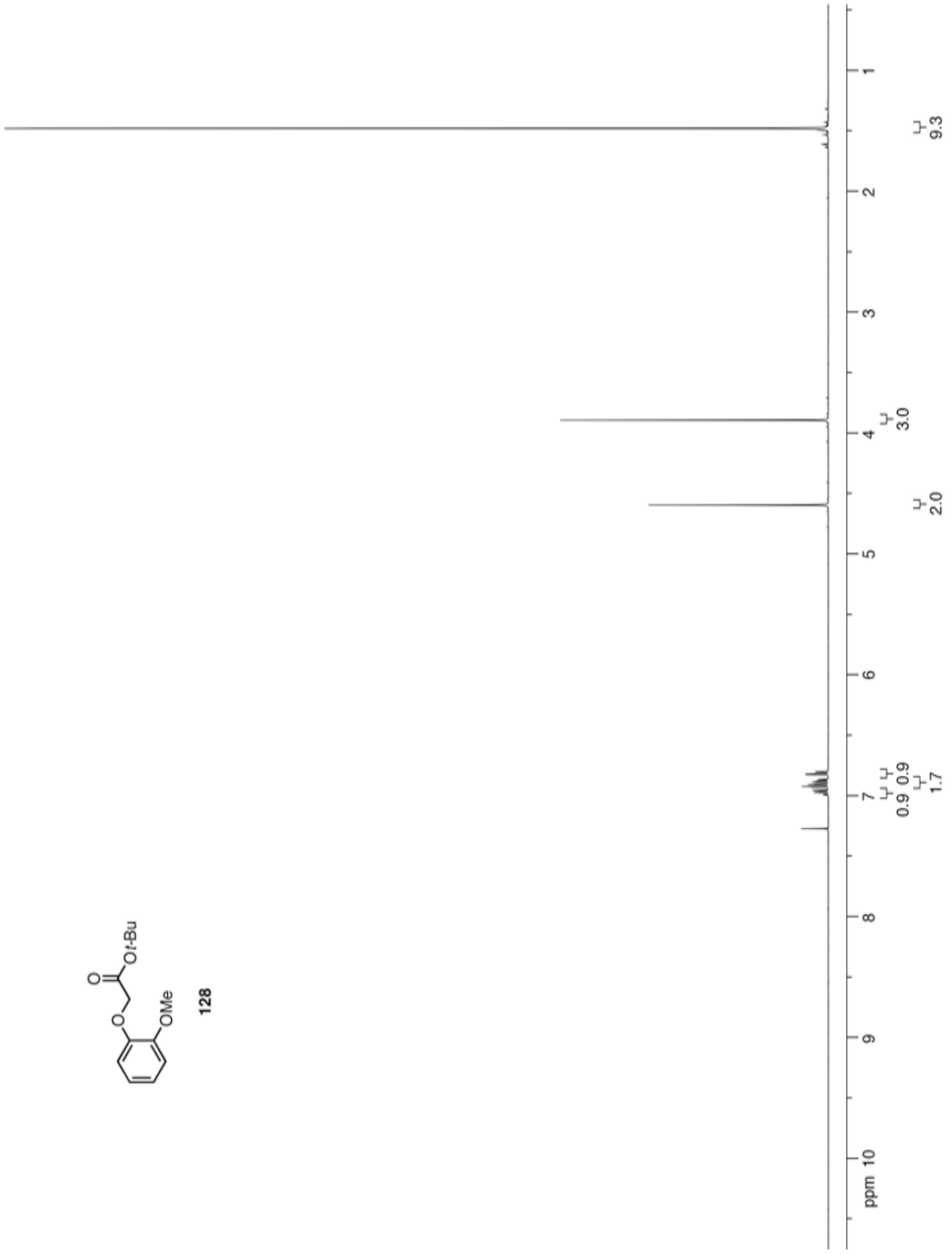
Ot-Bu
O
OMe
128
ppm 10
9
8
7
6
5
4
3
2
1
0.9 0.9
1.7
2.0
3.0
9.3

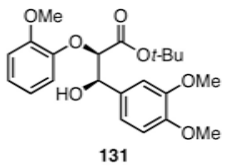

131

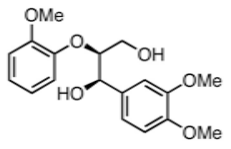
OMe
O
OH
HO
OMe
OMe

132

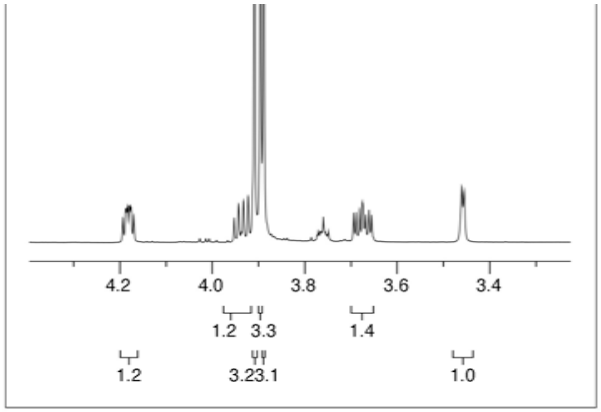
4.2
4.0
3.8
3.6
3.4
1.2
3.3
1.4
1.2
3.2
3.1
1.0

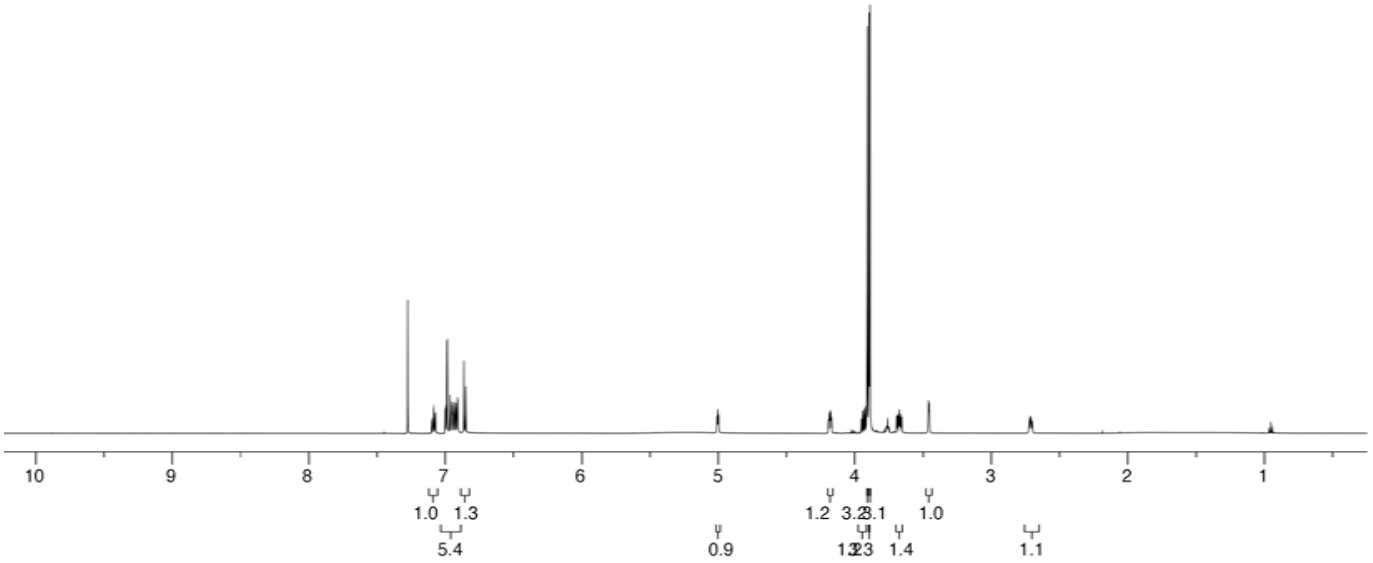
10
9
8
7
6
5
4
3
2
1
1.0
1.3
5.4
0.9
1.2
3.2
3.1
1.0
1.4
1.1

REFERENCES

[1] (a) Peroxy Compounds, Organic. *Ullmann's Encyclopedia of Industrial Chemistry*; VCH: Weinheim, Germany, 2000; Vol. 26, 325–360; (b) Braunecker, W.; Matyjaszewski, K. *Prog. Polym. Sci*. **2007**, *32*, 93–146; (c) Sciannamea, V.; Jerome, R.; Detrembleur, C. *Chem. Rev*. **2008**, *108*, 1104–1126.

[2] Thiboutot, D.; Weiss, J.; Bucko, A.; Eichenfield, L.; Jones, T.; Clark, S.; Liu, Y.; Graeber, M.; Kang, S. *J. Am. Acad. Dermatol.* **2007**, *57*, 791–799.

[3] (a) Montagnon, T.; Tofi, M.; Vassilikogiannakis, G. *Acc. Chem. Res.* **2008**, *41*, 1001–1011; (b) Kuehl Jr., F.; Humes, J.; Egan, R.; Ham, E.; Beveridge, G.; Van Arman, C. *Nature* **1977**, *265*, 170–173; (c) Hemler, M.; Graff, G.; Lands, W. *Biochem. Biophys. Res. Commun.* **1978**, *85*, 1325–1331.

[4] Bundy, G. *Tetrahedron Lett.* **1975**, *16*, 1957–1960.

[5] a) Dickey, F.; Cleland, G.; Lotz, C. *Proc. Natl. Acad. Sci. U.S.A.* **1949**, *35*, 581–586; (b) *For a review on the biological effects of oxidative stress, see:* Uttara, B.; Singh, A.; Zamboni, P.; Mahajan, R. T. *Curr Neuropharmacol*. **2009**, *7*, 65–74.

[6] (a) Gemma, S.; Martí, F.; Gabellieri, E.; Campiani, G.; Novellino, E.; Butini, S. *Tetrahedron Lett.* **2009**, *50*, 5719–5722; (b) Ghorai, P.; Dussault, P.; Hu, C. *Org. Lett.* **2008**, *10*, 2401–2404; (c) Schiaffo, C.; Rottman, M.; Wittlin, S.; Dussault, P. *ACS Med. Chem. Lett.* **2011**, *2*, 316–319; (d) Hartwig, C.L.; Rosenthal, A.S.;

D'Angelo, J.G.; Posner, G.H. and Cooper, R.A. *Biochem. Pharmacol.* **2009**, *77*, 322–336; (e) Posner, G.; Chang, W; Hess, L.; Woodard, L.; Sinishtai, S.; Usera, A.; Maio, W.; Rosenthal, A.; Kalinda, A.; D'Angelo, J.; Peterson, K.; Stohler, R.; Chollet, J.; Santo-Thomas, J.; Snyder, C.; Rottmann, M.; Wittlin, S.; Brun, R.; Shapiro, T. *J. Med. Chem.* **2008,** *51,* 1035–1042; (f) Woodard, L.; Chang, W.; Chen, X; Liu, J.; Shapiro, T.; Posner, G. *J. Med. Chem.* **2009**, *52*, 7458–7462

[7] (a) Moffit, W. *Trans. Faraday Soc.* **1949**, *45*, 373–385. (b) Longuet-Higgins, H. C. *J. Chem. Phys.* **1950**, *18*, 265–274.

[8] Hund, F. *Zeits. f. Physik.* **1928**, *51*, 759–795.

[9] Dowd, P. *J. Am. Chem. Soc.*, **1966**, *88*, 2587–2589.

[10] (a) Dowd, P.; Sachdev, K. *J. Am. Chem. Soc.* **1967**, *89*, 715–716; (b) Dowd, P. *Acc. Chem. Res.* **1972**, 5, 242–248.

[11] Berson, J.; Bushby, R.; McBride, J. M.; Tremelling, M. *J. Am. Chem. Soc.* **1971**, *93*, 1544–1546.

[12] (a) Berson, J. A., Corwin, L., Davis, J. *J. Am. Chem. Soc*., **1974**, *96*, 6177–6179; (b) Berson, J. *Acc. Chem. Res.* **1978**, *11*, 446–453.

[13] Carpenter, B.; Little, R. D.; Berson, J. *J. Am. Chem. Soc.*, **1976**, *98*, 5723–5725; (b) Platz, M.; McBride, J.M.; Little, R. D.; Harrison, J.; Shaw, A.; Potter, S.; Berson, J. *J. Am. Chem. Soc.* **1976**, *98*, 5725–5726.

[14] Borden, W.T. *Tetrahedron Lett*. **1967**, *8*, 259–264.

[15] Berson, J., Corwin, L., Davis, J. *J. Am. Chem. Soc*. **1974**, *96*, 6177–6179.

[16] (a) Borden, W. T. Salem, L. *J. Am. Chem. Soc.* **1973**, *95,* 932–933; (b) Borden, W. T. *J. Am. Chem. Soc.* **1975**, *97,* 2907–2908; (c) Borden, W. T. *J. Am. Chem. Soc.* **1976**, *98*, 2695–2700; (d) Borden, W. T. Davidson, E. R. *J. Chem. Phys.* **1976**, *64,* 663–666.

[17] Goodman, J. L.; Hermann, M. S. *J. Am. Chem. Soc.* **1988**, *110*, 2681–2683.

[18] (a) Berson, J. A.; Rule, M.; Mondo, J. A. *J. Am. Chem. Soc.* **1982**, *104*, 2209–2216; (b) Mazur, M. R.; Berson, J. A. *J. Am. Chem. Soc.* **1982**, *104*, 2217–2222; (c) Mazur, M. R.; Berson, J. A. *J. Am. Chem. Soc.* **1981**, *103*, 684–686.

[19] Weiss, F. *Q. Rev. Chem. Soc*. **1970**, *24*, 278–309.

[20] Schoeller, W. *J. Chem. Soc., Perkin Trans. II.* **1978**, 525–529.

[21] Siemionko, R., Shaw, A; O'Connell, G.; Little, R.D.; Carpenter, B.; Shen, L.; Berson, J. *Tetrahedron Lett.* **1978**, *38*, 3529–3532.

[22] (a) Masjedizadeh, M.; Dannecker-Doerig, I.; Little, R.D. *J. Org. Chem*. **1990**, *55*, 2742–2752; (b) Little, R. D.; Masjedizadeh, M.; Moeller, K.; Dannecker-Doerig, I. *Synlett* **1992**, 107–113.

[23] Little, R.D. *Chem. Rev*. **1996**, *96*, 93−114.

[24] Maiti, A.; Gerken, J.; Masjedizadeh, M.; Mimieux, Y.; Little, R.D. *J. Org. Chem.* **2004**, *69*, 8574–8582.

[25] Van Hijfte, L.; Little, R. D.; Petersen, J. L.; Moeller, K. D. *J. Org. Chem*. **1987**, *52*, 4647–4661.

[26] (a) Little, R.D.; Muller, G. *J. Am. Chem. Soc*. **1981**, *103*, 2744-2149; (b) Little, R.D.; Higby, R.; Moeller, K. *J. Org. Chem.* **1983**, *48*, 3139–3140.

[27] Little, R.D; Carroll, G.; Petersen, J. *J. Am. Chem. Soc.* **1983**, *105*, 928–932.

[28] Van Hijfte, L.; Little, R. D. *J. Org. Chem*. **1985**, *50*, 3940–3942.

[29] In this case, an approach to the synthesis of Taxol was reported rather than a total synthesis. *See:* Ott, M.; Little, R.D. *J. Org. Chem.* **1997**, *62*, 1610–1616.

[30] Zhong, W.; Little, R.D. *Tetrahedron Lett*. **2009**, *50*, 4994–4997.

[31] (a) Adam, W.; Finzel, R. *J. Am. Chem. Soc.* **1992**, *114*, 4563–4568. Pioneering work by Gajewski and coworkers demonstrated the radical nature of cyclohexane-1,4-diyl, which was determined to be a viable intermediate in the cope rearrangement. *See:* (b) Gajewski, J. J.; Conrad, N. D. *J. Am. Chem. Soc.* **1978**, *100*, 6268–6269; (c) Gajewski, J. J.; Conrad, N. D.; Emrani, J.; Gilbert, K. *ARKIVOC* **2002**, 18–29.

[32] Little, R. D.; Brown, L. M.; Masjedizadeh, M. R. *J. Am. Chem. Soc.* **1992**, *114*, 3071–3075.

[33] (a) Berson, J., Corwin, L., Davis, J. *J. Am. Chem. Soc*. **1974**, *96*, 6177–6179; (b) Berson, J. *Acc. Chem. Res.* **1978**, *11*, 446–453; (c) Masjedizadeh, M.; Dannecker-Doerig, I.; Little, R.D. *J. Org. Chem*. **1990**, *55*, 2742–2752; (d) Little, R. D.; Masjedizadeh, M.; Moeller, K.; Dannecker-Doerig, I. *Synlett* **1992**, 107–113.

[34]Little, R.D.; Losinski-Dang, L.; Venegas, M.; Merlic, C. *Tetrahedron Lett.* **1983**, *24*, 4499–4502.

[35] Losinski Dang, L. Pyrolysis of 7-Alkylidene-2,3-diazabicyclo[2.2.1]hept-2-enes in the Presence of Molecular Oxygen. Formation and Chemistry of Fused (3,4-Dioxabicyclo[3.3.0]oct-1(8)-enes) and Bridged (7-Alkylidene-2,3-dioxabicyclo[2.21]heptanes) Peroxides. Ph.D. Thesis, The University of California Santa Barbara, 1982.

[36] Stone, K.; Little, R.D. *J. Org. Chem*. **1984**, *49*, 1849–1853.

[37] Ott, M.; Little, R.D. *J. Org. Chem.* **1997**, *62*, 1610–1616; (b) Little, R.D.; Venegas, M. *J. Org. Chem.* **1978**, *43*, 2921–2923.

[38] Since the carbonyl unit of an aldehyde can serve as a diylophile in cycloaddition reactions with TMM diyls, mixtures of several regioisomeric products of this nature were isolated. *See:* Little, R.D.; Bode, H.; Stone, K.; Wallquist, O.; Dannecker, R. *J. Org. Chem*. **1985**, *50*, 2401–2403.

[39] (a) Adam, W.; Arce, J. *J. Am. Chem. Soc.* **1975**, *97*, 926–928.

[40] Wilson, R.M.; Geiser, F. *J. Am. Chem. Soc.* **1978**, *100*, 2225–2226.

[41] Stork, G.; Zhao, K. *Tetrahedron Lett.* **1989**, *30*, 287–290.

[42] (a) Nicolaou, K.C.; Mathison, C.; Montagnon, T. *Angew. Chem., Int. Ed.* **2003**, *42*, 4077–4082; (b) Fleming, F.; Funk, L.; Altundas, R.; Tu, Y. *J. Org. Chem*. **2001**, *66*, 6502–6504.

[43] Nugteren, D.; Hazelhof, E. *Biochim. Biophys. Acta* **1973**, *326*, 448–461.

[44] (a) Bartlett, P.; Nozaki, K. *J. Am. Chem. Soc.* **1947**, *69*, 2299–2306; (b) Greene, F.; Adam, W.; Cantrill, J. *J. Am. Chem. Soc.* **1961**, *83*, 3461–3468; (c) Walling,

C. *Pure Appl. Chem.* **1967**, *15*, 69–80; (d) Walling, C.; Waits, H.; Milovanovic, J.; Pappiaonnou, C. *J. Am. Chem. Soc.* **1970**, *92*, 4927–4932; (e) Pryor, W.; Bickley, H. *J. Org. Chem.* **1972**, *37*, 2885–2893; (f) Pryor, W.; Hendrickson, W. *J. Am. Chem. Soc.* **1975**, *97*, 1580–1582; (g) Pryor, W.; Hendrickson, W. *J. Am. Chem. Soc.* **1975**, *97*, 1582–1583; (h) Bravo, A.; Fontana, F.; Fronza, G.; Minisci, F.; Zhao, L. *J. Org. Chem.* **1998**, *63*, 254–263.

[45] (a) Roberfroid, M.; Buc Calderon, P. *Free Radicals and Oxidation Phenomena in Biological Systems*; Marcel Dekker: New York, 1995; (b) Cafferata, L.; Rimada, R. *Molecules*, **2003**, *8*, 655–662; (c) Minisci, F.; Gambarotti, C.; Pierini, M.; Porta, O.; Punta, C.; Recupero, F.; Lucarini, M.; Mugnaini, V. *Tetrahedron Lett.* **2006**, *47*, 1421–1424; (d) Leival, L.; Jorgel, N.; Romero, J.; Cafferata, L.; Varal, M.; Castro, E. *J. Argent. Chem. Soc.* **2008**, *96*, 111–122.

[46] Calculations predicted that hydrogen bonding occurs at the oxygen distal to the alkyl group in the peroxide bond.

[47] (a) Erden, I.; Amputch, M. *Tetrahedron Lett*. **1987**, *28*, 3779–3782; (b) Erden, I.; Drummond, J.; Alstad, R.; Xu, F. *Tetrahedron Lett*. **1993**, *34*, 1255–1258; (c) Erden, I.; Drummond, J.; Alstad, R.; Xu, F. *Tetrahedron Lett.* **1993**, *34*, 2291–2294; (d) Erden, I.; Xu, F.; Drummond, J.; Alstad, R. *J. Org. Chem*. **1993**, *58*, 3611–3612.

[48] We express our gratitude to Professor Dean J. Tantillo, Department of Chemistry at UC Davis, for carrying out the IRC calculations.

[49] (a) Thiele, J. *Chemische Berichte* **1900**, *33*, 666–673. (b) Thiele, J. *Justus Liebigs Ann. Chem.* **1908**, 348–362.

[50] (a) McLoughlin, J. I.; Little, R. D. *J. Org. Chem.* **1988**, *53*, 3624–3626; (b) Kyburg, R.; Schaltegger, H.; Neuenschwander, M. *Helv. Chim. Acta* **1971**, *54*, 1037–1046; (c) Neuenschwander, M.; Iseli, R. *Helv. Chim. Acta* **1977**, *60*, 1061–1072.

[51] (a) Büchi, G.; Berthet, D.; Decorzant, R.; Grieder, A.; Hauser, A. *J. Org. Chem*. **1976**, *41*, 3208–3209; (b) Freiesleben, W.; *Angew. Chem.* **1963**, *12*, 576.

[52] Stone, K.; Little, R.D. *J. Org. Chem*. **1984**, *49*, 1849–1853.

[53] Erden, I.; Xu, F.; Sadoun, A.; Smith, W.; Sheff, G.; Ossun, M. *J. Org. Chem.* **1995**, *60*, 813–820.

[54] Little, W.; Koestler, R. *J. Org. Chem.* **1961**, *26*, 3247–3250.

[55] Alt, H.; Köppl, A. *Chem. Rev*., **2000**, *100*, 1205−1221.

[56] Tacke, M.; Allen, L. T.; Cuffe, L.; Gallagher, W. M.; Lou, Y.; Menzoa, O.; Mueller-Bunz, H.; Rehnmann, F.-J.; Sweeny, N. *J. Organomet. Chem.* **2004**, *689,* 2242–2249.

[57] Neuenschwander, M. *Chem. Double-Bonded Funct. Groups* **1989**, *2*, 1131–1268.

[58] (a) Houk, K.N.; Luskus, L. J.; Bhacca, N. S. *J. Am. Chem. Soc.* **1970**, *92*, 6392–6394; (b) Houk, K. N.; Luskus, L. J. *Tetrahedron Lett.* **1970**, *11*, 4029–4031; (c) Houk, K. N.; Luskus, L. J. Bhacca, N. S. *Tetrahedron Lett.* **1972**, *13,* 2297–2300; (d) Houk, K. N.; Luskus, L. J. *J. Org. Chem.* **1973**, *38*, 3836–3843; (e) Dunn, L.

C.; Chang, Y.-M.; Houk, K. N. *J. Am. Chem. Soc.* **1976**, *98*, 7095–7096; (f) Reiter, E.; Dunn, L. C.; Houk, K. N. *J. Am. Chem. Soc.* **1977**, *99*, 4199–4201.

[59] Wu, T.-S.; Mareda, J.; Gupta, Y. N.; Houk, K. N. *J. Am. Chem. Soc.* **1983**, *105*, 6996–6997.

[60] Hong, B.-C.; Shr, Y.-J.; Wu, J.-L.; Gupta, A. K.; Lin, K.-J. *Org. Lett*. **2002**, *4*, 2249–2252.

[61] Hong, B.-C.; Chen, F.-L.; Chen, S.-H.; Liao, J.-H.; Lee, G.-H. *Org. Lett.* **2005**, *7*, 557–560.

[62] *For reviews*: (a) Yates, P. *Adv. Alicyclic. Chem.* **1968**, *2,* 59– 184; (b) Bergmann, E. D. *Chem. Rev.* **1968**, *68*, 41–84.

[63] Fry, A. J. *Synthetic Organic Electrochemistry, 2nd Ed.*; John Wiley & Sons:New York, 1989; p. 57.

[64] Seebach, D. *Angew. Chemie., Int. Ed.* **1979**, *18*, 239–336.

[65] Little, R. D.; Moeller, K. *Interface* **2002**, 36–42.

[66] Sowell, G.; Wolin, R.; Little, R. D. *Tetrahedron Lett.* **1990**, *31*, 485–488.

[67] Carroll, G. L.; Little, R.D. *Org. Lett*. **2000**, *2,* 2873−2876.

[68] Fry, A.; Little, R. D.; Leonetti, J. *J. Org. Chem.* **1994**, *59*, 5017–5026.

[69] (a) Enholm, E.; Trivellas, A. *Tetrahedron Lett.* **1989**, *30*, 1063–1066. (b) Shim, S.; Hwang, J.; Kang, H.; Chang, M. *Tetrahedron Lett.* **1990**, *31*, 4765–4768.

[70] Inokuchi, T.; Kawafuchi, H.; Torri, S. *J. Org. Chem.* **1991**, *56*, 4983–4985.

[71] Corey, E. J.; Pyne, S. *Tetrahedron Lett.* **1983**, *24*, 2821–2824.

[72] The results reported are for the solvent corrected calculations, without which delocalization of the radical anion across both subunits is evident.

[73] (a) Macías-Ruvalcaba, N.; Felton, G.; Evans, D. H. *J. Phys. Chem. C* **2009**, *113*, 338–345; (b) Macías-Ruvalcaba, N.; Evans, D. H. *J. Phys. Chem. C* **2010**, *114*, 1285–1292.

[74] Nicolaou, K. C.; Adsool, V.; Hale, C. *Org. Lett.* **2010**, *12*, 1552–1555.

[75] Helmholtz, H. *Ann. Rev.* **1879**, *30*, 337–382.

[76] Gouy, M. G. *J. Phys. Radium* **1910**, *9*, 457–468.

[77] (a) Stern, O. *Z. Elektrochem.* **1924**, *30*, 508–516; (b) Evans, D. H. *Acc. Chem. Res*. **1977**, *10*, 313–319.

[78] Bordwell, F.; Harrelson, J., Satish, A. *J. Org. Chem.* **1989**, *54*, 3101–3105.

[79] Little, R. D.; Fox, D.; Hijfte, L. V.; Dannecker, R.; Sowell, G.; Wolin, R. L.; Moens, L.; Baizer, M. *J. Org. Chem.* **1988**, *53*, 2287–2294.

[80] Moeller, K. D; Tinao, L. V. *J. Am. Chem. Soc.* **1992**, *114*, 1033–1041.

[81] Moëns, L.; Baizer, M. M.; Little, R. D. *J. Org. Chem.* **1986**, *51*, 4497–4498.

[82] Sitzmann, H.; Bock, H.; Boese, R.; Dezember, T.; Havlas, Z.; Kaim, W.; Moscherosch, M.; Zanathy, L. *J. Am. Chem. Soc.* **1993**, *115*, 12003–12009.

[83] Within the dimer/cyclized product mixture HPLC fraction, signals consistent with the "fused" structure, **95**, were identified using the 2D COSY NMR spectrum (see Figure 28). In particular, the signals at 6.3 (yellow line), 6.2 (red line), and 6.0 ppm (orange line) were correlated to a peak at 2.85 ppm (green line), assigned to the

doubly allylic proton, H_5, (see below – horizontal black lines drawn between colored lines indicate a correlation was observed in the 2D COSY spectrum). Futhermore, the peak at 2.85 ppm coupled to the peak at 2.0 ppm attributed to H_6, which coupled to the protons α to the ester at ca. 2.45 ppm (blue line).

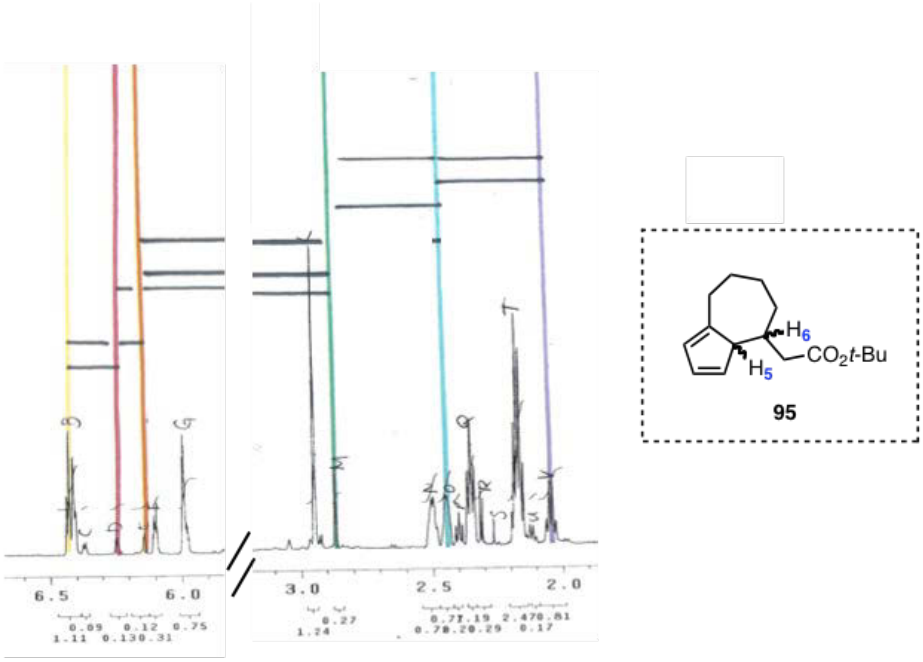

[84] (a) Tanasova, M.; Sturla, S. J.; *Chem. Rev.* **2012**, *112*, 3578–3610; (b) Bhandarkar, S.; Jaconi, M.; Fried, L.; Bonner, M.; Lefkove, B.; Govindarajan, B.; Perry, B.; Parhar, R.; Mackelfresh, J.; Sohn, A.; Stouffs, M.; Knaus, U.; Yancopoulos, G.; Reiss, Y.; Benest, A.; Augustin, H.; Arbiser, J. *J. Clin. Invest.* **2009**, *119*, 2359–2365.

[85] (a) Lane, R. F.; Hubbard, A. T. *J. Phys. Chem.* **1973**, *77*, 1401–1410; (b) Lane, R. F.; Hubbard, A. T. *J. Phys. Chem.* **1973**, *77*, 1411–1421.

[86] Moses, P. R.; Wier, L.; Murray, R. W. *Anal. Chem.* **1975**, *47*, 1882–1886.

[87] *For reviews:* (a) Snell, K. D.; Keenan, A. G. *Chem. Soc. Rev.* **1979**, ***8***, 259–282; (b) Murray, R. W. *Acc. Chem. Res.* **1980**, *13*, 135–141; (c) Murray, R. W. *Ann. Rev. Mater. Sci*. **1984**, *14*, 145–169; (d) Murray, R. W.; Ewing, A.; Durst, R. *Anal. Chem.* **1987**, *59*, 379A–390A.

[88] Martin, C. R.; Foss Jr., C. R. Chemically Modified Electrodes. In *Laboratory Techniques in Electroanalytical Chemistry;* Kissinger, P.T.; Heineman, W. R., Eds.; Marcel Dekker, Inc.:New York, 1994; pp 403–439.

[89] (a) Delamar, M.; Hitmi, R.; Pinson, J.; Savéant, J. M. *J. Am. Chem. Soc.* **1992**, *114*, 5883–5884; (b) Brooksby, P. A.; Downdard, A. J. *Langmuir* **2004**, *20*, 5038–5045; *For a review:* (c) Downard, A. *Electroanalysis* **2000**, *12,* 1085–1096 *and references therein*.

[90] Brown, A. P.; Anson, F. C. *Anal. Chem.* **1977**, *49*, 1589–1595.

[91] (a) Dubois, L. H.; Muzzo, R. G. *Ann. Rev. Phys. Chem.* **1992**, *43*, 437–463; (b) Walczak, M. M. ; Chung, C.; Stole, S. M.; Widrig, C. A.; Porter, M.D. *J. Am. Chem. Soc*. **1991**, *113*, 2370–2378.

[92] Facci, J. S. *Tech. Chem.* **1992**, *22*, 119.

[93] Miller, L. L.; Van de Mark, M. R. *J. Electroanal. Chem.* **1978**, *88*, 437–440.

[94] Merz, A.; Bard, A. J. *J. Am. Chem. Soc.* **1978**, *100*, 3222–3223.

[95] (a) Wrighton, M. S.; Austin, R. G.; Bocarsly, A. B.; Bolts, J. M.; Hass, O.; *J. Electroanal. Chem.* **1978**, *87*, 429–433; (b) Daum, P.; Lenhard, J. R.; Rolison, D. R; Murray, R. W. *J. Am. Chem. Soc.* **1980**, *102*, 4649–4653; (c) Nowak, R. J.;

Schultz, F. A.; Umana, M.; Lam, R.; Murray, R. W. *Anal. Chem.* **1980**, *52*, 315–321.

[96] Oyama, N.; Anson, F. C. *J. Am. Chem. Soc.* **1979**, *101*, 739–741.

[97] Szentirmay, M. Z.; Martin, C. R. *Anal. Chem.* **1984**, *56*, 1898–1902.

[98] Steckhan, E. *Angew. Chem. Int. Ed. Engl.* **1986**, *25*, 683–701.

[99] Steckhan, E.; Kuwana, T. *Ber. Bunsenges, Phys. Chem.* **1974**, *78*, 253–259.

[100] Park, Y. S.; Little, R. D. *J. Org. Chem.* **2008***, 73,* 6807-6815.

[101] Mayers, B. T.; Fry, A. J. *Org. Lett.* **2006**, *8*, 411-414.

[102] Ruther, R.; Rigsby, M.; Gerken, J.; Hogendoorn, S.; Landis, E.; Stahl, S.; Hamers, R. *J. Am. Chem. Soc.* **2011**, *133*, 5692–5694.

[103] Zhang, Y.; Murphy, C.; Jones, W. *Macromolecules* **2002**, *35*, 630–636.

[104] Collis, G.; Burrell A. *J. Org. Chem.* **2003**, *68*, 8974–8983.

[105] Collis, G.; Burrell, A.; Blandford, E.; Officer, D. *Tetrahedron* **2007**, *63*, 11141–11152.

[106] Rogers, S.; Melander, C. *Angew. Chem. Int. Ed.* **2008**, *47*, 5229–5231.

[107] Bandini, M.; Pietrangelo, A.; Sinisi, R.; Umani-Ronchi, A.; Wolf, M. *Eur. J. Org. Chem*. **2009**, 3554–3561.

[108] Wakeham, D.; Donne, S.; Belcher, W.; Dastoor, P. *Synth. Met.* **2008**, *158*, 661–669.

[109] Kennedy, K. G.; Miles, D. T. *Journal of undergraduate chemistry research* **2004**, *4*, 145–150.

[110] I am sincerely grateful for the assistance of Brian Stahl (Hawker Group, UCSB) in obtaining and processing the SEM and AFM images.

[111] (a) Zeng, C-C.; Zhang, N-T; Lam, C. M.; Little, R. D. *Org. Lett*. **2012**, *14,* 1314-1317; (b) Zhang, N-T; Zeng, C-C.; Lam, C. M.; Gbur, R. K.; Little, R. D. *J. Org. Chem.* **2013**, *78*, 2104–2110.

[112] Karimi-Jaberi, Z.; Barekat, M. *Chin. Chem. Lett.* **2010**, *21*, 1183–1186.

[113] Yalin, Y. C.; Wu, Y.; Henklein, P.; Li, X.; Hofmann, K. P.; Nakanishi, K.; Ernst, O. P. *Chem. Eur. J.* **2010**, *16*, 7389–7394.

[114] Wautelet, P.; Le Moigne, J.; Videva, V.; Turek, P. *J. Org. Chem.* **2003**, *68*, 8025–8036.

[115] Karimi-Jaberi, Z.; Barekat, M. *Chin. Chem. Lett.* **2010**, *21*, 1183–1186.

[116] (a) Patil, S. S.; Patil, S. V.; Bobade, V. D. *Synlett* **2011**, *8*, 1157–1159; (b) Chen, W-W.; Nguyen, R. V.; Li, C-J. *Tetrahedron Lett.* **2009**, *50*, 2895–2898; (c) Uhlig, N.; Li, C-J. *Org. Lett.* **2012**, *14*, 3000–3003; *Reviews and references therein:* (d) Yoo, W-J.; Zhao, L.; Li, C-J. *Aldrichimica Acta,* **2011**, *44*, 43–51; (e) Peshkov, V. A.; Pereshivko, O. P.; Van der Eycken, E. V. *Chem. Soc. Rev.* **2012**, *41*, 3790–3807.

[117] (a) Nadipuram, A.; David, W.; Kumar, D.; Kerwin, S. *Org. Lett.* **2002**, *4*, 4543–4546; (b) Nadipuram, A.; Kerwin, S. *Tetrahedron* **2006**, *62*, 3798–3808.

[118] Heravi, M. M.; Derikvand, F.; Haghighi, M. *Monatsh. Chem.* **2008**, *139*, 31–33.

[119] Brunner, K.; van Dijken, A.; Borner, H.; Bastiaansen, J.; Kiggen, N.; Langeveld, B. *J. Am. Chem. Soc.* **2004**, *126*, 6035–6042.

[120] (a) Seo, E.; Nelson, R. Fritsch, J.; Marcoux, L.; Leedy, R.; Adams, N. *J. Am. Chem. Soc.* **1966**, *88*, 3498–3503; (b) Ambrose, J.; Carpenter, L.; Nelson, R. *J. Electrochem. Soc.* **1975***, 122*, 876–894.

[121] Smith, K.; James, D. M.; Mistry, A. G.; Bye, M. R.; Faulkner, D. J. *Tetrahedron* **1992**, *48*, 7479–7488.

[122] Shklover, V. E.; Igonin, V. A.; Struchkov, Y. T.; Golding, I. R.; Vasnyova, N. A.; Chernoglazova, I. V.; Lazareva, O. L. Shchegolikhin, A. N. *Mol. Cryst. Liq. Cryst.* **1990**, *180B*, 417–423.

[123] (a) Vilas-Boas, M.; Freire, C.; de Castro, B.; Hillman, A. *J. Phys. Chem. B.* **1998**, *102*, 8533–8540; (b) Miranda, J.; Wade, C.; Little, R. D. *J. Org. Chem.* **2005**, *70*, 8017-8026.

[124] Chang, K.; Huang, C.; Liu, Y.; Hu, Y.; Chou, P. *Dalton Trans.* **2004**, 1731–1738.

[125] Stenberg, V.; Srinivas, V.; Baltisberger, R.; Woolsey, N. *J. Org. Chem.* **1983**, *48*, 1107–1110.

[126] Crossland, R. K.; Servis, K. L. *J. Org. Chem.* **1970**, *35*, 3195–3196

[127] (a) Gilhespy, M.; Lok, M.; Baucherel, X. *Chem.Commun.* **2005**, 1085–1086; (b) R. Barhdadi, R.; Commings, C.; Doherty, A. P.; Nedelec, J. Y.; O'Toole, S.; Troupel, M. *J Appl Electrochem*. **2007***, 37*, 723–728; (c) Kashiwagi, Y.; Tsunoda, M.; Ono, T. *Heterocycles* **2011**, *83*, 2517–2524

[128] Steckhan, E. *Angew. Chem. Int. Ed.* **1986**, *25,* 683–701.

[129] Lai, G.; Bu, X.; Santos, J.; Mintz, E. *Synlett* **1997**, 1275–1276.

[130] Chattise, P.; Ramaswamy, A.; Waghmode, S. *Tetrahedron Lett.* **2008**, *49*, 189–194.

[131] Takahashi, K.; Furusawa, T.; Sawamura, T.; Kuribayashi, S.; Inagi, S.; Fuchigami, T. *Electrochim. Acta* **2012**, *77,* 47–53.

[132] Matsumoto, K.; Iwata, T.; Suenaga, M.; Okudomi, M.; Nogawa, M.; Nakano, M.; Sugahara, A.; Bannai, Y.; Baba, K. *Heterocycles* **2010**, *81*, 2539–2553.

[133] Ono, T.; Tsunoda, M.; Takahashi, S.; Obata, T.; Sone, T.; Kashiwagi, Y. *Heterocycles* **2010**, *81*, 2771–2780.

[134] Buendia, J.; Mottweiler, J.; Bolm, C. *Chem. Eur. J.* **2011**, *17*, 13877–13882.

[135] Zanello, P. *Inorganic Electrochemistry: Theory, Practice, and Application*; Royal Society of Chemistry:Cambridge, 2003, pp 51–58.

[136] c-AFM images were obtained and processed in collaboration with Nick Economou (Buratto group, UCSB). I am fully appreciative of his patience and help during sample preparation and analysis.

[137] Initially, the c-AFM images were obtained from carbon paper electrodes modified using 5, 10, and 50 CV scans. Although an image was eventually obtained for the 50 scan sample (a,b), the roughness of the carbon paper surface proved less than ideal for this technique. In order to decrease surface roughness, subsequent polymerizations were carried out using FTO (fluorine-doped tin oxide) on glass as the working electrode. Although c-AFM images were more readily obtained on this substrate (c,d), it is apparent from the conductivity measurement that the

polymer film, right of the purple line in image (c), seems to be completely resistive (grey portion of image (d)).

(a) Surface morphology – carbon paper

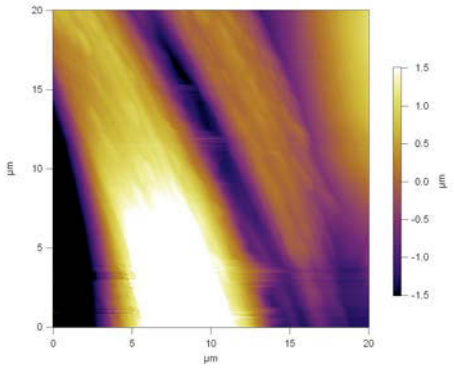

(b) Surface conductivity – carbon paper

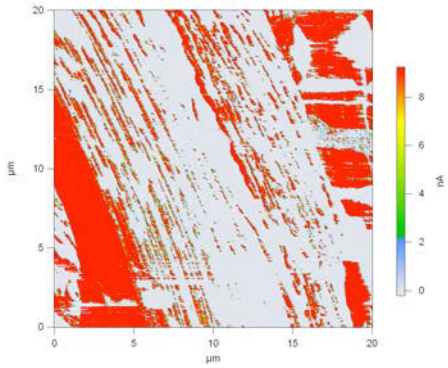

(c) Surface morphology – FTO

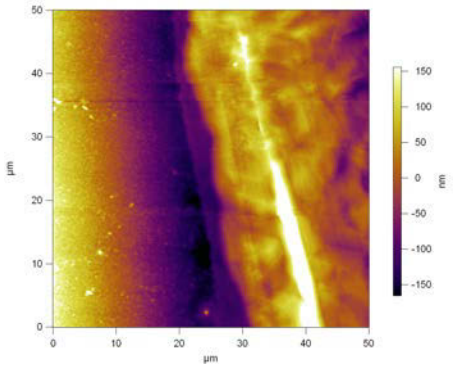

(d) Surface conductivity – FTO

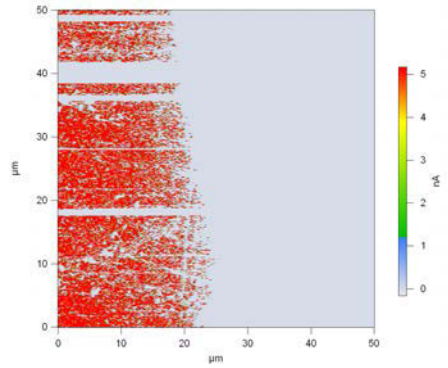

[138] Nicolaou, K. C.; Adsool, V.; Hale, C. *Org. Lett.* **2010**, *12*, 1552–1555.

[139] Cooke, M. P.; Burman, D. L. *J. Org. Chem.* **1982**, *47*, 4955–4963.

[140] Zhang, Y.; Murphy, C.; Jones, W. *Macromolecules* **2002**, *35*, 630–636.

[141] Collis, G.; Burrell, A. *J. Org. Chem.* **2003**, *68*, 8974–8983.

[142] Collis, G.; Burrell, A.; Blandford, E.; Officer, D. *Tetrahedron* **2007**, *63*, 11141–11152.

[143] Lai, G.; Bu, X.; Santos, J.; Mintz, E. *Synlett* **1997**, 1275–1276.

[144] Takahashi, K.; Furusawa, T.; Sawamura, T.; Kuribayashi, S.; Inagi, S.; Fuchigami, T. *Electrochim. Acta* **2012**, *77,* 47–53.

[145] Buendia, J.; Mottweiler, J.; Bolm, C. *Chem. Eur. J.* **2011**, *17*, 13877–13882.